

Global Carbon Budget 2023

Pierre Friedlingstein 1 2, Michael O'Sullivan 1, Matthew W. Jones 3, Robbie M. Andrew 4, Dorothee C. E. Bakker 5, Judith Hauck 6, Peter Landschützer 7, Corinne Le Quéré 3, Ingrid T. Lujikx 8, Glen P. Peters 4, Wouter Peters 8 9, Julia Pongratz 10 11, Clemens Schwingshackl 10, Stephen Sitch 1, Josep G. Canadell 12, Philippe Ciais 13, Robert B. Jackson 14, Simone R. Alin 15, Peter Anthoni 16, Leticia Barbero 17, Nicholas R. Bates 18 19, Meike Becker 20 21, Nicolas Bellouin 22, Bertrand Decharme 23, Laurent Bopp 2, Ida Bagus Mandhara Brasika 1 24, Patricia Cadule 25, Matthew A. Chamberlain 26, Naveen Chandra 27, Thuyet-Trang Chau 13, Frédéric Chevallier 13, Louise P. Chini 28, Margot Cronin 29, Xinyu Dou 30, Kazutaka Enyo 31, Wiley Evans 32, Stefanie Falk 10, Richard A. Feely 15, Liang Feng 33 34, Daniel J. Ford 1, Thomas Gasser 35, Josefine Ghattas 13, Thanos Gkritzalis 7, Giacomo Grassi 36, Luke Gregor 37, Nicolas Gruber 38, Özgür Gürses 6, Ian Harris 39, Matthew Hefner 40, Jens Heinke 41, Richard A. Houghton 42, George C. Hurtt 43, Yosuke Iida 31, Tatiana Ilyina 11, Andrew R. Jacobson 44 45, Atul Jain 46, Tereza Jarníková 47, Annika Jersild 11, Fei Jiang 48, Zhe Jin 49 50, Fortunat Joos 51 52, Etsushi Kato 53, Ralph F. Keeling 54, Daniel Kennedy 55, Kees Klein Goldewijk 56, Jürgen Knauer 57 12, Jan Ivar Korsbakken 4, Arne Körtzinger 58, Xin Lan 44 45, Nathalie Lefèvre 59, Hongmei Li 11, Junjie Liu 60 61, Zhiqiang Liu 62, Lei Ma 28, Greg Marland 40 63, Nicolas Mayot 3, Patrick C. McGuire 64, G.A. McKinley 65, Gesa Meyer 66, Eric J. Morgan 54, David R. Munro 44 67, Shin-Ichiro Nakaoka 68, Yosuke Niwa 68 69, Kevin M. O'Brien 70 15, Are Olsen 20 21, Abdírahman M. Omar 71 21, Tsuneo Ono 72, Melf E. Paulsen 58, Denis Pierrot 73, Katie Pocock 74, Benjamin Poulter 75, Carter M. Powis 76, Gregor Rehder 77, Laure Resplandy 78, Eddy Robertson 79, Christian Rödenbeck 80, Thais M Rosan 1, Jörg Schwinger 21 81, Roland Séférian 82, T. Luke Smallman 33, Stephen M. Smith 76, Reinel Sospedra-Alfonso 83, Qing Sun 51 52, Adrienne J. Sutton 15, Colm Sweeney 45, Shintaro Takao 68, Pieter P. Tans 84, Hanqin Tian 85, Bronte Tilbrook 86 87, Hiroyuki Tsujino 88, Francesco Tubiello 89, Guido R. van der Werf 8, Erik van Ooijen 86, Rik Wanninkhof 73, Michio Watanabe 90, Cathy Wimart-Rousseau 58, Dongxu Yang 91, Xiaojuan Yang 92, Wenping Yuan 93, Xu Yue 94, Sönke Zaehle 80, Jiye Zeng 68, Bo Zheng 95

1 Faculty of Environment, Science and Economy, University of Exeter, Exeter EX4 4QF, UK

2 Laboratoire de Météorologie Dynamique / Institut Pierre-Simon Laplace, CNRS, Ecole Normale Supérieure / Université PSL, Sorbonne Université, Ecole Polytechnique, Paris, France

3 Tyndall Centre for Climate Change Research, School of Environmental Sciences, University of East Anglia, Norwich Research Park, Norwich NR4 7TJ, UK

4 CICERO Center for International Climate Research, Oslo 0349, Norway

5 School of Environmental Sciences, University of East Anglia, Norwich NR4 7TJ, UK

6 Alfred-Wegener-Institut, Helmholtz-Zentrum für Polar- und Meeresforschung, Am Handelshafen 12, 27570 Bremerhaven

7 VLIZ Flanders Marine Institute, Jacobsenstraat 1, 8400, Ostend, Belgium

37 8 Wageningen University, Environmental Sciences Group, P.O. Box 47, 6700AA, Wageningen, The
38 Netherlands
39 9 University of Groningen, Centre for Isotope Research, Groningen, The Netherlands
40 10 Ludwig-Maximilians-Universität München, Luisenstr. 37, 80333 München, Germany
41 11 Max Planck Institute for Meteorology, Bundesstraße 53, 20146 Hamburg, Germany
42 12 CSIRO Environment, Canberra, ACT 2101, Australia
43 13 Laboratoire des Sciences du Climat et de l'Environnement, LSCE/IPSL, CEA-CNRS-UVSQ, Université
44 Paris-Saclay, F-91198 Gif-sur-Yvette, France
45 14 Department of Earth System Science, Woods Institute for the Environment, and Precourt Institute for
46 Energy, Stanford University, Stanford, CA 94305–2210, United States of America
47 15 National Oceanic and Atmospheric Administration, Pacific Marine Environmental Laboratory
48 (NOAA/PMEL), 7600 Sand Point Way NE, Seattle, WA 98115, USA
49 16 Karlsruhe Institute of Technology, Institute of Meteorology and Climate Research/Atmospheric
50 Environmental Research, 82467 Garmisch-Partenkirchen, Germany
51 17 Rosenstiel School of Marine Atmospheric and Earth Science, Cooperative Institute for Marine and
52 Atmospheric Studies (CIMAS), University of Miami, 4600 Rickenbacker Causeway, Miami, FL, USA
53 18 School of Ocean Futures, Julie Ann Wrigley Global Futures Laboratory, Arizona State University, Tempe,
54 Arizona, AZ 85287-5502, USA
55 19 Bermuda Institute of Ocean Sciences (BIOS), 17 Biological Lane, St. Georges, GE01, Bermuda
56 20 Geophysical Institute, University of Bergen, Allégaten 70, 5007 Bergen, Norway
57 21 Bjerknes Centre for Climate Research, Bergen, Norway
58 22 Department of Meteorology, University of Reading, Reading, RG6 6BB, UK
59 23 CNRM, Université de Toulouse, Météo-France, CNRS, Toulouse, France
60 24 Faculty of Marine Science & Fisheries, University of Udayana, Bali 80361, Indonesia
61 25 CNRS, Institut Pierre-Simon Laplace, Sorbonne Université, Paris, France
62 26 CSIRO Environment, Hobart, TAS, Australia
63 27 Research Institute for Global Change, JAMSTEC, 3173-25 Showa-machi, Kanazawa, Yokohama, 236-0001,
64 Japan
65 28 Department of Geographical Sciences, University of Maryland, College Park, MD 20742, USA
66 29 Marine Institute, Rinville, Oranmore, Co Galway H91 R673, Ireland
67 30 Department of Earth System Science, Tsinghua University, Beijing, China
68 31 Japan Meteorological Agency, 3-6-9 Toranomon, Minato City, Tokyo 105-8431, Japan
69 32 Hakai Institute, 1713 Hyacinthe Bay Rd, Heriot Bay, BC, V0P 1H0, Canada
70 33 National Centre for Earth Observation, University of Edinburgh, Edinburgh, EH9 3FE, UK
71 34 School of Geosciences, University of Edinburgh, UK
72 35 International Institute for Applied Systems Analysis (IIASA), Schlossplatz 1
73 A-2361 Laxenburg, Austria
74 36 European Commission, Joint Research Centre, 21027 Ispra (VA), Italy
75 37 ETH Zuerich

76 38 Environmental Physics Group, ETH Zürich, Institute of Biogeochemistry and Pollutant Dynamics and
77 Center for Climate Systems Modeling (C2SM)
78 39 NCAS-Climate, Climatic Research Unit, School of Environmental Sciences, University of East Anglia,
79 Norwich Research Park, Norwich, NR4 7TJ, UK
80 40 Research Institute for Environment, Energy, and Economics, Appalachian State University, Boone, North
81 Carolina, USA
82 41 Potsdam Institute for Climate Impact Research (PIK), member
83 of the Leibniz Association, P.O. Box 60 12 03, 14412 Potsdam, Germany
84 42 Woodwell Climate Research Center, Falmouth, MA 02540, USA
85 43 Department of Geographical Sciences, University of Maryland, College Park, Maryland 20742, USA
86 44 Cooperative Institute for Research in Environmental Sciences (CIRES), University of Colorado, Boulder,
87 CO 80305, USA
88 45 National Oceanic and Atmospheric Administration, Global Monitoring Laboratory (NOAA/GML), 325
89 Broadway R/GML, Boulder, CO 80305, USA
90 46 Department of Atmospheric Sciences, University of Illinois, Urbana, IL 61821, USA
91 47 School of Environmental Sciences, University of East Anglia, Norwich Research Park, Norwich NR4 7TJ,
92 UK
93 48 Jiangsu Provincial Key Laboratory of Geographic Information Science and Technology, International
94 Institute for Earth System Science, Nanjing University, Nanjing, 210023, China
95 Nanjing University, Nanjing, China
96 49 State Key Laboratory of Tibetan Plateau Earth System and Resource Environment, Institute of Tibetan
97 Plateau Research, Chinese Academy of Sciences, Beijing 100101, China
98 50 Institute of Carbon Neutrality, Peking University, Beijing 100871, China
99 51 Climate and Environmental Physics, Physics Institute, University of Bern, Bern, Switzerland
100 52 Oeschger Centre for Climate Change Research, University of Bern, Bern, Switzerland
101 53 Institute of Applied Energy (IAE), Minato-ku, Tokyo 105-0003, Japan
102 54 University of California, San Diego, Scripps Institution of Oceanography, La Jolla, CA 92093-0244, USA
103 55 National Center for Atmospheric Research, Climate and Global Dynamics, Terrestrial Sciences Section,
104 Boulder, CO 80305, USA
105 56 Utrecht University, Faculty of Geosciences, Department IMEW, Copernicus Institute of Sustainable
106 Development, Heidelberglaan 2, P.O. Box 80115, 3508 TC, Utrecht, the Netherlands
107 57 Hawkesbury Institute for the Environment, Western Sydney University, Penrith, New South Wales,
108 Australia
109 58 GEOMAR Helmholtz Centre for Ocean Research, Wischhofstr. 1-3, 24148 Kiel, Germany
110 59 LOCEAN/IPSL laboratory, Sorbonne Université, CNRS/IRD/MNHN, Paris, France
111 60 NASA JPL
112 61 Caltech
113 62 CMA Key Open Laboratory of Transforming Climate Resources to Economy, Chongqing Institute of
114 Meteorological Sciences, Chongqing 401147, China

115 63 Department of Geological and Environmental Sciences, Appalachian State University, Boone, North
116 Carolina, USA
117 64 Department of Meteorology & National Centre for Atmospheric Science (NCAS), University of Reading,
118 Reading, United Kingdom
119 65 Columbia University
120 66 Climate Research Division, Environment and Climate Change Canada, Victoria, BC, Canada
121 67 National Oceanic and Atmospheric Administration/Global Monitoring Laboratory (NOAA/GML), 325
122 Broadway R/GML, Boulder, CO 80305, USA
123 68 Earth System Division, National Institute for Environmental Studies, 16-2 Onogawa, Tsukuba, Ibaraki, 305-
124 8506 Japan
125 69 Department of Climate and Geochemistry Research, Meteorological Research Institute, 1-1 Nagamine,
126 Tsukuba, Ibaraki 305-0052, Japan
127 70 Cooperative Institute for Climate, Ocean and Ecosystem Studies (CICOES), University of Washington,
128 Seattle, WA 98105, USA
129 71 NORCE Norwegian Research Centre, Jahnebakken 5, 5007 Bergen, Norway
130 72 Marine Environment Division, Fisheries Resources Institute, Japan Fisheries Research and Education
131 Agency, 2-12-4 Fukuura, Kanazawa-Ku, Yokohama 236-8648, Japan
132 73 National Oceanic & Atmospheric Administration, Atlantic Oceanographic & Meteorological Laboratory
133 (NOAA/AOML), 4301 Rickenbacker Causeway, Miami, FL 33149, USA
134 74 Hakai Institute, 1713 Hyacinthe Bay Rd, Heriot Bay, BC, V0P 1H0, Canada
135 75 NASA Goddard Space Flight Center, Biospheric Sciences Laboratory, Greenbelt, Maryland 20771, USA
136 76 Smith School for Enterprise and the Environment, University of Oxford, Oxford, UK
137 77 Leibniz Institute for Baltic Sea Research Warnemünde (IOW), Seestrasse 15, 18119 Rostock, Germany
138 78 Princeton University, Department of Geosciences and Princeton Environmental Institute, Princeton, NJ,
139 USA
140 79 Met Office Hadley Centre, FitzRoy Road, Exeter EX1 3PB, UK
141 80 Max Planck Institute for Biogeochemistry, P.O. Box 600164, Hans-Knöll-Str. 10, 07745 Jena, Germany
142 81 NORCE Climate & Environment, Jahnebakken 5, 5007 Bergen, Norway
143 82 CNRM (Météo-France/CNRS)-UMR 3589
144 83 Canadian Centre for Climate Modelling and Analysis, Victoria BC, Canada
145 84 Institute of Arctic and Alpine Research, University of Colorado, Boulder, CO 80309, USA
146 85 Schiller Institute of Integrated Science and Society, Department of Earth and Environmental Sciences,
147 Boston College, Chestnut Hill, MA 02467, USA
148 86 CSIRO Environment, Castray Esplanade, Hobart, Tasmania 7004, Australia
149 87 Australian Antarctic Partnership Program, University of Tasmania, Hobart, Australia
150 88 JMA Meteorological Research Institute, Japan
151 89 Statistics Division, Food and Agriculture Organization of the United Nations, Via Terme di Caracalla, Rome
152 00153, Italy

153 90 Japan Agency for Marine-Earth Science and Technology (JAMSTEC), 3173-25, Showa-machi, Kanazawa-
154 ku, Yokohama, 236-0001, Japan
155 91 Institute of Atmospheric Physics, Chinese Academy of Sciences
156 92 Environmental Sciences Division and Climate Change Science Institute, Oak Ridge National Laboratory,
157 Oak Ridge, TN, 37831, USA
158 93 School of Atmospheric Sciences, Sun Yat-sen University, Zhuhai, Guangdong 510245, China
159 94 School of Environmental Science and Engineering, Nanjing University of Information Science and
160 Technology (NUIST)
161 95 Shenzhen Key Laboratory of Ecological Remediation and Carbon Sequestration, Institute of Environment
162 and Ecology, Tsinghua Shenzhen International Graduate School, Tsinghua University, Shenzhen 518055, China
163
164 *Correspondence to:* Pierre Friedlingstein (p.friedlingstein@exeter.ac.uk)

165 **Abstract**

166 Accurate assessment of anthropogenic carbon dioxide (CO₂) emissions and their redistribution among the
167 atmosphere, ocean, and terrestrial biosphere in a changing climate is critical to better understand the global
168 carbon cycle, support the development of climate policies, and project future climate change. Here we describe
169 and synthesise data sets and methodology to quantify the five major components of the global carbon budget
170 and their uncertainties. Fossil CO₂ emissions (E_{FOS}) are based on energy statistics and cement production data,
171 while emissions from land-use change (E_{LUC}), mainly deforestation, are based on land-use and land-use change
172 data and bookkeeping models. Atmospheric CO₂ concentration is measured directly, and its growth rate (G_{ATM})
173 is computed from the annual changes in concentration. The ocean CO₂ sink (S_{OCEAN}) is estimated with global
174 ocean biogeochemistry models and observation-based *f*CO₂-products. The terrestrial CO₂ sink (S_{LAND}) is
175 estimated with dynamic global vegetation models. Additional lines of evidence on land and ocean sinks are
176 provided by atmospheric inversions, atmospheric oxygen measurements and Earth System Models. The
177 resulting carbon budget imbalance (B_{IM}), the difference between the estimated total emissions and the
178 estimated changes in the atmosphere, ocean, and terrestrial biosphere, is a measure of imperfect data and
179 incomplete understanding of the contemporary carbon cycle. All uncertainties are reported as $\pm 1\sigma$.

180 For the year 2022, E_{FOS} increased by 0.9% relative to 2021, with fossil emissions at 9.9 ± 0.5 GtC yr⁻¹ ($10.2 \pm$
181 0.5 GtC yr⁻¹ when the cement carbonation sink is not included), E_{LUC} was 1.2 ± 0.7 GtC yr⁻¹, for a total
182 anthropogenic CO₂ emission (including the cement carbonation sink) of 11.1 ± 0.8 GtC yr⁻¹ (40.7 ± 3.2 GtCO₂
183 yr⁻¹). Also, for 2022, G_{ATM} was 4.6 ± 0.2 GtC yr⁻¹ (2.18 ± 0.1 ppm yr⁻¹), S_{OCEAN} was 2.8 ± 0.4 GtC yr⁻¹ and
184 S_{LAND} was 3.8 ± 0.8 GtC yr⁻¹, with a B_{IM} of -0.1 GtC yr⁻¹ (i.e. total estimated sources marginally too low or
185 sinks marginally too high). The global atmospheric CO₂ concentration averaged over 2022 reached 417.1 ± 0.1
186 ppm. Preliminary data for 2023, suggest an increase in E_{FOS} relative to 2022 of +1.1% (0.1% to 2.2%) globally,
187 and atmospheric CO₂ concentration reaching 419.3 ppm, 51% above pre-industrial level (around 278 ppm in
188 1750). Overall, the mean and trend in the components of the global carbon budget are consistently estimated

189 over the period 1959-2022, with a near-zero overall budget imbalance, although discrepancies of up to around
190 1 GtC yr⁻¹ persist for the representation of annual to semi-decadal variability in CO₂ fluxes. Comparison of
191 estimates from multiple approaches and observations shows: (1) a persistent large uncertainty in the estimate of
192 land-use changes emissions, (2) a low agreement between the different methods on the magnitude of the land
193 CO₂ flux in the northern extra-tropics, and (3) a discrepancy between the different methods on the strength of
194 the ocean sink over the last decade.

195 This living data update documents changes in methods and data sets applied to this most-recent global carbon
196 budget as well as evolving community understanding of the global carbon cycle. The data presented in this
197 work are available at <https://doi.org/10.18160/GCP-2023> (Friedlingstein et al., 2023).

198

199 **Executive Summary**

200 **Global fossil CO₂ emissions (including cement carbonation) are expected to further increase in 2023, to**
201 **1.4% above their pre-COVID-19 pandemic 2019 level.** The 2022 emission increase was 0.09 GtC yr⁻¹ (0.33
202 GtCO₂ yr⁻¹) relative to 2021, bringing 2022 fossil CO₂ emissions to 9.9 ± 0.5 GtC yr⁻¹ (36.4 ± 1.8 GtCO₂ yr⁻¹),
203 virtually equal to the emissions level of 2019. Preliminary estimates based on data available suggest fossil CO₂
204 emissions to increase further in 2023, by 1.1% relative to 2022 (0.1% to 2.2%), bringing emissions to 10.0 GtC
205 yr⁻¹ (36.8 GtCO₂ yr⁻¹), 1.4% above the 2019 level.

206 Emissions from coal, oil, and gas in 2023 are all expected to be slightly above their 2022 levels (by 1.3%, 1.5%
207 and 0.2% respectively). Regionally, fossil emissions in 2022 are expected to decrease by 7.4% in the European
208 Union (0.7 GtC, 2.6 GtCO₂), and by 3.0% in the United States (1.3 GtC, 4.9 GtCO₂), but to increase by 4.0% in
209 China (3.2 GtC, 11.9 GtCO₂), 8.7% in India (0.8 GtC, 3.1 GtCO₂) and 0.5% for the rest of the world (4.2 GtC,
210 15.2 GtCO₂).

211 **Fossil CO₂ emissions decreased in 18 countries during the decade 2013-2022.** Altogether, these 18 countries
212 contribute about 1.9 GtC yr⁻¹ (7.1 GtCO₂) fossil fuel CO₂ emissions over the last decade, representing about
213 20% of world CO₂ fossil emissions.

214 **Global CO₂ emissions from land-use, land-use change, and forestry (LULUCF) averaged 1.3 ± 0.7 GtC yr⁻¹**
215 **(4.7 ± 2.6 GtCO₂ yr⁻¹) for the 2013-2022 period with a preliminary projection for 2023 of 1.1 ± 0.7 GtC**
216 **yr⁻¹ (4.0 ± 2.6 GtCO₂ yr⁻¹). A small decrease over the past two decades is not robust given the large model**
217 **uncertainty.** Emissions from deforestation, the main driver of global gross sources, remain high at around 1.9
218 GtC yr⁻¹ over the 2013-2022 period, highlighting the strong potential of halting deforestation for emissions
219 reductions. Sequestration of 1.3 GtC yr⁻¹ through re-/afforestation and forestry offsets two third of the
220 deforestation emissions. Emissions from other land-use transitions and from peat drainage and peat fire add
221 further, smaller contributions. The highest emitters during 2013-2022 in descending order were Brazil,
222 Indonesia, and the Democratic Republic of the Congo, with these 3 countries contributing more than half of
223 global land-use CO₂ emissions.

224 **Total anthropogenic emissions were 11.1 GtC yr⁻¹ (40.7 GtCO₂ yr⁻¹) in 2022, with a similar preliminary**
225 **estimate of 11.2 GtC yr⁻¹ (40.9 GtCO₂ yr⁻¹) for 2023.**

226 **The remaining carbon budget for a 50% likelihood to limit global warming to 1.5°C, 1.7°C and 2°C has**
227 **respectively reduced to 75 GtC (275 GtCO₂), 175 GtC (625 GtCO₂) and 315 GtC (1150 GtCO₂) from the**
228 **beginning of 2024, equivalent to around 7, 15 and 28 years, assuming 2023 emissions levels.**

229 **The concentration of CO₂ in the atmosphere is set to reach 419.3 ppm in 2023, 51% above pre-industrial**
230 **levels.** The atmospheric CO₂ growth was 5.2 ± 0.02 GtC yr⁻¹ during the decade 2013-2022 (47% of total CO₂
231 emissions) with a preliminary 2023 growth rate estimate of around 5.1 GtC (2.4 ppm).

232 **The ocean CO₂ sink resumed a more rapid growth in the past two decades after low or no growth during**
233 **the 1991-2002 period, overlaid with imprints of climate variability.** The estimates based on *f*CO₂-products
234 and models diverge with the growth of the ocean CO₂ sink in the past decade being a factor 2.5 larger than in the
235 models. This discrepancy in the trend originates from all latitudes but is largest in the Southern Ocean. The
236 ocean CO₂ sink was 2.9 ± 0.4 GtC yr⁻¹ during the decade 2013-2022 (26% of total CO₂ emissions), and did not
237 grow since 2019 due to a triple La Niña event. A similar value of 2.9 GtC yr⁻¹ is preliminarily estimated for
238 2023, which marks an increase in the sink compared to the last two years due to the transition from La Niña to
239 El Niño conditions in 2023.

240 **The land CO₂ sink continued to increase during the 2013-2022 period primarily in response to increased**
241 **atmospheric CO₂, albeit with large interannual variability.** The land CO₂ sink was 3.3 ± 0.8 GtC yr⁻¹ during
242 the 2013-2022 decade (31% of total CO₂ emissions), 0.4 GtC yr⁻¹ larger than during the previous decade (2000-
243 2009), with a preliminary 2023 estimate of around 2.9 GtC yr⁻¹, significantly lower than in 2022, and attributed
244 to the response of the land biosphere to the emerging El Niño in 2023. Year to year variability in the land sink is
245 about 1 GtC yr⁻¹ and dominates the year-to-year changes in the global atmospheric CO₂ concentration, implying
246 that small annual changes in anthropogenic emissions (such as the fossil fuel emission decrease in 2020) are
247 hard to detect in the atmospheric CO₂ observations.

248 1 Introduction

249 The concentration of carbon dioxide (CO₂) in the atmosphere has increased from approximately 278 parts per
250 million (ppm) in 1750 (Gulev et al., 2021), the beginning of the Industrial Era, to 417.1 ± 0.1 ppm in 2022 (Lan
251 et al., 2023; Figure 1). The atmospheric CO₂ increase above pre-industrial levels was, initially, primarily caused
252 by the release of carbon to the atmosphere from deforestation and other land-use change activities (Canadell et
253 al., 2021). While emissions from fossil fuels started before the Industrial Era, they became the dominant source
254 of anthropogenic emissions to the atmosphere from around 1950 and their relative share has continued to
255 increase until present. Anthropogenic emissions occur on top of an active natural carbon cycle that circulates
256 carbon between the reservoirs of the atmosphere, ocean, and terrestrial biosphere on time scales from sub-daily
257 to millennia, while exchanges with geologic reservoirs occur at longer timescales (Archer et al., 2009).

258 The global carbon budget (GCB) presented here refers to the mean, variations, and trends in the perturbation of
259 CO₂ in the environment, referenced to the beginning of the Industrial Era (defined here as 1750). This paper
260 describes the components of the global carbon cycle over the historical period with a stronger focus on the
261 recent period (since 1958, onset of robust atmospheric CO₂ measurements), the last decade (2013-2022), the last
262 year (2022) and the current year (2023). Finally, it provides cumulative emissions from fossil fuels and land-use
263 change since the year 1750 (the pre-industrial period), and since the year 1850 (the reference year for historical
264 simulations in IPCC AR6) (Eyring et al., 2016).

265 We quantify the input of CO₂ to the atmosphere by emissions from human activities, the growth rate of
266 atmospheric CO₂ concentration, and the resulting changes in the storage of carbon in the land and ocean
267 reservoirs in response to increasing atmospheric CO₂ levels, climate change and variability, and other
268 anthropogenic and natural changes (Figure 2). An understanding of this perturbation budget over time and the
269 underlying variability and trends of the natural carbon cycle is necessary to understand the response of natural
270 sinks to changes in climate, CO₂ and land-use change drivers, and to quantify emissions compatible with a given
271 climate stabilisation target.

272 The components of the CO₂ budget that are reported annually in this paper include separate and independent
273 estimates for the CO₂ emissions from (1) fossil fuel combustion and oxidation from all energy and industrial
274 processes; also including cement production and carbonation (E_{FOS} ; GtC yr⁻¹) and (2) the emissions resulting
275 from deliberate human activities on land, including those leading to land-use change (E_{LUC} ; GtC yr⁻¹); and their
276 partitioning among (3) the growth rate of atmospheric CO₂ concentration (G_{ATM} ; GtC yr⁻¹), and the uptake of
277 CO₂ (the ‘CO₂ sinks’) in (4) the ocean (S_{OCEAN} ; GtC yr⁻¹) and (5) on land (S_{LAND} ; GtC yr⁻¹). The CO₂ sinks as
278 defined here conceptually include the response of the land (including inland waters and estuaries) and ocean
279 (including coastal and marginal seas) to elevated CO₂ and changes in climate and other environmental
280 conditions, although in practice not all processes are fully accounted for (see Section 2.10). Global emissions
281 and their partitioning among the atmosphere, ocean and land are in balance in the real world. Due to the
282 combination of imperfect spatial and/or temporal data coverage, errors in each estimate, and smaller terms not
283 included in our budget estimate (discussed in Section 2.10), the independent estimates (1) to (5) above do not

284 necessarily add up to zero. We therefore assess a set of additional lines of evidence derived from global
285 atmospheric inversion system results (Section 2.7), observed changes in oxygen concentration (Section 2.8) and
286 Earth System Models (ESMs) simulations (Section 2.9), all of which closing the global carbon balance. We also
287 estimate a budget imbalance (B_{IM}), which is a measure of the mismatch between the estimated emissions and the
288 estimated changes in the atmosphere, land and ocean, as follows:

$$289 \quad B_{IM} = E_{FOS} + E_{LUC} - (G_{ATM} + S_{OCEAN} + S_{LAND}) \quad (1)$$

290 G_{ATM} is usually reported in ppm yr⁻¹, which we convert to units of carbon mass per year, GtC yr⁻¹, using 1 ppm
291 = 2.124 GtC (Ballantyne et al., 2012; Table 1). All quantities are presented in units of gigatonnes of carbon
292 (GtC, 10¹⁵ gC), which is the same as petagrams of carbon (PgC; Table 1). Units of gigatonnes of CO₂ (or billion
293 tonnes of CO₂) used in policy are equal to 3.664 multiplied by the value in units of GtC.

294 We also quantify E_{FOS} and E_{LUC} by country, including both territorial and consumption-based accounting for
295 E_{FOS} (see Section 2), and discuss missing terms from sources other than the combustion of fossil fuels (see
296 Section 2.10, Supplement S1 and S2).

297 We now assess carbon dioxide removal (CDR) (see Sect. 2.2 and 2.3). Land-based CDR is significant, but
298 already accounted for in E_{LUC} in equation (1) (Sect 3.2.2). Other CDR methods, not based on vegetation, are
299 currently several orders of magnitude smaller than the other components of the budget (Sect. 3.3), hence these
300 are not included in equation (1), or in the global carbon budget tables or figures (with the exception of Figure 2
301 where CDR is shown primarily for illustrative purpose).

302 The global CO₂ budget has been assessed by the Intergovernmental Panel on Climate Change (IPCC) in all
303 assessment reports (Prentice et al., 2001; Schimel et al., 1995; Watson et al., 1990; Denman et al., 2007; Ciais et
304 al., 2013; Canadell et al., 2021), and by others (e.g. Ballantyne et al., 2012). The Global Carbon Project (GCP,
305 www.globalcarbonproject.org, last access: 9 November 2023) has coordinated this cooperative community
306 effort for the annual publication of global carbon budgets for the year 2005 (Raupach et al., 2007; including
307 fossil emissions only), year 2006 (Canadell et al., 2007), year 2007 (GCP, 2008), year 2008 (Le Quéré et al.,
308 2009), year 2009 (Friedlingstein et al., 2010), year 2010 (Peters et al., 2012a), year 2012 (Le Quéré et al., 2013;
309 Peters et al., 2013), year 2013 (Le Quéré et al., 2014), year 2014 (Le Quéré et al., 2015a; Friedlingstein et al.,
310 2014), year 2015 (Jackson et al., 2016; Le Quéré et al., 2015b), year 2016 (Le Quéré et al., 2016), year 2017 (Le
311 Quéré et al., 2018a; Peters et al., 2017), year 2018 (Le Quéré et al., 2018b; Jackson et al., 2018), year 2019
312 (Friedlingstein et al., 2019; Jackson et al., 2019; Peters et al., 2020), year 2020 (Friedlingstein et al., 2020; Le
313 Quéré et al., 2021), year 2021 (Friedlingstein et al., 2022a; Jackson et al., 2022) and most recently the year 2022
314 (Friedlingstein et al., 2022b). Each of these papers updated previous estimates with the latest available
315 information for the entire time series.

316 We adopt a range of ± 1 standard deviation (σ) to report the uncertainties in our global estimates, representing a
317 likelihood of 68% that the true value will be within the provided range if the errors have a gaussian distribution,
318 and no bias is assumed. This choice reflects the difficulty of characterising the uncertainty in the CO₂ fluxes

319 between the atmosphere and the ocean and land reservoirs individually, particularly on an annual basis, as well
320 as the difficulty of updating the CO₂ emissions from land-use change. A likelihood of 68% provides an
321 indication of our current capability to quantify each term and its uncertainty given the available information.
322 The uncertainties reported here combine statistical analysis of the underlying data, assessments of uncertainties
323 in the generation of the data sets, and expert judgement of the likelihood of results lying outside this range. The
324 limitations of current information are discussed in the paper and have been examined in detail elsewhere
325 (Ballantyne et al., 2015; Zscheischler et al., 2017). We also use a qualitative assessment of confidence level to
326 characterise the annual estimates from each term based on the type, amount, quality, and consistency of the
327 different lines of evidence as defined by the IPCC (Stocker et al., 2013).

328 This paper provides a detailed description of the data sets and methodology used to compute the global carbon
329 budget estimates for the industrial period, from 1750 to 2023, and in more detail for the period since 1959. This
330 paper is updated every year using the format of ‘living data’ to keep a record of budget versions and the changes
331 in new data, revision of data, and changes in methodology that lead to changes in estimates of the carbon
332 budget. Additional materials associated with the release of each new version will be posted at the Global Carbon
333 Project (GCP) website (<http://www.globalcarbonproject.org/carbonbudget>, last access: 9 November 2023), with
334 fossil fuel emissions also available through the Global Carbon Atlas (<http://www.globalcarbonatlas.org>, last
335 access: 9 November 2023). All underlying data used to produce the budget can also be found at
336 <https://globalcarbonbudget.org/> (last access: 9 November 2023). With this approach, we aim to provide the
337 highest transparency and traceability in the reporting of CO₂, the key driver of climate change.

338 **2 Methods**

339 Multiple organisations and research groups around the world generated the original measurements and data used
340 to complete the global carbon budget. The effort presented here is thus mainly one of synthesis, where results
341 from individual groups are collated, analysed, and evaluated for consistency. We facilitate access to original
342 data with the understanding that primary data sets will be referenced in future work (see Table 2 for how to cite
343 the data sets, and Section on data availability). Descriptions of the measurements, models, and methodologies
344 follow below, with more detailed descriptions of each component provided as Supplementary Information (S1 to
345 S5).

346 This is the 18th version of the global carbon budget and the 12th revised version in the format of a living data
347 update in Earth System Science Data. It builds on the latest published global carbon budget of Friedlingstein et
348 al. (2022b). The main changes this year are: the inclusion of (1) data to year 2022 and a projection for the global
349 carbon budget for year 2023; (2) CO₂ uptake from Carbon Dioxide Removal (CDR); (3) land and ocean net
350 carbon fluxes estimates from changes in atmospheric oxygen concentration; (4) land and ocean net carbon
351 fluxes estimates from ESMs; and (5) revised method to estimate the current year (2023) atmospheric CO₂. The
352 main methodological differences between recent annual carbon budgets (2019 to 2023) are summarised in Table
353 3 and previous changes since 2006 are provided in Table S8.

354 **2.1 Fossil CO₂ emissions (E_{FOS})**

355 **2.1.1 Historical period 1850-2022**

356 The estimates of global and national fossil CO₂ emissions (E_{FOS}) include the oxidation of fossil fuels through
357 both combustion (e.g., transport, heating) and chemical oxidation (e.g. carbon anode decomposition in
358 aluminium refining) activities, and the decomposition of carbonates in industrial processes (e.g. the production
359 of cement). We also include CO₂ uptake from the cement carbonation process. Several emissions sources are not
360 estimated or not fully covered: coverage of emissions from lime production are not global, and decomposition of
361 carbonates in glass and ceramic production are included only for the “Annex 1” countries of the United Nations
362 Framework Convention on Climate Change (UNFCCC) for lack of activity data. These omissions are
363 considered to be minor. Short-cycle carbon emissions - for example from combustion of biomass - are not
364 included here but are accounted for in the CO₂ emissions from land use (see Section 2.2).

365 Our estimates of fossil CO₂ emissions rely on data collection by many other parties. Our goal is to produce the
366 best estimate of this flux, and we therefore use a prioritisation framework to combine data from different
367 sources that have used different methods, while being careful to avoid double counting and undercounting of
368 emissions sources. The CDIAC-FF emissions dataset, derived largely from UN energy data, forms the
369 foundation, and we extend emissions to year Y-1 using energy growth rates reported by the Energy Institute (a
370 dataset formally produced by BP). We then proceed to replace estimates using data from what we consider to be
371 superior sources, for example Annex 1 countries’ official submissions to the UNFCCC. All data points are
372 potentially subject to revision, not just the latest year. For full details see Andrew and Peters (2022).

373 Other estimates of global fossil CO₂ emissions exist, and these are compared by Andrew (2020a). The most
374 common reason for differences in estimates of global fossil CO₂ emissions is a difference in which emissions
375 sources are included in the datasets. Datasets such as those published by the energy company BP, the US Energy
376 Information Administration, and the International Energy Agency’s ‘CO₂ emissions from fuel combustion’ are
377 all generally limited to emissions from combustion of fossil fuels. In contrast, datasets such as PRIMAP-hist,
378 CEDS, EDGAR, and GCP’s dataset aim to include all sources of fossil CO₂ emissions. See Andrew (2020a) for
379 detailed comparisons and discussion.

380 Cement absorbs CO₂ from the atmosphere over its lifetime, a process known as ‘cement carbonation’. We
381 estimate this CO₂ sink, from 1931, onwards as the average of two studies in the literature (Cao et al., 2020; Guo
382 et al., 2021). Both studies use the same model, developed by Xi et al. (2016), with different parameterisations
383 and input data, with the estimate of Guo and colleagues being a revision of Xi et al. (2016). The trends of the
384 two studies are very similar. Since carbonation is a function of both current and previous cement production, we
385 extend these estimates to 2022 by using the growth rate derived from the smoothed cement emissions (10-year
386 smoothing) fitted to the carbonation data. In the present budget, we always include the cement carbonation
387 carbon sink in the fossil CO₂ emission component (E_{FOS}).

388 We use the Kaya Identity for a simple decomposition of CO₂ emissions into the key drivers (Raupach et al.,
389 2007). While there are variations (Peters et al., 2017), we focus here on a decomposition of CO₂ emissions into
390 population, GDP per person, energy use per GDP, and CO₂ emissions per energy. Multiplying these individual
391 components together returns the CO₂ emissions. Using the decomposition, it is possible to attribute the change
392 in CO₂ emissions to the change in each of the drivers. This method gives a first-order understanding of what
393 causes CO₂ emissions to change each year.

394 **2.1.2 2023 projection**

395 We provide a projection of global fossil CO₂ emissions in 2022 by combining separate projections for China,
396 USA, EU, India, and for all other countries combined. The methods are different for each of these. For China we
397 combine monthly fossil fuel production data from the National Bureau of Statistics and trade data from the
398 Customs Administration, giving us partial data for the growth rates to date of natural gas, petroleum, and
399 cement, and of the apparent consumption itself for raw coal. We then use a regression model to project full-year
400 emissions based on historical observations. For the USA our projection is taken directly from the Energy
401 Information Administration's (EIA) Short-Term Energy Outlook (EIA, 2023), combined with the year-to-date
402 growth rate of cement clinker production. For the EU we use monthly energy data from Eurostat to derive
403 estimates of monthly CO₂ emissions through July, with coal emissions extended through September using a
404 statistical relationship with reported electricity generation from coal and other factors. For natural gas we use
405 Holt-Winters to project the last four months of the year. EU emissions from oil are derived using the EIA's
406 projection of oil consumption for Europe. EU cement emissions are based on available year-to-date data from
407 three of the largest producers, Germany, Poland, and Spain. India's projected emissions are derived from
408 estimates through August (July for coal) using the methods of Andrew (2020b) and extrapolated assuming
409 seasonal patterns from before 2019. Emissions for the rest of the world are derived using projected growth in
410 economic production from the IMF (2023) combined with extrapolated changes in emissions intensity of
411 economic production. More details on the E_{FOS} methodology and its 2023 projection can be found in
412 Supplement S.1.

413 **2.2 CO₂ emissions from land-use, land-use change and forestry (E_{LUC})**

414 **2.2.1 Historical period 1850-2022**

415 The net CO₂ flux from land-use, land-use change and forestry (E_{LUC}, called land-use change emissions in the
416 rest of the text) includes CO₂ fluxes from deforestation, afforestation, logging and forest degradation (including
417 harvest activity), shifting cultivation (cycle of cutting forest for agriculture, then abandoning), and regrowth of
418 forests (following wood harvest or agriculture abandonment). Emissions from peat burning and peat drainage
419 are added from external datasets, peat drainage being averaged from three spatially explicit independent datasets
420 (see Supplement S.2.1).

421 Three bookkeeping approaches (updated estimates each of BLUE (Hansis et al., 2015), OSCAR (Gasser et al.,
422 2020), and H&C2023 (Houghton and Castanho, 2023)) were used to quantify gross emissions and gross

423 removals and the resulting net E_{LUC} . Uncertainty estimates were derived from the Dynamic Global Vegetation
424 Models (DGVMs) ensemble for the time period prior to 1960, and using for the recent decades an uncertainty
425 range of ± 0.7 GtC yr⁻¹, which is a semi-quantitative measure for annual and decadal emissions and reflects our
426 best value judgement that there is at least 68% chance ($\pm 1\sigma$) that the true land-use change emission lies within
427 the given range, for the range of processes considered here.

428 Our E_{LUC} estimates follow the definition of global carbon cycle models of CO₂ fluxes related to land use and
429 land management and differ from IPCC definitions adopted in National GHG Inventories (NGHGI) for
430 reporting under the UNFCCC, which additionally generally include, through adoption of the IPCC so-called
431 managed land proxy approach, the terrestrial fluxes occurring on all land that countries define as managed. This
432 partly includes fluxes due to environmental change (e.g. atmospheric CO₂ increase), which are part of S_{LAND} in
433 our definition. This causes the global emission estimates to be smaller for NGHGI than for the global carbon
434 budget definition (Grassi et al., 2018). The same is the case for the Food Agriculture Organization (FAO)
435 estimates of carbon fluxes on forest land, which include both anthropogenic and natural sources on managed
436 land (Tubiello et al., 2021). We translate the two definitions to each other, to provide a comparison of the
437 anthropogenic carbon budget to the official country reporting to the climate convention.

438 E_{LUC} contains a range of fluxes that are related to Carbon Dioxide Removal (CDR). CDR can be defined as the
439 set of anthropogenic activities that remove CO₂ from the atmosphere and store it in durable form, such as in
440 forest biomass and soils, long-lived products, or in geological or ocean reservoirs. We quantify vegetation-based
441 CDR that is implicitly or explicitly captured by land-use fluxes consistent with our updated model estimates
442 (CDR not based on vegetation is discussed in Section 2.3; IPCC, 2023). We quantify re/afforestation from the
443 three bookkeeping estimates by separating forest regrowth in shifting cultivation cycles from permanent
444 increases in forest cover (see Supplement C.2.1). The latter count as CDR, but it should be noted that the
445 permanence of the storage under climate risks such as fire is increasingly questioned. Other CDR activities
446 contained in E_{LUC} include the transfer of carbon to harvested wood products (HWP), which is represented by the
447 bookkeeping models with varying details concerning product usage and their lifetimes; bioenergy with carbon
448 capture and storage (BECCS); and biochar production. Bookkeeping and TRENDY models currently only
449 represent BECCS and biochar with regard to the CO₂ removal through photosynthesis, but not for the durable
450 storage. HWP, BECCS, and biochar are typically counted as CDR when the transfer to the durable storage site
451 occurs and not when the CO₂ is removed from the atmosphere, which complicates a direct comparison to the
452 global carbon budgets approach to quantify annual fluxes to and from the atmosphere. Estimates for CDR
453 through HWP, BECCS, and biochar are thus not indicated in this budget, but can be found elsewhere (see
454 Section 3.2.2).

455 **2.2.2 2023 Projection**

456 We project the 2023 land-use emissions for BLUE, H&C2023, and OSCAR based on their E_{LUC} estimates for
457 2022 and adding the change in carbon emissions from peat fires and tropical deforestation and degradation fires
458 (2023 emissions relative to 2022 emissions) estimated using active fire data (MCD14ML; Giglio et al., 2016).

459 Peat drainage is assumed to be unaltered as it has low interannual variability. More details on the `ELUC`
460 methodology can be found in Supplement S.2.

461 **2.3 Carbon Dioxide Removal (CDR) not based on vegetation**

462 CDR not based on terrestrial vegetation currently relies on enhanced rock weathering and Direct Air Carbon
463 Capture and Storage (DACCS) projects. The majority of this (58%) derives from a single project: Climeworks'
464 Orca DACCS plant based in Hellisheidi, Iceland. The remainder is generated by 13 small-scale projects
465 including, for example, 500 tons of carbon dioxide sequestered through the spreading of crushed olivine on
466 agricultural areas by Eion Carbon. We use data from the State of CDR Report (Smith et al., 2023), which
467 quantifies all currently deployed CDR methods, including the land-use related activities already covered by
468 Section 2.2. The State of CDR Report (Smith et al., 2023) combines estimates of carbon storage in managed
469 land derived from NGHGI data with project-by-project storage rates obtained through 20 extant CDR databases
470 and registries (status as of mid-year 2022) by Powis et al. (2023). They assessed the data quality on existing
471 CDR projects to be poor, suffering from fragmentation, different reporting standards, limited geographical
472 coverage, and inclusion of a number of pilot plants with uncertain lifespans. As a consequence, these numbers
473 could change substantially from year-to-year in the near-term.

474 **2.4 Growth rate in atmospheric CO₂ concentration (G_{ATM})**

475 **2.4.1 Historical period 1850-2022**

476 The rate of growth of the atmospheric CO₂ concentration is provided for years 1959-2022 by the US National
477 Oceanic and Atmospheric Administration Global Monitoring Laboratory (NOAA/GML; Lan et al., 2023),
478 which includes recent revisions to the calibration scale of atmospheric CO₂ measurements (Hall et al., 2021).
479 For the 1959-1979 period, the global growth rate is based on measurements of atmospheric CO₂ concentration
480 averaged from the Mauna Loa and South Pole stations, as observed by the CO₂ Program at Scripps Institution of
481 Oceanography (Keeling et al., 1976). For the 1980-2021 time period, the global growth rate is based on the
482 average of multiple stations selected from the marine boundary layer sites with well-mixed background air
483 (Ballantyne et al., 2012), after fitting a smooth curve through the data for each station as a function of time, and
484 averaging by latitude band (Masarie and Tans, 1995). The annual growth rate is estimated by Lan et al. (2023)
485 from atmospheric CO₂ concentration by taking the average of the most recent December-January months
486 corrected for the average seasonal cycle and subtracting this same average one year earlier. The growth rate in
487 units of ppm yr⁻¹ is converted to units of GtC yr⁻¹ by multiplying by a factor of 2.124 GtC per ppm, assuming
488 instantaneous mixing of CO₂ throughout the atmosphere (Ballantyne et al., 2012; Table 1).

489 Since 2020, NOAA/GML provides estimates of atmospheric CO₂ concentrations with respect to a new
490 calibration scale, referred to as WMO-CO₂-X2019, in line with a recalibration agreed by the World
491 Meteorological Organization (WMO) Global Atmosphere Watch (GAW) community (Hall et al., 2021). The re-
492 calibrated data were first used to estimate G_{ATM} in the 2021 edition of the global carbon budget (Friedlingstein
493 et al., 2022a). Friedlingstein et al. (2022a) verified that the change of scales from WMO-CO₂-X2007 to WMO-

494 CO₂-X2019 made a negligible difference to the value of G_{ATM} (-0.06 GtC yr⁻¹ during 2010-2019 and -0.01 GtC
495 yr⁻¹ during 1959-2019, well within the uncertainty range reported below).

496 The uncertainty around the atmospheric growth rate is due to four main factors. First, the long-term
497 reproducibility of reference gas standards (around 0.03 ppm for 1 σ from the 1980s; Lan et al., 2023). Second,
498 small unexplained systematic analytical errors that may have a duration of several months to two years come
499 and go. They have been simulated by randomising both the duration and the magnitude (determined from the
500 existing evidence) in a Monte Carlo procedure. Third, the network composition of the marine boundary layer
501 with some sites coming or going, gaps in the time series at each site, etc (Lan et al., 2023). The latter uncertainty
502 was estimated by NOAA/GML with a Monte Carlo method by constructing 100 "alternative" networks (Masarie
503 and Tans, 1995; NOAA/GML, 2019). The second and third uncertainties, summed in quadrature, add up to
504 0.085 ppm on average (Lan et al., 2023). Fourth, the uncertainty associated with using the average CO₂
505 concentration from a surface network to approximate the true atmospheric average CO₂ concentration (mass-
506 weighted, in 3 dimensions) as needed to assess the total atmospheric CO₂ burden. In reality, CO₂ variations
507 measured at the stations will not exactly track changes in total atmospheric burden, with offsets in magnitude
508 and phasing due to vertical and horizontal mixing. This effect must be very small on decadal and longer time
509 scales, when the atmosphere can be considered well mixed. The CO₂ increase in the stratosphere lags the
510 increase (meaning lower concentrations) that we observe in the marine boundary layer, while the continental
511 boundary layer (where most of the emissions take place) leads the marine boundary layer with higher
512 concentrations. These effects nearly cancel each other. In addition, the growth rate is nearly the same
513 everywhere (Ballantyne et al, 2012). We therefore maintain an uncertainty around the annual growth rate based
514 on the multiple stations data set ranges between 0.11 and 0.72 GtC yr⁻¹, with a mean of 0.61 GtC yr⁻¹ for 1959-
515 1979 and 0.17 GtC yr⁻¹ for 1980-2022, when a larger set of stations were available as provided by Lan et al.
516 (2023). We estimate the uncertainty of the decadal averaged growth rate after 1980 at 0.02 GtC yr⁻¹ based on the
517 calibration and the annual growth rate uncertainty but stretched over a 10-year interval. For years prior to 1980,
518 we estimate the decadal averaged uncertainty to be 0.07 GtC yr⁻¹ based on a factor proportional to the annual
519 uncertainty prior and after 1980 ($0.02 * [0.61/0.17]$ GtC yr⁻¹).

520 We assign a high confidence to the annual estimates of G_{ATM} because they are based on direct measurements
521 from multiple and consistent instruments and stations distributed around the world (Ballantyne et al., 2012; Hall
522 et al., 2021).

523 To estimate the total carbon accumulated in the atmosphere since 1750 or 1850, we use an atmospheric CO₂
524 concentration of 278.3 ± 3 ppm or 285.1 ± 3 ppm, respectively (Gulev et al., 2021). For the construction of the
525 cumulative budget shown in Figure 3, we use the fitted estimates of CO₂ concentration from Joos and Spahni
526 (2008) to estimate the annual atmospheric growth rate using the conversion factors shown in Table 1. The
527 uncertainty of ± 3 ppm (converted to $\pm 1\sigma$) is taken directly from the IPCC's AR5 assessment (Ciais et al., 2013).
528 Typical uncertainties in the growth rate in atmospheric CO₂ concentration from ice core data are equivalent to
529 ± 0.1 - 0.15 GtC yr⁻¹ as evaluated from the Law Dome data (Etheridge et al., 1996) for individual 20-year intervals
530 over the period from 1850 to 1960 (Bruno and Joos, 1997).

531 **2.4.2 2023 projection**

532 We provide an assessment of G_{ATM} for 2023 as the average of two methods. The GCB regression method
533 models monthly global-average atmospheric CO_2 concentrations and derives the increment and annual average
534 from these. The model uses lagged observations of concentration (Lan et al., 2023): both a 12-month lag, and
535 the lowest lag that will allow model prediction to produce an estimate for the following January, recalling that
536 the G_{ATM} increment is derived from December/January pairs. The largest driver of interannual changes is the
537 ENSO signal (Betts et al., 2016), so the monthly ENSO 3.4 index (Huang et al., 2023) is included in the model.
538 Given the natural lag between sea-surface temperatures and effects on the biosphere, and in turn effects on
539 globally mixed atmospheric CO_2 concentration, a lagged ENSO index is used, and we use both a 5-month and a
540 6-month lag. The combination of the two lagged ENSO values helps reduce possible effects of noise in a single
541 month. To help characterise the seasonal variation, we add month as a categorical variable. Finally, we flag the
542 period affected by the Pinatubo eruption (August 1991 - November 1993) as a categorical variable. Note that
543 while emissions of CO_2 are the largest driver of the trend in atmospheric CO_2 concentration, our goal here is to
544 predict divergence from that trend. Because changes in emissions from year to year are relatively minor, this has
545 little effect on the variation of concentration from the trend line. Even the relatively large drop in emissions in
546 2020 due to the COVID-19 pandemic does not cause any problems for the model.

547 For the first time this year, we also use the multi-model mean and uncertainty of the 2023 G_{ATM} estimated by the
548 ESMS prediction system (see Section 2.9). We then take the average of the GCB regression and ESMS G_{ATM}
549 estimates, with their respective uncertainty combined quadratically.

550 Similarly, the projection of the 2023 global average CO_2 concentration (in ppm), is calculated as the average of
551 the estimates from the two methods. For the GCB regression method, it is the annual average of global
552 concentration over the 12 months of 2023; for the ESMS, it is the observed global average CO_2 concentration for
553 2022 plus the annual increase in 2023 of the global average CO_2 concentration predicted by the ESMS multi-
554 model mean.

555 **2.5 Ocean CO_2 sink**

556 **2.5.1 Historical period 1850-2022**

557 The reported estimate of the global ocean anthropogenic CO_2 sink S_{OCEAN} is derived as the average of two
558 estimates. The first estimate is derived as the mean over an ensemble of ten global ocean biogeochemistry
559 models (GOBMs, Table 4 and Table S2). The second estimate is obtained as the mean over an ensemble of
560 seven surface ocean fCO_2 -observation-based data-products (Table 4 and Table S3). An eighth fCO_2 -product
561 (Watson et al., 2020) is shown, but is not included in the ensemble average as it differs from the other products
562 by adjusting the flux to a cool, salty ocean surface skin (see Supplement S.3.1 for a discussion of the Watson
563 product). The GOBMs simulate both the natural and anthropogenic CO_2 cycles in the ocean. They constrain the
564 anthropogenic air-sea CO_2 flux (the dominant component of S_{OCEAN}) by the transport of carbon into the ocean
565 interior, which is also the controlling factor of present-day ocean carbon uptake in the real world. They cover

566 the full globe and all seasons and were recently evaluated against surface ocean carbon observations, suggesting
567 they are suitable to estimate the annual ocean carbon sink (Hauck et al., 2020). The $f\text{CO}_2$ -products are tightly
568 linked to observations of $f\text{CO}_2$ (fugacity of CO_2 , which equals $p\text{CO}_2$ corrected for the non-ideal behaviour of the
569 gas; Pfeil et al., 2013), which carry imprints of temporal and spatial variability, but are also sensitive to
570 uncertainties in gas-exchange parameterizations and data-sparsity (Gloege et al., 2021, Hauck et al., 2023).
571 Their asset is the assessment of the mean spatial pattern of variability and its seasonality (Hauck et al., 2020,
572 Gloege et al. 2021, Hauck et al., 2023). We further use two diagnostic ocean models to estimate So_{OCEAN} over the
573 industrial era (1781-1958).

574 The global $f\text{CO}_2$ -based flux estimates were adjusted to remove the pre-industrial ocean source of CO_2 to the
575 atmosphere of $0.65 \pm 0.3 \text{ GtC yr}^{-1}$ from river input to the ocean (Regnier et al., 2022), to satisfy our definition of
576 So_{OCEAN} (Hauck et al., 2020). The river flux adjustment was distributed over the latitudinal bands using the
577 regional distribution of Lacroix et al. (2020; North: 0.14 GtC yr^{-1} , Tropics: 0.42 GtC yr^{-1} , South: 0.09 GtC yr^{-1}).
578 Acknowledging that this distribution is based on only one model, the advantage is that a gridded field is
579 available, and the river flux adjustment can be calculated for the three latitudinal bands and the RECCAP
580 regions (REgional Carbon Cycle Assessment and Processes (RECCAP2; Ciais et al., 2020, Poulter et al., 2022,
581 DeVries et al., 2023). This data set suggests that more of the riverine outgassing is located in the tropics than in
582 the Southern Ocean and is thus opposed to the previously used data set of Aumont et al. (2001). Accordingly,
583 the regional distribution is associated with a major uncertainty in addition to the large uncertainty around the
584 global estimate (Crisp et al., 2022; Gruber et al., 2023). Anthropogenic perturbations of river carbon and
585 nutrient transport to the ocean are not considered (see Section 2.10 and Supplement S.6.3).

586 We derive So_{OCEAN} from GOBMs by using a simulation (sim A) with historical forcing of climate and
587 atmospheric CO_2 , accounting for model biases and drift from a control simulation (sim B) with constant
588 atmospheric CO_2 and normal year climate forcing. A third simulation (sim C) with historical atmospheric CO_2
589 increase and normal year climate forcing is used to attribute the ocean sink to CO_2 (sim C minus sim B) and
590 climate (sim A minus sim C) effects. A fourth simulation (sim D; historical climate forcing and constant
591 atmospheric CO_2) is used to compare the change in anthropogenic carbon inventory in the interior ocean (sim A
592 minus sim D) to the observational estimate of Gruber et al. (2019) with the same flux components (steady state
593 and non-steady state anthropogenic carbon flux). The $f\text{CO}_2$ -products are adjusted with respect to their original
594 publications to represent the full ice-free ocean area, including coastal zones and marginal seas, when the area
595 coverage is below 99%. This is done by either area filling following Fay et al. (2021) or a simple scaling
596 approach. GOBMs and $f\text{CO}_2$ -products fall within the observational constraints over the 1990s ($2.2 \pm 0.7 \text{ GtC yr}^{-1}$,
597 Ciais et al., 2013) after applying adjustments.

598 So_{OCEAN} is calculated as the average of the GOBM ensemble mean and the $f\text{CO}_2$ -product ensemble mean from
599 1990 onwards. Prior to 1990, it is calculated as the GOBM ensemble mean plus half of the offset between
600 GOBMs and $f\text{CO}_2$ -products ensemble means over 1990-2001.

601 We assign an uncertainty of $\pm 0.4 \text{ GtC yr}^{-1}$ to the ocean sink based on a combination of random (ensemble
602 standard deviation) and systematic uncertainties (GOBMs bias in anthropogenic carbon accumulation,

603 previously reported uncertainties in $f\text{CO}_2$ -products; see Supplement S.3.4). We assess a medium confidence
604 level to the annual ocean CO_2 sink and its uncertainty because it is based on multiple lines of evidence, it is
605 consistent with ocean interior carbon estimates (Gruber et al., 2019, see Section 3.6.5) and the interannual
606 variability in the GOBMs and data-based estimates is largely consistent and can be explained by climate
607 variability. We refrain from assigning a high confidence because of the systematic deviation between the
608 GOBM and $f\text{CO}_2$ -product trends since around 2002. More details on the SoCEAN methodology can be found in
609 Supplement S.3.

610 **2.5.2 2023 Projection**

611 The ocean CO_2 sink forecast for the year 2023 is based on the annual historical (Lan et al., 2023) and our
612 estimated 2023 atmospheric CO_2 concentration growth rate, the historical and our estimated 2023 annual global
613 fossil fuel emissions from this year's carbon budget, and the spring (March, April, May) Oceanic Niño Index
614 (ONI) (NCEP, 2023). Using a non-linear regression approach, i.e., a feed-forward neural network, atmospheric
615 CO_2 , ONI, and the fossil fuel emissions are used as training data to best match the annual ocean CO_2 sink (i.e.
616 combined SoCEAN estimate from GOBMs and data products) from 1959 through 2022 from this year's carbon
617 budget. Using this relationship, the 2023 SoCEAN can then be estimated from the projected 2022 input data using
618 the non-linear relationship established during the network training. To avoid overfitting, the neural network was
619 trained with a variable number of hidden neurons (varying between 2-5) and 20% of the randomly selected
620 training data were withheld for independent internal testing. Based on the best output performance (tested using
621 the 20% withheld input data), the best performing number of neurons was selected. In a second step, we trained
622 the network 10 times using the best number of neurons identified in step 1 and different sets of randomly
623 selected training data. The mean of the 10 trainings is considered our best forecast, whereas the standard
624 deviation of the 10 ensembles provides a first order estimate of the forecast uncertainty. This uncertainty is then
625 combined with the SoCEAN uncertainty (0.4 GtC yr^{-1}) to estimate the overall uncertainty of the 2023 projection.
626 As an additional line of evidence, we also assess the 2023 atmosphere-ocean carbon flux from the ESM
627 prediction system (see Section 2.9).

628 **2.6 Land CO_2 sink**

629 **2.6.1 Historical Period 1850-2022**

630 The terrestrial land sink (S_{LAND}) is thought to be due to the combined effects of fertilisation by rising
631 atmospheric CO_2 and N inputs on plant growth, as well as the effects of climate change such as the lengthening
632 of the growing season in northern temperate and boreal areas. S_{LAND} does not include land sinks directly
633 resulting from land-use and land-use change (e.g., regrowth of vegetation) as these are part of the land-use flux
634 (E_{LUC}), although system boundaries make it difficult to attribute exactly CO_2 fluxes on land between S_{LAND} and
635 E_{LUC} (Erb et al., 2013).

636 S_{LAND} is estimated from the multi-model mean of 20 DGVMs (Table S1) with an additional comparison of
637 DGVMs with a data-driven, carbon data model framework (CARDAMOM) (Bloom and Williams, 2015; Bloom

638 et al., 2016), see Supplement S4. DGVMs simulations include all climate variability and CO₂ effects over land.
639 In addition to the carbon cycle represented in all DGVMs, 14 models also account for the nitrogen cycle and
640 hence can include the effect of N inputs on S_{LAND}. The DGVMs estimate of S_{LAND} does not include the export of
641 carbon to aquatic systems or its historical perturbation, which is discussed in Supplement S.6.3. DGVMs need to
642 meet several criteria to be included in this assessment. In addition, we use the International Land Model
643 Benchmarking system (ILAMB; Collier et al., 2018) for the DGVMs evaluation (see Supplement S.4.2). The
644 uncertainty on S_{LAND} is taken from the GGVMs standard deviation (see Supplement S.4.3). More details on the
645 S_{LAND} methodology can be found in Supplement S.4.

646 **2.6.2 2023 Projection**

647 Like for the ocean forecast, the land CO₂ sink (S_{LAND}) forecast is based on the annual historical (Lan et al.,
648 2023) and our estimated 2023 atmospheric CO₂ concentration, historical and our estimated 2023 annual global
649 fossil fuel emissions from this year's carbon budget, and the summer (June, July, August) ONI (NCEP, 2022).
650 All training data are again used to best match S_{LAND} from 1959 through 2022 from this year's carbon budget
651 using a feed-forward neural network. To avoid overfitting, the neural network was trained with a variable
652 number of hidden neurons (varying between 2-15), larger than for So_{CEAN} prediction due to the stronger land
653 carbon interannual variability. As done for So_{CEAN}, a pre-training selects the optimal number of hidden neurons
654 based on 20% withheld input data, and in a second step, an ensemble of 10 forecasts is produced to provide the
655 mean forecast plus uncertainty. This uncertainty is then combined with the S_{LAND} uncertainty for 2022 (0.9 GtC
656 yr⁻¹) to estimate the overall uncertainty of the 2023 projection.

657 **2.7 Atmospheric inversion estimate**

658 The world-wide network of in-situ atmospheric measurements and satellite derived atmospheric CO₂ column
659 (xCO₂) observations put a strong constraint on changes in the atmospheric abundance of CO₂. This is true
660 globally (hence our large confidence in G_{ATM}), but also regionally in regions with sufficient observational
661 density found mostly in the extra-tropics. This allows atmospheric inversion methods to constrain the magnitude
662 and location of the combined total surface CO₂ fluxes from all sources, including fossil and land-use change
663 emissions and land and ocean CO₂ fluxes. The inversions assume E_{FOS} to be well known, and they solve for the
664 spatial and temporal distribution of land and ocean fluxes from the residual gradients of CO₂ between stations
665 that are not explained by fossil fuel emissions. By design, such systems thus close the carbon balance (B_{IM} = 0)
666 and thus provide an additional perspective on the independent estimates of the ocean and land fluxes.

667 This year's release includes fourteen inversion systems that are described in Table S4, of which thirteen are
668 included in the ensemble of inverse estimates presented in the text and figures. Each system is rooted in
669 Bayesian inversion principles but uses different methodologies. These differences concern the selection of
670 atmospheric CO₂ data or xCO₂, and the choice of a-priori fluxes to refine. They also differ in spatial and
671 temporal resolution, assumed correlation structures, and mathematical approach of the models (see references in
672 Table S4 for details). Importantly, the systems use a variety of transport models, which was demonstrated to be
673 a driving factor behind differences in atmospheric inversion-based flux estimates, and specifically their

674 distribution across latitudinal bands (Gaubert et al., 2019; Schuh et al., 2019). Six inversion systems (CAM-
675 FT23r1, CMS-flux, GONGGA, THU, COLA, GCASv2) used satellite $x\text{CO}_2$ retrievals from GOSAT and/or
676 OCO-2, scaled to the WMO 2019 calibration scale. Two inversions this year (CMS-Flux, COLA) used these
677 $x\text{CO}_2$ datasets in addition to the in-situ observational CO_2 mole fraction records.

678 The original products delivered by the inverse modellers were modified to facilitate the comparison to the other
679 elements of the budget, specifically on two accounts: (1) global total fossil fuel emissions including cement
680 carbonation CO_2 uptake, and (2) riverine CO_2 transport. Details are given below. We note that with these
681 adjustments the inverse results no longer represent the net atmosphere-surface exchange over land/ocean areas
682 as sensed by atmospheric observations. Instead, for land, they become the net uptake of CO_2 by vegetation and
683 soils that is not exported by fluvial systems, similar to the DGVMs estimates. For oceans, they become the net
684 uptake of anthropogenic CO_2 , similar to the GOBMs estimates.

685 The inversion systems prescribe global fossil fuel emissions based on e.g. the GCP's Gridded Fossil Emissions
686 Dataset versions 2023.1 (GCP-GridFED; Jones et al., 2023), which are updates to GCP-GridFEDv2021
687 presented by Jones et al. (2021b). GCP-GridFEDv2023 scales gridded estimates of CO_2 emissions from
688 EDGARv4.3.2 (Janssens-Maenhout et al., 2019) within national territories to match national emissions
689 estimates provided by the GCB for the years 1959-2022, which were compiled following the methodology
690 described in Section 2.1. Small differences between the systems due to for instance regridding to the transport
691 model resolution, or use of different fossil fuel emissions, are adjusted in the latitudinal partitioning we present,
692 to ensure agreement with the estimate of E_{FOS} in this budget. We also note that the ocean fluxes used as prior by
693 8 out of 14 inversions are part of the suite of the ocean process model or $f\text{CO}_2$ -products listed in Section 2.5.
694 Although these fluxes are further adjusted by the atmospheric inversions, it makes the inversion estimates of the
695 ocean fluxes not completely independent of S_{OCEAN} assessed here.

696 To facilitate comparisons to the independent S_{OCEAN} and S_{LAND} , we used the same corrections for transport and
697 outgassing of carbon transported from land to ocean, as done for the observation-based estimates of S_{OCEAN} (see
698 Supplement S.3).

699 The atmospheric inversions are evaluated using vertical profiles of atmospheric CO_2 concentrations (Figure S4).
700 More than 30 aircraft programs over the globe, either regular programs or repeated surveys over at least 9
701 months (except for SH programs), have been used to assess system performance (with space-time observational
702 coverage sparse in the SH and tropics, and denser in NH mid-latitudes; Table S7). The fourteen systems are
703 compared to the independent aircraft CO_2 measurements between 2 and 7 km above sea level between 2001 and
704 2022. Results are shown in Figure S4 and discussed in Supplement S.5.2. One inversion was flagged for
705 concerns after quality control with these observations, as well as assessment of their global growth rate. This
706 makes the number of systems included in the ensemble to be $N=13$.

707 With a relatively small ensemble of systems that cover at least one full decade ($N=9$), and which moreover share
708 some a-priori fluxes used with one another, or with the process-based models, it is difficult to justify using their
709 mean and standard deviation as a metric for uncertainty across the ensemble. We therefore report their full range

710 (min-max) without their mean. More details on the atmospheric inversions methodology can be found in
711 Supplement S.5.

712 **2.8 Atmospheric oxygen based estimate**

713 Long-term atmospheric O₂ and CO₂ observations allow estimation of the global ocean and land carbon sinks,
714 due to the coupling of O₂ and CO₂ with distinct exchange ratios for fossil fuel emissions and land uptake, and
715 uncoupled O₂ and CO₂ ocean exchange (Keeling and Manning, 2014). The global ocean and net land carbon
716 sinks were calculated following methods and constants used in Keeling and Manning (2014), modified to
717 include the effective O₂ source from metal refining (Battle et al., 2023), and using a value of 1.05 for the
718 exchange ratio of the net land sink, following Resplandy et al. (2019). Atmospheric O₂ is observed as $\delta(\text{O}_2/\text{N}_2)$
719 and combined with CO₂ mole fraction observations into Atmospheric Potential Oxygen (APO, Stephens et al.,
720 1998). The APO observations from 1990 to 2022 were taken from a weighted average of flask records from the
721 three stations in the Scripps O₂ program network (Alert, Canada (ALT), La Jolla, California (LJO), and Cape
722 Grim, Australia (CGO), weighted per Keeling and Manning (2014). Observed CO₂ was taken from the globally
723 averaged marine surface annual mean growth rate from the NOAA/GML Global Greenhouse Gas Reference
724 Network (Lan et al., 2023). The O₂ source from ocean warming is based on ocean heat content from updated
725 data from NOAA/NCEI (Levitus et al., 2012). The effective O₂ source from metal refining is based on
726 production data from Bray (2020), Flanagan (2021), and Tuck (2022). Uncertainty was determined through a
727 Monte Carlo approach with 5,000 iterations, using uncertainties prescribed in Keeling and Manning (2014),
728 including observational uncertainties from Keeling et al. (2007) and autoregressive errors in fossil fuel
729 emissions (Ballantyne et al., 2015). The reported uncertainty is 1 standard deviation of the ensemble.

730 **2.9 Earth System Models estimate**

731 Reconstructions and predictions from decadal prediction systems based on Earth system models (ESMs) provide
732 a novel line of evidence in assessing the atmosphere-land and atmosphere-ocean carbon fluxes in the past
733 decades and predicting their changes for the current year. The decadal prediction systems based on ESMs used
734 here consist of three sets of simulations: (i) uninitialized freely evolving historical simulations (1850-2014); (ii)
735 assimilation reconstruction incorporating observational data into the model (1980-2022); (iii) initialized
736 prediction simulations for the 1981-2023 period, starting every year from initial states obtained from the above
737 assimilation simulations. The assimilations are designed to reconstruct the actual evolution of the Earth system
738 by assimilating essential fields from data products. The assimilations' states, which are expected to be close to
739 observations, are used to start the initialized prediction simulations used for the current year (2023) global
740 carbon budget. Similar initialized prediction simulations starting every year (Nov. 1st or Jan. 1st) over the 1981-
741 2022 period (i.e., hindcasts) are also performed for predictive skill quantification and for bias correction. More
742 details on the illustration of a decadal prediction system based on an ESM can refer to Figure 1 of Li et al.
743 (2023).

744 By assimilating physical atmospheric and oceanic data products into the ESMs, the models are able to reproduce
745 the historical variations of the atmosphere-sea CO₂ fluxes, atmosphere-land CO₂ fluxes, and atmospheric CO₂

746 growth rate (Li et al., 2016, 2019; Lovenduski et al., 2019a,b; Ilyina et al., 2021; Li et al., 2023). Furthermore,
747 the ESM-based predictions have proven their skill in predicting the air-sea CO₂ fluxes for up to 6 years, the air-
748 land CO₂ fluxes and atmospheric CO₂ growth for 2 years (Lovenduski et al., 2019a,b; Ilyina et al., 2021; Li et
749 al., 2023). The reconstructions from the fully coupled model simulations ensure a closed budget within the Earth
750 system, i.e., no budget imbalance term.

751 Four ESMs, i.e., CanESM5 (Swart et al., 2019; Sospedra-Alfonso et al., 2021), IPSL-CM6A-CO2-LR (Boucher
752 et al., 2020), MIROC-ES2L (Watanabe et al., 2020), and MPI-ESM1-2-LR (Mauritsen et al., 2019; Li et al., 2023),
753 have performed the set of prediction simulations. Each ESM uses a different assimilation method and combination
754 of data products incorporated in the system, more details on the models configuration can be found in Table 4.
755 The ESMs use external forcings from the Coupled Model Intercomparison Project Phase 6 (CMIP6) historical
756 (1980-2014) plus SSP2-4.5 baseline and CovidMIP two-year blip scenario (2015-2023) (Eyring et al., 2016; Jones
757 et al., 2021a). The CO₂ emissions forcing from 2015-2023 are substituted by GCB-GridFED (v2023.1, Jones et
758 al., 2023) to provide a more realistic forcing. Reconstructions of atmosphere-ocean CO₂ fluxes (SOCEAN) and
759 atmosphere-land CO₂ fluxes (S_{LAND}-ELUC) for the time period from 1980-2022 are assessed here. Predictions of
760 the atmosphere-ocean CO₂ flux, atmosphere-land CO₂ flux, and atmospheric CO₂ growth for 2023 are calculated
761 based on the predictions at a lead time of 1 year. The predictions are bias-corrected using the 1985-2014
762 climatology mean of GCB2022 (Friedlingstein et al., 2022), more details on methods can be found in Boer et al.
763 (2016) and Li et al. (2023). The ensemble size of initialized prediction simulations is 10, and the ensemble mean
764 for each individual model is used here. The ESMs are used here to support the assessment of SOCEAN and net
765 atmosphere-land CO₂ flux (S_{LAND} - ELUC) over the 1980-2022 period, and to provide an estimate of the 2023
766 projection of G_{ATM}.

767 **2.10 Processes not included in the global carbon budget**

768 The contribution of anthropogenic CO and CH₄ to the global carbon budget is not fully accounted for in Eq. (1)
769 and is described in Supplement S.6.1. The contributions to CO₂ emissions of decomposition of carbonates not
770 accounted for is described in Supplement S.6.2. The contribution of anthropogenic changes in river fluxes is
771 conceptually included in Eq. (1) in SOCEAN and in S_{LAND}, but it is not represented in the process models used to
772 quantify these fluxes. This effect is discussed in Supplement S.6.3. Similarly, the loss of additional sink capacity
773 from reduced forest cover is missing in the combination of approaches used here to estimate both land fluxes
774 (ELUC and S_{LAND}) and its potential effect is discussed and quantified in Supplement S.6.4.

775 **3 Results**

776 For each component of the global carbon budget, we present results for three different time periods: the full
777 historical period, from 1850 to 2022, the decades in which we have atmospheric concentration records from
778 Mauna Loa (1960-2022), a specific focus on last year (2022), and the projection for the current year (2023).
779 Subsequently, we assess the estimates of the budget components of the last decades against the top-down
780 constraints from inverse modelling of atmospheric observations, the land/ocean partitioning derived from the
781 atmospheric O₂ measurements, and the budget components estimates from the ESMs assimilation simulations.

782 Atmospheric inversions further allow for an assessment of the budget components with a regional breakdown of
783 land and ocean sinks.

784 **3.1 Fossil CO₂ Emissions**

785 **3.1.1 Historical period 1850-2022**

786 Cumulative fossil CO₂ emissions for 1850-2022 were 477 ± 25 GtC, including the cement carbonation sink
787 (Figure 3, Table 8, with all cumulative numbers rounded to the nearest 5GtC). In this period, 46% of global
788 fossil CO₂ emissions came from coal, 35% from oil, 15% from natural gas, 3% from decomposition of
789 carbonates, and 1% from flaring. In 1850, the UK stood for 62% of global fossil CO₂ emissions. In 1891 the
790 combined cumulative emissions of the current members of the European Union reached and subsequently
791 surpassed the level of the UK. Since 1917 US cumulative emissions have been the largest. Over the entire
792 period 1850-2022, US cumulative emissions amounted to 115GtC (24% of world total), the EU27's to 80 GtC
793 (17%), China's to 70 GtC (15%), and India's to 15 GtC (3%).

794 In addition to the estimates of fossil CO₂ emissions that we provide here (see Methods), there are three global
795 datasets with long time series that include all sources of fossil CO₂ emissions: CDIAC-FF (Gilfillan and
796 Marland, 2021), CEDS version v_2021_04_21 (Hoesly et al., 2018; O'Rourke et al., 2021) and PRIMAP-hist
797 version 2.4.2 (Gütschow et al., 2016; Gütschow and Pflüger, 2023), although these datasets are not entirely
798 independent from each other (Andrew, 2020a). CDIAC-FF has the lowest cumulative emissions over 1750-2018
799 at 440 GtC, GCP has 444 GtC, CEDS 445 GtC, PRIMAP-hist TP 453 GtC, and PRIMAP-hist CR 452 GtC.
800 CDIAC-FF excludes emissions from lime production. CEDS has higher emissions from international shipping
801 in recent years, while PRIMAP-hist has higher fugitive emissions than the other datasets. However, in general
802 these four datasets are in relative agreement as to total historical global emissions of fossil CO₂.

803 **3.1.2 Recent period 1960-2022**

804 Global fossil CO₂ emissions, E_{FOS} (including the cement carbonation sink), have increased every decade from an
805 average of 3.0 ± 0.2 GtC yr⁻¹ for the decade of the 1960s to an average of 9.6 ± 0.5 GtC yr⁻¹ during 2013-2022
806 (Table 7, Figure 2 and Figure 5). The growth rate in these emissions decreased between the 1960s and the
807 1990s, from 4.3% yr⁻¹ in the 1960s (1960-1969), 3.2% yr⁻¹ in the 1970s (1970-1979), 1.6% yr⁻¹ in the 1980s
808 (1980-1989), to 1.0% yr⁻¹ in the 1990s (1990-1999). After this period, the growth rate began increasing again in
809 the 2000s at an average growth rate of 2.8% yr⁻¹, decreasing to 0.5% yr⁻¹ for the last decade (2013-2022).
810 China's emissions increased by +1.6% yr⁻¹ on average over the last 10 years dominating the global trend, and
811 India's emissions increased by +3.5% yr⁻¹, while emissions decreased in EU27 by -1.7% yr⁻¹, and in the USA
812 by -1.0% yr⁻¹. Figure 6 illustrates the spatial distribution of fossil fuel emissions for the 2013-2022 period.

813 E_{FOS} reported here includes the uptake of CO₂ by cement via carbonation which has increased with increasing
814 stocks of cement products, from an average of 18 MtC yr⁻¹ (0.018 GtC yr⁻¹) in the 1960s to an average of 197
815 MtC yr⁻¹ (0.197 GtC yr⁻¹) during 2013-2022 (Figure 5).

816 **3.1.3 Final year 2022**

817 Global fossil CO₂ emissions were slightly higher, 0.92%, in 2022 than in 2021, with an increase of less than 0.1
818 GtC to reach 9.9 ± 0.5 GtC (including the 0.2 GtC cement carbonation sink) in 2022 (Figure 5), distributed
819 among coal (42%), oil (32%), natural gas (21%), cement (4%), flaring (1%), and others (<1%). Compared to the
820 previous year, 2022 emissions from coal and oil increased by 1.6% and 3.2% respectively, while emissions from
821 gas and cement respectively decreased by 2.2% and 5.1%. All growth rates presented are adjusted for the leap
822 year, unless stated otherwise.

823 In 2022, the largest absolute contributions to global fossil CO₂ emissions were from China (31%), the USA
824 (14%), India (8%), and the EU27 (7%). These four regions account for 59% of global fossil CO₂ emissions,
825 while the rest of the world contributed 41%, including international aviation and marine bunker fuels (2.6% of
826 the total). Growth rates for these countries from 2021 to 2022 were 0.5% (China), 0.5% (USA), -1.6% (EU27),
827 and 5.8% (India), with +0.9% for the rest of the world. The per-capita fossil CO₂ emissions in 2022 were 1.3 tC
828 person⁻¹ yr⁻¹ for the globe, and were 4.1 (USA), 2.2 (China), 1.7 (EU27) and 0.5 (India) tC person⁻¹ yr⁻¹ for the
829 four highest emitters (Figure 5).

830 **3.1.4 Year 2023 Projection**

831 Globally, we estimate that global fossil CO₂ emissions (including cement carbonation) will grow by 1.1% in
832 2023 (0.1% to 2.2%) to 10.1 GtC (36.8 GtCO₂), exceeding the pre-COVID19 2019 emission levels of 9.9 GtC
833 (36.3 GtCO₂). Global increase in 2023 emissions per fuel types are projected to be +1.3% (range 0.0% to 2.6%)
834 for coal, +1.5% (range 0.5% to 2.5%) for oil, +0.2% (range -0.6% to 1.1%) for natural gas, and 1.4% (range -
835 0.3% to 3.0%) for cement.

836 For China, projected fossil emissions in 2023 are expected to increase by 4% (range 1.9% to 6.2%) compared
837 with 2022 emissions, bringing 2023 emissions for China around 3.2 GtC yr⁻¹ (11.9 GtCO₂ yr⁻¹). Changes in fuel
838 specific projections for China are 3.5% for coal, 7.7% for oil, 6.4% natural gas, and 0.2% for cement.

839 For the USA, the Energy Information Administration (EIA) emissions projection for 2023 combined with
840 cement clinker data from USGS gives an decrease of 3.0% (range -5.0% to -1.0%) compared to 2022, bringing
841 USA 2023 emissions to around 1.3 GtC yr⁻¹ (4.9 GtCO₂ yr⁻¹). This is based on separate projections for coal -
842 18.3%, oil -0.3%, natural gas +1.4%, and cement -4.0%.

843 For the European Union, our projection for 2023 is for a decrease of 7.4% (range -9.9% to -4.9%) over 2022,
844 with 2023 emissions around 0.7 GtC yr⁻¹ (2.6 GtCO₂ yr⁻¹). This is based on separate projections for coal of -
845 18.8%, oil -1.5%, natural gas -6.6%, and cement -8.7%.

846 For India, our projection for 2023 is an increase of 8.7% (range of 7.2% to 10.2%) over 2022, with 2023
847 emissions around 0.8 GtC yr⁻¹ (3.1 GtCO₂ yr⁻¹). This is based on separate projections for coal of +10.1%, oil
848 +5.3%, natural gas +5.6%, and cement +8.8%.

849 For the rest of the world, the expected growth rate for 2023 is 0.5% (range -1.2% to 2.2%) with 2023 emissions
850 around 4.2 GtC yr⁻¹ (15.2 GtCO₂ yr⁻¹). The fuel-specific projected 2023 growth rates for the rest of the world
851 are: +0.8% for coal, +0.8% for oil, -0.4% for natural gas, +2.4% for cement.

852 **3.2 Emissions from Land Use Changes**

853 **3.2.1 Historical period 1850-2022**

854 Cumulative CO₂ emissions from land-use changes (ELUC) for 1850-2022 were 220 ± 65 GtC (Table 8; Figure 3;
855 Figure 15). The cumulative emissions from ELUC show a large spread among individual estimates of 150 GtC
856 (H&C2023), 290 GtC (BLUE), and 215 GtC (OSCAR) for the three bookkeeping models and a similar wide
857 estimate of 210 ± 65 GtC for the DGVMs (all cumulative numbers are rounded to the nearest 5 GtC). These
858 estimates are broadly consistent with indirect constraints from vegetation biomass observations, giving
859 cumulative emissions of 155 ± 50 GtC over the 1901-2012 period (Li et al., 2017). However, given the large
860 spread, a best estimate is difficult to ascertain.

861 **3.2.2 Recent period 1960-2022**

862 In contrast to growing fossil emissions, CO₂ emissions from land-use, land-use change, and forestry remained
863 relatively constant over the 1960-1999 period. Since then, they have shown a slight decrease of about 0.1 GtC
864 per decade, reaching 1.3 ± 0.7 GtC yr⁻¹ for the 2013-2022 period (Table 7), but with large spread across
865 estimates (Table 5, Figure 7). Different from the bookkeeping average, the DGVMs average grows slightly
866 larger over the 1970-2022 period and shows no sign of decreasing emissions in the recent decades (Table 5,
867 Figure 7). This is, however, expected as DGVM-based estimates include the loss of additional sink capacity,
868 which grows with time, while the bookkeeping estimates do not (Supplement S.6.4).

869 We separate net ELUC into five component fluxes to gain further insight into the drivers of net emissions:
870 deforestation, forest (re-)growth, wood harvest and other forest management, peat drainage and peat fires, and
871 all other transitions (Figure 7c; Sec. C.2.1). We further decompose the deforestation and the forest (re-)growth
872 term into contributions from shifting cultivation vs permanent forest cover changes (Figure 7d). Averaged over
873 the 2013-2022 period and over the three bookkeeping estimates, fluxes from deforestation amount to 1.9 [1.5 to
874 2.4] GtC yr⁻¹ (Table 5), of which 1.1 [1.0, 1.2] GtC yr⁻¹ are from permanent deforestation. Fluxes from forest
875 (re-)growth amount to -1.3 [-1.5, -0.9] GtC yr⁻¹ (Table 5), of which -0.5 [-0.8 to -0.2] GtC yr⁻¹ are from
876 re/afforestation and the remainder from forest regrowth in shifting cultivation cycles. Emissions from wood
877 harvest and other forest management (0.2 [0.0, 0.6] GtC yr⁻¹), peat drainage and peat fires (0.3 [0.3, 0.3] GtC yr⁻¹)
878 and the net flux from other transitions (0.1 [0.0, 0.3] GtC yr⁻¹) are substantially less important globally (Table
879 5). However, the small net flux from wood harvest and other forest management contains substantial gross
880 fluxes that largely compensate each other (see Figure S7): 1.3 [0.9, 2.0] GtC yr⁻¹ emissions result from the
881 decomposition of slash and the decay of wood products and -1.1 [-1.3, -0.8] GtC yr⁻¹ removals result from
882 regrowth after wood harvesting. This split into component fluxes clarifies the potentials for emission reduction
883 and carbon dioxide removal: the emissions from permanent deforestation - the largest of our component fluxes -

884 could be halted (largely) without compromising carbon uptake by forests, contributing substantially to emissions
885 reduction. By contrast, reducing wood harvesting would have limited potential to reduce emissions as it would
886 be associated with less forest regrowth; removals and emissions cannot be decoupled here on long timescales. A
887 similar conclusion applies to removals and emissions from shifting cultivation, which we have therefore
888 separated out. Carbon Dioxide Removal (CDR) in forests could instead be increased by permanently increasing
889 the forest cover through re/afforestation. Our estimate of about -0.5 [-0.8 , -0.2] GtC yr^{-1} (of which about two
890 thirds are located in non-Annex-I countries, in particular in China) removed on average each year during 2013-
891 2022 by re/afforestation is very similar to independent estimates that were derived from NGHGs for 2022.
892 Re/afforestation constitutes the vast majority of all current CDR (Powis et al., 2023). Though they cannot be
893 compared directly to annual fluxes from the atmosphere, CDR through transfers between non-atmospheric
894 reservoirs such as in durable HWPs, biochar or BECCS comprise much smaller amounts of carbon. 61 MtC yr^{-1}
895 have been estimated to be transferred to HWPs in 2022, and BECCS projects have been estimated to store 0.5
896 MtC yr^{-1} in geological projects worldwide (Powis et al., 2023). “Blue carbon”, i.e. coastal wetland management
897 such as restoration of mangrove forests, saltmarshes and seagrass meadows, though at the interface of land and
898 ocean carbon fluxes, are counted towards the land-use sector as well. Currently, bookkeeping models do not
899 include blue carbon; however, current CDR deployment in coastal wetlands is small globally, less than
900 $0.003 \text{ MtC yr}^{-1}$ (Powis et al., 2023).

901 The small declining trend of E_{LUC} over the last three decades is a result of total deforestation emissions showing
902 no clear trend, while forest regrowth has provided steadily increasing removals. Since the processes behind
903 gross removals, foremost forest regrowth and soil recovery, are all slow, while gross emissions include a large
904 instantaneous component, short-term changes in land-use dynamics, such as a temporary decrease in
905 deforestation, influences gross emissions dynamics more than gross removals dynamics, which rather are a
906 response to longer-term dynamics. Component fluxes often differ more across the three bookkeeping estimates
907 than the net flux, which is expected due to different process representation; in particular, treatment of shifting
908 cultivation, which increases both gross emissions and removals, differs across models, but also net and gross
909 wood harvest fluxes show high uncertainty. By contrast, models agree relatively well for emissions from
910 permanent deforestation emissions and removals by re/afforestation.

911 Overall, highest land-use emissions occur in the tropical regions of all three continents. The top three emitters
912 (both cumulatively 1959-2022 and on average over 2013-2022) are Brazil (in particular the Amazon Arc of
913 Deforestation), Indonesia and the Democratic Republic of the Congo, with these 3 countries contributing 0.7
914 GtC yr^{-1} or 55% of the global net land-use emissions (average over 2013-2022) (Figure 6b). This is related to
915 massive expansion of cropland, particularly in the last few decades in Latin America, Southeast Asia, and sub-
916 Saharan Africa (Hong et al., 2021), to a substantial part for export of agricultural products (Pendrill et al., 2019).
917 Emission intensity is high in many tropical countries, particularly of Southeast Asia, due to high rates of land
918 conversion in regions of carbon-dense and often still pristine, undegraded natural forests (Hong et al., 2021).
919 Emissions are further increased by peat fires in equatorial Asia (GFED4s, van der Werf et al., 2017). Uptake due
920 to land-use change occurs, particularly in Europe, partly related to expanding forest area as a consequence of the

921 forest transition in the 19th and 20th century and subsequent regrowth of forest (Figure 6b) (Mather 2001;
922 McGrath et al., 2015).

923 While the mentioned patterns are robust and supported by independent literature, we acknowledge that model
924 spread is substantially larger on regional than global levels, as has been shown for bookkeeping models (Bastos
925 et al., 2021) as well as DGVMs (Obermeier et al., 2021). Assessments for individual regions will be performed
926 as part of REgional Carbon Cycle Assessment and Processes (RECCAP2; Ciais et al., 2020, Poulter et al., 2022)
927 or already exist for selected regions (e.g., for Europe by Petrescu et al., 2020, for Brazil by Rosan et al., 2021,
928 for 8 selected countries/regions in comparison to inventory data by Schwingshackl et al., 2022).

929 As mentioned before, the NGHGI data under the LULUCF sector or data submitted by countries to FAOSTAT
930 differ from the global models' definition of E_{LUC} . In the NGHGI reporting, the natural fluxes (S_{LAND}) are
931 counted towards E_{LUC} when they occur on managed land (Grassi et al., 2018). To compare our results to the
932 NGHGI approach, we perform a translation of our E_{LUC} estimates by subtracting S_{LAND} in managed forest from
933 the DGVMs simulations (following the methodology described in Grassi et al., 2023) from the bookkeeping
934 E_{LUC} estimate (see Supplement S.2.3). For the 2013-2022 period, we estimate that 2.0 GtC yr⁻¹ of S_{LAND}
935 occurred in managed forests. Subtracting this value from E_{LUC} changes E_{LUC} from being a source of 1.3 GtC yr⁻¹
936 to a sink of 0.8 GtC yr⁻¹, very similar to the NGHGI estimate that yields a sink of 0.7 GtC yr⁻¹ (Table 9). The
937 translation approach has been shown to be generally applicable also on country-level (Grassi et al., 2023;
938 Schwingshackl et al., 2022). Country-level analysis suggests, e.g., that the bookkeeping method estimates higher
939 deforestation emissions than the national report in Indonesia, but less CO₂ removal by afforestation than the
940 national report in China. The fraction of the natural CO₂ sinks that the NGHGI estimates include differs
941 substantially across countries, related to varying proportions of managed vs total forest areas (Schwingshackl et
942 al., 2022). By comparing E_{LUC} and NGHGI on the basis of the component fluxes used above, we find that our
943 estimates reproduce very closely the NGHGI estimates for emissions from permanent deforestation (1.1 GtC yr⁻¹
944 averaged over 2013-2022). Forest fluxes, that is, (re-)growth from re/afforestation plus the net flux from wood
945 harvesting and other forest management, constitute a large sink in the NGHGI (-1.9 GtC yr⁻¹ averaged over
946 2013-2022), since they also include S_{LAND} in managed forests. Summing up the bookkeeping estimates of (re-
947)growth from re/afforestation and the net flux from wood harvesting and other forest management and adding
948 S_{LAND} in managed forests yields a flux of -2.3 GtC yr⁻¹ (averaged over 2013-2022), which compares well with
949 the NGHGI estimate. Emissions from organic soils in NGHGI are similar to the estimates based on the
950 bookkeeping approach and the external peat drainage and burning datasets. The net flux from other transitions is
951 small in both NGHGI and bookkeeping estimates, but a difference in sign (small source in bookkeeping
952 estimates, small sink in NGHGI) creates a notable difference between NGHGI and bookkeeping estimates.
953 Though estimates between NGHGI, FAOSTAT and the translated budget estimates still differ in value and need
954 further analysis, the approach suggested by Grassi et al. (2023), which we adopt here, provides a feasible way to
955 relate the global models' and NGHGI approach to each other and thus link the anthropogenic carbon budget
956 estimates of land CO₂ fluxes directly to the Global Stocktake, as part of UNFCCC Paris Agreement.

957 3.2.3 Final year 2022

958 The global CO₂ emissions from land-use change are estimated as 1.2 ± 0.7 GtC in 2022, similar to the 2020 and
959 2021 estimates. However, confidence in the annual change remains low. Effects of the COVID-19 pandemic on
960 land-use change have turned out to be country-specific as global market mechanisms, national economics and
961 changes in household income all could act to curb or enhance deforestation (Wunder et al., 2021). Concerns
962 about enhanced deforestation due to weakened environmental protection and monitoring in tropical countries
963 (Brancalion et al., 2020, Vale et al., 2021) have been confirmed only for some countries (Cespedes et al., 2023).
964 For example, a recent study suggests slightly increased deforestation rates for the Democratic Republic of
965 Congo linked in particular to post-pandemic economic recovery in the mining sector, while deforestation trends
966 in Brazil seem to have been unaffected. Land use dynamics may be further altered by the Russian invasion of
967 Ukraine, but scientific evidence related to international dependencies (like a shift to tropical palm oil to alleviate
968 dependencies on sunflower oil) so far is very limited and recent changes will not be reflected by the land-use
969 forcing applied in the global models. High food prices, which preceded but were exacerbated by the war (FAO,
970 2022), are generally linked to higher deforestation (Angelsen and Kaimowitz, 1999). A new wave of cropland
971 abandonment in the conflict region may increase the substantial Eastern European carbon sink due to land-use
972 changes, but sanctions being placed on trade may also incentivise domestic agricultural production, thus leading
973 to recultivation of abandoned areas in Russia (Winkler et al., 2023).

974 3.2.4 Year 2023 Projection

975 In Indonesia, peat fire emissions are below average (12 Tg C through September 29 2023) despite El Niño
976 conditions, which in general lead to more fires. Tropical deforestation and degradation fires in Indonesia are
977 around average (13 Tg C through September 29 2023), but higher than in the previous year, which had a
978 relatively wet dry season (GFED4.1s, van der Werf et al., 2017; see also
979 https://www.geo.vu.nl/~gwerf/GFED/GFED4/tables/GFED4.1s_C.txt). In South America, emissions from
980 tropical deforestation and degradation fires are among the lowest over the last decades (64 Tg C through
981 September 29 2023). Effects of the El Niño in the Amazon, such as droughts, are not expected before 2024.
982 Disentangling the degree to which interannual variability in rainfall patterns and stronger environmental
983 protection measures in both Indonesia after their 2015 high fire season and in Brazil after the change in
984 government in Brazil play a role in this is an important research topic. Cumulative fire emission estimates
985 through September 29 2023 are 155 Tg C for global deforestation and degradation fires and 12 Tg C for
986 peatland fires in Indonesia (https://www.geo.vu.nl/~gwerf/GFED/GFED4/tables/GFED4.1s_C.txt).

987 Based on these estimates, we expect E_{LUC} emissions of around 1.1 GtC (4.1 GtCO₂) in 2023. Our preliminary
988 estimate of E_{LUC} for 2023 is substantially lower than the 2013-2022 average, which saw years of anomalously
989 dry conditions in Indonesia and high deforestation fires in South America (Friedlingstein et al., 2022b). Note
990 that although our extrapolation includes tropical deforestation and degradation fires, degradation attributable to
991 selective logging, edge-effects or fragmentation is not captured. Further, deforestation and fires in deforestation
992 zones may become more disconnected, partly due to changes in legislation in some regions. For example, Van

993 Wees et al. (2021) found that the contribution from fires to forest loss decreased in the Amazon and in Indonesia
994 over the period of 2003-2018.

995 **3.3 CDR not based on vegetation**

996 Besides the CDR through land-use (Sec. 3.2), the atmosphere to geosphere flux of carbon resulting from carbon
997 dioxide removal (CDR) activity is currently 0.003 MtC/yr, with 0.002 MtC/yr of DACCS and 0.001 MtC/yr of
998 enhanced weathering projects. This is more than a million times smaller than current fossil CO₂ emissions.

999 **3.4 Total anthropogenic emissions**

1000 Cumulative anthropogenic CO₂ emissions for 1850-2022 totalled 695 ± 70 GtC (2550 ± 260 GtCO₂), of which
1001 70% (485 GtC) occurred since 1960 and 33% (235 GtC) since 2000 (Table 7 and 8). Total anthropogenic
1002 emissions more than doubled over the last 60 years, from 4.6 ± 0.7 GtC yr⁻¹ for the decade of the 1960s to an
1003 average of 10.9 ± 0.8 GtC yr⁻¹ during 2013-2022 and reaching 11.1 ± 0.9 GtC (40.7 ± 3.3 GtCO₂) in 2022. For
1004 2023, we project global total anthropogenic CO₂ emissions from fossil and land use changes to be also around
1005 11.2 GtC (40.9 GtCO₂). All values here include the cement carbonation sink (currently about 0.2 GtC yr⁻¹).

1006 During the historical period 1850-2022, 31% of historical emissions were from land use change and 69% from
1007 fossil emissions. However, fossil emissions have grown significantly since 1960 while land use changes have
1008 not, and consequently the contributions of land use change to total anthropogenic emissions were smaller during
1009 recent periods (18% during the period 1960-2022 and down to 12% over the 2013-2022 period).

1010 **3.5 Atmospheric CO₂**

1011 **3.5.1 Historical period 1850-2022**

1012 Atmospheric CO₂ concentration was approximately 278 parts per million (ppm) in 1750, reaching 300 ppm in
1013 the 1910s, 350 ppm in the late 1980s, and reaching 417.07 ± 0.1 ppm in 2022 (Lan et al., 2023; Figure 1). The
1014 mass of carbon in the atmosphere increased by 48% from 590 GtC in 1750 to 886 GtC in 2022. Current CO₂
1015 concentrations in the atmosphere are unprecedented in the last 2 million years and the current rate of
1016 atmospheric CO₂ increase is at least 10 times faster than at any other time during the last 800,000 years
1017 (Canadell et al., 2021).

1018 **3.5.2 Recent period 1960-2022**

1019 The growth rate in atmospheric CO₂ level increased from 1.7 ± 0.07 GtC yr⁻¹ in the 1960s to 5.2 ± 0.02 GtC yr⁻¹
1020 during 2013-2022 with important decadal variations (Table 7, Figure 3 and Figure 4). During the last decade
1021 (2013-2022), the growth rate in atmospheric CO₂ concentration continued to increase, albeit with large
1022 interannual variability (Figure 4).

1023 The airborne fraction (AF), defined as the ratio of atmospheric CO₂ growth rate to total anthropogenic
1024 emissions:

$$1025 \quad AF = G_{ATM} / (E_{FOS} + E_{LUC}) \quad (2)$$

1026 provides a diagnostic of the relative strength of the land and ocean carbon sinks in removing part of the
1027 anthropogenic CO₂ perturbation. The evolution of AF over the last 60 years shows no significant trend,
1028 remaining at around 44%, albeit showing a large interannual and decadal variability driven by the year-to-year
1029 variability in G_{ATM} (Figure 9). The observed stability of the airborne fraction over the 1960-2020 period
1030 indicates that the ocean and land CO₂ sinks have been removing on average about 56% of the anthropogenic
1031 emissions (see Sections 3.6.2 and 3.7.2).

1032 **3.5.3 Final year 2022**

1033 The growth rate in atmospheric CO₂ concentration was 4.6 ± 0.2 GtC (2.18 ± 0.08 ppm) in 2022 (Figure 4; Lan
1034 et al., 2023), below the 2021 growth rate (5.2 ± 0.2 GtC) or the 2013-2022 average (5.2 ± 0.02 GtC).

1035 **3.5.4 Year 2023 Projection**

1036 The 2023 growth in atmospheric CO₂ concentration (G_{ATM}) is projected to be about 5.1 GtC (2.4 ppm). This is
1037 the average of the GCB regression method (5.07 GtC, 2.39 ppm) and ESMs the multi-model mean (5.11 GtC,
1038 2.41 ppm). The 2023 atmospheric CO₂ concentration, averaged over the year, is expected to reach the level of
1039 419.3 ppm, 51% over the pre-industrial level.

1040 **3.6 Ocean Sink**

1041 **3.6.1 Historical period 1850-2022**

1042 Cumulated since 1850, the ocean sink adds up to 180 ± 35 GtC, with more than two thirds of this amount (125
1043 GtC) being taken up by the global ocean since 1960. Over the historical period, the ocean sink increased in pace
1044 with the anthropogenic emissions exponential increase (Figure 3). Since 1850, the ocean has removed 26% of
1045 total anthropogenic emissions.

1046 **3.6.2 Recent period 1960-2022**

1047 The ocean CO₂ sink increased from 1.1 ± 0.4 GtC yr⁻¹ in the 1960s to 2.8 ± 0.4 GtC yr⁻¹ during 2013-2022
1048 (Table 7), with interannual variations of the order of a few tenths of GtC yr⁻¹ (Figure 10). The ocean-borne
1049 fraction ($S_{OCEAN}/(E_{FOS}+E_{LUC})$) has been remarkably constant around 25% on average (Figure 9c), with variations
1050 around this mean illustrating the decadal variability of the ocean carbon sink. So far, there is no indication of a
1051 decrease in the ocean-borne fraction from 1960 to 2022. The increase of the ocean sink is primarily driven by
1052 the increased atmospheric CO₂ concentration, with the strongest CO₂ induced signal in the North Atlantic and
1053 the Southern Ocean (Figure 11a). The effect of climate change is much weaker, reducing the ocean sink globally

1054 by $0.16 \pm 0.04 \text{ GtC yr}^{-1}$ (-6.7% of S_{OCEAN}) during 2013-2022 (all models simulate a weakening of the ocean sink
1055 by climate change, range -4.3 to -10.3%), and does not show clear spatial patterns across the GOBMs ensemble
1056 (Figure 11b). This is the combined effect of change and variability in all atmospheric forcing fields, previously
1057 attributed, in one model, to wind and temperature changes (LeQuéré et al., 2010).

1058 The global net air-sea CO_2 flux is a residual of large natural and anthropogenic CO_2 fluxes into and out of the
1059 ocean with distinct regional and seasonal variations (Figure 6 and B1). Natural fluxes dominate on regional
1060 scales, but largely cancel out when integrated globally (Gruber et al., 2009). Mid-latitudes in all basins and the
1061 high-latitude North Atlantic dominate the ocean CO_2 uptake where low temperatures and high wind speeds
1062 facilitate CO_2 uptake at the surface (Takahashi et al., 2009). In these regions, formation of mode, intermediate
1063 and deep-water masses transport anthropogenic carbon into the ocean interior, thus allowing for continued CO_2
1064 uptake at the surface. Outgassing of natural CO_2 occurs mostly in the tropics, especially in the equatorial
1065 upwelling region, and to a lesser extent in the North Pacific and polar Southern Ocean, mirroring a well-
1066 established understanding of regional patterns of air-sea CO_2 exchange (e.g., Takahashi et al., 2009, Gruber et
1067 al., 2009). These patterns are also noticeable in the Surface Ocean CO_2 Atlas (SOCAT) dataset, where an ocean
1068 $f\text{CO}_2$ value above the atmospheric level indicates outgassing (Figure S1). This map further illustrates the data-
1069 sparsity in the Indian Ocean and the southern hemisphere in general.

1070 Interannual variability of the ocean carbon sink is driven by climate variability with a first-order effect from a
1071 stronger ocean sink during large El Niño events (e.g., 1997-1998) (Figure 10; Rödenbeck et al., 2014, Hauck et
1072 al., 2020; McKinley et al. 2017). The GOBMs show the same patterns of decadal variability as the mean of the
1073 $f\text{CO}_2$ -products, with a stagnation of the ocean sink in the 1990s and a strengthening since the early 2000s
1074 (Figure 10; Le Quéré et al., 2007; Landschützer et al., 2015, 2016; DeVries et al., 2017; Hauck et al., 2020;
1075 McKinley et al., 2020, Gruber et al., 2023). Different explanations have been proposed for this decadal
1076 variability, ranging from the ocean's response to changes in atmospheric wind and pressure systems (e.g., Le
1077 Quéré et al., 2007, Keppler and Landschützer, 2019), including variations in upper ocean overturning circulation
1078 (DeVries et al., 2017) to the eruption of Mount Pinatubo and its effects on sea surface temperature and slowed
1079 atmospheric CO_2 growth rate in the 1990s (McKinley et al., 2020). The main origin of the decadal variability is
1080 a matter of debate with a number of studies initially pointing to the Southern Ocean (see review in Canadell et
1081 al., 2021), but also contributions from the North Atlantic and North Pacific (Landschützer et al., 2016, DeVries
1082 et al., 2019), or a global signal (McKinley et al., 2020) were proposed.

1083 Although all individual GOBMs and $f\text{CO}_2$ -products fall within the observational constraint, the ensemble means
1084 of GOBMs, and $f\text{CO}_2$ -products adjusted for the riverine flux diverge over time with a mean offset increasing
1085 from 0.30 GtC yr^{-1} in the 1990s to 0.57 GtC yr^{-1} in the decade 2013-2022 and reaching 0.61 GtC yr^{-1} in 2022.
1086 The S_{OCEAN} positive trend over time diverges by a factor two since 2002 (GOBMs: $0.24 \pm 0.07 \text{ GtC yr}^{-1}$ per
1087 decade, $f\text{CO}_2$ -products: $0.48 \pm 0.11 \text{ GtC yr}^{-1}$ per decade, S_{OCEAN} : 0.36 GtC yr^{-1} per decade) and by a factor of 2.5
1088 since 2010 (GOBMs: $0.16 \pm 0.15 \text{ GtC yr}^{-1}$ per decade, $f\text{CO}_2$ -products: $0.42 \pm 0.18 \text{ GtC yr}^{-1}$ per decade, S_{OCEAN} :
1089 0.29 GtC yr^{-1} per decade). The $f\text{CO}_2$ -product estimate is slightly different compared to Friedlingstein et al.

1090 (2022b) as a result of an updated submission of the NIES-ML3 product (previously NIES-NN), however the
1091 difference in the integrated mean flux is small.

1092 The discrepancy between the two types of estimates stems from a larger S_{OCEAN} trend in the northern and
1093 southern extra-tropics since around 2002 (Figure 13). Note that the discrepancy in the mean flux, which was
1094 located in the Southern Ocean in previous versions of the GCB, has been reduced due to the choice of the
1095 regional river flux adjustment (Lacroix et al., 2020 instead of Aumont et al., 2001). This comes at the expense of
1096 a new discrepancy in the mean S_{OCEAN} of about 0.2 GtC yr^{-1} in the tropics. Likely explanations for the
1097 discrepancy in the trends in the high-latitudes are data sparsity and uneven data distribution (Bushinsky et al.,
1098 2019, Gloege et al., 2021, Hauck et al., 2023). In particular, two $f\text{CO}_2$ -products that are part of the GCB
1099 ensemble were shown to overestimate the Southern Ocean CO_2 flux trend by 50 and 130% based on current
1100 sampling in a model subsampling experiment (Hauck et al., 2023). Another likely contributor to the discrepancy
1101 between GOBMs and $f\text{CO}_2$ -products are model biases (as indicated by the large model spread in the South,
1102 Figure 13, and the larger model-data $f\text{CO}_2$ mismatch, Figure S2).

1103 In previous GCB releases, the ocean sink 1959-1989 was only estimated by GOBMs due to the absence of $f\text{CO}_2$
1104 observations. Now, the first data-based estimates extending back to 1957/58 are becoming available (Jena-MLS,
1105 Rödenbeck et al., 2022, LDEO-HPD, Bennington et al., 2022; Gloege et al., 2022). These are based on a multi-
1106 linear regression of $p\text{CO}_2$ with environmental predictors (Rödenbeck et al., 2022) or on model-data $p\text{CO}_2$ misfits
1107 and their relation to environmental predictors (Bennington et al., 2022). The Jena-MLS and LDEO-HPD
1108 estimates fall well within the range of GOBM estimates and have a correlation of 0.99 and 0.98 respectively
1109 with S_{OCEAN} for the period 1959-2022 (and 0.98 and 0.97 for the 1959-1989 period). They agree well on the
1110 mean S_{OCEAN} estimate since 1977 with a slightly higher amplitude of variability (Figure 10). Until 1976, Jena-
1111 MLS and LDEO-HPD are respectively about 0.25 GtCyr^{-1} and about 0.1 GtCyr^{-1} below the central S_{OCEAN}
1112 estimate. The agreement especially on phasing of variability is impressive in both products, and the
1113 discrepancies in the mean flux 1959-1976 could be explained by an overestimated trend of Jena-MLS
1114 (Rödenbeck et al., 2022). Bennington et al. (2022) report a larger flux into the pre-1990 ocean than in Jena-
1115 MLS, although lower than S_{OCEAN} .

1116 The reported S_{OCEAN} estimate from GOBMs and $f\text{CO}_2$ -products is $2.2 \pm 0.4 \text{ GtC yr}^{-1}$ over the period 1994 to
1117 2007, which is in excellent agreement with the ocean interior estimate of $2.2 \pm 0.4 \text{ GtC yr}^{-1}$, which accounts for
1118 the climate effect on the natural CO_2 flux of $-0.4 \pm 0.24 \text{ GtC yr}^{-1}$ (Gruber et al., 2019) to match the
1119 definition of S_{OCEAN} used here (Hauck et al., 2020). This comparison depends critically on the estimate of the
1120 climate effect on the natural CO_2 flux, which is smaller from the GOBMs (-0.1 GtC yr^{-1}) than in Gruber et al.
1121 (2019). Uncertainties of these two estimates would also overlap when using the GOBM estimate of the climate
1122 effect on the natural CO_2 flux.

1123 During 2010-2016, the ocean CO_2 sink appears to have intensified in line with the expected increase from
1124 atmospheric CO_2 (McKinley et al., 2020). This effect is slightly stronger in the $f\text{CO}_2$ -products (Figure 10, ocean
1125 sink 2016 minus 2010, GOBMs: $+0.42 \pm 0.10 \text{ GtC yr}^{-1}$, $f\text{CO}_2$ -products: $+0.48 \pm 0.10 \text{ GtC yr}^{-1}$). The reduction of

1126 $-0.14 \text{ GtC yr}^{-1}$ (range: -0.39 to $+0.01 \text{ GtC yr}^{-1}$) in the ocean CO_2 sink in 2017 is consistent with the return to
1127 normal conditions after the El Niño in 2015/16, which caused an enhanced sink in previous years. After an
1128 increasing S_{OCEAN} in 2018 and 2019, 2017, the GOBM and $f\text{CO}_2$ -product ensemble means suggest a decrease of
1129 S_{OCEAN} , related to the triple La Niña event 2020-2023.

1130 **3.6.3 Final year 2022**

1131 The estimated ocean CO_2 sink is $2.8 \pm 0.4 \text{ GtC}$ for 2022. This is a small decrease of 0.05 GtC compared to 2021,
1132 in line with the expected sink weakening from persistent La Niña conditions. GOBM and $f\text{CO}_2$ -product
1133 estimates consistently result in a near-stagnation of S_{OCEAN} (GOBMs: $-0.01 \pm 0.05 \text{ GtC}$, $f\text{CO}_2$ -products: -0.09
1134 $\pm 0.10 \text{ GtC}$). Four models and six $f\text{CO}_2$ -products show a decrease in S_{OCEAN} (GOBMs down to -0.09 GtC , $f\text{CO}_2$ -
1135 products down to -0.25 GtC), while one model shows no change and five models and two $f\text{CO}_2$ -products show
1136 an increase in S_{OCEAN} (GOBMs up to 0.07 GtC , $f\text{CO}_2$ -products up to 0.15 GtC ; Figure 10). The $f\text{CO}_2$ -products
1137 have a larger uncertainty at the end of the reconstructed time series (tail effect, e.g., Watson et al., 2020).
1138 Specifically, the $f\text{CO}_2$ -products' estimate of the last year is regularly adjusted in the following release owing to
1139 the tail effect and an incrementally increasing data availability. While the monthly grid cells covered may have a
1140 lag of only about a year (Figure 10 inset), the values within grid cells may change with 1-5 years lag (see
1141 absolute number of observations plotted in previous GCB releases).

1142 **3.6.4 Year 2023 Projection**

1143 Using a feed-forward neural network method (see Section 2.5.2) we project an ocean sink of 2.9 GtC for 2023.
1144 This is slightly higher than for the year 2022 (2.8 GtC) and could mark a reversal of the slight decrease of
1145 S_{OCEAN} sink since 2019, due to the transition from persisting La Niña conditions to emerging El Niño conditions
1146 in 2023. The new set of ESMs predictions support this estimate with a 2023 ocean sink of around $3.1 [2.9, 3.2]$
1147 GtC .

1148 **3.6.5 Ocean Models Evaluation**

1149 The process-based model evaluation draws a generally positive picture with GOBMs scattered around the
1150 observational values for Southern Ocean sea-surface salinity, Southern Ocean stratification index and surface
1151 ocean Revelle factor (Section C3.3 and Table S10). However, the Atlantic Meridional Overturning Circulation
1152 at 26°N is underestimated by 8 out of 10 GOBMs. It is planned to derive skill scores for the GOBMs in future
1153 releases based on these metrics.

1154 The model simulations allow to separate the anthropogenic carbon component (steady state and non-steady
1155 state, $\text{sim D} - \text{sim A}$) and to compare the model flux and DIC inventory change directly to the interior ocean
1156 estimate of Gruber et al. (2019) without further assumptions (Table S10). The GOBMs ensemble average of
1157 anthropogenic carbon inventory changes 1994-2007 amounts to 2.4 GtC yr^{-1} and is thus lower than the 2.6 ± 0.3
1158 GtC yr^{-1} estimated by Gruber et al. (2019) although within the uncertainty. Only four models with the highest
1159 sink estimate fall within the range reported by Gruber et al. (2019). This suggests that the majority of the

1160 GOBMs underestimate anthropogenic carbon uptake by 10-20%. Analysis of Earth System Models indicate that
1161 an underestimation by about 10% may be due to biases in ocean carbon transport and mixing from the surface
1162 mixed layer to the ocean interior (Goris et al., 2018, Terhaar et al., 2021, Bourgeois et al., 2022, Terhaar et al.,
1163 2022), biases in the chemical buffer capacity (Revelle factor) of the ocean (Vaittinada Ayar et al., 2022; Terhaar
1164 et al., 2022) and partly due to a late starting date of the simulations (mirrored in atmospheric CO₂ chosen for the
1165 preindustrial control simulation, Table S2, Bronselaer et al., 2017, Terhaar et al., 2022). Interestingly, and in
1166 contrast to the uncertainties in the surface CO₂ flux, we find the largest mismatch in interior ocean carbon
1167 accumulation in the tropics (96% of the mismatch), with minor contributions from the north (3%) and the south
1168 (<1%). These numbers deviate slightly from GCB2021 because of submission of the ACCESS model with a
1169 high anthropogenic carbon accumulation, particularly in the Southern Ocean. The large discrepancy in
1170 accumulation in the tropics highlights the role of interior ocean carbon redistribution for those inventories
1171 (Khatiwala et al., 2009, DeVries et al., 2023).

1172 The evaluation of the ocean estimates with the *f*CO₂ observations from the SOCAT v2023 dataset for the period
1173 1990-2022 shows an RMSE from annually detrended data of 0.4 to 2.4 μatm for the seven *f*CO₂-products over
1174 the globe (Figure S2). The GOBMs RMSEs are larger and range from 2.9 to 5.4 μatm. The RMSEs are
1175 generally larger at high latitudes compared to the tropics, for both the *f*CO₂-products and the GOBMs. The
1176 *f*CO₂-products have RMSEs of 0.3 to 2.8 μatm in the tropics, 0.7 to 2.3 μatm in the north, and 0.7 to 2.8 μatm in
1177 the south. Note that the *f*CO₂-products are based on the SOCAT v2023 database, hence the SOCAT is not an
1178 independent dataset for the evaluation of the *f*CO₂-products. The GOBMs RMSEs are more spread across
1179 regions, ranging from 2.5 to 5.0 μatm in the tropics, 3.0 to 7.2 μatm in the North, and 3.7 to 8.5 μatm in the
1180 South. The higher RMSEs occur in regions with stronger climate variability, such as the northern and southern
1181 high latitudes (poleward of the subtropical gyres). The upper range of the model RMSEs have increased
1182 somewhat relative to Friedlingstein et al. (2022b).

1183 **3.7 Land Sink**

1184 **3.7.1 Historical period 1850-2022**

1185 Cumulated since 1850, the terrestrial CO₂ sink amounts to 225 ± 55 GtC, 32% of total anthropogenic emissions.
1186 Over the historical period, the sink increased in pace with the anthropogenic emissions exponential increase
1187 (Figure 3).

1188 **3.7.2 Recent period 1960-2022**

1189 The terrestrial CO₂ sink *S*_{LAND} increased from 1.3 ± 0.5 GtC yr⁻¹ in the 1960s to 3.3 ± 0.8 GtC yr⁻¹ during 2013-
1190 2022, with important interannual variations of up to 2 GtC yr⁻¹ generally showing a decreased land sink during
1191 El Niño events (Figure 8), responsible for the corresponding enhanced growth rate in atmospheric CO₂
1192 concentration. The larger land CO₂ sink during 2013-2022 compared to the 1960s is reproduced by all the
1193 DGVMs in response to the increase in both atmospheric CO₂, nitrogen deposition, and the changes in climate,
1194 and is consistent with constraints from the other budget terms (Table 5).

1195 Over the period 1960 to present the increase in the global terrestrial CO₂ sink is largely attributed to the CO₂
1196 fertilisation effect (Prentice et al., 2001, Piao et al., 2009, Schimel et al., 2015) and increased nitrogen
1197 deposition (Huntzinger et al., 2017, O’Sullivan et al., 2019), directly stimulating plant photosynthesis and
1198 increased plant water use in water limited systems, with a small negative contribution of climate change (Figure
1199 11). There is a range of evidence to support a positive terrestrial carbon sink in response to increasing
1200 atmospheric CO₂, albeit with uncertain magnitude (Walker et al., 2021). As expected from theory, the greatest
1201 CO₂ effect is simulated in the tropical forest regions, associated with warm temperatures and long growing
1202 seasons (Hickler et al., 2008) (Figure 11a). However, evidence from tropical intact forest plots indicate an
1203 overall decline in the land sink across Amazonia (1985-2011), attributed to enhanced mortality offsetting
1204 productivity gains (Brienen et al., 2015, Hubau et al., 2020). During 2013-2022 the land sink is positive in all
1205 regions (Figure 6) with the exception of eastern Brazil, Bolivia, Paraguay, northern Venezuela, Southwest USA,
1206 central Europe and Central Asia, North and South Africa, and eastern Australia, where the negative effects of
1207 climate variability and change (i.e. reduced rainfall and/or increased temperature) counterbalance CO₂ effects.
1208 This is clearly visible on Figure 11 where the effects of CO₂ (Figure 11a) and climate (Figure 11b) as simulated
1209 by the DGVMs are isolated. The negative effect of climate is the strongest in most of South America, Central
1210 America, Southwest US, Central Europe, western Sahel, southern Africa, Southeast Asia and southern China,
1211 and eastern Australia (Figure 11b). Globally, over the 2013-2022 period, climate change reduces the land sink
1212 by $0.68 \pm 0.62 \text{ GtC yr}^{-1}$ (20% of S_{LAND}).

1213 Most DGVMs have similar S_{LAND} averaged over 2013-2022, and 14/20 models fall within the 1σ range of the
1214 residual land sink [$2.0\text{-}3.8 \text{ GtC yr}^{-1}$] (see Table 5), and all but one model are within the 2σ range [$1.1\text{-}4.7 \text{ GtC yr}^{-1}$].
1215 The ED model is an outlier, with a land sink estimate of 5.7 GtC yr^{-1} , driven by a strong CO₂ fertilisation
1216 effect (6.6 GtC yr^{-1} in the CO₂ only (S1) simulation), that is offset by correspondingly high land-use emissions.
1217 There are no direct global observations of the land sink, or the CO₂ fertilisation effect, and so we are not yet in a
1218 position to rule out models based on component fluxes if the net land sink ($S_{\text{LAND}} - E_{\text{LUC}}$) is within the
1219 observational uncertainty provided by atmospheric O₂ measurements (Table 5). Overall, therefore the spread
1220 among models for the estimate of S_{LAND} over the last decade has increased this year (0.8 GtC yr^{-1}) compared to
1221 GCB2022 (0.6 GtC yr^{-1}).

1222 Furthermore, DGVMs were compared against a data-constrained intermediate complexity model of the land
1223 carbon cycle (CARDAMOM) (Bloom and Williams, 2015; Bloom et al., 2016). Results suggest good
1224 correspondence between approaches at the interannual timescales, but divergence in the recent trend with
1225 CARDAMOM simulating a stronger trend than the DGVMs (Figure S8).

1226 Since 2020 the globe has experienced La Niña conditions which would be expected to lead to an increased land
1227 carbon sink. A clear peak in the global land sink is not evident in S_{LAND} , and we find that a La Niña- driven
1228 increase in tropical land sink is offset by a reduced high latitude extra-tropical land sink, which may be linked to
1229 the land response to recent climate extremes. A notable difference from GCB2022 (2012-2021 S_{LAND} mean) is
1230 the reduced carbon losses across tropical drylands. Further, central Europe has switched from a sink of carbon to
1231 a source, with the summer heatwave of 2022 (and associated drought and wildfire) causing widespread losses

1232 (Peters et al., 2023). In the past years several regions experienced record-setting fire events. While global
1233 burned area has declined over the past decades mostly due to declining fire activity in savannas (Andela et al.,
1234 2017), forest fire emissions are rising and have the potential to counter the negative fire trend in savannas
1235 (Zheng et al., 2021). Noteworthy events include the 2019-2020 Black Summer event in Australia (emissions of
1236 roughly 0.2 GtC; van der Velde et al., 2021) and Siberia in 2021 where emissions approached 0.4 GtC or three
1237 times the 1997-2020 average according to GFED4s. While other regions, including Western US and
1238 Mediterranean Europe, also experienced intense fire seasons in 2021 their emissions are substantially lower.

1239 Despite these regional negative effects of climate change on S_{LAND} , the efficiency of land to remove
1240 anthropogenic CO_2 emissions has remained broadly constant over the last six decades, with a land-borne
1241 fraction ($S_{\text{LAND}}/(E_{\text{FOS}}+E_{\text{LUC}})$) of around 30% (Figure 9b).

1242 **3.7.3 Final year 2022**

1243 The terrestrial CO_2 sink from the DGVMs ensemble was 3.8 ± 0.8 GtC in 2022, above the decadal average of
1244 3.3 ± 0.8 GtC yr^{-1} (Figure 4, Table 7), and slightly above the 2021 sink of 3.5 ± 1.0 GtC, likely driven by the
1245 persistent La Niña conditions. We note that the DGVMs estimate for 2022 is similar to the 3.7 ± 1.0 GtC yr^{-1}
1246 estimate from the residual sink from the global budget ($E_{\text{FOS}}+E_{\text{LUC}}-G_{\text{ATM}}-S_{\text{OCEAN}}$) (Table 5).

1247 **3.7.4 Year 2023 Projection**

1248 Using a feed-forward neural network method we project a land sink of 2.9 GtC for 2023, 0.9 GtC smaller than
1249 the 2022 estimate. As for the ocean sink, we attribute this to the emerging El Niño conditions in 2023, leading to
1250 a reduced land sink. The ESMs do not provide an additional estimate of S_{LAND} as they only simulate the net
1251 atmosphere-land carbon flux ($S_{\text{LAND}}-E_{\text{LUC}}$).

1252 **3.7.5 Land Models Evaluation**

1253 The evaluation of the DGVMs shows generally high skill scores across models for runoff, and to a lesser extent
1254 for vegetation biomass, GPP, and ecosystem respiration. These conclusions are supported by a more
1255 comprehensive analysis of DGVM performance in comparison with benchmark data (Seiler et al., 2022). A
1256 relative comparison of DGVM performance (Figure S3) suggests several DGVMs (CABLE-POP, CLASSIC,
1257 OCN, ORCHIDEE) may outperform others at multiple carbon and water cycle benchmarks. However, results
1258 from Seiler et al., 2022, also show how DGVM differences are often of similar magnitude compared with the
1259 range across observational datasets. All models score high enough over the metrics tests to support their use
1260 here. There are a few anomalously low scores for individual metrics from a single model, and these can direct
1261 the effort to improve models for use in future budgets.

1262 3.8 Partitioning the carbon sinks

1263 3.8.1 Global sinks and spread of estimates

1264 In the period 2013-2022, the bottom-up view of global net ocean and land carbon sinks provided by the GCB,
1265 S_{OCEAN} for the ocean and $S_{\text{LAND}} - E_{\text{LUC}}$ for the land, agrees closely with the top-down global carbon sinks
1266 delivered by the atmospheric inversions. This is shown in Figure 12, which visualises the individual decadal
1267 mean atmosphere-land and atmosphere-ocean fluxes from each, along with the constraints on their sum offered
1268 by the global fossil CO₂ emissions flux minus the atmospheric growth rate ($E_{\text{FOS}} - G_{\text{ATM}}$, $4.5 \pm 0.5 \text{ Gt C yr}^{-1}$,
1269 Table 7, shown as diagonal line on Figure 12). The GCB estimate for net atmosphere-to-surface flux ($S_{\text{OCEAN}} +$
1270 $S_{\text{LAND}} - E_{\text{LUC}}$) during 2013-2022 is $4.9 \pm 1.2 \text{ Gt C yr}^{-1}$ (Table 7), with the difference to the diagonal representing
1271 the budget imbalance (B_{IM}) of 0.4 GtC yr^{-1} discussed in Section 3.9. By virtue of the inversion methodology, the
1272 imbalance of the top-down estimates is $< 0.1 \text{ GtC yr}^{-1}$ and thus scatter across the diagonal, inverse models
1273 trading land for ocean fluxes in their solution. The independent constraint on the net atmosphere-to-surface flux
1274 based on atmospheric O₂ is $4.5 \pm 1.0 \text{ GtC yr}^{-1}$ over the 2013-2022 period (orange symbol on Figure 12), while
1275 the ESMs estimate for the net atmosphere-to-surface flux over that period is $5.0 [4.2, 5.5] \text{ Gt C yr}^{-1}$, consistent
1276 with the GCB estimate (Tables 5 and 6).

1277 The distributions based on the individual models and data products reveal substantial spread but converge near
1278 the decadal means quoted in Tables 5 to 7. Sink estimates for S_{OCEAN} and from inverse systems are mostly non-
1279 Gaussian, while the ensemble of DGVMs appears more normally distributed justifying the use of a multi-model
1280 mean and standard deviation for their errors in the budget. Noteworthy is that the tails of the distributions
1281 provided by the land and ocean bottom-up estimates would not agree with the global constraint provided by the
1282 fossil fuel emissions and the observed atmospheric CO₂ growth rate. This illustrates the power of the
1283 atmospheric joint constraint from G_{ATM} and the global CO₂ observation network it derives from.

1284 3.8.1.1 Net atmosphere-to-land fluxes

1285 The GCB net atmosphere-to-land fluxes ($S_{\text{LAND}} - E_{\text{LUC}}$), calculated as the difference between S_{LAND} from the
1286 DGVMs and E_{LUC} from the bookkeeping models, amounts to a $2.1 \pm 1.1 \text{ GtC yr}^{-1}$ sink during 2013-2022 (Table
1287 5). Estimates of net atmosphere-to-land fluxes ($S_{\text{LAND}} - E_{\text{LUC}}$) from the DGVMs alone ($1.7 \pm 0.6 \text{ GtC yr}^{-1}$, Table
1288 5, green symbol on Figure 12) are slightly lower, within the uncertainty of the GCB estimate and also with the
1289 global carbon budget constraint from the ocean sink ($E_{\text{FOS}} - G_{\text{ATM}} - S_{\text{OCEAN}}$, $1.6 \pm 0.6 \text{ GtC yr}^{-1}$; Table 7). For the
1290 last decade (2013-2022), the inversions estimate the net atmosphere-to-land uptake to be $1.6 [0.5, 2.3] \text{ GtC yr}^{-1}$,
1291 similar to the DGVMs estimates (purple symbol on Figure 12). The ESMs estimate for the net atmosphere-to-
1292 land uptake during 2013-2022 is $2.4 [1.8, 3.3] \text{ GtC yr}^{-1}$, consistent with the GCB and DGVMs estimates of
1293 $S_{\text{LAND}} - E_{\text{LUC}}$ (Figure 13 top row). The independent constraint based on atmospheric O₂ is significantly lower,
1294 $1.2 \pm 0.8 \text{ GtC yr}^{-1}$, although its relatively high uncertainty range overlaps with the central estimates from other
1295 approaches.

1296 3.8.1.2 Net atmosphere-to-ocean fluxes

1297 For the 2013-2022 period, the GOBMs ($2.6 \pm 0.4 \text{ GtC yr}^{-1}$) produce a lower estimate for the ocean sink than the
1298 $f\text{CO}_2$ -products ($3.1 [2.6, 3.3] \text{ GtC yr}^{-1}$), which shows up in Figure 12 as separate peaks in the distribution from
1299 the GOBMs (dark blue symbols) and from the $f\text{CO}_2$ -products (light blue symbols). Atmospheric inversions (3.0
1300 $[2.4, 4.1] \text{ GtC yr}^{-1}$) suggest an ocean uptake more in line with the $f\text{CO}_2$ -products for the recent decade (Table 7),
1301 although the inversions range includes both the GOBMs and $f\text{CO}_2$ -products estimates (Figure 13 top row). The
1302 ESMs $2.6 [2.2, 3.4] \text{ GtC yr}^{-1}$ suggest a moderate estimate for the ocean carbon sink, comparable to the GOBMs
1303 estimate with regard to mean and spread. Conversely, the independent constraint based on atmospheric O_2
1304 suggests a larger ocean sink ($3.3 \pm 0.5 \text{ GtC yr}^{-1}$), more consistent with the $f\text{CO}_2$ -products and atmospheric
1305 inversions. We caution that the riverine transport of carbon taken up on land and outgassing from the ocean is a
1306 substantial ($0.65 \pm 0.3 \text{ GtC yr}^{-1}$) and uncertain term (Crisp et al., 2022; Gruber et al., 2023; DeVries et al., 2023)
1307 that separates the GOBMs, ESMs and oxygen-based estimates on the one hand from the $f\text{CO}_2$ -products and
1308 atmospheric inversions on the other hand. However, the high ocean sink estimate based on atmospheric oxygen
1309 that is not subject to river flux adjustment, provides another line of evidence that most GOBMs and ESMs
1310 underestimate the ocean sink.

1311 3.8.2 Regional partitioning

1312 Figure 13 shows the latitudinal partitioning of the global atmosphere-to-ocean (SOCEAN), atmosphere-to-land
1313 ($\text{SLAND} - \text{ELUC}$), and their sum ($\text{SOCEAN} + \text{SLAND} - \text{ELUC}$) according to the estimates from GOBMs and ocean
1314 $f\text{CO}_2$ -products (SOCEAN), DGVMs ($\text{SLAND} - \text{ELUC}$), and from atmospheric inversions (SOCEAN and $\text{SLAND} - \text{ELUC}$).

1315 3.8.2.1 North

1316 Despite being one of the most densely observed and studied regions of our globe, annual mean carbon sink
1317 estimates in the northern extra-tropics (north of 30°N) continue to differ. The atmospheric inversions suggest an
1318 atmosphere-to-surface sink ($\text{SOCEAN} + \text{SLAND} - \text{ELUC}$) for 2013-2022 of $2.8 [1.7 \text{ to } 3.3] \text{ GtC yr}^{-1}$, which is higher
1319 than the process models' estimate of $2.2 \pm 0.4 \text{ GtC yr}^{-1}$ (Figure 13). The GOBMs ($1.2 \pm 0.2 \text{ GtC yr}^{-1}$), $f\text{CO}_2$ -
1320 products ($1.3 [1.2-1.4] \text{ GtC yr}^{-1}$), and inversion systems ($1.2 [0.7 \text{ to } 1.4] \text{ GtC yr}^{-1}$) produce consistent estimates of
1321 the ocean sink. Thus, the difference mainly arises from the net land flux ($\text{SLAND} - \text{ELUC}$) estimate, which is $1.0 \pm$
1322 0.4 GtC yr^{-1} in the DGVMs compared to $1.6 [0.4 \text{ to } 2.6] \text{ GtC yr}^{-1}$ in the atmospheric inversions (Figure 13,
1323 second row). We note that the range among inversions driven by OCO-2 satellite data is smaller though ($1.6 -$
1324 $2.2 \text{ GtC yr}^{-1} \text{ N}=6$), supporting the notion that northern extra-tropics land uptake was larger than suggested by the
1325 DGVMs at least in the 2015-2022 period covered by this data product.

1326 Discrepancies in the northern land fluxes conforms with persistent issues surrounding the quantification of the
1327 drivers of the global net land CO_2 flux (Arneeth et al., 2017; Huntzinger et al., 2017; O'Sullivan et al., 2022) and
1328 the distribution of atmosphere-to-land fluxes between the tropics and high northern latitudes (Baccini et al.,
1329 2017; Schimel et al., 2015; Stephens et al., 2007; Ciais et al., 2019; Gaubert et al., 2019).

1330 In the northern extra-tropics, the process models, inversions, and $f\text{CO}_2$ -products consistently suggest that most
1331 of the variability stems from the land (Figure 13). Inversions generally estimate similar interannual variations
1332 (IAV) over land to DGVMs (0.28-0.35 vs 0.8-0.64 GtC yr^{-1} , averaged over 1990-2022), and they have higher
1333 IAV in ocean fluxes (0.05-0.10 GtC yr^{-1}) relative to GOBMs (0.02-0.06 GtC yr^{-1} , Figure S2), and $f\text{CO}_2$ -
1334 products (0.03-0.10 GtC yr^{-1}).

1335 **3.8.2.2 Tropics**

1336 In the tropics (30°S-30°N), both the atmospheric inversions and process models estimate a net carbon balance
1337 ($\text{SoCEAN} + \text{SLAND} - \text{ELUC}$) that is close to neutral over the past decade. The GOBMs ($-0.03 \pm 0.24 \text{ GtC yr}^{-1}$), $f\text{CO}_2$ -
1338 products (0.2 [0.2, 0.3] GtC yr^{-1}), and inversion systems ($-0.3 [-0.1, 0.8] \text{ GtC yr}^{-1}$) all indicate an approximately
1339 neutral tropical ocean flux (see Figure S1 for spatial patterns). DGVMs indicate a net land sink ($\text{SLAND} - \text{ELUC}$) of
1340 $0.6 \pm 0.4 \text{ GtC yr}^{-1}$, whereas the inversion systems indicate a net land flux of $0.03 [-0.8, 1.1] \text{ GtC yr}^{-1}$, though with
1341 high uncertainty (Figure 13, third row).

1342 The tropical lands are the origin of most of the atmospheric CO_2 interannual variability (Ahlström et al., 2015),
1343 consistently among the process models and inversions (Figure 13). The interannual variability in the tropics is
1344 similar among the ocean $f\text{CO}_2$ -products (0.07-0.16 GtC yr^{-1}) and the GOBMs (0.07-0.16 GtC yr^{-1} ,
1345 Figure S2), which is the highest ocean sink variability of all regions. The DGVMs and inversions indicate that
1346 atmosphere-to-land CO_2 fluxes are more variable than atmosphere-to-ocean CO_2 fluxes in the tropics, with
1347 interannual variability of 0.35 to 1.61 and 0.77-0.92 GtC yr^{-1} for DGVMs and inversions, respectively.

1348 **3.8.2.3 South**

1349 In the southern extra-tropics (south of 30°S), the atmospheric inversions suggest a net atmosphere-to-surface
1350 sink ($\text{SoCEAN} + \text{SLAND} - \text{ELUC}$) for 2013-2022 of $1.5 [1.2, 1.9] \text{ GtC yr}^{-1}$, slightly higher than the process models'
1351 estimate of $1.5 \pm 0.4 \text{ GtC yr}^{-1}$ (Figure 13). An approximately neutral net land flux ($\text{SLAND} - \text{ELUC}$) for the southern
1352 extra-tropics is estimated by both the DGVMs ($0.05 \pm 0.07 \text{ GtC yr}^{-1}$) and the inversion systems (sink of $0.02 [-$
1353 $0.2, 0.2] \text{ GtC yr}^{-1}$). This means nearly all carbon uptake is due to oceanic sinks south of 30°S. The Southern
1354 Ocean flux in the $f\text{CO}_2$ -products ($1.6 [1.3, 1.7] \text{ GtC yr}^{-1}$) and inversion estimates ($1.5 [1.3, 1.9] \text{ GtCyr}^{-1}$) is
1355 slightly higher than in the GOBMs ($1.4 \pm 0.3 \text{ GtC yr}^{-1}$) (Figure 13, bottom row). This discrepancy in the mean
1356 flux is smaller this year than in previous releases due to the change in data set of the regional distribution of the
1357 river flux adjustment applied to $f\text{CO}_2$ -products and inverse systems to isolate the anthropogenic SoCEAN flux.
1358 The data set used (Lacroix et al., 2020) has less river-induced carbon outgassing in the Southern Ocean than the
1359 previously used data set (Aumont et al., 2001). Nevertheless, the time-series of atmospheric inversions and
1360 $f\text{CO}_2$ -products diverge from the GOBMs. A substantial overestimation of the trends in the $f\text{CO}_2$ -products could
1361 be explained by sparse and unevenly distributed observations, especially in wintertime (Figure S1; Hauck et al.,
1362 2023; Gloege et al., 2021). Model biases may contribute as well, with biases in mode water formation,
1363 stratification, and the chemical buffer capacity known to play a role in Earth System Models (Terhaar et al.,
1364 2021, Bourgeois et al., 2022, Terhaar et al., 2022).

1365 The interannual variability in the southern extra-tropics is low because of the dominance of ocean areas with
1366 low variability compared to land areas. The split between land ($S_{\text{LAND-ELUC}}$) and ocean (S_{OCEAN}) shows a
1367 substantial contribution to variability in the south coming from the land, with no consistency between the
1368 DGVMs and the inversions or among inversions. This is expected due to the difficulty of separating exactly the
1369 land and oceanic fluxes when viewed from atmospheric observations alone. The S_{OCEAN} interannual variability
1370 was found to be higher in the $f\text{CO}_2$ -products (0.04-0.18 GtC yr⁻¹) compared to GOBMs (0.03 to 0.06 GtC yr⁻¹)
1371 in 1990-2022 (Figure S2). Model subsampling experiments recently illustrated that $f\text{CO}_2$ -products may
1372 overestimate decadal variability in the Southern Ocean carbon sink by 30% and the trend since 2000 by 50-
1373 130% due to data sparsity, based on one and two $f\text{CO}_2$ -products with strong variability (Gloege et al., 2021,
1374 Hauck et al., 2023).

1375 **3.8.2.4 RECCAP2 regions**

1376 Aligning with the RECCAP-2 initiative (Ciais et al., 2022; Poulter et al., 2022; DeVries et al., 2023), we
1377 provide a breakdown of this GCB paper estimate of the E_{LUC} , S_{LAND} , Net land ($S_{\text{LAND}} - E_{\text{LUC}}$), and S_{OCEAN} fluxes
1378 over the 10 land, and 5 ocean RECCAP-2 regions, averaged over the period 2013-2022. The DGVMs and
1379 inversions suggest a positive net land sink in all regions, except for South America and Africa, where the
1380 inversions indicate a small net source of respectively -0.1 [-0.5, 0.3] GtC yr⁻¹ and -0.3 [-0.6, -0.1] GtC yr⁻¹,
1381 compared to a small sink of 0.1 ± 0.3 GtC yr⁻¹ and 0.3 ± 0.2 GtC yr⁻¹ for the DGVMs. However, for South
1382 America, there is substantial uncertainty in both products (ensembles span zero). For the DGVMs, this is driven
1383 by uncertainty in both S_{LAND} (0.6 ± 0.5 GtC yr⁻¹) and E_{LUC} (0.4 ± 0.2 GtC yr⁻¹). The bookkeeping models also
1384 suggest an E_{LUC} source of around 0.4 GtC yr⁻¹ in South America and Africa, in line with the DGVMs estimates.
1385 Bookkeeping models and DGVMs similarly estimate a source of 0.4 GtC yr⁻¹ in Southeast Asia, with DGVMs
1386 suggesting a near neutral net land sink (0.03 ± 0.12 GtC yr⁻¹). This contrasts with the inversion estimate of a 0.2
1387 [-0.3, 0.6] GtC yr⁻¹ sink, although the inversions spread is substantial. The inversions suggest the largest net
1388 land sinks are located in North America (0.5 [-0.1, 0.8] GtC yr⁻¹), Russia (0.7 [0.5, 1.1] GtC yr⁻¹), and East Asia
1389 (0.3 [0.0, 0.9] GtC yr⁻¹). This agrees well with the DGVMs in North America (0.4 ± 0.2 GtC yr⁻¹), which
1390 indicate a large natural land sink (S_{LAND}) of 0.6 ± 0.2 GtC yr⁻¹, being slightly reduced by land-use related carbon
1391 losses (0.2 ± 0.1 GtC yr⁻¹). The DGVMs suggest a smaller net land sink in Russia compared to inversions
1392 (0.4 ± 0.2 GtC yr⁻¹), and a similar net sink in East Asia (0.2 ± 0.1 GtC yr⁻¹).

1393 There is generally a higher level of agreement in the estimates of regional S_{OCEAN} between the different data
1394 streams (GOBMs, $f\text{CO}_2$ -products and atmospheric inversions) on decadal scale, compared to the agreement
1395 between the different land flux estimates. All data streams agree that the largest contribution to S_{OCEAN} stems
1396 from the Southern Ocean due to a combination of high flux density and large surface area, but with important
1397 contributions also from the Atlantic (high flux density) and Pacific (large area) basins. In the Southern Ocean,
1398 GOBMs suggest a sink of 1.0 ± 0.3 GtC yr⁻¹, in line with the $f\text{CO}_2$ -products (1.1 [0.9, 1.2] GtC yr⁻¹) and
1399 atmospheric inversions (1.0 [0.8, 1.4] GtC yr⁻¹). There is similar agreement in the Pacific Ocean, with GOBMs,

1400 $f\text{CO}_2$ -products, and atmospheric inversions indicating a sink of $0.5 \pm 0.1 \text{ GtC yr}^{-1}$, $0.7 [0.5, 0.9] \text{ GtC yr}^{-1}$, and
1401 $0.6 [0.2, 1.0] \text{ GtC yr}^{-1}$, respectively. However, in the Atlantic Ocean, GOBMs simulate a sink of $0.5 \pm 0.1 \text{ GtC}$
1402 yr^{-1} , noticeably lower than both the $f\text{CO}_2$ -products ($0.8 [0.7, 0.9] \text{ GtC yr}^{-1}$) and atmospheric inversions (0.8
1403 $[0.5, 1.2] \text{ GtC yr}^{-1}$). It is important to note the $f\text{CO}_2$ -products and atmospheric inversions have a substantial and
1404 uncertain river flux adjustment in the Atlantic Ocean (0.3 GtC yr^{-1}) that also leads to a mean offset between
1405 GOBMs and $f\text{CO}_2$ -products/inversions in the latitude band of the tropics (Figure 13). The Indian Ocean due its
1406 smaller size and the Arctic Ocean due to its size and sea-ice cover that prevents air-sea gas-exchange are
1407 responsible for smaller but non negligible S_{OCEAN} fluxes (Indian Ocean: ($0.3 [0.2, 0.4] \text{ GtC yr}^{-1}$, $0.3 [0.3, 0.4]$
1408 GtC yr^{-1} , and $0.4 [0.3, 0.6] \text{ GtC yr}^{-1}$ for GOBMs, $f\text{CO}_2$ -products, and atmospheric inversions, respectively, and
1409 Arctic Ocean: ($0.1 [0.1, 0.1] \text{ GtC yr}^{-1}$, $0.2 [0.2, 0.2] \text{ GtC yr}^{-1}$, and $0.1 [0.1, 0.1] \text{ GtC yr}^{-1}$ for GOBMs, $f\text{CO}_2$ -
1410 products, and atmospheric inversions, respectively). Note that the S_{OCEAN} numbers presented here deviate from
1411 numbers reported in RECCAP-2 where the net air-sea CO_2 flux is reported (i.e. without river flux adjustment for
1412 $f\text{CO}_2$ -products and inversions, and with river flux adjustment subtracted from GOBMs in most chapters, or
1413 comparing unadjusted data sets with discussion of uncertain regional riverine fluxes as major uncertainty, e.g.
1414 Sarma et al., 2023, DeVries et al., 2023).

1415 **3.8.2.5 Tropical vs northern land uptake**

1416 A continuing conundrum is the partitioning of the global atmosphere-land flux between the northern hemisphere
1417 land and the tropical land (Stephens et al., 2017; Pan et al., 2011; Gaubert et al., 2019). It is of importance
1418 because each region has its own history of land-use change, climate drivers, and impact of increasing
1419 atmospheric CO_2 and nitrogen deposition. Quantifying the magnitude of each sink is a prerequisite to
1420 understanding how each individual driver impacts the tropical and mid/high-latitude carbon balance.

1421 We define the North-South (N-S) difference as net atmosphere-land flux north of 30°N minus the net
1422 atmosphere-land flux south of 30°N . For the inversions, the N-S difference ranges from -0.5 GtC yr^{-1} to $+3.0$
1423 GtC yr^{-1} across this year's inversion ensemble, but with a clear cluster of solutions driven by the OCO-2 satellite
1424 product with a NH land sink of $1.6\text{-}2.2 \text{ GtC yr}^{-1}$, along with a tropical land flux of -0.6 to $+0.2 \text{ GtC yr}^{-1}$, and a
1425 dipole between $+1.4$ and $+2.8 \text{ GtC yr}^{-1}$ for the period 2015-2022. Whether this tighter clustering relative to the
1426 surface-observation based inversions is driven by (a) additional information on tropical fluxes delivered by
1427 tropical retrievals contained in OCO-2, (b) a tighter constraint on the NH land sink from that same product, or
1428 (c) a reduced sensitivity to vertical transport differences between models when using CO_2 column integrals,
1429 requires further investigation.

1430 In the ensemble of DGVMs the N-S difference is $0.5 \pm 0.6 \text{ GtC yr}^{-1}$, a much narrower range than the one from
1431 atmospheric inversions. Five DGVMs have a N-S difference larger than 1.0 GtC yr^{-1} , compared to only two
1432 from last year's ensemble. This is still only 25% of DGVMs, compared to most inversion systems simulating a
1433 difference at least this large. The smaller spread across DGVMs than across inversions is to be expected as there
1434 is no correlation between Northern and Tropical land sinks in the DGVMs as opposed to the inversions where

1435 the sum of the two regions being well-constrained by atmospheric observations leads to an anti-correlation
1436 between these two regions. This atmospheric N-S gradient could be used as an additional way to evaluate
1437 tropical and NH uptake in DGVMs, if their fluxes were combined with multiple transport models. Vice versa,
1438 the much smaller spread in the N-S difference between the DGVMs could help to scrutinise the inverse systems
1439 further. For example, a large northern land sink and a tropical land source in an inversion would suggest a large
1440 sensitivity to CO₂ fertilisation (the dominant factor driving the land sinks) for Northern ecosystems, which
1441 would be not mirrored by tropical ecosystems. Such a combination could be hard to reconcile with the process
1442 understanding gained from the DGVM ensembles and independent measurements (e.g. Free Air CO₂
1443 Enrichment experiments).

1444 **3.8.3 Fire Emissions in 2023**

1445 Fire emissions so far in 2023 have been above the average of recent decades, due to an extreme wildfire season
1446 in North America. Figure S9 shows global and regional emissions estimates for the period 1st Jan-30th
1447 September in each year 2003-2023. Estimates derive from two global fire emissions products: the global fire
1448 emissions database (GFED, version 4.1s; van der Werf et al., 2017), and the global fire assimilation system
1449 (GFAS, operated by the Copernicus Atmosphere Service; Di Giuseppe et al., 2018). The two products estimate
1450 that global emissions from fires were 1.9-2.3 GtC yr⁻¹ during January-October 2023. These estimates are 19-
1451 33% above the 2013-2022 average for the same months (1.6-1.7 GtC yr⁻¹) and 10-28% above the 2003-2022
1452 average (1.8 GtC yr⁻¹ in both products).

1453 The above-average global fire emissions during January-October 2023 have occurred despite below-average fire
1454 emissions from major source regions. On average during 2013-2022, 75-80% of global fire emissions through
1455 October occur in the tropics (1.2-1.4 GtC yr⁻¹) and around 41-48% of global fire emissions through October
1456 occur in Africa (0.7-0.8 GtC yr⁻¹). This year, through October, fire emissions in the tropics were approximately
1457 equal to the 2013-2022 average and 7-9% below the 2003-2022 average, while in Africa the fire emissions were
1458 approximately equal to the 2013-2022 average and 4-13% below the 2003-2022 average.

1459 In contrast, fire emissions from the Northern extra-tropics so far in 2023 have exceeded the values of all
1460 previous years. Northern extra-tropical fire emissions during January-October 2023 (0.7-0.9 GtC yr⁻¹) were 84-
1461 183% above the average for the same months in 2013-2022 (0.3-0.4 GtC yr⁻¹) and 76-190% above the average
1462 for the same months in 2003-2022 (0.3-0.4 GtC yr⁻¹). Fire emissions in North America alone (0.5-0.8 GtC yr⁻¹)
1463 were 239-438% above the average of 2013-2022 (0.2 GtC yr⁻¹ for both products) and 215-410% above the
1464 average for 2003-2022 (0.2 GtC yr⁻¹ for both products). Extreme fires in Canada were the largest contributor to
1465 the anomaly in 2023, with emissions reaching 0.5-0.8 GtC yr⁻¹ or 527-874% above the 2013-2022 average (0.1
1466 Gt C yr⁻¹ in both products) and 450-709% above the 2003-2022 average (0.1 Gt C yr⁻¹ in both products).

1467 While the fire emission fluxes presented above point towards a highly unusual Northern Hemisphere fire season
1468 so far in 2023, we caution that the fluxes presented should not be compared directly with other fluxes of the
1469 budget (e.g. S_{LAND} or E_{LUC}) due to incompatibilities between the observable fire emission fluxes and what is
1470 quantified in the S_{LAND} and E_{LUC} components of the budget. The fire emission estimates from global fire

1471 products relate to all fire types that can be observed in Earth Observations (Giglio et al., 2018; Randerson et al.,
1472 2012; Kaiser et al., 2012), including (i) fires occurring as part of natural disturbance-recovery cycles that would
1473 also have occurred in the pre-industrial period (Yue et al., 2016; Keeley and Pausas, 2019; Zou et al., 2019), (ii)
1474 fires occurring above and beyond natural disturbance-recovery cycle due to changes in climate, CO₂ and N
1475 fertilisation and to an increased frequency of extreme drought and heatwave events (Abatzoglou et al., 2019;
1476 Jones et al., 2022; Zheng et al., 2021; Burton et al., 2023), and (iii) fires occurring in relation to land use and
1477 land use change, such as deforestation fires and agricultural fires (van der Werf et al., 2010; Magi et al., 2012).
1478 In the context of the global carbon budget, only the portion of fire emissions associated with (ii) should be
1479 included in the S_{LAND} component, and fire emissions associated with (iii) should already be accounted for in the
1480 E_{LUC} component. Emissions associated with (i) should not be included in the global carbon budget. It is not
1481 currently possible to derive specific estimates for fluxes (i), (ii), and (iii) using global fire emission products
1482 such as GFED or GFAS. In addition, the fire emissions estimates from global fire emissions products represent
1483 a gross flux of carbon to the atmosphere, whereas the S_{LAND} component of the budget is a net flux that should
1484 also include post-fire recovery fluxes. Even if emissions from fires of type (ii) could be separated from those of
1485 type (i), these fluxes may be partially or wholly offset in subsequent years by post-fire fluxes as vegetation
1486 recovers, sequestering carbon from the atmosphere to the terrestrial biosphere (Yue et al., 2016).

1487 **3.9 Closing the Global Carbon Cycle**

1488 **3.9.1 Partitioning of Cumulative Emissions and Sink Fluxes**

1489 The global carbon budget over the historical period (1850-2021) is shown in Figure 3.

1490 Emissions during the period 1850-2022 amounted to 695 ± 70 GtC and were partitioned among the atmosphere
1491 (280 ± 5 GtC; 40%), ocean (180 ± 35 GtC; 26%), and land (225 ± 55 GtC; 32%). The cumulative land sink is
1492 almost equal to the cumulative land-use emissions (220 ± 70 GtC), making the global land nearly neutral over
1493 the whole 1850-2022 period.

1494 The use of nearly independent estimates for the individual terms of the global carbon budget shows a cumulative
1495 budget imbalance of 15 GtC (2% of total emissions) during 1850-2022 (Figure 3, Table 8), which, if correct,
1496 suggests that emissions could be slightly too high by the same proportion (2%) or that the combined land and
1497 ocean sinks are slightly underestimated (by about 3%), although these are well within the uncertainty range of
1498 each component of the budget. Nevertheless, part of the imbalance could originate from the estimation of
1499 significant increase in E_{FOS} and E_{LUC} between the mid 1920s and the mid 1960s which is unmatched by a similar
1500 growth in atmospheric CO₂ concentration as recorded in ice cores (Figure 3). However, the known loss of
1501 additional sink capacity of 30-40 GtC (over the 1850-2020 period) due to reduced forest cover has not been
1502 accounted for in our method and would exacerbate the budget imbalance (see Section 2.10 and Supplement
1503 S.6.4).

1504 For the more recent 1960-2022 period where direct atmospheric CO₂ measurements are available, total
1505 emissions (E_{FOS} + E_{LUC}) amounted to 485 ± 50 GtC, of which 395 ± 20 GtC (82%) were caused by fossil CO₂

1506 emissions, and 90 ± 45 GtC (18%) by land-use change (Table 8). The total emissions were partitioned among
1507 the atmosphere (215 ± 5 GtC; 44%), ocean (125 ± 25 GtC; 25%), and the land (150 ± 35 GtC; 31%), with a near
1508 zero (-5 GtC) unattributed budget imbalance. All components except land-use change emissions have
1509 significantly grown since 1960, with important interannual variability in the growth rate in atmospheric CO₂
1510 concentration and in the land CO₂ sink (Figure 4), and some decadal variability in all terms (Table 7).
1511 Differences with previous budget releases are documented in Figure S5.

1512 The global carbon budget averaged over the last decade (2013-2022) is shown in Figure 2, Figure 14 (right
1513 panel) and Table 7. For this period, 88% of the total emissions ($E_{\text{FOS}} + E_{\text{LUC}}$) were from fossil CO₂ emissions
1514 (E_{FOS}), and 12% from land-use change (E_{LUC}). The total emissions were partitioned among the atmosphere
1515 (47%), ocean (26%) and land (31%), with a small unattributed budget imbalance ($\sim 4\%$). For single years, the
1516 budget imbalance can be larger (Figure 4). For 2022, the combination of our estimated sources (11.1 ± 0.9 GtC
1517 yr^{-1}) and sinks (11.2 ± 0.9 GtC yr^{-1}) leads to a B_{IM} of -0.09 GtC, suggesting a near closure of the global carbon
1518 budget, although there is relatively high uncertainty on B_{IM} (± 1.3 GtC for 2022) as this is calculated as the
1519 residual of the five budget terms.

1520 **3.9.2 Trend and Variability in the Carbon Budget Imbalance**

1521 The carbon budget imbalance (B_{IM} ; Eq. 1, Figure 4) quantifies the mismatch between the estimated total
1522 emissions and the estimated changes in the atmosphere, land, and ocean reservoirs. The budget imbalance from
1523 1960 to 2022 is very small (-3.0 GtC over the period, i.e. average of 0.05 GtC yr^{-1}) and shows no trend over the
1524 full time series (Figure 4e). The process models (GOBMs and DGVMs) and data-products have been selected to
1525 match observational constraints in the 1990s, but no further constraints have been applied to their representation
1526 of trend and variability. Therefore, the near-zero mean and trend in the budget imbalance is seen as evidence of
1527 a coherent community understanding of the emissions and their partitioning on those time scales (Figure 4).
1528 However, the budget imbalance shows substantial variability of the order of ± 1 GtC yr^{-1} , particularly over semi-
1529 decadal time scales, although most of the variability is within the uncertainty of the estimates. The positive
1530 carbon imbalance during the 1960s, and early 1990s, indicates that either the emissions were overestimated, or
1531 the sinks were underestimated during these periods. The reverse is true for the 1970s, and to a lesser extent for
1532 the 1980s and 2013-2022 period (Figure 4, Table 7).

1533 We cannot attribute the cause of the variability in the budget imbalance with our analysis, we only note that the
1534 budget imbalance is unlikely to be explained by errors or biases in the emissions alone because of its large semi-
1535 decadal variability component, a variability that is atypical of emissions and has not changed in the past 60 years
1536 despite a near tripling in emissions (Figure 4). Errors in S_{LAND} and S_{OCEAN} are more likely to be the main cause
1537 for the budget imbalance, especially on interannual to semi-decadal timescales. For example, underestimation of
1538 the S_{LAND} by DGVMs has been reported following the eruption of Mount Pinatubo in 1991 possibly due to
1539 missing responses to changes in diffuse radiation (Mercado et al., 2009). Although since GCB2021 we
1540 accounted for aerosol effects on solar radiation quantity and quality (diffuse vs direct), most DGVMs only used
1541 the former as input (i.e., total solar radiation) (Table S1). Thus, the ensemble mean may not capture the full

1542 effects of volcanic eruptions, i.e. associated with high light scattering sulphate aerosols, on the land carbon sink
1543 (O’Sullivan et al., 2021). DGVMs are suspected to overestimate the land sink in response to the wet decade of
1544 the 1970s (Sitch et al., 2008). Quasi-decadal variability in the ocean sink has also been reported, with all
1545 methods agreeing on a smaller than expected ocean CO₂ sink in the 1990s and a larger than expected sink in the
1546 2000s (Figure 10; Landschützer et al., 2016, DeVries et al., 2019, Hauck et al., 2020, McKinley et al., 2020,
1547 Gruber et al., 2023) and the climate-driven variability could be substantial but is not well constrained (DeVries
1548 et al., 2023, Müller et al., 2023). Errors in sink estimates could also be driven by errors in the climatic forcing
1549 data, particularly precipitation for S_{LAND} and wind for S_{OCEAN}. Also, the B_{IM} shows substantial departure from
1550 zero on yearly time scales (Figure 4e), highlighting unresolved variability of the carbon cycle, likely in the land
1551 sink (S_{LAND}), given its large year to year variability (Figure 4d and 8).

1552 Both the budget imbalance (B_{IM}, Table 7) and the residual land sink from the global budget (E_{FOS}+E_{ELUC}-G_{ATM}-
1553 S_{OCEAN}, Table 5) include an error term due to the inconsistencies that arises from combining E_{ELUC} from
1554 bookkeeping models with S_{LAND} from DGVMs, most notably the loss of additional sink capacity (see Section
1555 2.10 and Supplement S.6.4). Other differences include a better accounting of land use changes practices and
1556 processes in bookkeeping models than in DGVMs, or the bookkeeping models error of having present-day
1557 observed carbon densities fixed in the past. That the budget imbalance shows no clear trend towards larger
1558 values over time is an indication that these inconsistencies probably play a minor role compared to other errors
1559 in S_{LAND} or S_{OCEAN}.

1560 Although the budget imbalance is near zero for the recent decades, it could be due to a compensation of errors.
1561 We cannot exclude an overestimation of CO₂ emissions, particularly from land-use change, given their large
1562 uncertainty, as has been suggested elsewhere (Piao et al., 2018), and/or an underestimate of the sinks. A larger
1563 DGVM estimate of the atmosphere-land CO₂ flux (S_{LAND}-E_{ELUC}) over the extra-tropics would reconcile model
1564 results with inversion estimates for fluxes in the total land during the past decade (Figure 13; Table 5).
1565 Likewise, a larger S_{OCEAN} is also possible given the higher estimates from the fCO₂-products (see Section 3.6.2,
1566 Figure 10 and Figure 13), the underestimation of interior ocean anthropogenic carbon accumulation in the
1567 GOBMs (Section 3.6.5), and the recently suggested upward adjustments of the ocean carbon sink in Earth
1568 System Models (Terhaar et al., 2022), and in fCO₂-products, here related to a potential temperature bias and skin
1569 effects (Watson et al., 2020; Dong et al., 2022; Figure 10). If S_{OCEAN} were to be based on fCO₂-products alone,
1570 with all fCO₂-products including this adjustment, this would result in a 2013-2022 S_{OCEAN} of 3.7 GtC yr⁻¹ (Dong
1571 et al., 2022) or >3.9 GtC yr⁻¹ (Watson et al., 2020), i.e., outside of the range supported by the atmospheric
1572 inversions and with an implied negative B_{IM} of more than -1 GtC yr⁻¹ indicating that a closure of the budget
1573 could only be achieved with either anthropogenic emissions being significantly larger and/or the net land sink
1574 being substantially smaller than estimated here. A recent model study suggests that the skin effect is smaller
1575 (about 0.1 GtC yr⁻¹ or 5%) due to feedbacks with surface carbon concentration (Bellenger et al., 2023), which
1576 would nevertheless lead to a larger S_{OCEAN} even in the GOBMs. More integrated use of observations in the
1577 Global Carbon Budget, either on their own or for further constraining model results, should help resolve some of
1578 the budget imbalance (Peters et al., 2017).

1579 4 Tracking progress towards mitigation targets

1580 The average growth in global fossil CO₂ emissions peaked at nearly +3% per year during the 2000s, driven by
1581 the rapid growth in emissions in China. In the last decade, however, the global growth rate has slowly declined,
1582 reaching a low +0.5% per year over 2013-2022. While this slowdown in global fossil CO₂ emissions growth is
1583 welcome, global fossil CO₂ emissions continue to grow, far from the rapid emission decreases needed to be
1584 consistent with the temperature goals of the Paris Agreement.

1585 Since the 1990s, the average growth rate of fossil CO₂ emissions has continuously declined across the group of
1586 developed countries of the Organisation for Economic Co-operation and Development (OECD), with emissions
1587 peaking in around 2005 and now declining at around 1% yr⁻¹ (Le Quéré et al., 2021). In the decade 2013-2022,
1588 territorial fossil CO₂ emissions decreased significantly (at the 95% confidence level) in 26 countries/economies
1589 whose economies grew significantly : Belgium, Brazil, Czechia, Denmark, Estonia, Finland, France, Germany,
1590 Greece, Hong Kong, Israel, Italy, Jamaica, Japan, Luxembourg, Netherlands, Norway, Portugal, Romania,
1591 Slovenia, South Africa, Sweden, Switzerland, United Kingdom, USA, Zimbabwe (updated from Le Quéré et al.,
1592 2019). Altogether, these 26 countries emitted 2.7 GtC yr⁻¹ (10.0 GtCO₂ yr⁻¹) on average over the last decade,
1593 about 28% of world CO₂ fossil emissions. For comparison, 22 countries showed a significant decrease in
1594 territorial fossil CO₂ emissions over the previous decade (2003-2012). Figure 16 shows that the emission
1595 declines in the USA and the EU27 are primarily driven by slightly weaker economic growth in the last decade
1596 compared to the 1990s, sustained declines in energy per GDP (though, weakening in the USA), and sustained
1597 declines in CO₂ emissions per unit energy (decarbonisation) with a slight acceleration in the USA in the last
1598 decade.

1599 In contrast, fossil CO₂ emissions continue to grow in non-OECD countries, although the growth rate has slowed
1600 from more than 6% yr⁻¹ during the 2000s to less than 2% yr⁻¹ in the last decade. Representing 47% of non-
1601 OECD emissions in 2022, a large part of this slowdown is due to China, which has seen emissions growth
1602 decline from 9% yr⁻¹ in the 2000s to 1.6% yr⁻¹ in the last decade. Excluding China, non-OECD emissions grew
1603 at 3.1% yr⁻¹ in the 2000s compared to 1.5% yr⁻¹ in the last decade. China has had weaker economic growth in
1604 the 2000s compared to the 2010s and a higher decarbonisation rate from 2005 to 2015 comparable to the highs
1605 in the 1990s, though the decarbonisation rate has slowed considerably since 2016 (Figure 16). India and the rest
1606 of the world have strong economic growth that is not offset by decarbonisation or declines in energy per GDP,
1607 driving up fossil CO₂ emissions. Despite the high deployment of renewables in some countries (e.g., India),
1608 fossil energy sources continue to grow to meet growing energy demand (Le Quéré et al., 2019).

1609 Globally, fossil CO₂ emissions growth is slowing, and this is due in part to the emergence of climate policy
1610 (Eskander and Fankhauser 2020; Le Quere et al 2019) and technological change, which is leading to a shift from
1611 coal to gas and growth in renewable energies, and reduced expansion of coal capacity. At the aggregated global
1612 level, decarbonisation shows a strong and growing signal in the last decade, with smaller contributions from
1613 lower economic growth and declines in energy per GDP. Altogether, global emissions are still growing (average

1614 of 0.5% per year over the 2013-2022 decade), far from the reductions needed to meet the ambitious climate
1615 goals of the UNFCCC Paris agreement.

1616 This year we updated the remaining carbon budget (RCB) based on two studies, the IPCC AR6 (Canadell et al,
1617 2021) as used in GCB2022, and a recent revision of the IPCC AR6 estimates (Forster et al 2023, Lamboll et al.,
1618 2023). We update the RCB assessed by the IPCC AR6 (Canadell et al., 2021), accounting for the 2020 to 2023
1619 estimated emissions from fossil fuel combustion (E_{FOS}) and land use changes (E_{LUC}). From January 2024, the
1620 IPCC AR6 RCB (50% likelihood) for limiting global warming to 1.5°C, 1.7°C and 2°C is estimated to amount
1621 to 95, 190, and 325 GtC (340, 690, 1190 GtCO₂). The Forster et al. (2023) study proposed a significantly lower
1622 RCB than IPCC AR6, with the largest reduction being due to an update of the climate emulator (MAGICC)
1623 used to estimate the warming contribution of non-CO₂ agents, and to the warming (i.e. emissions) that occurred
1624 over the 2020-2022 period. We update the Forster et al., budget accounting for the 2023 estimated emissions
1625 from fossil fuel combustion (E_{FOS}) and land use changes (E_{LUC}). From January 2024, the Forster et al., (2023)
1626 RCB (50% likelihood) for limiting global warming to 1.5°C, 1.7°C and 2°C is estimated to amount to 55, 155,
1627 and 305 GtC (210, 560, 1110 GtCO₂), significantly smaller than the updated IPCC AR6 estimate. Both the
1628 original IPCC AR6 and Forster et al. (2023) estimates include an uncertainty due to the climate response to
1629 cumulative CO₂ emissions, which is reflected through the percent likelihood of exceeding the given temperature
1630 threshold, an additional uncertainty of 220GtCO₂ due to alternative non-CO₂ emission scenarios, and other
1631 sources of uncertainties (see Canadell et al., 2021). The two sets of estimates overlap when considering all
1632 uncertainties. The IPCC AR6 estimates have the advantage of a consensus building approach, while the Forster
1633 et al. (2023) estimates include significant update estimates but without the backing of the IPCC yet. Here, we
1634 take the average of our update of both IPCC AR6 and Forster et al. (2023) estimates, giving a remaining carbon
1635 (50% likelihood) for limiting global warming to 1.5°C, 1.7°C and 2°C of respectively 75, 175, and 315 GtC
1636 (275, 625, 1150 GtCO₂) starting from January 2024. We emphasise the large uncertainties, particularly when
1637 close to the global warming limit of 1.5°C. These 1.5°C, 1.7°C and 2°C average remaining carbon budgets
1638 correspond respectively to about 7, 15 and 28 years from the beginning of 2024, at the 2023 level of total
1639 anthropogenic CO₂ emissions. Reaching net-zero CO₂ emissions by 2050 entails cutting total anthropogenic
1640 CO₂ emissions by about 0.4 GtC (1.5 GtCO₂) each year on average, comparable to the decrease in E_{FOS}
1641 observed in 2020 during the COVID-19 pandemic. However, this would lead to cumulative emissions over
1642 2024-2050 of 150 GtC (550 GtCO₂), well above the remaining carbon budget of 75 GtC to limit global warming
1643 to 1.5°C, but still below the remaining budget of 175 GtC to limit warming to 1.7°C (in phase with the “well
1644 below 2°C” ambition of the Paris Agreement). Even reaching net zero CO₂ globally by 2040, which would
1645 require annual emissions cuts of 0.7 GtC (2.4 GtCO₂) on average, would still exceed the remaining carbon
1646 budget, with 95 GtC (350 GtCO₂) cumulative emissions over 2024-2050, unless the global emissions trajectory
1647 becomes net negative (i.e. more anthropogenic CO₂ sinks than emissions) after 2040.

1648 **5 Discussion**

1649 Each year when the global carbon budget is published, each flux component is updated for all previous years to
1650 consider corrections that are the result of further scrutiny and verification of the underlying data in the primary

1651 input data sets. Annual estimates may be updated with improvements in data quality and timeliness (e.g., to
1652 eliminate the need for extrapolation of forcing data such as land-use). Of all terms in the global budget, only the
1653 fossil CO₂ emissions and the growth rate in atmospheric CO₂ concentration are based primarily on empirical
1654 inputs supporting annual estimates in this carbon budget. The carbon budget imbalance, yet an imperfect
1655 measure, provides a strong indication of the limitations in observations, in understanding and representing
1656 processes in models, and/or in the integration of the carbon budget components.

1657 The persistent unexplained variability in the carbon budget imbalance limits our ability to verify reported
1658 emissions (Peters et al., 2017) and suggests we do not yet have a complete understanding of the underlying
1659 carbon cycle dynamics on annual to decadal timescales. Resolving most of this unexplained variability should
1660 be possible through different and complementary approaches. First, as intended with our annual updates, the
1661 imbalance as an error term should be reduced by improvements of individual components of the global carbon
1662 budget that follow from improving the underlying data and statistics and by improving the models through the
1663 resolution of some of the key uncertainties detailed in Table 10. Second, additional clues to the origin and
1664 processes responsible for the variability in the budget imbalance could be obtained through a closer scrutiny of
1665 carbon variability in light of other Earth system data (e.g., heat balance, water balance), and the use of a wider
1666 range of biogeochemical observations to better understand the land-ocean partitioning of the carbon imbalance
1667 such as the constraint from atmospheric oxygen included this year. Finally, additional information could also be
1668 obtained through better inclusion of process knowledge at the regional level, and through the introduction of
1669 inferred fluxes such as those based on satellite xCO₂ retrievals. The limit of the resolution of the carbon budget
1670 imbalance is yet unclear, but most certainly not yet reached given the possibilities for improvements that lie
1671 ahead.

1672 Estimates of global fossil CO₂ emissions from different datasets are in relatively good agreement when the
1673 different system boundaries of these datasets are considered (Andrew, 2020a). But while estimates of E_{FOS} are
1674 derived from reported activity data requiring much fewer complex transformations than some other components
1675 of the budget, uncertainties remain, and one reason for the apparently low variation between datasets is precisely
1676 the reliance on the same underlying reported energy data. The budget excludes some sources of fossil CO₂
1677 emissions, which available evidence suggests are relatively small (<1%). We have added emissions from lime
1678 production in China and the US, but these are still absent in most other non-Annex I countries, and before 1990
1679 in other Annex I countries.

1680 Estimates of E_{LUC} suffer from a range of intertwined issues, including the poor quality of historical land-cover
1681 and land-use change maps, the rudimentary representation of management processes in most models, and the
1682 confusion in methodologies and boundary conditions used across methods (e.g., Arneth et al., 2017; Pongratz et
1683 al., 2014, see also Supplement S.6.4 on the loss of sink capacity; Bastos et al., 2021). Uncertainties in current
1684 and historical carbon stocks in soils and vegetation also add uncertainty in the E_{LUC} estimates. Unless a major
1685 effort to resolve these issues is made, little progress is expected in the resolution of E_{LUC}. This is particularly
1686 concerning given the growing importance of E_{LUC} for climate mitigation strategies, and the large issues in the
1687 quantification of the cumulative emissions over the historical period that arise from large uncertainties in E_{LUC}.

1688 By adding the DGVMs estimates of CO₂ fluxes due to environmental change from countries' managed forest
1689 areas (part of S_{LAND} in this budget) to the budget E_{LUC} estimate, we successfully reconciled the large gap
1690 between our E_{LUC} estimate and the land use flux from NGHGs using the approach described in Grassi et al.
1691 (2021) for future scenarios and in Grassi et al. (2023) using data from the Global Carbon Budget 2021. The
1692 updated data presented here can be used as potential adjustment in the policy context, e.g., to help assess the
1693 collective countries' progress towards the goal of the Paris Agreement and avoiding double-accounting for the
1694 sink in managed forests. In the absence of this adjustment, collective progress would hence appear better than it
1695 is (Grassi et al., 2021). The application of this adjustment is also recommended in the UNFCCC Synthesis
1696 report for the first Global Stocktake (UNFCCC, 2022) whenever a comparison between LULUCF fluxes
1697 reported by countries and the global emission estimates of the IPCC is conducted. However, this adjustment
1698 should be seen as a short-term and pragmatic fix based on existing data, rather than a definitive solution to
1699 bridge the differences between global models and national inventories. Additional steps are needed to
1700 understand and reconcile the remaining differences, some of which are relevant at the country level (Grassi, et
1701 al., 2023, Schwingshackl, et al., 2022).

1702 The comparison of GOBMs, f CO₂-products, and inversions highlights substantial discrepancy in the temporal
1703 evolution of S_{OCEAN} in the Southern Ocean and northern high-latitudes (Figure 13, Hauck et al., 2023) and in the
1704 mean S_{OCEAN} in the tropics. A large part of the uncertainty in the mean fluxes stems from the regional
1705 distribution of the river flux adjustment term. The current distribution simulates the largest share of the
1706 outgassing to occur in the tropics (Lacroix et al., 2020) in contrast to the regional distribution previously used
1707 with the largest riverine outgassing flux south of 20°S (Aumont et al., 2001). The long-standing sparse data
1708 coverage of f CO₂ observations in the Southern compared to the Northern Hemisphere (e.g., Takahashi et al.,
1709 2009) continues to exist (Bakker et al., 2016, 2022, Figure S1) and to lead to substantially higher uncertainty in
1710 the S_{OCEAN} estimate for the Southern Hemisphere (Watson et al., 2020, Gloege et al., 2021, Hauck et al., 2023).
1711 This discrepancy, which also hampers model improvement, points to the need for increased high-quality f CO₂
1712 observations especially in the Southern Ocean. At the same time, model uncertainty is illustrated by the large
1713 spread of individual GOBM estimates (indicated by shading in Figure 13) and highlights the need for model
1714 improvement. The diverging trends in S_{OCEAN} from different methods is a matter of concern. Recent and on-
1715 going work suggests that the f CO₂-products may overestimate the trend (Hauck et al., 2023), though many
1716 products remain to be tested, whereas evidence is accumulating that GOBMs likely underestimate the mean flux
1717 (Section 3.6.2, Terhaar et al., 2022, DeVries et al., 2023, Müller et al., 2023). The independent constraint from
1718 atmospheric oxygen measurements is consistent within errors with the relatively larger ocean sink in the f CO₂-
1719 products. The assessment of the net land-atmosphere exchange from DGVMs and atmospheric inversions also
1720 shows substantial discrepancy, particularly for the estimate of the net land flux over the northern extra-tropic.
1721 This discrepancy highlights the difficulty to quantify complex processes (CO₂ fertilisation, nitrogen deposition
1722 and fertilisers, climate change and variability, land management, etc.) that collectively determine the net land
1723 CO₂ flux. Resolving the differences in the Northern Hemisphere land sink will require the consideration and
1724 inclusion of larger volumes of observations.

1725 We provide metrics for the evaluation of the ocean and land models and the atmospheric inversions (Figures B2
1726 to B4, Table S10). These metrics expand the use of observations in the global carbon budget, helping 1) to
1727 support improvements in the ocean and land carbon models that produce the sink estimates, and 2) to constrain
1728 the representation of key underlying processes in the models and to allocate the regional partitioning of the CO₂
1729 fluxes. The introduction of process-based metrics targeted to evaluate the simulation of SOCEAN in the ocean
1730 biogeochemistry models is an important addition to the evaluation based on ocean carbon observations. This is
1731 an initial step towards the introduction of a broader range of observations and more stringent model evaluation
1732 that we hope will support continued improvements in the annual estimates of the global carbon budget.

1733 We assessed before that a sustained decrease of –1% in global emissions could be detected at the 66%
1734 likelihood level after a decade only (Peters et al., 2017). Similarly, a change in behaviour of the land and/or
1735 ocean carbon sink would take as long to detect, and much longer if it emerges more slowly. To continue
1736 reducing the carbon imbalance on annual to decadal time scales, regionalising the carbon budget, and integrating
1737 multiple variables are powerful ways to shorten the detection limit and ensure the research community can
1738 rapidly identify issues of concern in the evolution of the global carbon cycle under the current rapid and
1739 unprecedented changing environmental conditions.

1740 **6 Conclusions**

1741 The estimation of global CO₂ emissions and sinks is a major effort by the carbon cycle research community that
1742 requires a careful compilation and synthesis of measurements, statistical estimates, and model results. The
1743 delivery of an annual carbon budget serves two purposes. First, there is a large demand for up-to-date
1744 information on the state of the anthropogenic perturbation of the climate system and its underpinning causes. A
1745 broad stakeholder community relies on the data sets associated with the annual carbon budget including
1746 scientists, policy makers, businesses, journalists, and non-governmental organisations engaged in adapting to
1747 and mitigating human-driven climate change. Second, over the last decades we have seen unprecedented
1748 changes in the human and biophysical environments (e.g., changes in the growth of fossil fuel emissions, impact
1749 of COVID-19 pandemic, Earth’s warming, and strength of the carbon sinks), which call for frequent
1750 assessments of the state of the planet, a better quantification of the causes of changes in the contemporary global
1751 carbon cycle, and an improved capacity to anticipate its evolution in the future. Building this scientific
1752 understanding to meet the extraordinary climate mitigation challenge requires frequent, robust, transparent, and
1753 traceable data sets and methods that can be scrutinised and replicated. This paper via ‘living data’ helps to keep
1754 track of new budget updates.

1755 **Data availability**

1756 The data presented here are made available in the belief that their wide dissemination will lead to greater
1757 understanding and new scientific insights of how the carbon cycle works, how humans are altering it, and how
1758 we can mitigate the resulting human-driven climate change. Full contact details and information on how to cite
1759 the data shown here are given at the top of each page in the accompanying database and summarised in Table 2.

1760 The accompanying database includes three Excel files organised in the following spreadsheets:

1761 File `Global_Carbon_Budget_2023v1.0.xlsx` includes the following:

- 1762 1. Summary
- 1763 2. The global carbon budget (1959-2022);
- 1764 3. The historical global carbon budget (1750-2022);
- 1765 4. Global CO₂ emissions from fossil fuels and cement production by fuel type, and the per-capita emissions
1766 (1850-2022);
- 1767 5. CO₂ emissions from land-use change from the individual bookkeeping models (1959-2022);
- 1768 6. Ocean CO₂ sink from the individual global ocean biogeochemistry models and f CO₂-products (1959-
1769 2022);
- 1770 7. Terrestrial CO₂ sink from the individual DGVMs (1959-2022);
- 1771 8. Cement carbonation CO₂ sink (1959-2022).

1772 File `National_Fossil_Carbon_Emissions_2023v1.0.xlsx` includes the following:

- 1773 1. Summary
- 1774 2. Territorial country CO₂ emissions from fossil fuels and cement production (1850-2022);
- 1775 3. Consumption country CO₂ emissions from fossil fuels and cement production and emissions transfer from
1776 the international trade of goods and services (1990-2020) using CDIAC/UNFCCC data as reference;
- 1777 4. Emissions transfers (Consumption minus territorial emissions; 1990-2020);
- 1778 5. Country definitions.

1779 File `National_LandUseChange_Carbon_Emissions_2023v1.0.xlsx` includes the following:

- 1780 1. Summary
- 1781 2. Territorial country CO₂ emissions from Land Use Change (1850-2022) from three bookkeeping models;

1782 All three spreadsheets are published by the Integrated Carbon Observation System (ICOS) Carbon Portal and
1783 are available at <https://doi.org/10.18160/GCP-2023> (Friedlingstein et al., 2023). National emissions data are also
1784 available on Zenodo (Andrew and Peters, 2022), from the Global Carbon Atlas
1785 (<http://www.globalcarbonatlas.org/>, last access: 9 November 2023) and from Our World in Data
1786 (<https://ourworldindata.org/co2-emissions>, last access: 9 November 2023).

1787 **Author contributions**

1788 PF, MO, MWJ, RMA, DCEB, JH, PL, CLQ, ITL, GPP, WP, JP, CSc, and SSi designed the study, conducted the
1789 analysis, and wrote the paper with input from JGC, PCi and RBJ. RMA, GPP and JIK produced the fossil CO₂
1790 emissions and their uncertainties and analysed the emissions data. MH and GMa provided fossil fuel emission
1791 data. JP, TGa, CSc and RAH provided the bookkeeping land-use change emissions with synthesis by JP and
1792 CSc. FJo provided peat drainage emission estimates. SSm and CMP provided the estimates of non-vegetation
1793 CDR fluxes. LBo, MCh, ÖG, NG, TI, TJ, LR, JS, RS, and HiT provided an update of the global ocean
1794 biogeochemical models, TTTC, DF, LG, YI, AJ, GMc, ChR, and JZ provided an update of the ocean *f*CO₂-data
1795 products, with synthesis on both streams by JH, PL and NMa. SRA, LBa, NRB, MB, MCr, KE, WE, RAF, TGk,
1796 AK, NL, DRM, SN, AO, AMO, TO, MEP, DP, KP, GR, AJS, CSw, ST, BT, EvO, RW, and CWR provided
1797 ocean *f*CO₂ measurements for the year 2022, with synthesis by DCEB and KMO. PA, DB, SF, JG, HJ, AKJ,
1798 EK, DK, JK, GMe, LM, PM, MO, BP, TLS, QS, HTi, WY, XYua, XYue, and SZ provided an update of the
1799 Dynamic Global Vegetation Models, with synthesis by SSi and MO. HL, RSA, MW, and PCa provided
1800 estimates of land and ocean sinks from Earth System Models, as well as a projection of the atmospheric growth
1801 rate for 2023. FC, ITL, NC, LF, ARJ, FJi, JL, ZJin, ZLiu, YN, CR, DY, and BZ provided an updated
1802 atmospheric inversion, WP, FC, and ITL developed the protocol and produced the synthesis and evaluation of
1803 the atmospheric inversions. RMA provided projections of the 2023 fossil emissions and atmospheric CO₂
1804 growth rate. PL provided the predictions of the 2023 ocean and land sinks. IBMB, LPC, GCH, KKG, TMR, and
1805 GRvdW provided forcing data for land-use change. FT and GG provided data for the land-use change NGHGI
1806 harmonisation. RK provided key atmospheric CO₂ data. EJM and RFK provided the atmospheric oxygen
1807 constraint on surface net carbon sinks. XL, PPT and MWJ provided the historical atmospheric CO₂
1808 concentration and growth rate. MO and NB produced the aerosol diffuse radiative forcing for the DGVMs. IH
1809 provided the climate forcing data for the DGVMs. ER provided the evaluation of the DGVMs. MWJ provided
1810 the emissions prior for use in the inversion systems. XD provided seasonal emissions data for most recent years
1811 for the emission prior. PF, MO and MWJ coordinated the effort, revised all figures, tables, text and numbers to
1812 ensure the update was clear from the 2022 edition and in line with the globalcarbonatlas.org.

1813 **Competing interests.**

1814 At least one of the (co-)authors is a member of the editorial board of Earth System Science Data

1815 **Acknowledgements**

1816 We thank all people and institutions who provided the data used in this global carbon budget 2023 and the Global
1817 Carbon Project members for their input throughout the development of this publication. We thank Nigel Hawtin
1818 for producing Figure 2 and Figure 15. We thank Alex Vermeulen and Hanna Ritchie for respectively hosting the
1819 Global Carbon Budget datasets on the ICOS portal and the Our World in Data website. We thank Ian G. C. Ashton,
1820 Sebastian Brune, Fatemeh Cheginig, Sam Ditkovsky, Christian Ethé, Amanda R. Fay, Lonneke Goddijn-Murphy,
1821 T. Holding, Yawen Kong, Fabrice Lacroix, Yi Liu, Damian Loher, Naiqing Pan, Paridhi Rustogi, Shijie Shu, J.
1822 D. Shutler, Richard Sims, Phillip Townsend, Jing Wang, Andrew J. Watson, and David K. Woolf for their
1823 involvement in the development, use and analysis of the models and data-products used here. We thank Toste
1824 Tanhua, Marcos Fontela, Claire Lo Monaco and Nicolas Metzl who contributed to the provision of surface ocean
1825 CO₂ observations for the year 2022 (see Table S6). We also thank Stephen D. Jones of the Ocean Thematic Centre
1826 of the EU Integrated Carbon Observation System (ICOS) Research Infrastructure, Eugene Burger of NOAA's
1827 Pacific Marine Environmental Laboratory and Alex Kozyr of NOAA's National Centers for Environmental
1828 Information, for their contribution to surface ocean CO₂ data and metadata management. This is PMEL
1829 contribution 5550. We thank the scientists, institutions, and funding agencies responsible for the collection and
1830 quality control of the data in SOCAT as well as the International Ocean Carbon Coordination Project (IOCCP),
1831 the Surface Ocean Lower Atmosphere Study (SOLAS) and the Integrated Marine Biosphere Research (IMBeR)
1832 program for their support. We thank Nadine Goris and Lavinia Patara for support in calculating observational
1833 ocean evaluation metrics. We thank Fortunat Joos, Samar Khatiwala and Timothy DeVries for providing historical
1834 atmospheric and ocean data. We thank data providers ObsPack GLOBALVIEWplus v8.0 and NRT v8.1 for
1835 atmospheric CO₂ observations. Ingrid T Lujikx and Wouter Peters thank the CarbonTracker Europe team at
1836 Wageningen University, including Remco de Kok, Joram Hooghiem, Linda Kooijmans and Auke van der Woude.
1837 Daniel Kennedy thanks all the scientists, software engineers, and administrators who contributed to the
1838 development of CESM2. Josefine Ghattas thanks the whole ORCHIDEE group. Ian Harris thanks the Japan
1839 Meteorological Agency (JMA) for producing the Japanese 55-year Reanalysis (JRA-55). Reinel Sospedra-
1840 Alfonso thanks Barbara Winter, Woosung Lee, and William J. Merryfield for their contribution to the preparation

1841 and production of CanESM5 runs. Patricia Cadule thanks Olivier Torres, Juliette Mignot, Didier Swingedouw,
1842 and Laurent Bopp for contributions to the IPSL-CM6-LR-ESMCO2 simulations. Yosuke Niwa thanks CSIRO,
1843 EC, EMPA, FMI, IPEN, JMA, LSCE, NCAR, NIES, NILU, NIWA, NOAA, SIO, and TU/NIPR for providing
1844 data for NISMON-CO2. Zhe Jin thanks Xiangjun Tian, Yilong Wang, Hongqin Zhang, Min Zhao, Tao Wang,
1845 Jinzhi Ding and Shilong Piao for their contributions to the GONGGA inversion system. Bo Zheng thanks Yawen
1846 Kong for running the THU inversion system. Frédéric Chevallier thanks Zoé Lloret who maintained the
1847 atmospheric transport model for the CAMS inversions. Frédéric Chevallier and Thi-Tuyet-Trang Chau thank
1848 Marion Gehlen for her contribution to the CMEMS-LSCE-FFNNv2 product. Lian Fang thanks Paul I. Palmer and
1849 acknowledges ongoing support from the National Centre for Earth Observation. Junjie Liu thanks the Jet
1850 Propulsion Laboratory, California Institute of Technology. Zhiqiang Liu thanks Ning Zeng, Yun Liu, Eugenia
1851 Kalnay, and Gassem Asrar for their contributions to the COLA system. Fei Jiang acknowledges ongoing support
1852 from Frontiers Science Center for Critical Earth Material Cycling, Nanjing University. Andy Jacobson thanks the
1853 team at NOAA GML, Boulder, Colorado, USA, who provided the CarbonTracker CT2022 and CT-NRT.v2023-
1854 3 results from the website at <http://carbontracker.noaa.gov>. Meike Becker and Are Olsen thank Sparebanken Vest
1855 / Agenda Vestlandet for their support for the observations on the Statsraad Lehmkuhl. Margot Cronin thanks
1856 Anthony English, Clynt Gregory and Gordon Furey (P&O Maritime Services), Tobias Steinhoff and Aodhan
1857 Fitzgerald (Marine Institute) for their support. Wiley Evans and Katie Pocock thank the Tula Foundation for
1858 funding support. Thanos Gkritzalis and the VLIZ ICOS team are thankful to the crew of the research vessel Simon
1859 Stevin for all the support and help they provide. Data providers Nicolas Metzl and Claire LoMonaco thank the
1860 French Institut National des Sciences de l'Univers (INSU), Institut Polaire français, Paul-Emile Victor(IPEV),
1861 Observatoire des sciences de l'univers Ecce-Terra (OSU at Sorbonne Université), Institut de recherche français
1862 sur les ressources marines (IFREMER), French Oceanographic Fleet (FOF) for the Marion Dufresne data set
1863 (<http://dx.doi.org/10.17600/18001858>). Bronte Tilbrook and Erik van Ooijen thank Australia's Integrated Marine
1864 Observing System (IMOS) for sourcing of CO₂ data. IMOS is enabled by the National Collaborative Research
1865 Infrastructure Strategy (NCRIS). FAOSTAT is funded by FAO member states through their contributions to the
1866 FAO Regular Programme, data contributions by national experts are greatly acknowledged. The views expressed
1867 in this paper are the authors' only and do not necessarily reflect those of FAO. Finally, we thank all funders who
1868 have supported the individual and joint contributions to this work (see details below), as well as the two
1869 anonymous reviewers of this manuscript, and the many researchers who have provided feedback.

1870 **Financial and computing support**

1871 This research was supported by the following sources of funding: Integrated Marine Observing System (IMOS)
1872 [Australia]; ICOS Flanders [Belgium]; Research Foundation Flanders (grant no. I001821N) [Belgium]; Tula
1873 Foundation [Canada]; Chinese Academy of Science Project for Young Scientists in Basic Research (Grant No.
1874 YSBR-037) [China]; National Key R&D Program of China (Grant No: 2020YFA0607504); National Natural
1875 Science Foundation (grant no. 42141020, 42275128) [China]; National Natural Science Foundation (grant no.
1876 42275128) [China]; National Natural Science Foundation (grant no. 41921005) [China]; Scientific Research Start-
1877 up Funds (grant no. QD2021024C) from Tsinghua Shenzhen International Graduate School [China]; Second
1878 Tibetan Plateau Scientific Expedition and Research Program (Grant: 2022QZKK0101) [China]; Young Elite
1879 Scientists Sponsorship Program by CAST (grant no. YESS20200135) [China]; Copernicus Atmosphere
1880 Monitoring Service, implemented by ECMWF (Grant: CAMS2 55) [EC]; Copernicus Marine Environment
1881 Monitoring Service, implemented by MOi (Grant: CAMS2 55) [EC]; H2020 (Horizon 2020) 4C (grant no.
1882 821003) [European Commission, EC]; H2020 ESM2025 – Earth System Models for the Future (grant no.
1883 101003536) [European Commission, EC]; H2020 EuroSea (grant no. 862626) [EC]; H2020 GEORGE (grant no.
1884 101094716) [EC]; H2020 JERICO-S3 (grant no. 871153) [EC]; ICOS France [France]; Institut de Recherche pour
1885 le Développement (IRD) [France]; Federal Ministry of Education and Research (BMBF) (grant no. 03F0885AL1)
1886 [Germany]; Federal Ministry of Education and Research, collaborative project C-SCOPE (Towards Marine
1887 Carbon Observations 2.0: Socializing, COncnecting, Perfecting and Expanding, project no. 03F0877A) [Germany];
1888 Helmholtz Association ATMO programme [Germany]; Helmholtz Association of German Research Centres
1889 (project MOSES; Modular Observation Solutions for Earth Systems) [Germany]; ICOS (Integrated Carbon
1890 Observation System) Germany [Germany]; Ludwig-Maximilians-University Munich, Department of Geography
1891 [Germany]; Marine Institute [Ireland]; Arctic Challenge for Sustainability phase II project (ArCS-II; grant no. JP-
1892 MXD1420318865) [Japan]; Environment Research and Technology Development Fund (grant no. JP-
1893 MEERF21S20800) [Japan]; Fundamental Research Funds for the Central Universities (Grant No:
1894 090414380031); Global Environmental Research Coordination System, Ministry of the Environment (grant no.
1895 E2252) [Japan]; Japan Meteorological Agency [Japan]; Ministry of Education, Culture, Sports, Science and
1896 Technology, MEXT program for the advanced studies of climate change projection (SENTAN) (grant numbers
1897 JPMXD0722680395, JPMXD0722681344) [Japan]; Ministry of Environment, Environmental Restoration and
1898 Conservation Agency, Environment Research and Technology Development Fund (grant no.

1899 JPMEERF21S20810) [Japan]; National Institute for Environmental Studies [Japan]; Research Council of Norway
1900 (N-ICOS-2, grant no. 296012) [Norway]; Swiss National Science Foundation (grant no. 200020-200511)
1901 [Switzerland]; National Centre for Atmospheric Science [UK]; NERC (Natural Environment Research Council)
1902 Independent Research Fellowship (NE/V01417X/1) [UK]; NERC (NE/R016518/1) [UK]; Royal Society (grant
1903 no. RP\R1\191063) [UK]; UK Research and Innovation (UKRI) for Horizon Europe (GreenFeedBack, grant no.
1904 10040851) [UK]; NASA Carbon Monitoring System program (80NSSC21K1059) [USA]; NASA OCO Science
1905 team program (80NM0018F0583) [USA]; National Center for Atmospheric Research (NCAR) cooperative
1906 agreement (NSF No. 1852977) [USA]; National Oceanic and Atmospheric Administration (NOAA) cooperative
1907 agreement (NA22OAR4320151) [USA]; National Science Foundation (NSF- 831361857) [USA]; NOAA
1908 (NA20OAR4320278) [USA]; NOAA Cooperative Agreement, Cooperative Institute for Climate, Ocean, &
1909 Ecosystem Studies (CIOCES; NA20OAR4320271) [USA]; NOAA Cooperative Agreement, Cooperative Institute
1910 for Marine and Atmospheric Studies (CIMAS) / University of Miami (NA20OAR4320472) [USA]; NOAA
1911 Global Ocean Monitoring and Observing Program (grant no. 100018302, 100007298, NA-03-AR4320179)
1912 [USA]; NOAA Ocean Acidification Program [USA]; National Science Foundation (OPP-1922922) [USA]. We
1913 also acknowledge support from the following computing facilities: Adapter Allocation Scheme from the National
1914 Computational Infrastructure (NCI) [Australia]; High-Performance Computing Center (HPCC) of Nanjing
1915 University [China]; GENCI -TGCC (A0130102201, A0130106328, A0140107732 and A0130107403) [France],
1916 CCRT awarded by CEA/DRF (CCRT2023-p24cheva) [France]; HPC cluster Aether at the University of Bremen,
1917 financed by DFG within the scope of the Excellence Initiative [Germany], the State of Baden-Württemberg,
1918 through bwHPC [Germany]; Earth Simulator (ES4) at JAMSTEC [Japan], JAMSTEC's Super Computer system
1919 [Japan], NIES supercomputer system [Japan], NIES (SX-Aurora) and MRI (FUJITSU Server PRIMERGY
1920 CX2550M5) [Japan]; ADA HPC cluster at the University of East Anglia [UK], UK CEDA JASMIN
1921 supercomputer [UK]; Cheyenne NCAR HPC resources managed by CISL (doi:10.5065/D6RX99HX) [USA].
1922
1923

1924 **References**

- 1925 Ahlström, A., Raupach, M. R., Schurgers, G., Smith, B., Arneth, A., Jung, M., Reichstein, M., Canadell, J. G.,
1926 Friedlingstein, P., Jain, A. K., Kato, E., Poulter, B., Sitch, S., Stocker, B. D., Viovy, N., Wang, Y. P., Wiltshire, A., Zaehle,
1927 S., and Zeng, N.: The dominant role of semi-arid ecosystems in the trend and variability of the land CO₂ sink, 348, 895–899,
1928 <https://doi.org/10.1126/science.aaa1668>, 2015.
- 1929 Amador-Jiménez, M., Millner, N., Palmer, C., Pennington, R. T., and Sileci, L.: The Unintended Impact of Colombia’s
1930 Covid-19 Lockdown on Forest Fires, *Environ Resource Econ*, 76, 1081–1105, <https://doi.org/10.1007/s10640-020-00501-5>,
1931 2020.
- 1932 Andela, N., Morton, D. C., Giglio, L., Chen, Y., van der Werf, G. R., Kasibhatla, P. S., DeFries, R. S., Collatz, G. J.,
1933 Hantson, S., Kloster, S., Bachelet, D., Forrest, M., Lasslop, G., Li, F., Mangeon, S., Melton, J. R., Yue, C., and Randerson, J.
1934 T.: A human-driven decline in global burned area, *Science*, 356, 1356–1362, <https://doi.org/10.1126/science.aal4108>, 2017.
- 1935 Andrew, R. M.: A comparison of estimates of global carbon dioxide emissions from fossil carbon sources, *Earth Syst. Sci.*
1936 *Data*, 12, 1437–1465, <https://doi.org/10.5194/essd-12-1437-2020>, 2020a.
- 1937 Andrew, R. M.: Timely estimates of India’s annual and monthly fossil CO₂ emissions, *Earth Syst. Sci. Data*, 12, 2411–2421,
1938 <https://doi.org/10.5194/essd-12-2411-2020>, 2020b.
- 1939 Andrew, R. M. and Peters, G. P.: The Global Carbon Project’s fossil CO₂ emissions dataset (2022v27), [https://doi.org/](https://doi.org/10.5281/zenodo.7215364)
1940 [10.5281/zenodo.7215364](https://doi.org/10.5281/zenodo.7215364), 2022.
- 1941 Angelsen, A. and Kaimowitz, D.: Rethinking the Causes of Deforestation: Lessons from Economic Models, *World Bank*
1942 *Res. Obs.*, 14, 73–98, <https://doi.org/10.1093/wbro/14.1.73>, 1999.
- 1943 Aragão, L. E. O. C., Anderson, L. O., Fonseca, M. G., Rosan, T. M., Vedovato, L. B., Wagner, F. H., Silva, C. V. J., Silva
1944 Junior, C. H. L., Arai, E., Aguiar, A. P., Barlow, J., Berenguer, E., Deeter, M. N., Domingues, L. G., Gatti, L., Gloor, M.,
1945 Malhi, Y., Marengo, J. A., Miller, J. B., Phillips, O. L., and Saatchi, S.: 21st Century drought-related fires counteract the
1946 decline of Amazon deforestation carbon emissions, *Nat Commun*, 9, 536, <https://doi.org/10.1038/s41467-017-02771-y>,
1947 2018.
- 1948 Archer, D., Eby, M., Brovkin, V., Ridgwell, A., Cao, L., Mikolajewicz, U., Caldeira, K., Matsumoto, K., Munhoven, G.,
1949 Montenegro, A., and Tokos, K.: Atmospheric Lifetime of Fossil Fuel Carbon Dioxide, *Annu. Rev. Earth Planet. Sci.*, 37,
1950 117–134, <https://doi.org/10.1146/annurev.earth.031208.100206>, 2009.
- 1951 Arneth, A., Sitch, S., Pongratz, J., Stocker, B. D., Ciais, P., Poulter, B., Bayer, A. D., Bondeau, A., Calle, L., Chini, L. P.,
1952 Gasser, T., Fader, M., Friedlingstein, P., Kato, E., Li, W., Lindeskog, M., Nabel, J. E. M. S., Pugh, T. A. M., Robertson, E.,
1953 Viovy, N., Yue, C., and Zaehle, S.: Historical carbon dioxide emissions caused by land-use changes are possibly larger than
1954 assumed, *Nature Geosci*, 10, 79–84, <https://doi.org/10.1038/ngeo2882>, 2017.
- 1955 Asaadi, A., Arora, V. K., Melton, J. R., and Bartlett, P.: An improved parameterization of leaf area index (LAI) seasonality
1956 in the Canadian Land Surface Scheme (CLASS) and Canadian Terrestrial Ecosystem Model (CTEM) modelling framework,
1957 15, 6885–6907, <https://doi.org/10.5194/bg-15-6885-2018>, 2018.

- 1958 Aumont, O., Orr, J. C., Monfray, P., Ludwig, W., Amiotte-Suchet, P., and Probst, J.-L.: Riverine-driven interhemispheric
1959 transport of carbon, *Global Biogeochem. Cycles*, 15, 393–405, <https://doi.org/10.1029/1999GB001238>, 2001.
- 1960 Aumont, O., Ethé, C., Tagliabue, A., Bopp, L., and Gehlen, M.: PISCES-v2: an ocean biogeochemical model for carbon and
1961 ecosystem studies, 8, 2465–2513, <https://doi.org/10.5194/gmd-8-2465-2015>, 2015.
- 1962 Baccini, A., Walker, W., Carvalho, L., Farina, M., Sulla-Menashe, D., and Houghton, R. A.: Tropical forests are a net carbon
1963 source based on aboveground measurements of gain and loss, *Science*, 358, 230–234,
1964 <https://doi.org/10.1126/science.aam5962>, 2017.
- 1965 Bakker, D. C. E., Pfeil, B., Landa, C. S., Metzl, N., O'Brien, K. M., Olsen, A., Smith, K., Cosca, C., Harasawa, S., Jones, S.
1966 D., Nakaoka, S., Nojiri, Y., Schuster, U., Steinhoff, T., Sweeney, C., Takahashi, T., Tilbrook, B., Wada, C., Wanninkhof, R.,
1967 Alin, S. R., Balestrini, C. F., Barbero, L., Bates, N. R., Bianchi, A. A., Bonou, F., Boutin, J., Bozec, Y., Burger, E. F., Cai,
1968 W.-J., Castle, R. D., Chen, L., Chierici, M., Currie, K., Evans, W., Featherstone, C., Feely, R. A., Fransson, A., Goyet, C.,
1969 Greenwood, N., Gregor, L., Hankin, S., Hardman-Mountford, N. J., Harlay, J., Hauck, J., Hoppema, M., Humphreys, M. P.,
1970 Hunt, C. W., Huss, B., Ibáñez, J. S. P., Johannessen, T., Keeling, R., Kitidis, V., Körtzinger, A., Kozyr, A., Krasakopoulou,
1971 E., Kuwata, A., Landschützer, P., Lauvset, S. K., Lefèvre, N., Lo Monaco, C., Manke, A., Mathis, J. T., Merlivat, L.,
1972 Millero, F. J., Monteiro, P. M. S., Munro, D. R., Murata, A., Newberger, T., Omar, A. M., Ono, T., Paterson, K., Pearce, D.,
1973 Pierrot, D., Robbins, L. L., Saito, S., Salisbury, J., Schlitzer, R., Schneider, B., Schweitzer, R., Sieger, R., Skjelvan, I.,
1974 Sullivan, K. F., Sutherland, S. C., Sutton, A. J., Tadokoro, K., Telszewski, M., Tuma, M., van Heuven, S. M. A. C.,
1975 Vandemark, D., Ward, B., Watson, A. J., and Xu, S.: A multi-decade record of high-quality CO₂ data in version 3 of the
1976 Surface Ocean CO₂ Atlas (SOCAT), *Earth Syst. Sci. Data*, 8, 383–413, <https://doi.org/10.5194/essd-8-383-2016>, 2016.
- 1977 Bakker, Dorothee C. E.; Alin, Simone R.; Bates, Nicholas; Becker, Meike; Feely, Richard A.; Gkritzalis, Thanos; Jones,
1978 Steve D.; Kozyr, Alex; Lauvset, Siv K.; Metzl, Nicolas; Munro, David R.; Nakaoka, Shin-ichiro; Nojiri, Yukihiko; O'Brien,
1979 Kevin M.; Olsen, Are; Pierrot, Denis; Rehder, Gregor; Steinhoff, Tobias; Sutton, Adrienne J.; Sweeney, Colm; Tilbrook,
1980 Bronte; Wada, Chisato; Wanninkhof, Rik; Akl, John; Barbero, Leticia; Beatty, Cory M.; Berghoff, Carla F.; Bittig, Henry
1981 C.; Bott, Randy; Burger, Eugene F.; Cai, Wei-Jun; Castaño-Primo, Rocío; Corredor, Jorge E.; Cronin, Margot; De Carlo,
1982 Eric H.; DeGrandpre, Michael D.; Dietrich, Colin; Drennan, William M.; Emerson, Steven R.; Enochs, Ian C.; Enyo,
1983 Kazutaka; Epherra, Lucía; Evans, Wiley; Fiedler, Björn; Fontela, Marcos; Frangoulis, Constantin; Gehrung, Martina;
1984 Giannoudi, Louisa; Glockzin, Michael; Hales, Burke; Howden, Stephan D.; Ibáñez, J. Severino P.; Kamb, Linus;
1985 Körtzinger, Arne; Lefèvre, Nathalie; Lo Monaco, Claire; Lutz, Vivian A.; Macovei, Vlad A.; Maenner Jones, Stacy;
1986 Manalang, Dana; Manzello, Derek P.; Metzl, Nicolas; Mickett, John; Millero, Frank J.; Monacci, Natalie M.; Morell, Julio
1987 M.; Musielewicz, Sylvia; Neill, Craig; Newberger, Tim; Newton, Jan; Noakes, Scott; Ólafsdóttir, Sólveig Rósa; Ono,
1988 Tsuneo; Osborne, John; Padín, Xose A.; Paulsen, Melf; Perivoliotis, Leonidas; Petersen, Wilhelm; Petihakis, George;
1989 Plueddemann, Albert J.; Rodriguez, Carmen; Rutgersson, Anna; Sabine, Christopher L.; Salisbury, Joseph E.; Schlitzer,
1990 Reiner; Skjelvan, Ingunn; Stamatakis, Natalia; Sullivan, Kevin F.; Sutherland, Stewart C.; T'Jampens, Michiel; Tadokoro,
1991 Kazuaki; Tanhua, Toste; Telszewski, Maciej; Theetaert, Hannelore; Tomlinson, Michael; Vandemark, Douglas; Velo,
1992 Antón; Voynova, Yoana G.; Weller, Robert A.; Whitehead, Chris; Wimart-Rousseau, Cathy (2023). Surface Ocean CO₂
1993 Atlas Database Version 2023 (SOCATv2023) (NCEI Accession 0278913). [indicate subset used]. NOAA National Centers
1994 for Environmental Information. Dataset. <https://doi.org/10.25921/r7xa-bt92>, 2023.
- 1995 Ballantyne, A. P., Alden, C. B., Miller, J. B., Tans, P. P., and White, J. W. C.: Increase in observed net carbon dioxide
1996 uptake by land and oceans during the past 50 years, *Nature*, 488, 70–72, <https://doi.org/10.1038/nature11299>, 2012.

- 1997 Ballantyne, A. P., Andres, R., Houghton, R., Stocker, B. D., Wanninkhof, R., Anderegg, W., Cooper, L. A., DeGrandpre,
1998 M., Tans, P. P., Miller, J. B., Alden, C., and White, J. W. C.: Audit of the global carbon budget: estimate errors and their
1999 impact on uptake uncertainty, *Biogeosciences*, 12, 2565–2584, <https://doi.org/10.5194/bg-12-2565-2015>, 2015.
- 2000 Bastos, A., Hartung, K., Nützel, T. B., Nabel, J. E. M. S., Houghton, R. A., and Pongratz, J.: Comparison of uncertainties in
2001 land-use change fluxes from bookkeeping model parameterisation, 12, 745–762, <https://doi.org/10.5194/esd-12-745-2021>,
2002 2021.
- 2003 Battle, M. O., Raynor, R., Kesler, S., and Keeling, R.: Technical Note: The impact of industrial activity on the amount of
2004 atmospheric O₂, *Atmospheric Chem. Phys. Discuss.*, 1–17, <https://doi.org/10.5194/acp-2022-765>, 2023.
- 2005 Beckman, J. and Countryman, A. M.: The Importance of Agriculture in the Economy: Impacts from COVID-19, *Am. J. Agr.*
2006 *Econ.*, 103, 1595–1611, <https://doi.org/10.1111/ajae.12212>, 2021.
- 2007 Bellenger, H., Bopp, L., Ethé, C., Ho, D., Duvel, J. P., Flavoni, S., Guez, L., Kataoka, T., Perrot, X., Parc, L., and Watanabe,
2008 M.: Sensitivity of the Global Ocean Carbon Sink to the Ocean Skin in a Climate Model, *J. Geophys. Res. Oceans*, 128,
2009 e2022JC019479, <https://doi.org/10.1029/2022JC019479>, 2023.
2010
- 2011 Bennington, V., Gloege, L., and McKinley, G. A.: Variability in the Global Ocean Carbon Sink From 1959 to 2020 by
2012 Correcting Models with Observations, *Geophys. Res. Lett.*, 49, e2022GL098632, <https://doi.org/10.1029/2022GL098632>,
2013 2022.
- 2014 Berthet, S., Sférian, R., Bricaud, C., Chevallier, M., Voldoire, A., and Ethé, C.: Evaluation of an Online Grid-Coarsening
2015 Algorithm in a Global Eddy-Admitting Ocean Biogeochemical Model, *J. Adv. Model Earth Sy.*, 11, 1759–1783,
2016 <https://doi.org/10.1029/2019MS001644>, 2019.
- 2017 Betts, R. A., Jones, C. D., Knight, J. R., Keeling, R. F., and Kennedy, J. J.: El Niño and a record CO₂ rise, *Nat. Clim.*
2018 *Change*, 6, 806–810, <https://doi.org/10.1038/nclimate3063>, 2016.
- 2019 Bloom, A. A. and Williams, M.: Constraining ecosystem carbon dynamics in a data-limited world: integrating ecological
2020 “common sense” in a model–data fusion framework, *Biogeosciences*, 12, 1299–1315, [https://doi.org/10.5194/bg-12-1299-](https://doi.org/10.5194/bg-12-1299-2015)
2021 2015, 2015.
2022
- 2023 Bloom, A. A., Exbrayat, J.-F., van der Velde, I. R., Feng, L., and Williams, M.: The decadal state of the terrestrial carbon
2024 cycle: Global retrievals of terrestrial carbon allocation, pools, and residence times, *Proc. Natl. Acad. Sci.*, 113, 1285–1290,
2025 <https://doi.org/10.1073/pnas.1515160113>, 2016.
2026
- 2027 Boer, G. J., Smith, D. M., Cassou, C., Doblus-Reyes, F., Danabasoglu, G., Kirtman, B., Kushnir, Y., Kimoto, M., Meehl, G.
2028 A., Msadek, R., Mueller, W. A., Taylor, K. E., Zwiers, F., Rixen, M., Ruprich-Robert, Y., and Eade, R.: The Decadal
2029 Climate Prediction Project (DCPP) contribution to CMIP6, *Geosci. Model Dev.*, 9, 3751–3777, [https://doi.org/10.5194/gmd-](https://doi.org/10.5194/gmd-9-3751-2016)
2030 9-3751-2016, 2016.
2031
- 2032 Boucher, O., Servonnat, J., Albright, A. L., Aumont, O., Balkanski, Y., Bastrikov, V., Bekki, S., Bonnet, R., Bony, S., Bopp,
2033 L., Braconnot, P., Brockmann, P., Cadule, P., Caubel, A., Cheruy, F., Codron, F., Cozic, A., Cugnet, D., D’Andrea, F.,
2034 Davini, P., de Lavergne, C., Denvil, S., Deshayes, J., Devilliers, M., Ducharne, A., Dufresne, J.-L., Dupont, E., Éthé, C.,
2035 Fairhead, L., Falletti, L., Flavoni, S., Foujols, M.-A., Gardoll, S., Gastineau, G., Ghattas, J., Grandpeix, J.-Y., Guenet, B.,

- 2036 Guez, E., Lionel, Guilyardi, E., Guimberteau, M., Hauglustaine, D., Hourdin, F., Idelkadi, A., Joussaume, S., Kageyama, M.,
 2037 Khodri, M., Krinner, G., Lebas, N., Levavasseur, G., Lévy, C., Li, L., Lott, F., Lurton, T., Luyssaert, S., Madec, G.,
 2038 Madeleine, J.-B., Maignan, F., Marchand, M., Marti, O., Mellul, L., Meurdesoif, Y., Mignot, J., Musat, I., Ottlé, C., Peylin,
 2039 P., Planton, Y., Polcher, J., Rio, C., Rochetin, N., Rousset, C., Sepulchre, P., Sima, A., Swingedouw, D., Thiéblemont, R.,
 2040 Traore, A. K., Vancoppenolle, M., Vial, J., Vialard, J., Viovy, N., and Vuichard, N.: Presentation and Evaluation of the
 2041 IPSL-CM6A-LR Climate Model, *J. Adv. Model. Earth Syst.*, 12, e2019MS002010, <https://doi.org/10.1029/2019MS002010>,
 2042 2020.
- 2043 Bourgeois, T., Goris, N., Schwinger, J., and Tjiputra, J. F.: Stratification constrains future heat and carbon uptake in the
 2044 Southern Ocean between 30°S and 55°S, *Nat. Commun.*, 13, 340, <https://doi.org/10.1038/s41467-022-27979-5>, 2022.
- 2045 Bray, E.: 2017 Minerals Yearbook: Aluminum [Advance Release], Tech. rep., U.S. Geological Survey, [https://d9-wret.s3-us-](https://d9-wret.s3-us-west-2.amazonaws.com/assets/palladium/production/atoms/files/myb1-2017-alumi.pdf)
 2046 [west-2.amazonaws.com/assets/palladium/production/atoms/files/myb1-2017-alumi.pdf](https://d9-wret.s3-us-west-2.amazonaws.com/assets/palladium/production/atoms/files/myb1-2017-alumi.pdf), 2020.
- 2047 Brancalion, P. H. S., Broadbent, E. N., de-Miguel, S., Cardil, A., Rosa, M. R., Almeida, C. T., Almeida, D. R. A.,
 2048 Chakravarty, S., Zhou, M., Gamarra, J. G. P., Liang, J., Crouzeilles, R., Hérault, B., Aragão, L. E. O. C., Silva, C. A., and
 2049 Almeyda-Zambrano, A. M.: Emerging threats linking tropical deforestation and the COVID-19 pandemic, *Perspectives in*
 2050 *Ecology and Conservation*, 18, 243–246, <https://doi.org/10.1016/j.pecon.2020.09.006>, 2020.
- 2051 Brienens, R. J. W., Caldwell, L., Duchesne, L., Voelker, S., Barichivich, J., Baliva, M., Ceccantini, G., Di Filippo, A.,
 2052 Helama, S., Locosselli, G. M., Lopez, L., Piovesan, G., Schöngart, J., Villalba, R., and Gloor, E.: Forest carbon sink
 2053 neutralized by pervasive growth-lifespan trade-offs, *Nat. Commun.*, 11, 4241, <https://doi.org/10.1038/s41467-020-17966-z>,
 2054 2020.
- 2055 Brienens, R. J. W., Phillips, O. L., Feldpausch, T. R., Gloor, E., Baker, T. R., Lloyd, J., Lopez-Gonzalez, G., Monteagudo-
 2056 Mendoza, A., Malhi, Y., Lewis, S. L., Vásquez Martínez, R., Alexiades, M., Álvarez Dávila, E., Alvarez-Loayza, P.,
 2057 Andrade, A., Aragão, L. E. O. C., Araujo-Murakami, A., Arets, E. J. M. M., Arroyo, L., Aymard C., G. A., Bánki, O. S.,
 2058 Baraloto, C., Barroso, J., Bonal, D., Boot, R. G. A., Camargo, J. L. C., Castilho, C. V., Chama, V., Chao, K. J., Chave, J.,
 2059 Comiskey, J. A., Cornejo Valverde, F., da Costa, L., de Oliveira, E. A., Di Fiore, A., Erwin, T. L., Fauset, S., Forsthofer, M.,
 2060 Galbraith, D. R., Grahame, E. S., Groot, N., Hérault, B., Higuchi, N., Honorio Coronado, E. N., Keeling, H., Killeen, T. J.,
 2061 Laurance, W. F., Laurance, S., Licona, J., Magnussen, W. E., Marimon, B. S., Marimon-Junior, B. H., Mendoza, C., Neill,
 2062 D. A., Nogueira, E. M., Núñez, P., Pallqui Camacho, N. C., Parada, A., Pardo-Molina, G., Peacock, J., Peña-Claros, M.,
 2063 Pickavance, G. C., Pitman, N. C. A., Poorter, L., Prieto, A., Quesada, C. A., Ramírez, F., Ramírez-Angulo, H., Restrepo, Z.,
 2064 Roopsind, A., Rudas, A., Salomão, R. P., Schwarz, M., Silva, N., Silva-Espejo, J. E., Silveira, M., Stropp, J., Talbot, J., ter
 2065 Steege, H., Teran-Aguilar, J., Terborgh, J., Thomas-Caesar, R., Toledo, M., Torello-Raventos, M., Umetsu, R. K., van der
 2066 Heijden, G. M. F., van der Hout, P., Guimarães Vieira, I. C., Vieira, S. A., Vilanova, E., Vos, V. A., and Zagt, R. J.: Long-
 2067 term decline of the Amazon carbon sink, 519, 344–348, <https://doi.org/10.1038/nature14283>, 2015.
- 2068 Bronselaer, B., Winton, M., Russell, J., Sabine, C. L., and Khatiwala, S.: Agreement of CMIP5 Simulated and Observed
 2069 Ocean Anthropogenic CO₂ Uptake, *Geophys. Res. Lett.*, 44, 12,298–12,305, <https://doi.org/10.1002/2017GL074435>, 2017.
- 2070 Bruno, M. and Joos, F.: Terrestrial carbon storage during the past 200 years: A Monte Carlo Analysis of CO₂ data from ice
 2071 core and atmospheric measurements, *Global Biogeochem. Cycles*, 11, 111–124, <https://doi.org/10.1029/96GB03611>, 1997.

2072 Burrows, S. M., Maltrud, M., Yang, X., Zhu, Q., Jeffery, N., Shi, X., Ricciuto, D., Wang, S., Bisht, G., Tang, J., Wolfe, J.,
2073 Harrop, B. E., Singh, B., Brent, L., Baldwin, S., Zhou, T., Cameron-Smith, P., Keen, N., Collier, N., Xu, M., Hunke, E. C.,
2074 Elliott, S. M., Turner, A. K., Li, H., Wang, H., Golaz, J.-C., Bond-Lamberty, B., Hoffman, F. M., Riley, W. J., Thornton, P.
2075 E., Calvin, K., and Leung, L. R.: The DOE E3SM v1.1 Biogeochemistry Configuration: Description and Simulated
2076 Ecosystem-Climate Responses to Historical Changes in Forcing, *J. Adv. Model. Earth Syst.*, 12, e2019MS001766,
2077 <https://doi.org/10.1029/2019MS001766>, 2020.

2078 Burton, C., Betts, R., Cardoso, M., Feldpausch, T. R., Harper, A., Jones, C. D., Kelley, D. I., Robertson, E., and Wiltshire,
2079 A.: Representation of fire, land-use change and vegetation dynamics in the Joint UK Land Environment Simulator vn4.9
2080 (JULES), *Geosci. Model Dev.*, 12, 179–193, <https://doi.org/10.5194/gmd-12-179-2019>, 2019.

2081 Burton, C. et al.: Global burned area increasingly explained by climate change, *under review*,
2082 <https://doi.org/10.21203/rs.3.rs-3168150/v1>, 2023.

2083 Bushinsky, S. M., Landschützer, P., Rödenbeck, C., Gray, A. R., Baker, D., Mazloff, M. R., Resplandy, L., Johnson, K. S.,
2084 and Sarmiento, J. L.: Reassessing Southern Ocean Air-Sea CO₂ Flux Estimates With the Addition of Biogeochemical Float
2085 Observations, *Global Biogeochem. Cycles*, 33, 1370–1388, <https://doi.org/10.1029/2019GB006176>, 2019.

2086 Canadell, J. G., Le Quere, C., Raupach, M. R., Field, C. B., Buitenhuis, E. T., Ciais, P., Conway, T. J., Gillett, N. P.,
2087 Houghton, R. A., and Marland, G.: Contributions to accelerating atmospheric CO₂ growth from economic activity, carbon
2088 intensity, and efficiency of natural sinks, *Proceedings of the National Academy of Sciences*, 104, 18866–18870,
2089 <https://doi.org/10.1073/pnas.0702737104>, 2007.

2090 Canadell, J. G., Monteiro, P. M. S., Costa, M. H., Cotrim da Cunha, L., Cox, P. M., Eliseev, A. V., Henson, S., Ishii, M.,
2091 Jaccard, S., Koven, C., Lohila, A., Patra, P. K., Piao, S., Rogelj, J., Syampungani, S., Zaehle, S., and Zickfeld, K.: Global
2092 Carbon and other Biogeochemical Cycles and Feedbacks. In: *Climate Change 2021: The Physical Science Basis*.
2093 Contribution of Working Group I to the Sixth Assessment Report of the Intergovernmental Panel on Climate Change
2094 [Masson-Delmotte, V., P. Zhai, A. Pirani, S. L. Connors, C. Péan, S. Berger, N. Caud, Y. Chen, L. Goldfarb, M. I. Gomis,
2095 M. Huang, K. Leitzell, E. Lonnoy, J.B.R. Matthews, T. K. Maycock, T. Waterfield, O. Yelekçi, R. Yu and B. Zhou (eds.)].
2096 Cambridge University Press, Cambridge, United Kingdom and New York, NY, USA, pp. 673–816, doi:
2097 10.1017/9781009157896.007., 2021.

2098 Cao, Z., Myers, R. J., Lupton, R. C., Duan, H., Sacchi, R., Zhou, N., Reed Miller, T., Cullen, J. M., Ge, Q., and Liu, G.: The
2099 sponge effect and carbon emission mitigation potentials of the global cement cycle, *Nat Commun*, 11, 3777,
2100 <https://doi.org/10.1038/s41467-020-17583-w>, 2020.

2101 Céspedes, J., Sylvester, J. M., Pérez-Marulanda, L., Paz-García, P., Reymondin, L., Khodadadi, M., Tello, J. J., and Castro-
2102 Nunez, A.: Has global deforestation accelerated due to the COVID-19 pandemic?, *J. For. Res.*, 34, 1153–1165,
2103 <https://doi.org/10.1007/s11676-022-01561-7>, 2023.

2104 Chandra, N., Patra, P. K., Niwa, Y., Ito, A., Iida, Y., Goto, D., Morimoto, S., Kondo, M., Takigawa, M., Hajima, T., and
2105 Watanabe, M.: Estimated regional CO₂ flux and uncertainty based on an ensemble of atmospheric CO₂ inversions,
2106 *Atmospheric Chem. Phys.*, 22, 9215–9243, <https://doi.org/10.5194/acp-22-9215-2022>, 2022.

2107 Chatfield, C.: The Holt-Winters Forecasting Procedure, *J. Roy. Stat. Soc. C.*, 27, 264–279, <https://doi.org/10.2307/2347162>,
2108 1978.

- 2109 Chau, T. T. T., Gehlen, M., and Chevallier, F.: A seamless ensemble-based reconstruction of surface ocean $p\text{CO}_2$ and air–sea
 2110 CO_2 fluxes over the global coastal and open oceans, *Biogeosciences*, 19, 1087–1109, [https://doi.org/10.5194/bg-19-1087-](https://doi.org/10.5194/bg-19-1087-2022)
 2111 2022, 2022.
- 2112 Chevallier, F., Fisher, M., Peylin, P., Serrar, S., Bousquet, P., Bréon, F.-M., Chédin, A., and Ciais, P.: Inferring CO_2
 2113 sources and sinks from satellite observations: Method and application to TOVS data, *J. Geophys. Res.*, 110, D24309,
 2114 <https://doi.org/10.1029/2005JD006390>, 2005.
- 2115 Ciais, P., Sabine, C., Bala, G., Bopp, L., Brovkin, V., Canadell, J. G., Chhabra, A., DeFries, R., Galloway, J., Heimann, M.,
 2116 Jones, C., Le Quéré, C., Myneni, R., Piao, S., Thornton, P., Willem, J., Friedlingstein, P., and Munhoven, G.: Carbon and
 2117 Other Biogeochemical Cycles, in *Climate Change 2013: The Physical Science Basis, Contribution of Working Group I to the*
 2118 *Fifth Assessment Report of the Intergovernmental Panel on Climate Change*, edited by: Intergovernmental Panel on Climate
 2119 Change, Cambridge University Press, Cambridge, United Kingdom and New York, NY, USA.
 2120 [doi:10.1017/CBO9781107415324.015](https://doi.org/10.1017/CBO9781107415324.015), 2013.
- 2121 Ciais, P., Tan, J., Wang, X., Roedenbeck, C., Chevallier, F., Piao, S.-L., Moriarty, R., Broquet, G., Le Quéré, C., Canadell, J.
 2122 G., Peng, S., Poulter, B., Liu, Z., and Tans, P.: Five decades of northern land carbon uptake revealed by the interhemispheric
 2123 CO_2 gradient, *Nature*, 568, 221–225, <https://doi.org/10.1038/s41586-019-1078-6>, 2019.
- 2124 Ciais, P., Bastos, A., Chevallier, F., Lauerwald, R., Poulter, B., Canadell, P., Hugelius, G., Jackson, R. B., Jain, A., Jones,
 2125 M., Kondo, M., Lujckx, I. T., Patra, P. K., Peters, W., Pongratz, J., Petrescu, A. M. R., Piao, S., Qiu, C., Von Randow, C.,
 2126 Regnier, P., Saunois, M., Scholes, R., Shvidenko, A., Tian, H., Yang, H., Wang, X., and Zheng, B.: Definitions and methods
 2127 to estimate regional land carbon fluxes for the second phase of the REgional Carbon Cycle Assessment and Processes
 2128 Project (RECCAP-2), *Geosci. Model Dev.*, 15, 1289–1316, <https://doi.org/10.5194/gmd-15-1289-2022>, 2022.
- 2129 Collier, N., Hoffman, F. M., Lawrence, D. M., Keppel-Aleks, G., Koven, C. D., Riley, W. J., Mu, M., and Randerson, J. T.:
 2130 The International Land Model Benchmarking (ILAMB) System: Design, Theory, and Implementation, *J. Adv. Model. Earth*
 2131 *Syst.*, 10, 2731–2754, <https://doi.org/10.1029/2018MS001354>, 2018.
- 2132 Cox, P. M., Pearson, D., Booth, B. B., Friedlingstein, P., Huntingford, C., Jones, C. D., and Luke, C. M.: Sensitivity of
 2133 tropical carbon to climate change constrained by carbon dioxide variability, *Nature*, 494, 341–344,
 2134 <https://doi.org/10.1038/nature11882>, 2013.
- 2135 De Kauwe, M. G., Medlyn, B. E., Zaehle, S., Walker, A. P., Dietze, M. C., Wang, Y.-P., Luo, Y., Jain, A. K., El-Masri, B.,
 2136 Hickler, T., Wårlind, D., Weng, E., Parton, W. J., Thornton, P. E., Wang, S., Prentice, I. C., Asao, S., Smith, B., McCarthy,
 2137 H. R., Iversen, C. M., Hanson, P. J., Warren, J. M., Oren, R., and Norby, R. J.: Where does the carbon go? A model–data
 2138 intercomparison of vegetation carbon allocation and turnover processes at two temperate forest free-air CO_2 enrichment
 2139 sites, *New Phytol.*, 203, 883–899, <https://doi.org/10.1111/nph.12847>, 2014.
- 2140 Delire, C., Séférian, R., Decharme, B., Alkama, R., Calvet, J.-C., Carrer, D., Gibelin, A.-L., Joetzjer, E., Morel, X., Rocher,
 2141 M., and Tzanos, D.: The Global Land Carbon Cycle Simulated With ISBA-CTRIP: Improvements Over the Last Decade, *J.*
 2142 *Adv. Model. Earth Syst.*, 12, e2019MS001886, <https://doi.org/10.1029/2019MS001886>, 2020.
- 2143 Denman, K. L., Brasseur, G., Chidthaisong, A., Ciais, P., Cox, P. M., Dickinson, R. E., Hauglustaine, D., Heinze, C.,
 2144 Holland, E., Jacob, D., Lohmann, U., Ramachandran, S., Leite da Silva Dias, P., Wofsy, S. C., and Zhang, X.: Couplings
 2145 Between Changes in the Climate System and Biogeochemistry, in: *Climate Change 2007: The Physical Science Basis*.

2146 Contribution of Working Group I to the Fourth Assessment Report of the Intergovernmental Panel on Climate Change,
2147 edited by: Solomon, S., Qin, D., Manning, M., Marquis, M., Averyt, K., Tignor, M. M. B., Miller, H. L., and Chen, Z. L.,
2148 Cambridge University Press, Cambridge, UK and New York, USA, 499–587, ISBN: 9780521705967, 2007.

2149 Denvil-Sommer, A., Gehlen, M., and Vrac, M.: Observation system simulation experiments in the Atlantic Ocean for
2150 enhanced surface ocean pCO₂ reconstructions, *Ocean Sci.*, 17, 1011–1030, <https://doi.org/10.5194/os-17-1011-2021>, 2021.

2151 DeVries, T., Holzer, M., and Primeau, F.: Recent increase in oceanic carbon uptake driven by weaker upper-ocean
2152 overturning, *Nature*, 542, 215–218, <https://doi.org/10.1038/nature21068>, 2017.

2153 DeVries, T., Quéré, C. L., Andrews, O., Berthet, S., Hauck, J., Ilyina, T., Landschützer, P., Lenton, A., Lima, I. D., Nowicki,
2154 M., Schwinger, J., and Séférian, R.: Decadal trends in the ocean carbon sink, *PNAS*, 116, 11646–11651,
2155 <https://doi.org/10.1073/pnas.1900371116>, 2019.

2156 DeVries, T., Yamamoto, K., Wanninkhof, R., Gruber, N., Hauck, J., Müller, J. D., Bopp, L., Carroll, D., Carter, B., Chau,
2157 T.-T.-T., Doney, S. C., Gehlen, M., Gloege, L., Gregor, L., Henson, S., Kim, J. H., Iida, Y., Ilyina, T., Landschützer, P., Le
2158 Quéré, C., Munro, D., Nissen, C., Patara, L., Pérez, F. F., Resplandy, L., Rodgers, K. B., Schwinger, J., Séférian, R., Sicardi,
2159 V., Terhaar, J., Triñanes, J., Tsujino, H., Watson, A., Yasunaka, S., and Zeng, J.: Magnitude, trends, and variability of the
2160 global ocean carbon sink from 1985–2018, *Glob. Biogeochem. Cycles*, n/a, e2023GB007780,
2161 <https://doi.org/10.1029/2023GB007780>, 2023.
2162

2163 Forster, P. M., Smith, C. J., Walsh, T., Lamb, W. F., Lamboll, R., Hauser, M., Ribes, A., Rosen, D., Gillett, N., Palmer, M.
2164 D., Rogelj, J., von Schuckmann, K., Seneviratne, S. I., Trewin, B., Zhang, X., Allen, M., Andrew, R., Birt, A., Borger, A.,
2165 Boyer, T., Broersma, J. A., Cheng, L., Dentener, F., Friedlingstein, P., Gutiérrez, J. M., Gütschow, J., Hall, B., Ishii, M.,
2166 Jenkins, S., Lan, X., Lee, J.-Y., Morice, C., Kadow, C., Kennedy, J., Killick, R., Minx, J. C., Naik, V., Peters, G. P., Pirani,
2167 A., Pongratz, J., Schleussner, C.-F., Szopa, S., Thorne, P., Rohde, R., Rojas Corradi, M., Schumacher, D., Vose, R.,
2168 Zickfeld, K., Masson-Delmotte, V., and Zhai, P.: Indicators of Global Climate Change 2022: annual update of large-scale
2169 indicators of the state of the climate system and human influence, *Earth Syst. Sci. Data*, 15, 2295–2327,
2170 <https://doi.org/10.5194/essd-15-2295-2023>, 2023.

2171 Doney, S. C., Lima, I., Feely, R. A., Glover, D. M., Lindsay, K., Mahowald, N., Moore, J. K., and Wanninkhof, R.:
2172 Mechanisms governing interannual variability in upper-ocean inorganic carbon system and air–sea CO₂ fluxes: Physical
2173 climate and atmospheric dust, *Deep Sea Research Part II: Topical Studies in Oceanography*, 56, 640–655,
2174 <https://doi.org/10.1016/j.dsr2.2008.12.006>, 2009.

2175 Dong, Y., Bakker, D. C. E., Bell, T. G., Huang, B., Landschützer, P., Liss, P. S., and Yang, M.: Update on the Temperature
2176 Corrections of Global Air–Sea CO₂ Flux Estimates, *Glob. Biogeochem. Cycles*, 36, e2022GB007360,
2177 <https://doi.org/10.1029/2022GB007360>, 2022.
2178

2179 Dou, X., Wang, Y., Ciais, P., Chevallier, F., Davis, S. J., Crippa, M., Janssens-Maenhout, G., Guizzardi, D., Solazzo, E.,
2180 Yan, F., Huo, D., Zheng, B., Zhu, B., Cui, D., Ke, P., Sun, T., Wang, H., Zhang, Q., Gentine, P., Deng, Z., and Liu, Z.: Near-
2181 real-time global gridded daily CO₂ emissions, *The Innovation*, 3, 100182, <https://doi.org/10.1016/j.xinn.2021.100182>, 2022.

2182 Edson, J. B., Jampana, V., Weller, R. A., Bigorre, S. P., Plueddemann, A. J., Fairall, C. W., Miller, S. D., Mahrt, L., Vickers,
2183 D., and Hersbach, H.: On the Exchange of Momentum over the Open Ocean, *J. Phys. Oceanogr.*, 43, 1589–1610,
2184 <https://doi.org/10.1175/JPO-D-12-0173.1>, 2013.

2185 EIA. Short-Term Energy Outlook: September 2023. U.S. Energy Information Administration. Available at:
2186 <http://www.eia.gov/forecasts/steo/outlook.cfm>, last access: 9 November 2023, 2023.

2187 Erb, K.-H., Kastner, T., Luysaert, S., Houghton, R. A., Kuemmerle, T., Olofsson, P., and Haberl, H.: Bias in the attribution
2188 of forest carbon sinks, *Nature Clim Change*, 3, 854–856, <https://doi.org/10.1038/nclimate2004>, 2013.

2189 Erb, K.-H., Kastner, T., Plutzer, C., Bais, A. L. S., Carvalhais, N., Fetzel, T., Gingrich, S., Haberl, H., Lauk, C.,
2190 Niedertscheider, M., Pongratz, J., Thurner, M., and Luysaert, S.: Unexpectedly large impact of forest management and
2191 grazing on global vegetation biomass, *Nature*, 553, 73–76, <https://doi.org/10.1038/nature25138>, 2018.

2192 Eskander, S. M. S. U. and Fankhauser, S.: Reduction in greenhouse gas emissions from national climate legislation, *Nat.*
2193 *Clim. Chang.*, 10, 750–756, <https://doi.org/10.1038/s41558-020-0831-z>, 2020.

2194 Etheridge, D. M., Steele, L. P., Langenfelds, R. L., Francey, R. J., Barnola, J.-M., and Morgan, V. I.: Natural and
2195 anthropogenic changes in atmospheric CO₂ over the last 1000 years from air in Antarctic ice and firn, *J. Geophys. Res.*,
2196 101, 4115–4128, <https://doi.org/10.1029/95JD03410>, 1996.

2197 Eyring, V., Bony, S., Meehl, G. A., Senior, C. A., Stevens, B., Stouffer, R. J., and Taylor, K. E.: Overview of the Coupled
2198 Model Intercomparison Project Phase 6 (CMIP6) experimental design and organization, *Geosci. Model Dev.*, 9, 1937–1958,
2199 <https://doi.org/10.5194/gmd-9-1937-2016>, 2016.

2200 FAO, Impact of the Ukraine-Russia conflict on global food security and related matters under the mandate of the Food and
2201 Agriculture Organization of the United Nations (FAO), Hundred and Seventieth Session of the Council,
2202 <https://www.fao.org/3/nj164en/nj164en.pdf>, last access: 9 November 2023, 2023.

2203 Fay, A. R., Gregor, L., Landschützer, P., McKinley, G. A., Gruber, N., Gehlen, M., Iida, Y., Laruelle, G. G., Rödenbeck, C.,
2204 Roobaert, A., and Zeng, J.: SeaFlux: harmonization of air–sea CO₂ fluxes from surface pCO₂ data products using a
2205 standardized approach, *Earth System Science Data*, 13, 4693–4710, <https://doi.org/10.5194/essd-13-4693-2021>, 2021.

2206 Feng, L., Palmer, P. I., Bösch, H., and Dance, S.: Estimating surface CO₂ fluxes from space-borne CO₂ dry air mole fraction
2207 observations using an ensemble Kalman Filter, *Atmospheric Chem. Phys.*, 9, 2619–2633, [https://doi.org/10.5194/acp-9-](https://doi.org/10.5194/acp-9-2619-2009)
2208 2619-2009, 2009.

2209 Feng, L., Palmer, P. I., Parker, R. J., Deutscher, N. M., Feist, D. G., Kivi, R., Morino, I., and Sussmann, R.: Estimates of
2210 European uptake of CO₂ inferred from GOSAT XCO₂ retrievals: sensitivity to measurement bias inside and outside Europe,
2211 *Atmos. Chem. Phys.*, 16, 1289–1302, <https://doi.org/10.5194/acp-16-1289-2016>, 2016.

2212 Flanagan, D.: 2017 Minerals Yearbook: Copper [Advance Release], Tech. rep., U.S. Geological Survey,
2213 <https://pubs.usgs.gov/myb/vol1/2017/myb1-2017-copper.pdf>, 2021.

2214 Friedlingstein, P., Houghton, R. A., Marland, G., Hackler, J., Boden, T. A., Conway, T. J., Canadell, J. G., Raupach, M. R.,
2215 Ciais, P., and Le Quéré, C.: Update on CO₂ emissions, *Nature Geosci*, 3, 811–812, <https://doi.org/10.1038/ngeo1022>, 2010.

- 2216 Friedlingstein, P., Andrew, R. M., Rogelj, J., Peters, G. P., Canadell, J. G., Knutti, R., Luderer, G., Raupach, M. R.,
 2217 Schaeffer, M., van Vuuren, D. P., and Le Quéré, C.: Persistent growth of CO₂ emissions and implications for reaching
 2218 climate targets, *Nature Geosci*, 7, 709–715, <https://doi.org/10.1038/ngeo2248>, 2014.
- 2219 Friedlingstein, P., Jones, M. W., O’Sullivan, M., Andrew, R. M., Hauck, J., Peters, G. P., Peters, W., Pongratz, J., Sitch, S.,
 2220 Le Quéré, C., Bakker, D. C. E., Canadell, J. G., Ciais, P., Jackson, R. B., Anthoni, P., Barbero, L., Bastos, A., Bastrikov, V.,
 2221 Becker, M., Bopp, L., Buitenhuis, E., Chandra, N., Chevallier, F., Chini, L. P., Currie, K. I., Feely, R. A., Gehlen, M.,
 2222 Gilfillan, D., Gkritzalis, T., Goll, D. S., Gruber, N., Gutekunst, S., Harris, I., Haverd, V., Houghton, R. A., Hurtt, G., Ilyina,
 2223 T., Jain, A. K., Joetzier, E., Kaplan, J. O., Kato, E., Klein Goldewijk, K., Korsbakken, J. I., Landschützer, P., Lauvset, S. K.,
 2224 Lefèvre, N., Lenton, A., Lienert, S., Lombardozi, D., Marland, G., McGuire, P. C., Melton, J. R., Metzl, N., Munro, D. R.,
 2225 Nabel, J. E. M. S., Nakaoka, S.-I., Neill, C., Omar, A. M., Ono, T., Peregon, A., Pierrot, D., Poulter, B., Rehder, G.,
 2226 Resplandy, L., Robertson, E., Rödenbeck, C., Séférian, R., Schwinger, J., Smith, N., Tans, P. P., Tian, H., Tilbrook, B.,
 2227 Tubiello, F. N., van der Werf, G. R., Wiltshire, A. J., and Zaehle, S.: Global Carbon Budget 2019, *Earth Syst. Sci. Data*, 11,
 2228 1783–1838, <https://doi.org/10.5194/essd-11-1783-2019>, 2019.
- 2229 Friedlingstein, P., O’Sullivan, M., Jones, M. W., Andrew, R. M., Hauck, J., Olsen, A., Peters, G. P., Peters, W., Pongratz, J.,
 2230 Sitch, S., Le Quéré, C., Canadell, J. G., Ciais, P., Jackson, R. B., Alin, S., Aragão, L. E. O. C., Arneeth, A., Arora, V., Bates,
 2231 N. R., Becker, M., Benoit-Cattin, A., Bittig, H. C., Bopp, L., Bultan, S., Chandra, N., Chevallier, F., Chini, L. P., Evans, W.,
 2232 Florentie, L., Forster, P. M., Gasser, T., Gehlen, M., Gilfillan, D., Gkritzalis, T., Gregor, L., Gruber, N., Harris, I., Hartung,
 2233 K., Haverd, V., Houghton, R. A., Ilyina, T., Jain, A. K., Joetzier, E., Kadono, K., Kato, E., Kitidis, V., Korsbakken, J. I.,
 2234 Landschützer, P., Lefèvre, N., Lenton, A., Lienert, S., Liu, Z., Lombardozi, D., Marland, G., Metzl, N., Munro, D. R.,
 2235 Nabel, J. E. M. S., Nakaoka, S.-I., Niwa, Y., O’Brien, K., Ono, T., Palmer, P. I., Pierrot, D., Poulter, B., Resplandy, L.,
 2236 Robertson, E., Rödenbeck, C., Schwinger, J., Séférian, R., Skjelvan, I., Smith, A. J. P., Sutton, A. J., Tanhua, T., Tans, P. P.,
 2237 Tian, H., Tilbrook, B., van der Werf, G., Vuichard, N., Walker, A. P., Wanninkhof, R., Watson, A. J., Willis, D., Wiltshire,
 2238 A. J., Yuan, W., Yue, X., and Zaehle, S.: Global Carbon Budget 2020, *Earth Syst. Sci. Data*, 12, 3269–3340,
 2239 <https://doi.org/10.5194/essd-12-3269-2020>, 2020.
- 2240 Friedlingstein, P., Jones, M. W., O’Sullivan, M., Andrew, R. M., Bakker, D. C. E., Hauck, J., Le Quéré, C., Peters, G. P.,
 2241 Peters, W., Pongratz, J., Sitch, S., Canadell, J. G., Ciais, P., Jackson, R. B., Alin, S. R., Anthoni, P., Bates, N. R., Becker, M.,
 2242 Bellouin, N., Bopp, L., Chau, T. T. T., Chevallier, F., Chini, L. P., Cronin, M., Currie, K. I., Decharme, B., Djetchouang, L.
 2243 M., Dou, X., Evans, W., Feely, R. A., Feng, L., Gasser, T., Gilfillan, D., Gkritzalis, T., Grassi, G., Gregor, L., Gruber, N.,
 2244 Gürses, Ö., Harris, I., Houghton, R. A., Hurtt, G. C., Iida, Y., Ilyina, T., Luijkx, I. T., Jain, A., Jones, S. D., Kato, E.,
 2245 Kennedy, D., Klein Goldewijk, K., Knauer, J., Korsbakken, J. I., Körtzinger, A., Landschützer, P., Lauvset, S. K., Lefèvre,
 2246 N., Lienert, S., Liu, J., Marland, G., McGuire, P. C., Melton, J. R., Munro, D. R., Nabel, J. E. M. S., Nakaoka, S.-I., Niwa,
 2247 Y., Ono, T., Pierrot, D., Poulter, B., Rehder, G., Resplandy, L., Robertson, E., Rödenbeck, C., Rosan, T. M., Schwinger, J.,
 2248 Schwingshackl, C., Séférian, R., Sutton, A. J., Sweeney, C., Tanhua, T., Tans, P. P., Tian, H., Tilbrook, B., Tubiello, F., van
 2249 der Werf, G. R., Vuichard, N., Wada, C., Wanninkhof, R., Watson, A. J., Willis, D., Wiltshire, A. J., Yuan, W., Yue, C.,
 2250 Yue, X., Zaehle, S., and Zeng, J.: Global Carbon Budget 2021, *Earth Syst. Sci. Data*, 14, 1917–2005,
 2251 <https://doi.org/10.5194/essd-14-1917-2022>, 2022a.
- 2252 Friedlingstein, P. and co-authors of the current study, Supplemental data of the Global Carbon Budget 2023, ICOS-ERIC
 2253 Carbon Portal, <https://doi.org/10.18160/GCP-2023>, 2023.
- 2254 Friedlingstein, P., O’Sullivan, M., Jones, M. W., Andrew, R. M., Gregor, L., Hauck, J., Le Quéré, C., Luijkx, I. T., Olsen,
 2255 A., Peters, G. P., Peters, W., Pongratz, J., Schwingshackl, C., Sitch, S., Canadell, J. G., Ciais, P., Jackson, R. B., Alin, S. R.,

- 2256 Alkama, R., Arneth, A., Arora, V. K., Bates, N. R., Becker, M., Bellouin, N., Bittig, H. C., Bopp, L., Chevallier, F., Chini, L.
 2257 P., Cronin, M., Evans, W., Falk, S., Feely, R. A., Gasser, T., Gehlen, M., Gkritzalis, T., Gloege, L., Grassi, G., Gruber, N.,
 2258 Gürses, Ö., Harris, I., Hefner, M., Houghton, R. A., Hurtt, G. C., Iida, Y., Ilyina, T., Jain, A. K., Jersild, A., Kadono, K.,
 2259 Kato, E., Kennedy, D., Klein Goldewijk, K., Knauer, J., Korsbakken, J. I., Landschützer, P., Lefèvre, N., Lindsay, K., Liu,
 2260 J., Liu, Z., Marland, G., Mayot, N., McGrath, M. J., Metzl, N., Monacci, N. M., Munro, D. R., Nakaoka, S.-I., Niwa, Y.,
 2261 O'Brien, K., Ono, T., Palmer, P. I., Pan, N., Pierrot, D., Pocock, K., Poulter, B., Resplandy, L., Robertson, E., Rödenbeck,
 2262 C., Rodriguez, C., Rosan, T. M., Schwinger, J., Séférian, R., Shutler, J. D., Skjelvan, I., Steinhoff, T., Sun, Q., Sutton, A. J.,
 2263 Sweeney, C., Takao, S., Tanhua, T., Tans, P. P., Tian, X., Tian, H., Tilbrook, B., Tsujino, H., Tubiello, F., van der Werf, G.
 2264 R., Walker, A. P., Wanninkhof, R., Whitehead, C., Willstrand Wranne, A., et al.: Global Carbon Budget 2022, *Earth Syst.*
 2265 *Sci. Data*, 14, 4811–4900, <https://doi.org/10.5194/essd-14-4811-2022>, 2022b.
- 2266 Ganzenmüller, R., Bultan, S., Winkler, K., Fuchs, R., Zabel, F., and Pongratz, J.: Land-use change emissions based on high-
 2267 resolution activity data substantially lower than previously estimated, *Environ. Res. Lett.*, 17, 064050,
 2268 <https://doi.org/10.1088/1748-9326/ac70d8>, 2022.
- 2269 Gasser, T., Crepin, L., Quilcaille, Y., Houghton, R. A., Ciais, P., and Obersteiner, M.: Historical CO₂ emissions from land
 2270 use and land cover change and their uncertainty, *Biogeosciences*, 17, 4075–4101, <https://doi.org/10.5194/bg-17-4075-2020>,
 2271 2020.
- 2272 Gaubert, B., Stephens, B. B., Basu, S., Chevallier, F., Deng, F., Kort, E. A., Patra, P. K., Peters, W., Rödenbeck, C., Saeki,
 2273 T., Schimel, D., Van der Laan-Luijckx, I., Wofsy, S., and Yin, Y.: Global atmospheric CO₂ inverse models converging on
 2274 neutral tropical land exchange, but disagreeing on fossil fuel and atmospheric growth rate, *Biogeosciences*, 16, 117–134,
 2275 <https://doi.org/10.5194/bg-16-117-2019>, 2019.
- 2276 GCP: The Global Carbon Budget 2007, available at: <http://www.globalcarbonproject.org/carbonbudget/archive.htm>, last
 2277 access: 9 November 2023, 2007.
- 2278 Giglio, L., Schroeder, W., and Justice, C. O.: The collection 6 MODIS active fire detection algorithm and fire products,
 2279 *Remote Sensing of Environment*, 178, 31–41, <https://doi.org/10.1016/j.rse.2016.02.054>, 2016.
- 2280 Gloege, L., McKinley, G. A., Landschützer, P., Fay, A. R., Frölicher, T. L., Fyfe, J. C., Ilyina, T., Jones, S., Lovenduski, N.
 2281 S., Rodgers, K. B., Schlunegger, S., and Takano, Y.: Quantifying Errors in Observationally Based Estimates of Ocean
 2282 Carbon Sink Variability, *Global Biogeochem. Cy.*, 35, e2020GB006788, <https://doi.org/10.1029/2020GB006788>, 2021.
- 2283 Gloege, L., Yan, M., Zheng, T., and McKinley, G. A.: Improved Quantification of Ocean Carbon Uptake by Using Machine
 2284 Learning to Merge Global Models and pCO₂ Data, *J. Adv. Model. Earth Syst.*, 14, e2021MS002620,
 2285 <https://doi.org/10.1029/2021MS002620>, 2022.
- 2286 Golar, G., Malik, A., Muis, H., Herman, A., Nurudin, N., and Lukman, L.: The social-economic impact of COVID-19
 2287 pandemic: implications for potential forest degradation, *Heliyon*, 6, e05354, <https://doi.org/10.1016/j.heliyon.2020.e05354>,
 2288 2020.
- 2289 Goris, N., Tjiputra, J. F., Olsen, A., Schwinger, J., Lauvset, S. K., and Jeansson, E.: Constraining Projection-Based Estimates
 2290 of the Future North Atlantic Carbon Uptake, *J. Clim.*, 31, 3959–3978, <https://doi.org/10.1175/JCLI-D-17-0564.1>, 2018.
- 2291 Grassi, G., House, J., Kurz, W. A., Cescatti, A., Houghton, R. A., Peters, G. P., Sanz, M. J., Viñas, R. A., Alkama, R.,
 2292 Arneth, A., Bondeau, A., Dentener, F., Fader, M., Federici, S., Friedlingstein, P., Jain, A. K., Kato, E., Koven, C. D., Lee,

2293 D., Nabel, J. E. M. S., Nassikas, A. A., Perugini, L., Rossi, S., Sitch, S., Viovy, N., Wiltshire, A., and Zaehle, S.:

2294 Reconciling global-model estimates and country reporting of anthropogenic forest CO₂ sinks, *Nature Clim Change*, 8, 914–

2295 920, <https://doi.org/10.1038/s41558-018-0283-x>, 2018.

2296 Grassi, G., Stehfest, E., Rogelj, J., van Vuuren, D., Cescatti, A., House, J., Nabuurs, G.-J., Rossi, S., Alkama, R., Viñas, R.

2297 A., Calvin, K., Ceccherini, G., Federici, S., Fujimori, S., Gusti, M., Hasegawa, T., Havlik, P., Humpenöder, F., Korosuo, A.,

2298 Perugini, L., Tubiello, F. N., and Popp, A.: Critical adjustment of land mitigation pathways for assessing countries' climate

2299 progress, *Nat. Clim. Chang.*, 11, 425–434, <https://doi.org/10.1038/s41558-021-01033-6>, 2021.

2300 Grassi, G., Schwingshackl, C., Gasser, T., Houghton, R. A., Sitch, S., Canadell, J. G., Cescatti, A., Ciais, P., Federici, S.,

2301 Friedlingstein, P., Kurz, W. A., Sanz Sanchez, M. J., Abad Viñas, R., Alkama, R., Bultan, S., Ceccherini, G., Falk, S., Kato,

2302 E., Kennedy, D., Knauer, J., Korosuo, A., Melo, J., McGrath, M. J., Nabel, J. E. M. S., Poulter, B., Romanovskaya, A. A.,

2303 Rossi, S., Tian, H., Walker, A. P., Yuan, W., Yue, X., and Pongratz, J.: Harmonising the land-use flux estimates of global

2304 models and national inventories for 2000–2020, *Earth Syst. Sci. Data*, 15, 1093–1114, [https://doi.org/10.5194/essd-15-1093-](https://doi.org/10.5194/essd-15-1093-2023)

2305 2023, 2023.

2306 Gregor, L. and Gruber, N.: OceanSODA-ETHZ: a global gridded data set of the surface ocean carbonate system for seasonal

2307 to decadal studies of ocean acidification, 13, 777–808, <https://doi.org/10.5194/essd-13-777-2021>, 2021.

2308 Gruber, N., Bakker, D. C. E., DeVries, T., Gregor, L., Hauck, J., Landschützer, P., McKinley, G. A., and Müller, J. D.:

2309 Trends and variability in the ocean carbon sink, *Nat. Rev. Earth Environ.*, 4, 119–134, [https://doi.org/10.1038/s43017-022-](https://doi.org/10.1038/s43017-022-00381-x)

2310 00381-x, 2023.

2311 Gruber, N., Clement, D., Carter, B. R., Feely, R. A., van Heuven, S., Hoppema, M., Ishii, M., Key, R. M., Kozyr, A.,

2312 Lauvset, S. K., Lo Monaco, C., Mathis, J. T., Murata, A., Olsen, A., Perez, F. F., Sabine, C. L., Tanhua, T., and Wanninkhof,

2313 R.: The oceanic sink for anthropogenic CO₂ from 1994 to 2007, 363, 1193–1199, <https://doi.org/10.1126/science.aau5153>,

2314 2019.

2315 Guan, D., Liu, Z., Geng, Y., Lindner, S., and Hubacek, K.: The gigatonne gap in China's carbon dioxide inventories, *Nature*

2316 *Clim Change*, 2, 672–675, <https://doi.org/10.1038/nclimate1560>, 2012.

2317 Gulev, S. K., Thorne, P. W., Ahn, J., Dentener, F. J., Domingues, C. M., Gerland, S., Gong, D. S., Kaufman, S., Nnamchi,

2318 H. C., Quaas, J., Rivera, J. A., Sathyendranath, S., Smith, S. L., Trewin, B., von Shuckmann, K., and Vose, R. S.: Changing

2319 State of the Climate System. In: *Climate Change 2021: The Physical Science Basis. Contribution of Working Group I to the*

2320 *Sixth Assessment Report of the Intergovernmental Panel on Climate Change* [Masson-Delmotte, V., Zhai, P., Pirani, A.,

2321 Connors, S. L., Péan, C., Berger, S., Caud, N., Chen, Y., Goldfarb, L., Gomis, M. I., Huang, M., Leitzell, K., Lonnoy, E.,

2322 Matthews, J.B.R., Maycock, T.K., Waterfield, T., Yelekçi, O., Yu, R. and Zhou, B. (eds.)]. Cambridge University Press,

2323 Cambridge, United Kingdom and New York, NY, USA, pp. 287–422, doi:10.1017/9781009157896.004, 2021.

2324 Guo, R., Wang, J., Bing, L., Tong, D., Ciais, P., Davis, S. J., Andrew, R. M., Xi, F., and Liu, Z.: Global CO₂ uptake by

2325 cement from 1930 to 2019, 13, 1791–1805, <https://doi.org/10.5194/essd-13-1791-2021>, 2021.

2326 Gürses, Ö., Oziel, L., Karakuş, O., Sidorenko, D., Völker, C., Ye, Y., Zeising, M., Butzin, M., and Hauck, J.: Ocean

2327 biogeochemistry in the coupled ocean–sea ice–biogeochemistry model FESOM2.1–REcoM3, *Geosci. Model Dev.*, 16,

2328 4883–4936, <https://doi.org/10.5194/gmd-16-4883-2023>, 2023.

- 2329 Gütschow, J., Jeffery, M. L., Gieseke, R., Gebel, R., Stevens, D., Krapp, M., and Rocha, M.: The PRIMAP-hist national
2330 historical emissions time series, 8, 571–603, <https://doi.org/10.5194/essd-8-571-2016>, 2016.
- 2331 Gütschow, J., and Pflüger, M. (2023): The PRIMAP-hist national historical emissions time series v2.4.2 (1750-2021)
2332 [dataset]. <https://doi.org/10.5281/zenodo.7727475>, 2023.
- 2333 Hall, B. D., Crotwell, A. M., Kitzis, D. R., Mefford, T., Miller, B. R., Schibig, M. F., and Tans, P. P.: Revision of the World
2334 Meteorological Organization Global Atmosphere Watch (WMO/GAW) CO₂ calibration scale, 14, 3015–3032,
2335 <https://doi.org/10.5194/amt-14-3015-2021>, 2021.
- 2336 Hansis, E., Davis, S. J., and Pongratz, J.: Relevance of methodological choices for accounting of land use change carbon
2337 fluxes, *Global Biogeochem. Cycles*, 29, 1230–1246, <https://doi.org/10.1002/2014GB004997>, 2015.
- 2338 Hauck, J., Nissen, C., Landschützer, P., Rödenbeck, C., Bushinsky, S., and Olsen, A.: Sparse observations induce large
2339 biases in estimates of the global ocean CO₂ sink: an ocean model subsampling experiment, *Philos. Trans. R. Soc. Math.*
2340 *Phys. Eng. Sci.*, 381, 20220063, <https://doi.org/10.1098/rsta.2022.0063>, 2023.
- 2341 Hauck, J., Zeising, M., Le Quéré, C., Gruber, N., Bakker, D. C. E., Bopp, L., Chau, T. T. T., Gürses, Ö., Ilyina, T.,
2342 Landschützer, P., Lenton, A., Resplandy, L., Rödenbeck, C., Schwinger, J., and Séférian, R.: Consistency and Challenges in
2343 the Ocean Carbon Sink Estimate for the Global Carbon Budget, *Front. Mar. Sci.*, 7, 571720,
2344 <https://doi.org/10.3389/fmars.2020.571720>, 2020.
- 2345 Haverd, V., Smith, B., Nieradzic, L., Briggs, P. R., Woodgate, W., Trudinger, C. M., Canadell, J. G., and Cuntz, M.: A new
2346 version of the CABLE land surface model (Subversion revision r4601) incorporating land use and land cover change, woody
2347 vegetation demography, and a novel optimisation-based approach to plant coordination of photosynthesis, *Geosci. Model*
2348 *Dev.*, 11, 2995–3026, <https://doi.org/10.5194/gmd-11-2995-2018>, 2018.
- 2349 Heinke, J., Rolinski, S., and Müller, C.: Modelling the role of livestock grazing in C and N cycling in grasslands with
2350 LPJmL5.0-grazing, *Geosci. Model Dev.*, 16, 2455–2475, <https://doi.org/10.5194/gmd-16-2455-2023>, 2023.
- 2351 Hefner, M., Marland, G., Boden, T., Andres, R.: Global, Regional, and National Fossil-Fuel CO₂ Emissions: 1751-2020
2352 CDIAC-FF [dataset], available at: <https://energy.appstate.edu/cdiac-appstate/data-products>, last access: 9 November 2023,
2353 2023.
- 2354 Hickler, T., Smith, B., Prentice, I. C., Mjöfors, K., Miller, P., Arneth, A., and Sykes, M. T.: CO₂ fertilization in temperate
2355 FACE experiments not representative of boreal and tropical forests, *Glob. Change Biol.*, 14, 1531–1542,
2356 <https://doi.org/10.1111/j.1365-2486.2008.01598.x>, 2008.
- 2357 Hoesly, R. M., Smith, S. J., Feng, L., Klimont, Z., Janssens-Maenhout, G., Pitkanen, T., Seibert, J. J., Vu, L., Andres, R. J.,
2358 Bolt, R. M., Bond, T. C., Dawidowski, L., Kholod, N., Kurokawa, J., Li, M., Liu, L., Lu, Z., Moura, M. C. P., O'Rourke, P.
2359 R., and Zhang, Q.: Historical (1750–2014) anthropogenic emissions of reactive gases and aerosols from the Community
2360 Emissions Data System (CEDs), *Geosci. Model Dev.*, 11, 369–408, <https://doi.org/10.5194/gmd-11-369-2018>, 2018.
- 2361 Hong, C., Burney, J. A., Pongratz, J., Nabel, J. E. M. S., Mueller, N. D., Jackson, R. B., and Davis, S. J.: Global and regional
2362 drivers of land-use emissions in 1961–2017, *Nature*, 589, 554–561, <https://doi.org/10.1038/s41586-020-03138-y>, 2021.

- 2363 Holding, T., Ashton, I. G., Shutler, J. D., Land, P. E., Nightingale, P. D., Rees, A. P., Brown, I., Piolle, J.-F., Kock, A.,
 2364 Bange, H. W., Woolf, D. K., Goddijn-Murphy, L., Pereira, R., Paul, F., Girard-Ardhuin, F., Chapron, B., Rehder, G.,
 2365 Ardhuin, F., and Donlon, C. J.: The FluxEngine air–sea gas flux toolbox: simplified interface and extensions for in situ
 2366 analyses and multiple sparingly soluble gases, *Ocean Sci.*, 15, 1707–1728, <https://doi.org/10.5194/os-15-1707-2019>, 2019.
- 2367 Houghton, R. A. and Castanho, A.: Annual emissions of carbon from land use, land-use change, and forestry from 1850 to
 2368 2020, *Earth Syst. Sci. Data*, 15, 2025–2054, <https://doi.org/10.5194/essd-15-2025-2023>, 2023.
- 2369 Houghton, R. A., House, J. I., Pongratz, J., van der Werf, G. R., DeFries, R. S., Hansen, M. C., Le Quéré, C., and
 2370 Ramankutty, N.: Carbon emissions from land use and land-cover change, *Biogeosciences*, 9, 5125–5142,
 2371 <https://doi.org/10.5194/bg-9-5125-2012>, 2012.
- 2372 Huang, B., Thorne, P. W., Banzon, V. F., Boyer, T., Chepurin, G., Lawrimore, J. H., Menne, M. J., Smith, T. M., Vose, R.
 2373 S., and Zhang, H.-M.: NOAA Extended Reconstructed Sea Surface Temperature (ERSST), Version 5,
 2374 <https://doi.org/10.7289/V5T72FNM>, 2017.
- 2375 Hubau, W., Lewis, S.L., Phillips, O.L., Affum-Baffoe, K., Beeckman, H., Cuní-Sanchez, A., Daniels, A.K., Ewango, C.E.N.,
 2376 Fauset, S., Mukinzi, J.M., Sheil, D., Sonké, B., Sullivan, M.J.P., Sunderland, T.C.H., Taedoumg, H., Thomas, S.C., White,
 2377 L.J.T., Abernethy, K.A., Adu-Bredu, S., Amani, C.A., Baker, T.R., Banin, L.F., Baya, F., Begne, S.K., Bennett, A.C.,
 2378 Benedet, F., Bitariho, R., Bocko, Y.E., Boeckx, P., Boundja, P., Brienen, R.J.W., Brncic, T., Chezeaux, E., Chuyong, G.B.,
 2379 Clark, C.J., Collins, M., Comiskey, J.A., Coomes, D.A., Dargie, G.C., de Haulleville, T., Kamdem, M.N.D., Doucet, J.-L.,
 2380 Esquivel-Muelbert, A., Feldpausch, T.R., Fofanah, A., Foli, E.G., Gilpin, M., Gloor, E., Gonmadje, C., Gourlet-Fleury, S.,
 2381 Hall, J.S., Hamilton, A.C., Harris, D.J., Hart, T.B., Hockemba, M.B.N., Hladik, A., Ifo, S.A., Jeffery, K.J., Jucker, T.,
 2382 Yakusu, E.K., Kearsley, E., Kenfack, D., Koch, A., Leal, M.E., Levesley, A., Lindsell, J.A., Lisingo, J., Lopez-Gonzalez, G.,
 2383 Lovett, J.C., Makana, J.-R., Malhi, Y., Marshall, A.R., Martin, J., Martin, E.H., Mbayu, F.M., Medjibe, V.P., Mihindou, V.,
 2384 Mitchard, E.T.A., Moore, S., Munishi, P.K.T., Bengone, N.N., Ojo, L., Ondo, F.E., Peh, K.S.-H., Pickavance, G.C., Poulsen,
 2385 A.D., Poulsen, J.R., Qie, L., Reitsma, J., Rovero, F., Swaine, M.D., Talbot, J., Taplin, J., Taylor, D.M., Thomas, D.W.,
 2386 Toirambe, B., Mukendi, J.T., Tuagben, D., Umunay, P.M., van der Heijden, G.M.F., Verbeeck, H., Vleminckx, J., Willcock,
 2387 S., Wöll, H., Woods, J.T., Zomagho, L.: Asynchronous carbon sink saturation in African and Amazonian tropical forests,
 2388 *Nature*, 579, 80–87, <https://doi.org/10.1038/s41586-020-2035-0>, 2020.
- 2389 Humphrey, V., Zscheischler, J., Ciais, P., Gudmundsson, L., Sitch, S., and Seneviratne, S. I.: Sensitivity of atmospheric CO₂
 2390 growth rate to observed changes in terrestrial water storage, *Nature*, 560, 628–631, [https://doi.org/10.1038/s41586-018-](https://doi.org/10.1038/s41586-018-0424-4)
 2391 0424-4, 2018.
- 2392 Humphrey, V., Berg, A., Ciais, P., Gentile, P., Jung, M., Reichstein, M., Seneviratne, S. I., and Frankenberg, C.: Soil
 2393 moisture–atmosphere feedback dominates land carbon uptake variability, *Nature*, 592, 65–69,
 2394 <https://doi.org/10.1038/s41586-021-03325-5>, 2021.
- 2395 Huntzinger, D. N., Michalak, A. M., Schwalm, C., Ciais, P., King, A. W., Fang, Y., Schaefer, K., Wei, Y., Cook, R. B.,
 2396 Fisher, J. B., Hayes, D., Huang, M., Ito, A., Jain, A. K., Lei, H., Lu, C., Maignan, F., Mao, J., Parazoo, N., Peng, S., Poulter,
 2397 B., Ricciuto, D., Shi, X., Tian, H., Wang, W., Zeng, N., and Zhao, F.: Uncertainty in the response of terrestrial carbon sink to
 2398 environmental drivers undermines carbon-climate feedback predictions, *Sci Rep*, 7, 4765, [https://doi.org/10.1038/s41598-](https://doi.org/10.1038/s41598-017-03818-2)
 2399 017-03818-2, 2017.

2400 Iida, Y., Takatani, Y., Kojima, A., and Ishii, M.: Global trends of ocean CO₂ sink and ocean acidification: an observation-
2401 based reconstruction of surface ocean inorganic carbon variables, *J Oceanogr*, 77, 323–358, [https://doi.org/10.1007/s10872-](https://doi.org/10.1007/s10872-020-00571-5)
2402 020-00571-5, 2021.

2403 Ilyina, T., Li, H., Spring, A., Müller, W. A., Bopp, L., Chikamoto, M. O., Danabasoglu, G., Dobrynin, M., Dunne, J.,
2404 Fransner, F., Friedlingstein, P., Lee, W., Lovenduski, N. S., Merryfield, W. J., Mignot, J., Park, J. Y., Séférian, R., Sospedra-
2405 Alfonso, R., Watanabe, M., and Yeager, S.: Predictable Variations of the Carbon Sinks and Atmospheric CO₂ Growth in a
2406 Multi-Model Framework, *Geophys. Res. Lett.*, 48, e2020GL090695, <https://doi.org/10.1029/2020GL090695>, 2021.

2407 IMF: International Monetary Fund: World Economic Outlook, available at: <http://www.imf.org>, last access: 9 November
2408 2023, 2023.

2409 IPCC: Annex II: Glossary [Möller, V, J.B.R. Matthews, R. van Diemen, C. Méndez, S. Semenov, J.S. Fuglestedt, A.
2410 Reisinger (eds.)]. In: *Climate Change 2022: Impacts, Adaptation, and Vulnerability. Contribution of Working Group II to the*
2411 *Sixth Assessment Report of the Intergovernmental Panel on Climate Change* [H.-O. Pörtner, D.C. Roberts, M. Tignor, E.S.
2412 Poloczanska, K. Mintenbeck, A. Alegría, M. Craig, S. Langsdorf, S. Löschke, V. Möller, A. Okem, B. Rama (eds.)], in:
2413 *Climate Change 2022 – Impacts, Adaptation and Vulnerability: Working Group II Contribution to the Sixth Assessment*
2414 *Report of the Intergovernmental Panel on Climate Change* [Möller, V, J.B.R. Matthews, R. van Diemen, C. Méndez, S.
2415 Semenov, J.S. Fuglestedt, A. Reisinger (eds.)], Cambridge University Press, Cambridge, UK and New York, NY, 2897–
2416 2930, <https://doi.org/10.1017/9781009325844.029>, 2023.

2417 Ito, A. and Inatomi, M.: Use of a process-based model for assessing the methane budgets of global terrestrial ecosystems and
2418 evaluation of uncertainty, 9, 759–773, <https://doi.org/10.5194/bg-9-759-2012>, 2012.

2419 Jackson, R. B., Canadell, J. G., Le Quéré, C., Andrew, R. M., Korsbakken, J. I., Peters, G. P., and Nakicenovic, N.:
2420 Reaching peak emissions, *Nature Clim Change*, 6, 7–10, <https://doi.org/10.1038/nclimate2892>, 2016.

2421 Jackson, R. B., Le Quéré, C., Andrew, R. M., Canadell, J. G., Korsbakken, J. I., Liu, Z., Peters, G. P., and Zheng, B.: Global
2422 energy growth is outpacing decarbonization, *Environ. Res. Lett.*, 13, 120401, <https://doi.org/10.1088/1748-9326/aaf303>,
2423 2018.

2424 Jackson, R. B., Friedlingstein, P., Andrew, R. M., Canadell, J. G., Le Quéré, C., and Peters, G. P.: Persistent fossil fuel
2425 growth threatens the Paris Agreement and planetary health, *Environ. Res. Lett.*, 14, 121001, [https://doi.org/10.1088/1748-](https://doi.org/10.1088/1748-9326/ab57b3)
2426 9326/ab57b3, 2019.

2427 Jackson, R. B., Friedlingstein, P., Quéré, C. L., Abernethy, S., Andrew, R. M., Canadell, J. G., Ciais, P., Davis, S. J., Deng,
2428 Z., Liu, Z., Korsbakken, J. I., and Peters, G. P.: Global fossil carbon emissions rebound near pre-COVID-19 levels, *Environ.*
2429 *Res. Lett.*, 17, 031001, <https://doi.org/10.1088/1748-9326/ac55b6>, 2022.

2430 Jacobson, A. R., Schuldt, K. N., Tans, P., Arlyn Andrews, Miller, J. B., Oda, T., Mund, J., Weir, B., Ott, L., Aalto, T.,
2431 Abshire, J. B., Aikin, K., Aoki, S., Apadula, F., Arnold, S., Baier, B., Bartyzel, J., Beyersdorf, A., Biermann, T., Biraud, S.
2432 C., Boenisch, H., Brailsford, G., Brand, W. A., Chen, G., Huilin Chen, Lukasz Chmura, Clark, S., Colomb, A., Commane,
2433 R., Conil, S., Couret, C., Cox, A., Cristofanelli, P., Cuevas, E., Curcoll, R., Daube, B., Davis, K. J., De Wekker, S., Coletta,
2434 J. D., Delmotte, M., DiGangi, E., DiGangi, J. P., Di Sarra, A. G., Dlugokencky, E., Elkins, J. W., Emmenegger, L., Shuangxi
2435 Fang, Fischer, M. L., Forster, G., Frumau, A., Galkowski, M., Gatti, L. V., Gehrlein, T., Gerbig, C., Francois Gheusi, Gloor,

- 2436 E., Gomez-Trueba, V., Goto, D., Griffis, T., Hammer, S., Hanson, C., Haszpra, L., Hatakka, J., Heimann, M., Heliasz, M.,
 2437 Hensen, A., Hermansen, O., Hintsä, E., Holst, J., Ivakhov, V., Jaffe, D. A., Jordan, A., Joubert, W., Karion, A., Kawa, S. R.,
 2438 Kazan, V., Keeling, R. F., Keronen, P., Kneuer, T., Kolari, P., Kateřina Komínková, Kort, E., Kozlova, E., Krummel, P.,
 2439 Kubistin, D., Labuschagne, C., Lam, D. H. Y., Lan, X., Langenfelds, R. L., Laurent, O., Laurila, T., Lauvaux, T., Lavric, J.,
 2440 Law, B. E., Lee, J., Lee, O. S. M., Lehner, I., Lehtinen, K., Leppert, R., et al.: CarbonTracker CT2022,
 2441 <https://doi.org/10.25925/Z1GJ-3254>, 2023a.
- 2442 Jacobson, A. R., Schuldt, K. N., Tans, P., Arlyn Andrews, Miller, J. B., Oda, T., Mund, J., Weir, B., Ott, L., Aalto, T.,
 2443 Abshire, J. B., Aikin, K., Aoki, S., Apadula, F., Arnold, S., Baier, B., Bartyzel, J., Beyersdorf, A., Biermann, T., Biraud, S.
 2444 C., Boenisch, H., Brailsford, G., Brand, W. A., Chen, G., Huilin Chen, Lukasz Chmura, Clark, S., Colomb, A., Commane,
 2445 R., Conil, S., Couret, C., Cox, A., Cristofanelli, P., Cuevas, E., Curcoll, R., Daube, B., Davis, K. J., De Wekker, S., Coletta,
 2446 J. D., Delmotte, M., DiGangi, E., DiGangi, J. P., Di Sarra, A. G., Dlugokencky, E., Elkins, J. W., Emmenegger, L., Shuangxi
 2447 Fang, Fischer, M. L., Forster, G., Frumau, A., Galkowski, M., Gatti, L. V., Gehrlein, T., Gerbig, C., Francois Gheusi, Gloor,
 2448 E., Gomez-Trueba, V., Goto, D., Griffis, T., Hammer, S., Hanson, C., Haszpra, L., Hatakka, J., Heimann, M., Heliasz, M.,
 2449 Hensen, A., Hermansen, O., Hintsä, E., Holst, J., Ivakhov, V., Jaffe, D. A., Jordan, A., Joubert, W., Karion, A., Kawa, S. R.,
 2450 Kazan, V., Keeling, R. F., Keronen, P., Kneuer, T., Kolari, P., Kateřina Komínková, Kort, E., Kozlova, E., Krummel, P.,
 2451 Kubistin, D., Labuschagne, C., Lam, D. H. Y., Lan, X., Langenfelds, R. L., Laurent, O., Laurila, T., Lauvaux, T., Lavric, J.,
 2452 Law, B. E., Lee, J., Lee, O. S. M., Lehner, I., Lehtinen, K., Leppert, R., et al.: CarbonTracker CT-NRT.v2023-3,
 2453 <https://doi.org/10.25925/7TAF-J322>, 2023b.
- 2454 Janssens-Maenhout, G., Crippa, M., Guizzardi, D., Muntean, M., Schaaf, E., Dentener, F., Bergamaschi, P., Pagliari, V.,
 2455 Olivier, J. G. J., Peters, J. A. H. W., van Aardenne, J. A., Monni, S., Doering, U., Petrescu, A. M. R., Solazzo, E., and
 2456 Oreggioni, G. D.: EDGAR v4.3.2 Global Atlas of the three major greenhouse gas emissions for the period 1970–2012, *Earth*
 2457 *Syst. Sci. Data*, 11, 959–1002, <https://doi.org/10.5194/essd-11-959-2019>, 2019.
- 2458 Jean-Michel, L., Eric, G., Romain, B.-B., Gilles, G., Angélique, M., Marie, D., Clément, B., Mathieu, H., Olivier, L. G.,
 2459 Charly, R., Tony, C., Charles-Emmanuel, T., Florent, G., Giovanni, R., Mounir, B., Yann, D., and Pierre-Yves, L. T.: The
 2460 Copernicus Global 1/12° Oceanic and Sea Ice GLORYS12 Reanalysis, *Front. Earth Sci.*, 9, 2021.
- 2461 Jiang, F., Ju, W., He, W., Wu, M., Wang, H., Wang, J., Jia, M., Feng, S., Zhang, L., and Chen, J. M.: A 10-year global
 2462 monthly averaged terrestrial net ecosystem exchange dataset inferred from the ACOS GOSAT v9 XCO₂ retrievals
 2463 (GCAS2021), *Earth Syst. Sci. Data*, 14, 3013–3037, <https://doi.org/10.5194/essd-14-3013-2022>, 2022.
- 2464 Jiang, F., Wang, H., Chen, J. M., Ju, W., Tian, X., Feng, S., Li, G., Chen, Z., Zhang, S., Lu, X., Liu, J., Wang, H., Wang, J.,
 2465 He, W., and Wu, M.: Regional CO₂ fluxes from 2010 to 2015 inferred from GOSAT XCO₂ retrievals using a new version
 2466 of the Global Carbon Assimilation System, *Atmospheric Chem. Phys.*, 21, 1963–1985, [https://doi.org/10.5194/acp-21-1963-](https://doi.org/10.5194/acp-21-1963-2021)
 2467 2021, 2021.
- 2468
- 2469 Jin, Z., Wang, T., Zhang, H., Wang, Y., Ding, J., and Tian, X.: Constraint of satellite CO₂ retrieval on the global carbon
 2470 cycle from a Chinese atmospheric inversion system, *Sci. China Earth Sci.*, 66, 609–618, [https://doi.org/10.1007/s11430-022-](https://doi.org/10.1007/s11430-022-1036-7)
 2471 1036-7, 2023.
- 2472 Joos, F. and Spahni, R.: Rates of change in natural and anthropogenic radiative forcing over the past 20,000 years,
 2473 *Proceedings of the National Academy of Sciences*, 105, 1425–1430, <https://doi.org/10.1073/pnas.0707386105>, 2008.

2474 Jones, C. D., Hickman, J. E., Rumbold, S. T., Walton, J., Lamboll, R. D., Skeie, R. B., Fiedler, S., Forster, P. M., Rogelj, J.,
2475 Abe, M., Botzet, M., Calvin, K., Cassou, C., Cole, J. N. S., Davini, P., Deushi, M., Dix, M., Fyfe, J. C., Gillett, N. P., Ilyina,
2476 T., Kawamiya, M., Kelley, M., Kharin, S., Koshiro, T., Li, H., Mackallah, C., Müller, W. A., Nabat, P., van Noije, T., Nolan,
2477 P., Ohgaito, R., Olivié, D., Oshima, N., Parodi, J., Reerink, T. J., Ren, L., Romanou, A., Séférian, R., Tang, Y., Timmreck,
2478 C., Tjiputra, J., Tourigny, E., Tsigaridis, K., Wang, H., Wu, M., Wyser, K., Yang, S., Yang, Y., and Ziehn, T.: The Climate
2479 Response to Emissions Reductions Due to COVID-19: Initial Results From CovidMIP, *Geophys. Res. Lett.*, 48,
2480 e2020GL091883, <https://doi.org/10.1029/2020GL091883>, 2021a.

2481

2482 Jones, M. W., Abatzoglou, J. T., Veraverbeke, S., Andela, N., Lasslop, G., Forkel, M., Smith, A. J. P., Burton, C., Betts, R.
2483 A., van der Werf, G. R., Sitch, S., Canadell, J. G., Santín, C., Kolden, C., Doerr, S. H., and Le Quéré, C.: Global and
2484 Regional Trends and Drivers of Fire Under Climate Change, *Rev. Geophys.*, 60, e2020RG000726,
2485 <https://doi.org/10.1029/2020RG000726>, 2022.

2486 Jones, M. W., Andrew, R. M., Peters, G. P., Janssens-Maenhout, G., De-Gol, A. J., Ciais, P., Patra, P. K., Chevallier, F., and
2487 Le Quéré, C.: Gridded fossil CO₂ emissions and related O₂ combustion consistent with national inventories 1959–2018, *Sci*
2488 *Data*, 8, 2, <https://doi.org/10.1038/s41597-020-00779-6>, 2021b.

2489 Jones, M. W., Andrew, R. M., Peters, G. P., Janssens-Maenhout, G., De-Gol, A. J., Dou, X., Liu, Z., Pickers, P., Ciais, P.,
2490 Patra, P. K., Chevallier, F., and Le Quéré, C.: Gridded fossil CO₂ emissions and related O₂ combustion consistent with
2491 national inventories 1959–2022, Zenodo [dataset], <https://doi.org/10.5281/zenodo.8386803>, 2023.

2492 Jung, M., Reichstein, M., Schwalm, C. R., Huntingford, C., Sitch, S., Ahlström, A., Arneeth, A., Camps-Valls, G., Ciais, P.,
2493 Friedlingstein, P., Gans, F., Ichii, K., Jain, A. K., Kato, E., Papale, D., Poulter, B., Raduly, B., Rödenbeck, C., Tramontana,
2494 G., Viovy, N., Wang, Y.-P., Weber, U., Zaehle, S., and Zeng, N.: Compensatory water effects link yearly global land CO₂
2495 sink changes to temperature, *Nature*, 541, 516–520, <https://doi.org/10.1038/nature20780>, 2017.

2496 Kaiser, J. W., Heil, A., Andreae, M. O., Benedetti, A., Chubarova, N., Jones, L., Morcrette, J.-J., Razinger, M., Schultz, M.
2497 G., Suttie, M., and van der Werf, G. R.: Biomass burning emissions estimated with a global fire assimilation system based
2498 on observed fire radiative power, *Biogeosciences*, 9, 527–554, <https://doi.org/10.5194/bg-9-527-2012>, 2012.

2499 Kato, E., Kinoshita, T., Ito, A., Kawamiya, M., and Yamagata, Y.: Evaluation of spatially explicit emission scenario of land-
2500 use change and biomass burning using a process-based biogeochemical model, *J. Land Use Sci.*, 8, 104–122,
2501 <https://doi.org/10.1080/1747423X.2011.628705>, 2013.

2502 Kawasaki, T., Hasumi, H., and Tanaka, Y.: Role of tide-induced vertical mixing in the deep Pacific Ocean circulation, *J.*
2503 *Oceanogr.*, 77, 173–184, <https://doi.org/10.1007/s10872-020-00584-0>, 2021.

2504 Keeley, J. E. and Pausas, J. G.: Distinguishing disturbance from perturbations in fire-prone ecosystems, *Int. J. Wildland Fire*,
2505 28, 282–287, <https://doi.org/10.1071/WF18203>, 2019.

2506 Keeling, C. D., Bacastow, R. B., Bainbridge, A. E., Ekdahl, C. A., Guenther, P. R., Waterman, L. S., and Chin, J. F. S.:
2507 Atmospheric carbon dioxide variations at Mauna Loa Observatory, Hawaii, *Tellus A.*, 28, 538–551,
2508 <https://doi.org/10.1111/j.2153-3490.1976.tb00701.x>, 1976.

- 2509 Keeling, R. F., Manning, A. C., Paplawsky, W. J., and Cox, A. C.: On the long-term stability of reference gases for
2510 atmospheric O₂/N₂ and CO₂ measurements, *Tellus B Chem. Phys. Meteorol.*, 59, 3–14, [https://doi.org/10.1111/j.1600-](https://doi.org/10.1111/j.1600-0889.2006.00196.x)
2511 [0889.2006.00196.x](https://doi.org/10.1111/j.1600-0889.2006.00196.x), 2007.
- 2512
- 2513 Keeling, R. F. and Manning, A. C.: 5.15 - Studies of Recent Changes in Atmospheric O₂ Content, in: *Treatise on*
2514 *Geochemistry (Second Edition)*, edited by: Holland, H. D. and Turekian, K. K., Elsevier, Oxford, 385–404,
2515 <https://doi.org/10.1016/B978-0-08-095975-7.00420-4>, 2014.
- 2516 Keppler, L. and Landschützer, P.: Regional Wind Variability Modulates the Southern Ocean Carbon Sink, *Sci Rep*, 9, 7384,
2517 <https://doi.org/10.1038/s41598-019-43826-y>, 2019.
- 2518 Khatiwala, S., Primeau, F., and Hall, T.: Reconstruction of the history of anthropogenic CO₂ concentrations in the ocean,
2519 *Nature*, 462, 346–349, <https://doi.org/10.1038/nature08526>, 2009.
- 2520 Khatiwala, S., Tanhua, T., Mikaloff Fletcher, S., Gerber, M., Doney, S. C., Graven, H. D., Gruber, N., McKinley, G. A.,
2521 Murata, A., Ríos, A. F., and Sabine, C. L.: Global ocean storage of anthropogenic carbon, *Biogeosciences*, 10, 2169–2191,
2522 <https://doi.org/10.5194/bg-10-2169-2013>, 2013.
- 2523 Kong, Y., Zheng, B., Zhang, Q., and He, K.: Global and regional carbon budget for 2015–2020 inferred from OCO-2 based
2524 on an ensemble Kalman filter coupled with GEOS-Chem, *Atmospheric Chem. Phys.*, 22, 10769–10788,
2525 <https://doi.org/10.5194/acp-22-10769-2022>, 2022.
- 2526 Korsbakken, J. I., Peters, G. P., and Andrew, R. M.: Uncertainties around reductions in China’s coal use and CO₂ emissions,
2527 *Nature Clim Change*, 6, 687–690, <https://doi.org/10.1038/nclimate2963>, 2016.
- 2528 Krinner, G., Viovy, N., de Noblet-Ducoudré, N., Ogée, J., Polcher, J., Friedlingstein, P., Ciais, P., Sitch, S., and Prentice, I.
2529 C.: A dynamic global vegetation model for studies of the coupled atmosphere-biosphere system: DVGCM for coupled climate
2530 studies, *Global Biogeochem. Cycles*, 19, GB1015, <https://doi.org/10.1029/2003GB002199>, 2005.
- 2531 Lacroix, F., Ilyina, T., and Hartmann, J.: Oceanic CO₂ outgassing and biological production hotspots induced by pre-
2532 industrial river loads of nutrients and carbon in a global modeling approach, *Biogeosciences*, 17, 55–88,
2533 <https://doi.org/10.5194/bg-17-55-2020>, 2020.
- 2534 Lacroix, F., Ilyina, T., Mathis, M., Laruelle, G. G., and Regnier, P.: Historical increases in land-derived nutrient inputs may
2535 alleviate effects of a changing physical climate on the oceanic carbon cycle, *Glob Change Biol*, 27, 5491–5513,
2536 <https://doi.org/10.1111/gcb.15822>, 2021.
- 2537 Lamboll, R. D., Nicholls, Z. R. J., Smith, C. J., Kikstra, J. S., Byers, E., and Rogelj, J.: Assessing the size and uncertainty of
2538 remaining carbon budgets, *Nat. Clim. Change*, <https://doi.org/10.1038/s41558-023-01848-5>, 2023.
- 2539 Lan, X., Tans, P. and K.W. Thoning: Trends in globally-averaged CO₂ determined from NOAA Global Monitoring
2540 Laboratory measurements, Version 2023-09. National Oceanic and Atmospheric Administration, Global Monitoring
2541 Laboratory (NOAA/GML), available at: <https://gml.noaa.gov/ccgg/trends/global.html>, last access: 9 November 2023, 2023.

- 2542 Landschützer, P., Gruber, N., Haumann, F. A., Rödenbeck, C., Bakker, D. C. E., van Heuven, S., Hoppema, M., Metzl, N.,
 2543 Sweeney, C., Takahashi, T., Tilbrook, B., and Wanninkhof, R.: The reinvigoration of the Southern Ocean carbon sink,
 2544 *Science*, 349, 1221–1224, <https://doi.org/10.1126/science.aab2620>, 2015.
- 2545 Landschützer, P., Gruber, N., and Bakker, D. C. E.: Decadal variations and trends of the global ocean carbon sink: decadal
 2546 air-sea CO₂ flux variability, *Global Biogeochem. Cycles*, 30, 1396–1417, <https://doi.org/10.1002/2015GB005359>, 2016.
- 2547 Law, R. M., Ziehn, T., Matear, R. J., Lenton, A., Chamberlain, M. A., Stevens, L. E., Wang, Y.-P., Srbinovsky, J., Bi, D.,
 2548 Yan, H., and Vohralik, P. F.: The carbon cycle in the Australian Community Climate and Earth System Simulator
 2549 (ACCESS-ESM1) – Part 1: Model description and pre-industrial simulation, *Geosci. Model Dev.*, 10, 2567–2590,
 2550 <https://doi.org/10.5194/gmd-10-2567-2017>, 2017.
- 2551 Lawrence, D. M., Fisher, R. A., Koven, C. D., Oleson, K. W., Swenson, S. C., Bonan, G., Collier, N., Ghimire, B., van
 2552 Kampenhout, L., Kennedy, D., Kluzek, E., Lawrence, P. J., Li, F., Li, H., Lombardozzi, D., Riley, W. J., Sacks, W. J., Shi,
 2553 M., Vertenstein, M., Wieder, W. R., Xu, C., Ali, A. A., Badger, A. M., Bisht, G., van den Broeke, M., Brunke, M. A., Burns,
 2554 S. P., Buzan, J., Clark, M., Craig, A., Dahlin, K., Drewniak, B., Fisher, J. B., Flanner, M., Fox, A. M., Gentine, P., Hoffman,
 2555 F., Keppel-Aleks, G., Knox, R., Kumar, S., Lenaerts, J., Leung, L. R., Lipscomb, W. H., Lu, Y., Pandey, A., Pelletier, J. D.,
 2556 Perket, J., Randerson, J. T., Ricciuto, D. M., Sanderson, B. M., Slater, A., Subin, Z. M., Tang, J., Thomas, R. Q., Val Martin,
 2557 M., and Zeng, X.: The Community Land Model Version 5: Description of New Features, Benchmarking, and Impact of
 2558 Forcing Uncertainty, *J. Adv. Model Earth, Sy.*, 11, 4245–4287, <https://doi.org/10.1029/2018MS001583>, 2019.
- 2559 Le Quéré, C., Rödenbeck, C., Buitenhuis, E. T., Conway, T. J., Langenfelds, R., Gomez, A., Labuschagne, C., Ramonet, M.,
 2560 Nakazawa, T., Metzl, N., Gillett, N., and Heimann, M.: Saturation of the Southern Ocean CO₂ Sink Due to Recent Climate
 2561 Change, *Science*, 316, 1735–1738, <https://doi.org/10.1126/science.1136188>, 2007.
- 2562 Le Quéré, C., Raupach, M. R., Canadell, J. G., Marland, G., Bopp, L., Ciais, P., Conway, T. J., Doney, S. C., Feely, R. A.,
 2563 Foster, P., Friedlingstein, P., Gurney, K., Houghton, R. A., House, J. I., Huntingford, C., Levy, P. E., Lomas, M. R., Majkut,
 2564 J., Metzl, N., Ometto, J. P., Peters, G. P., Prentice, I. C., Randerson, J. T., Running, S. W., Sarmiento, J. L., Schuster, U.,
 2565 Sitch, S., Takahashi, T., Viovy, N., van der Werf, G. R., and Woodward, F. I.: Trends in the sources and sinks of carbon
 2566 dioxide, *Nature Geosci*, 2, 831–836, <https://doi.org/10.1038/ngeo689>, 2009.
- 2567 Le Quéré, C., Andres, R. J., Boden, T., Conway, T., Houghton, R. A., House, J. I., Marland, G., Peters, G. P., van der Werf,
 2568 G. R., Ahlström, A., Andrew, R. M., Bopp, L., Canadell, J. G., Ciais, P., Doney, S. C., Enright, C., Friedlingstein, P.,
 2569 Huntingford, C., Jain, A. K., Jourdain, C., Kato, E., Keeling, R. F., Klein Goldewijk, K., Levis, S., Levy, P., Lomas, M.,
 2570 Poulter, B., Raupach, M. R., Schwinger, J., Sitch, S., Stocker, B. D., Viovy, N., Zaehle, S., and Zeng, N.: The global carbon
 2571 budget 1959–2011, *Earth Syst. Sci. Data*, 5, 165–185, <https://doi.org/10.5194/essd-5-165-2013>, 2013.
- 2572 Le Quéré, C., Peters, G. P., Andres, R. J., Andrew, R. M., Boden, T. A., Ciais, P., Friedlingstein, P., Houghton, R. A.,
 2573 Marland, G., Moriarty, R., Sitch, S., Tans, P., Arneth, A., Arvanitis, A., Bakker, D. C. E., Bopp, L., Canadell, J. G., Chini, L.
 2574 P., Doney, S. C., Harper, A., Harris, I., House, J. I., Jain, A. K., Jones, S. D., Kato, E., Keeling, R. F., Klein Goldewijk, K.,
 2575 Körtzinger, A., Koven, C., Lefèvre, N., Maignan, F., Omar, A., Ono, T., Park, G.-H., Pfeil, B., Poulter, B., Raupach, M. R.,
 2576 Regnier, P., Rödenbeck, C., Saito, S., Schwinger, J., Segsneider, J., Stocker, B. D., Takahashi, T., Tilbrook, B., van
 2577 Heuven, S., Viovy, N., Wanninkhof, R., Wiltshire, A., and Zaehle, S.: Global carbon budget 2013, *Earth Syst. Sci. Data*, 6,
 2578 235–263, <https://doi.org/10.5194/essd-6-235-2014>, 2014.

- 2579 Le Quéré, C., Moriarty, R., Andrew, R. M., Peters, G. P., Ciais, P., Friedlingstein, P., Jones, S. D., Sitch, S., Tans, P.,
2580 Arneth, A., Boden, T. A., Bopp, L., Bozec, Y., Canadell, J. G., Chini, L. P., Chevallier, F., Cosca, C. E., Harris, I.,
2581 Hoppema, M., Houghton, R. A., House, J. I., Jain, A. K., Johannessen, T., Kato, E., Keeling, R. F., Kitidis, V., Klein
2582 Goldewijk, K., Koven, C., Landa, C. S., Landschützer, P., Lenton, A., Lima, I. D., Marland, G., Mathis, J. T., Metzl, N.,
2583 Nojiri, Y., Olsen, A., Ono, T., Peng, S., Peters, W., Pfeil, B., Poulter, B., Raupach, M. R., Regnier, P., Rödenbeck, C., Saito,
2584 S., Salisbury, J. E., Schuster, U., Schwinger, J., Séférian, R., Segschneider, J., Steinhoff, T., Stocker, B. D., Sutton, A. J.,
2585 Takahashi, T., Tilbrook, B., van der Werf, G. R., Viovy, N., Wang, Y.-P., Wanninkhof, R., Wiltshire, A., and Zeng, N.:
2586 Global carbon budget 2014, *Earth Syst. Sci. Data*, 7, 47–85, <https://doi.org/10.5194/essd-7-47-2015>, 2015a.
- 2587 Le Quéré, C., Moriarty, R., Andrew, R. M., Canadell, J. G., Sitch, S., Korsbakken, J. I., Friedlingstein, P., Peters, G. P.,
2588 Andres, R. J., Boden, T. A., Houghton, R. A., House, J. I., Keeling, R. F., Tans, P., Arneth, A., Bakker, D. C. E., Barbero,
2589 L., Bopp, L., Chang, J., Chevallier, F., Chini, L. P., Ciais, P., Fader, M., Feely, R. A., Gkritzalis, T., Harris, I., Hauck, J.,
2590 Ilyina, T., Jain, A. K., Kato, E., Kitidis, V., Klein Goldewijk, K., Koven, C., Landschützer, P., Lauvset, S. K., Lefèvre, N.,
2591 Lenton, A., Lima, I. D., Metzl, N., Millero, F., Munro, D. R., Murata, A., Nabel, J. E. M. S., Nakaoka, S., Nojiri, Y.,
2592 O'Brien, K., Olsen, A., Ono, T., Pérez, F. F., Pfeil, B., Pierrot, D., Poulter, B., Rehder, G., Rödenbeck, C., Saito, S.,
2593 Schuster, U., Schwinger, J., Séférian, R., Steinhoff, T., Stocker, B. D., Sutton, A. J., Takahashi, T., Tilbrook, B., van der
2594 Laan-Luijkx, I. T., van der Werf, G. R., van Heuven, S., Vandemark, D., Viovy, N., Wiltshire, A., Zaehle, S., and Zeng, N.:
2595 Global Carbon Budget 2015, *Earth Syst. Sci. Data*, 7, 349–396, <https://doi.org/10.5194/essd-7-349-2015>, 2015b.
- 2596 Le Quéré, C., Andrew, R. M., Canadell, J. G., Sitch, S., Korsbakken, J. I., Peters, G. P., Manning, A. C., Boden, T. A., Tans,
2597 P. P., Houghton, R. A., Keeling, R. F., Alin, S., Andrews, O. D., Anthoni, P., Barbero, L., Bopp, L., Chevallier, F., Chini, L.
2598 P., Ciais, P., Currie, K., Delire, C., Doney, S. C., Friedlingstein, P., Gkritzalis, T., Harris, I., Hauck, J., Haverd, V.,
2599 Hoppema, M., Klein Goldewijk, K., Jain, A. K., Kato, E., Körtzinger, A., Landschützer, P., Lefèvre, N., Lenton, A., Lienert,
2600 S., Lombardozi, D., Melton, J. R., Metzl, N., Millero, F., Monteiro, P. M. S., Munro, D. R., Nabel, J. E. M. S., Nakaoka, S.,
2601 O'Brien, K., Olsen, A., Omar, A. M., Ono, T., Pierrot, D., Poulter, B., Rödenbeck, C., Salisbury, J., Schuster, U., Schwinger,
2602 J., Séférian, R., Skjelvan, I., Stocker, B. D., Sutton, A. J., Takahashi, T., Tian, H., Tilbrook, B., van der Laan-Luijkx, I. T.,
2603 van der Werf, G. R., Viovy, N., Walker, A. P., Wiltshire, A. J., and Zaehle, S.: Global Carbon Budget 2016, *Earth Syst. Sci.*
2604 *Data*, 8, 605–649, <https://doi.org/10.5194/essd-8-605-2016>, 2016.
- 2605 Le Quéré, C., Andrew, R. M., Friedlingstein, P., Sitch, S., Pongratz, J., Manning, A. C., Korsbakken, J. I., Peters, G. P.,
2606 Canadell, J. G., Jackson, R. B., Boden, T. A., Tans, P. P., Andrews, O. D., Arora, V. K., Bakker, D. C. E., Barbero, L.,
2607 Becker, M., Betts, R. A., Bopp, L., Chevallier, F., Chini, L. P., Ciais, P., Cosca, C. E., Cross, J., Currie, K., Gasser, T.,
2608 Harris, I., Hauck, J., Haverd, V., Houghton, R. A., Hunt, C. W., Hurtt, G., Ilyina, T., Jain, A. K., Kato, E., Kautz, M.,
2609 Keeling, R. F., Klein Goldewijk, K., Körtzinger, A., Landschützer, P., Lefèvre, N., Lenton, A., Lienert, S., Lima, I.,
2610 Lombardozi, D., Metzl, N., Millero, F., Monteiro, P. M. S., Munro, D. R., Nabel, J. E. M. S., Nakaoka, S., Nojiri, Y., Padin,
2611 X. A., Peregon, A., Pfeil, B., Pierrot, D., Poulter, B., Rehder, G., Reimer, J., Rödenbeck, C., Schwinger, J., Séférian, R.,
2612 Skjelvan, I., Stocker, B. D., Tian, H., Tilbrook, B., Tubiello, F. N., van der Laan-Luijkx, I. T., van der Werf, G. R., van
2613 Heuven, S., Viovy, N., Vuichard, N., Walker, A. P., Watson, A. J., Wiltshire, A. J., Zaehle, S., and Zhu, D.: Global Carbon
2614 Budget 2017, *Earth Syst. Sci. Data*, 10, 405–448, <https://doi.org/10.5194/essd-10-405-2018>, 2018a.
- 2615 Le Quéré, C., Andrew, R. M., Friedlingstein, P., Sitch, S., Hauck, J., Pongratz, J., Pickers, P. A., Korsbakken, J. I., Peters, G.
2616 P., Canadell, J. G., Arneth, A., Arora, V. K., Barbero, L., Bastos, A., Bopp, L., Chevallier, F., Chini, L. P., Ciais, P., Doney,
2617 S. C., Gkritzalis, T., Goll, D. S., Harris, I., Haverd, V., Hoffman, F. M., Hoppema, M., Houghton, R. A., Hurtt, G., Ilyina, T.,
2618 Jain, A. K., Johannessen, T., Jones, C. D., Kato, E., Keeling, R. F., Klein Goldewijk, K., Landschützer, P., Lefèvre, N.,

- 2619 Lienert, S., Liu, Z., Lombardozi, D., Metzl, N., Munro, D. R., Nabel, J. E. M. S., Nakaoka, S., Neill, C., Olsen, A., Ono, T.,
2620 Patra, P., Peregon, A., Peters, W., Peylin, P., Pfeil, B., Pierrot, D., Poulter, B., Rehder, G., Resplandy, L., Robertson, E.,
2621 Rocher, M., Rödenbeck, C., Schuster, U., Schwinger, J., Séférian, R., Skjelvan, I., Steinhoff, T., Sutton, A., Tans, P. P.,
2622 Tian, H., Tilbrook, B., Tubiello, F. N., van der Laan-Luijkx, I. T., van der Werf, G. R., Viovy, N., Walker, A. P., Wiltshire,
2623 A. J., Wright, R., Zaehle, S., and Zheng, B.: Global Carbon Budget 2018, *Earth Syst. Sci. Data*, 10, 2141–2194,
2624 <https://doi.org/10.5194/essd-10-2141-2018>, 2018b.
- 2625 Le Quéré, C., Korsbakken, J. I., Wilson, C., Tosun, J., Andrew, R., Andres, R. J., Canadell, J. G., Jordan, A., Peters, G. P.,
2626 and van Vuuren, D. P.: Drivers of declining CO₂ emissions in 18 developed economies, *Nat. Clim. Chang.*, 9, 213–217,
2627 <https://doi.org/10.1038/s41558-019-0419-7>, 2019.
- 2628 Le Quéré, C., Peters, G. P., Friedlingstein, P., Andrew, R. M., Canadell, J. G., Davis, S. J., Jackson, R. B., and Jones, M. W.:
2629 Fossil CO₂ emissions in the post-COVID-19 era, *Nat. Clim. Chang.*, 11, 197–199, [https://doi.org/10.1038/s41558-021-](https://doi.org/10.1038/s41558-021-01001-0)
2630 [01001-0](https://doi.org/10.1038/s41558-021-01001-0), 2021.
- 2631 Levitus, S., Antonov, J. I., Boyer, T. P., Baranova, O. K., Garcia, H. E., Locarnini, R. A., Mishonov, A. V., Reagan, J. R.,
2632 Seidov, D., Yarosh, E. S., and Zweng, M. M.: World ocean heat content and thermocline sea level change (0–2000 m),
2633 1955–2010, *Geophys. Res. Lett.*, 39, <https://doi.org/10.1029/2012GL051106>, 2012.
2634
- 2635 Li, H., Ilyina, T., Müller, W. A., and Sienz, F.: Decadal predictions of the North Atlantic CO₂ uptake, *Nat. Commun.*, 7,
2636 11076, <https://doi.org/10.1038/ncomms11076>, 2016.
2637
- 2638 Li, H., Ilyina, T., Müller, W. A., and Landschützer, P.: Predicting the variable ocean carbon sink, *Sci. Adv.*, 5, eaav6471,
2639 <https://doi.org/10.1126/sciadv.aav6471>, 2019.
2640
- 2641 Li, H., Ilyina, T., Loughran, T., Spring, A., and Pongratz, J.: Reconstructions and predictions of the global carbon budget
2642 with an emission-driven Earth system model, *Earth Syst. Dyn.*, 14, 101–119, <https://doi.org/10.5194/esd-14-101-2023>, 2023.
- 2643 Li, W., Ciais, P., Peng, S., Yue, C., Wang, Y., Thurner, M., Saatchi, S. S., Arneeth, A., Avitabile, V., Carvalhais, N., Harper,
2644 A. B., Kato, E., Koven, C., Liu, Y. Y., Nabel, J. E. M. S., Pan, Y., Pongratz, J., Poulter, B., Pugh, T. A. M., Santoro, M.,
2645 Sitch, S., Stocker, B. D., Viovy, N., Wiltshire, A., Yousefpour, R., and Zaehle, S.: Land-use and land-cover change carbon
2646 emissions between 1901 and 2012 constrained by biomass observations, *Biogeosciences*, 14, 5053–5067,
2647 <https://doi.org/10.5194/bg-14-5053-2017>, 2017.
- 2648 Liao, E., Resplandy, L., Liu, J., and Bowman, K. W.: Amplification of the Ocean Carbon Sink During El Niños: Role of
2649 Poleward Ekman Transport and Influence on Atmospheric CO₂, *Global Biogeochem. Cy.*, 34, e2020GB006574,
2650 <https://doi.org/10.1029/2020GB006574>, 2020.
- 2651 Lienert, S. and Joos, F.: A Bayesian ensemble data assimilation to constrain model parameters and land-use carbon
2652 emissions, *Biogeosciences*, 15, 2909–2930, <https://doi.org/10.5194/bg-15-2909-2018>, 2018.
- 2653 Liu, J., Baskaran, L., Bowman, K., Schimel, D., Bloom, A. A., Parazoo, N. C., Oda, T., Carroll, D., Menemenlis, D., Joiner,
2654 J., Commane, R., Daube, B., Gatti, L. V., McKain, K., Miller, J., Stephens, B. B., Sweeney, C., and Wofsy, S.: Carbon
2655 Monitoring System Flux Net Biosphere Exchange 2020 (CMS-Flux NBE 2020), 13, 299–330, [https://doi.org/10.5194/essd-](https://doi.org/10.5194/essd-13-299-2021)
2656 [13-299-2021](https://doi.org/10.5194/essd-13-299-2021), 2021.

- 2657 Liu, Z., Guan, D., Wei, W., Davis, S. J., Ciais, P., Bai, J., Peng, S., Zhang, Q., Hubacek, K., Marland, G., Andres, R. J.,
 2658 Crawford-Brown, D., Lin, J., Zhao, H., Hong, C., Boden, T. A., Feng, K., Peters, G. P., Xi, F., Liu, J., Li, Y., Zhao, Y.,
 2659 Zeng, N., and He, K.: Reduced carbon emission estimates from fossil fuel combustion and cement production in China,
 2660 *Nature*, 524, 335–338, <https://doi.org/10.1038/nature14677>, 2015.
- 2661 Liu, Z., Zeng, N., Liu, Y., Kalnay, E., Asrar, G., Wu, B., Cai, Q., Liu, D., and Han, P.: Improving the joint estimation of
 2662 CO₂ and surface carbon fluxes using a constrained ensemble Kalman filter in COLA (v1.0), *Geosci. Model Dev.*, 15, 5511–
 2663 5528, <https://doi.org/10.5194/gmd-15-5511-2022>, 2022.
- 2664
 2665 Lovenduski, N. S., Bonan, G. B., Yeager, S. G., Lindsay, K., and Lombardozzi, D. L.: High predictability of terrestrial
 2666 carbon fluxes from an initialized decadal prediction system, *Environ. Res. Lett.*, 14, 124074, <https://doi.org/10.1088/1748-9326/ab5c55>, 2019a.
- 2667
 2668
 2669 Lovenduski, N. S., Yeager, S. G., Lindsay, K., and Long, M. C.: Predicting near-term variability in ocean carbon uptake,
 2670 *Earth Syst. Dyn.*, 10, 45–57, <https://doi.org/10.5194/esd-10-45-2019>, 2019b.
- 2671 Lutz, F., Herzfeld, T., Heinke, J., Rolinski, S., Schaphoff, S., von Bloh, W., Stoorvogel, J. J., and Müller, C.: Simulating the
 2672 effect of tillage practices with the global ecosystem model LPJmL (version 5.0-tillage), *Geosci. Model Dev.*, 12, 2419–2440,
 2673 <https://doi.org/10.5194/gmd-12-2419-2019>, 2019.
- 2674 Ma, L., Hurtt, G., Ott, L., Sahajpal, R., Fisk, J., Lamb, R., Tang, H., Flanagan, S., Chini, L., Chatterjee, A., and Sullivan, J.:
 2675 Global evaluation of the Ecosystem Demography model (ED v3.0), *Geosci. Model Dev.*, 15, 1971–1994,
 2676 <https://doi.org/10.5194/gmd-15-1971-2022>, 2022.
- 2677
 2678 Magi, B. I., Rabin, S., Shevliakova, E., and Pacala, S.: Separating agricultural and non-agricultural fire seasonality at
 2679 regional scales, *Biogeosciences*, 9, 3003–3012, <https://doi.org/10.5194/bg-9-3003-2012>, 2012.
- 2680 Masarie, K. A. and Tans, P. P.: Extension and integration of atmospheric carbon dioxide data into a globally consistent
 2681 measurement record, *J. Geophys. Res.*, 100, 11593, <https://doi.org/10.1029/95JD00859>, 1995.
- 2682 Mather, A. S.: The transition from deforestation to reforestation in Europe, in: *Agricultural technologies and tropical*
 2683 *deforestation* (eds. Angelsen, A.; Kaimowitz, D.), CABI in association with centre for international Forestry Research, 35–
 2684 52, 2001.
- 2685 Mauritsen, T., Bader, J., Becker, T., Behrens, J., Bittner, M., Brokopf, R., Brovkin, V., Claussen, M., Crueger, T., Esch, M.,
 2686 Fast, I., Fiedler, S., Fläschner, D., Gayler, V., Giorgetta, M., Goll, D. S., Haak, H., Hagemann, S., Hedemann, C.,
 2687 Hohensee, C., Ilyina, T., Jahns, T., Jimenez-de-la-Cuesta, D., Jungclaus, J., Kleinen, T., Kloster, S., Kracher, D., Kinne,
 2688 S., Kleberg, D., Lasslop, G., Kornbluh, L., Marotzke, J., Matei, D., Meraner, K., Mikolajewicz, U., Modali, K., Möbis, B.,
 2689 Müller, W. A., Nabel, J. E. M. S., Nam, C. C. W., Notz, D., Nyawira, S.-S., Paulsen, H., Peters, K., Pincus, R., Pohlmann,
 2690 H., Pongratz, J., Popp, M., Raddatz, T. J., Rast, S., Redler, R., Reick, C. H., Rohrschneider, T., Schemann, V., Schmidt, H.,
 2691 Schnur, R., Schulzweida, U., Six, K. D., Stein, L., Stemmler, I., Stevens, B., von Storch, J.-S., Tian, F., Voigt, A., Vrese, P.,
 2692 Wieners, K.-H., Wilkenskjaeld, S., Winkler, A., and Roeckner, E.: Developments in the MPI-M Earth System Model version
 2693 1.2 (MPI-ESM1.2) and Its Response to Increasing CO₂, *J. Adv. Model Earth Sy.*, 11, 998–1038,
 2694 <https://doi.org/10.1029/2018MS001400>, 2019.

- 2695 McGrath, M. J., Luysaert, S., Meyfroidt, P., Kaplan, J. O., Bürgi, M., Chen, Y., Erb, K., Gimmi, U., McNerney, D., Naudts,
2696 K., Otto, J., Pasztor, F., Ryder, J., Schelhaas, M.-J., and Valade, A.: Reconstructing European forest management from 1600
2697 to 2010, 12, 4291–4316, <https://doi.org/10.5194/bg-12-4291-2015>, 2015.
- 2698 McKinley, G. A., Fay, A. R., Eddebbbar, Y. A., Gloege, L., and Lovenduski, N. S.: External Forcing Explains Recent
2699 Decadal Variability of the Ocean Carbon Sink, *AGU Advances*, 1, e2019AV000149,
2700 <https://doi.org/10.1029/2019AV000149>, 2020.
- 2701 McKinley, G. A., Fay, A. R., Lovenduski, N. S., and Pilcher, D. J.: Natural Variability and Anthropogenic Trends in the
2702 Ocean Carbon Sink, *Annu. Rev. Mar. Sci.*, 9, 125–150, <https://doi.org/10.1146/annurev-marine-010816-060529>, 2017.
- 2703 Meiyappan, P., Jain, A. K., and House, J. I.: Increased influence of nitrogen limitation on CO₂ emissions from future land
2704 use and land use change, *Global Biogeochem. Cycles*, 29, 1524–1548, <https://doi.org/10.1002/2015GB005086>, 2015.
- 2705 Melton, J. R., Arora, V. K., Wisernig-Cojoc, E., Seiler, C., Fortier, M., Chan, E., and Teckentrup, L.: CLASSIC v1.0: the
2706 open-source community successor to the Canadian Land Surface Scheme (CLASS) and the Canadian Terrestrial Ecosystem
2707 Model (CTEM) – Part 1: Model framework and site-level performance, *Geosci. Model Dev.*, 13, 2825–2850,
2708 <https://doi.org/10.5194/gmd-13-2825-2020>, 2020.
- 2709 Mercado, L. M., Bellouin, N., Sitch, S., Boucher, O., Huntingford, C., Wild, M., and Cox, P. M.: Impact of changes in
2710 diffuse radiation on the global land carbon sink, *Nature*, 458, 1014–1017, <https://doi.org/10.1038/nature07949>, 2009.
- 2711 Merchant, C. J., Embury, O., Bulgin, C. E., Block, T., Corlett, G. K., Fiedler, E., Good, S. A., Mittaz, J., Rayner, N. A.,
2712 Berry, D., Eastwood, S., Taylor, M., Tsushima, Y., Waterfall, A., Wilson, R., and Donlon, C.: Satellite-based time-series of
2713 sea-surface temperature since 1981 for climate applications, *Sci. Data*, 6, 223, <https://doi.org/10.1038/s41597-019-0236-x>,
2714 2019.
- 2715 Moorcroft, P. R., Hurtt, G. C., and Pacala, S. W.: A Method for Scaling Vegetation Dynamics: The Ecosystem Demography
2716 Model (ed), *Ecol. Monogr.*, 71, 557–586, [https://doi.org/10.1890/0012-9615\(2001\)071\[0557:AMFSVD\]2.0.CO;2](https://doi.org/10.1890/0012-9615(2001)071[0557:AMFSVD]2.0.CO;2), 2001.
- 2717 Müller, J. D., Gruber, N., Carter, B., Feely, R., Ishii, M., Lange, N., Lauvset, S. K., Murata, A., Olsen, A., Pérez, F. F.,
2718 Sabine, C., Tanhua, T., Wanninkhof, R., and Zhu, D.: Decadal Trends in the Oceanic Storage of Anthropogenic Carbon
2719 From 1994 to 2014, *AGU Adv.*, 4, e2023AV000875, <https://doi.org/10.1029/2023AV000875>, 2023.
- 2720 Nakano, H., Tsujino, H., Hirabara, M., Yasuda, T., Motoi, T., Ishii, M., and Yamanaka, G.: Uptake mechanism of
2721 anthropogenic CO₂ in the Kuroshio Extension region in an ocean general circulation model, *J. Oceanogr.*, 67, 765–783,
2722 <https://doi.org/10.1007/s10872-011-0075-7>, 2011.
- 2723 NCEP: National Centers for Environmental Prediction. ONI Index. Cold & Warm Episodes by Season, available at:
2724 https://origin.cpc.ncep.noaa.gov/products/analysis_monitoring/ensostuff/ONI_v5.php, last access: 9 November 2023, 2023.
- 2725 Niu, G.-Y., Yang, Z.-L., Mitchell, K. E., Chen, F., Ek, M. B., Barlage, M., Kumar, A., Manning, K., Niyogi, D., Rosero, E.,
2726 Tewari, M., and Xia, Y.: The community Noah land surface model with multiparameterization options (Noah-MP): 1. Model
2727 description and evaluation with local-scale measurements, *J. Geophys. Res. Atmospheres*, 116,
2728 <https://doi.org/10.1029/2010JD015139>, 2011.

- 2729 Niwa, Y., Ishijima, K., Ito, A., and Iida, Y.: Toward a long-term atmospheric CO₂ inversion for elucidating natural carbon
 2730 fluxes: technical notes of NISMON-CO₂ v2021.1, *Prog. Earth Planet Sci.*, 9, 42, [https://doi.org/10.1186/s40645-022-00502-](https://doi.org/10.1186/s40645-022-00502-6)
 2731 6, 2022.
- 2732 Niwa, Y., Langenfelds, R., Krummel, P., Loh, Zoe, Worthy, Doug, Hatakka, Juha, Aalto, Tuula, Ramonet, Michel,
 2733 Delmotte, Marc, Schmidt, Martina, Gheusi, Francois, Mihalopoulos, N., Morgui, J.A., Andrews, Arlyn, Dlugokencky, Ed,
 2734 Lee, John, Sweeney, Colm, Thoning, Kirk, Tans, Pieter, De Wekker, Stephan, Fischer, Marc L., Jaffe, Dan, McKain,
 2735 Kathryn, Viner, Brian, Miller, John B., Karion, Anna, Miller, Charles, Sloop, Christopher D., Saito, Kazuyuki, Aoki, Shuji,
 2736 Morimoto, Shinji, Goto, Daisuke, Steinbacher, Martin, Myhre, Cathrine Lund, Hermanssen, Ove, Stephens, Britton, Keeling,
 2737 Ralph, Afshar, Sara, Paplawsky, Bill, Cox, Adam, Walker, Stephen, Schuldt, Kenneth, Mukai, Hitoshi, Machida, Toshinobu,
 2738 Sasakawa, Motoki, Nomura, Shohei, Ito, Akihiko, Iida, Yosuke, and Jones, Matthew W.: Long-term global CO₂ fluxes
 2739 estimated by NICAM-based Inverse Simulation for Monitoring CO₂ (NISMON-CO₂) (ver.2022.1), National Institute for
 2740 Environmental Studies Japan [dataset], <https://doi.org/10.17595/20201127.001>, 2020.
- 2741 Obermeier, W. A., Nabel, J. E. M. S., Loughran, T., Hartung, K., Bastos, A., Havermann, F., Anthoni, P., Arneth, A., Goll,
 2742 D. S., Lienert, S., Lombardozzi, D., Luysaert, S., McGuire, P. C., Melton, J. R., Poulter, B., Sitch, S., Sullivan, M. O., Tian,
 2743 H., Walker, A. P., Wiltshire, A. J., Zaehle, S., and Pongratz, J.: Modelled land use and land cover change emissions – a
 2744 spatio-temporal comparison of different approaches, 12, 635–670, <https://doi.org/10.5194/esd-12-635-2021>, 2021.
- 2745 O'Rourke, P. R., Smith, S. J., Mott, A., Ahsan, H., McDuffie, E. E., Crippa, M., Klimont, Z., McDonald, B., Wang, S.,
 2746 Nicholson, M. B., Feng, L., and Hoesly, R. M.: CEDS v_2021_04_21 Release Emission Data,
 2747 <https://doi.org/10.5281/zenodo.4741285>, 2021.
- 2748 O'Sullivan, M., Zhang, Y., Bellouin, N., Harris, I., Mercado, L. M., Sitch, S., Ciais, P., and Friedlingstein, P.: Aerosol–light
 2749 interactions reduce the carbon budget imbalance, *Environ. Res. Lett.*, 16, 124072, <https://doi.org/10.1088/1748-9326/ac3b77>,
 2750 2021.
- 2751 O'Sullivan, M., Friedlingstein, P., Sitch, S., Anthoni, P., Arneth, A., Arora, V. K., Bastrikov, V., Delire, C., Goll, D. S., Jain,
 2752 A., Kato, E., Kennedy, D., Knauer, J., Lienert, S., Lombardozzi, D., McGuire, P. C., Melton, J. R., Nabel, J. E. M. S.,
 2753 Pongratz, J., Poulter, B., Séférian, R., Tian, H., Vuichard, N., Walker, A. P., Yuan, W., Yue, X., and Zaehle, S.: Process-
 2754 oriented analysis of dominant sources of uncertainty in the land carbon sink, *Nat. Commun.*, 13, 4781,
 2755 <https://doi.org/10.1038/s41467-022-32416-8>, 2022.
- 2756 O'Sullivan, M., Spracklen, D. V., Batterman, S. A., Arnold, S. R., Gloor, M., and Buermann, W.: Have Synergies Between
 2757 Nitrogen Deposition and Atmospheric CO₂ Driven the Recent Enhancement of the Terrestrial Carbon Sink?, *Glob.*
 2758 *Biogeochem. Cycles*, 33, 163–180, <https://doi.org/10.1029/2018GB005922>, 2019.
- 2759 Palmer, P. I., Feng, L., Baker, D., Chevallier, F., Bösch, H., and Somkuti, P.: Net carbon emissions from African biosphere
 2760 dominate pan-tropical atmospheric CO₂ signal, *Nat Commun*, 10, 3344, <https://doi.org/10.1038/s41467-019-11097-w>, 2019.
- 2761 Pan, Y., Birdsey, R. A., Fang, J., Houghton, R., Kauppi, P. E., Kurz, W. A., Phillips, O. L., Shvidenko, A., Lewis, S. L.,
 2762 Canadell, J. G., Ciais, P., Jackson, R. B., Pacala, S. W., McGuire, A. D., Piao, S., Rautiainen, A., Sitch, S., and Hayes, D.: A
 2763 Large and Persistent Carbon Sink in the World's Forests, *Science*, 333, 988–993, <https://doi.org/10.1126/science.1201609>,
 2764 2011.

- 2765 Pendrill, F., Persson, U. M., Godar, J., Kastner, T., Moran, D., Schmidt, S., and Wood, R.: Agricultural and forestry trade
2766 drives large share of tropical deforestation emissions, *Global Environmental Change*, 56, 1–10,
2767 <https://doi.org/10.1016/j.gloenvcha.2019.03.002>, 2019.
- 2768 Peters, G. P., Minx, J. C., Weber, C. L., and Edenhofer, O.: Growth in emission transfers via international trade from 1990 to
2769 2008, *Proceedings of the National Academy of Sciences*, 108, 8903–8908, <https://doi.org/10.1073/pnas.1006388108>, 2011a.
- 2770 Peters, G. P., Marland, G., Le Quéré, C., Boden, T., Canadell, J. G., and Raupach, M. R.: Rapid growth in CO₂ emissions
2771 after the 2008–2009 global financial crisis, *Nature Clim Change*, 2, 2–4, <https://doi.org/10.1038/nclimate1332>, 2012a.
- 2772 Peters, G. P., Andrew, R. M., Boden, T., Canadell, J. G., Ciais, P., Le Quéré, C., Marland, G., Raupach, M. R., and Wilson,
2773 C.: The challenge to keep global warming below 2 °C, *Nature Clim Change*, 3, 4–6, <https://doi.org/10.1038/nclimate1783>,
2774 2013.
- 2775 Peters, G. P., Le Quéré, C., Andrew, R. M., Canadell, J. G., Friedlingstein, P., Ilyina, T., Jackson, R. B., Joos, F.,
2776 Korsbakken, J. I., McKinley, G. A., Sitch, S., and Tans, P.: Towards real-time verification of CO₂ emissions, *Nature Clim*
2777 *Change*, 7, 848–850, <https://doi.org/10.1038/s41558-017-0013-9>, 2017.
- 2778 Peters, G. P., Andrew, R. M., Canadell, J. G., Friedlingstein, P., Jackson, R. B., Korsbakken, J. I., Le Quéré, C., and
2779 Peregón, A.: Carbon dioxide emissions continue to grow amidst slowly emerging climate policies, *Nat. Clim. Chang.*, 10, 3–
2780 6, <https://doi.org/10.1038/s41558-019-0659-6>, 2020.
- 2781 Peters, W., Miller, J. B., Whitaker, J., Denning, A. S., Hirsch, A., Krol, M. C., Zupanski, D., Bruhwiler, L., and Tans, P. P.:
2782 An ensemble data assimilation system to estimate CO₂ surface fluxes from atmospheric trace gas observations, *J. Geophys.*
2783 *Res. Atmospheres*, 110, <https://doi.org/10.1029/2005JD006157>, 2005.
- 2784 Peters W, Woude Avd, Luijkx I, Joetzer E, Lafont S, Loubet B, Herig-Coimbra P, Loustau D, Koren G, Ciais P, Ramonet
2785 M, Xu Y, Bastos A, Sitch S, Kneuer T, Kubistin D, De Kok R, Botía S. Temperature extremes of 2022 reduced carbon
2786 uptake by forests in Europe. doi:10.21203/rs.3.rs-2841861/v1. PPR:PPR653515, 2023.
- 2787 Petrescu, A. M. R., Peters, G. P., Janssens-Maenhout, G., Ciais, P., Tubiello, F. N., Grassi, G., Nabuurs, G.-J., Leip, A.,
2788 Carmona-García, G., Winiwarter, W., Höglund-Isaksson, L., Günther, D., Solazzo, E., Kiesow, A., Bastos, A., Pongratz, J.,
2789 Nabel, J. E. M. S., Conchedda, G., Pilli, R., Andrew, R. M., Schelhaas, M.-J., and Dolman, A. J.: European anthropogenic
2790 AFOLU greenhouse gas emissions: a review and benchmark data, *Earth Syst. Sci. Data*, 12, 961–1001,
2791 <https://doi.org/10.5194/essd-12-961-2020>, 2020.
- 2792 Pfeil, B., Olsen, A., Bakker, D. C. E., Hankin, S., Koyuk, H., Kozyr, A., Malczyk, J., Manke, A., Metz, N., Sabine, C. L.,
2793 Akl, J., Alin, S. R., Bates, N., Bellerby, R. G. J., Borges, A., Boutin, J., Brown, P. J., Cai, W.-J., Chavez, F. P., Chen, A.,
2794 Cosca, C., Fassbender, A. J., Feely, R. A., González-Dávila, M., Goyet, C., Hales, B., Hardman-Mountford, N., Heinze, C.,
2795 Hood, M., Hoppema, M., Hunt, C. W., Hydes, D., Ishii, M., Johannessen, T., Jones, S. D., Key, R. M., Körtzinger, A.,
2796 Landschützer, P., Lauvset, S. K., Lefèvre, N., Lenton, A., Lourantou, A., Merlivat, L., Midorikawa, T., Mintrop, L.,
2797 Miyazaki, C., Murata, A., Nakadate, A., Nakano, Y., Nakaoka, S., Nojiri, Y., Omar, A. M., Padin, X. A., Park, G.-H.,
2798 Paterson, K., Perez, F. F., Pierrot, D., Poisson, A., Ríos, A. F., Santana-Casiano, J. M., Salisbury, J., Sarma, V. V. S. S.,
2799 Schlitzer, R., Schneider, B., Schuster, U., Sieger, R., Skjelvan, I., Steinhoff, T., Suzuki, T., Takahashi, T., Tedesco, K.,
2800 Telszewski, M., Thomas, H., Tilbrook, B., Tjiputra, J., Vandemark, D., Veness, T., Wanninkhof, R., Watson, A. J., Weiss,

- 2801 R., Wong, C. S., and Yoshikawa-Inoue, H.: A uniform, quality controlled Surface Ocean CO₂ Atlas (SOCAT), *Earth Syst.*
2802 *Sci. Data*, 5, 125–143, <https://doi.org/10.5194/essd-5-125-2013>, 2013.
- 2803 Piao, S., Ciais, P., Friedlingstein, P., de Noblet-Ducoudré, N., Cadule, P., Viovy, N., and Wang, T.: Spatiotemporal patterns
2804 of terrestrial carbon cycle during the 20th century, *Global Biogeochem. Cy.*, 23, GB4026,
2805 <https://doi.org/10.1029/2008GB003339>, 2009.
- 2806 Piao, S., Huang, M., Liu, Z., Wang, X., Ciais, P., Canadell, J. G., Wang, K., Bastos, A., Friedlingstein, P., Houghton, R. A.,
2807 Le Quéré, C., Liu, Y., Myneni, R. B., Peng, S., Pongratz, J., Sitch, S., Yan, T., Wang, Y., Zhu, Z., Wu, D., and Wang, T.:
2808 Lower land-use emissions responsible for increased net land carbon sink during the slow warming period, *Nature Geosci.*, 11,
2809 739–743, <https://doi.org/10.1038/s41561-018-0204-7>, 2018.
- 2810 Pongratz, J., Reick, C. H., Houghton, R. A., and House, J. I.: Terminology as a key uncertainty in net land use and land
2811 cover change carbon flux estimates, *Earth Syst. Dynam.*, 5, 177–195, <https://doi.org/10.5194/esd-5-177-2014>, 2014.
- 2812 Poulter, B., Bastos, A., Canadell, J., Ciais, P., Gruber, N., Hauck, J., Jackson, R., Ishii, M., Müller, J., Patra, P., and Tian, H.:
2813 Inventorying Earth’s Land and Ocean Greenhouse Gases, *Eos*, 103, <https://doi.org/10.1029/2022EO179084>, 2022.
- 2814 Poulter, B., Frank, D. C., Hodson, E. L., and Zimmermann, N. E.: Impacts of land cover and climate data selection on
2815 understanding terrestrial carbon dynamics and the CO₂ airborne fraction, *Biogeosciences*, 8, 2027–2036,
2816 <https://doi.org/10.5194/bg-8-2027-2011>, 2011.
- 2817 Poulter, B., Freeborn, P. H., Jolly, W. M., and Varner, J. M.: COVID-19 lockdowns drive decline in active fires in
2818 southeastern United States, *PNAS*, 118, e2105666118, <https://doi.org/10.1073/pnas.2105666118>, 2021.
- 2819 Powis, C. M., Smith, S. M., Minx, J. C., and Gasser, T.: Quantifying global carbon dioxide removal deployment, *Environ.*
2820 *Res. Lett.*, 18, 024022, <https://doi.org/10.1088/1748-9326/acb450>, 2023.
- 2821 Prentice, I. C., Farquhar, G. D., Fasham, M. J. R., Goulden, M. L., Heimann, M., Jaramillo, V. J., Kheshgi, H. S., Le Quéré,
2822 C., Scholes, R. J., and Wallace, D. W. R.: The Carbon Cycle and Atmospheric Carbon Dioxide, in *Climate Change 2001:
2823 The Scientific Basis. Contribution of Working Group I to the Third Assessment Report of the Intergovernmental Panel on
2824 Climate Change*, edited by: Houghton, J. T., Ding, Y., Griggs, D. J., Noguer, M., van der Linden, P. J., Dai, X., Maskell, K.,
2825 and Johnson, C. A., Cambridge University Press, Cambridge, United Kingdom and New York, NY, USA, 183–237, ISBN:
2826 978-0521014953, 2001.
- 2827 Price, J. T. and Warren, R.: Literature Review of the Potential of “Blue Carbon” Activities to Reduce Emissions, available
2828 at: [https://avoid-net-uk.cc.ic.ac.uk/wp-content/uploads/delightful-downloads/2016/03/Literature-review-of-the-potential-of-
2829 blue-carbon-activities-to-reduce-emissions-AVOID2-WPE2.pdf](https://avoid-net-uk.cc.ic.ac.uk/wp-content/uploads/delightful-downloads/2016/03/Literature-review-of-the-potential-of-blue-carbon-activities-to-reduce-emissions-AVOID2-WPE2.pdf), last access: 9 November 2023, 2016.
- 2830 Qin, Y., Xiao, X., Wigneron, J.-P., Ciais, P., Brandt, M., Fan, L., Li, X., Crowell, S., Wu, X., Doughty, R., Zhang, Y., Liu,
2831 F., Sitch, S., and Moore, B.: Carbon loss from forest degradation exceeds that from deforestation in the Brazilian Amazon,
2832 *Nat. Clim. Chang.*, 11, 442–448, <https://doi.org/10.1038/s41558-021-01026-5>, 2021.
- 2833 Randerson, J. T., Chen, Y., van der Werf, G. R., Rogers, B. M., and Morton, D. C.: Global burned area and biomass burning
2834 emissions from small fires: BURNED AREA FROM SMALL FIRES, *J. Geophys. Res. Biogeosciences*, 117, n/a-n/a,
2835 <https://doi.org/10.1029/2012JG002128>, 2012.

- 2836 Raupach, M. R., Marland, G., Ciais, P., Le Quere, C., Canadell, J. G., Klepper, G., and Field, C. B.: Global and regional
2837 drivers of accelerating CO₂ emissions, *Proceedings of the National Academy of Sciences*, 104, 10288–10293,
2838 <https://doi.org/10.1073/pnas.0700609104>, 2007.
- 2839 Regnier, P., Resplandy, L., Najjar, R. G., and Ciais, P.: The land-to-ocean loops of the global carbon cycle, *Nature*, 603,
2840 401–410, <https://doi.org/10.1038/s41586-021-04339-9>, 2022.
- 2841 Reick, C. H., Gayler, V., Goll, D., Hagemann, S., Heidkamp, M., Nabel, J. E. M. S., Raddatz, T., Roeckner, E., Schnur, R.,
2842 110 and Wilkenskjaeld, S.: JSBACH 3 – The land component of the MPI Earth System Model: documentation of version 3.2,
2843 available at: <https://doi.org/10.17617/2.3279802>, 2021.
- 2844 Remaud, M., Chevallier, F., Cozic, A., Lin, X., and Bousquet, P.: On the impact of recent developments of the LMDz
2845 atmospheric general circulation model on the simulation of CO₂ transport, 11, 4489, [https://doi.org/10.5194/gmd-11-4489-](https://doi.org/10.5194/gmd-11-4489-2018)
2846 2018, 2018.
- 2847 Resplandy, L., Keeling, R. F., Rödenbeck, C., Stephens, B. B., Khatiwala, S., Rodgers, K. B., Long, M. C., Bopp, L., and
2848 Tans, P. P.: Revision of global carbon fluxes based on a reassessment of oceanic and riverine carbon transport, *Nature*
2849 *Geosci*, 11, 504–509, <https://doi.org/10.1038/s41561-018-0151-3>, 2018.
- 2850 Rodenbeck, C., Houweling, S., Gloor, M., and Heimann, M.: CO₂ flux history 1982–2001 inferred from atmospheric data
2851 using a global inversion of atmospheric transport, *Atmos Chem Phys*, 3, 1919–1964, 2003.
- 2852 Rödenbeck, C., Bakker, D. C. E., Metz, N., Olsen, A., Sabine, C., Cassar, N., Reum, F., Keeling, R. F., and Heimann, M.:
2853 Interannual sea–air CO₂ flux variability from an observation-driven ocean mixed-layer scheme, 11, 4599–4613,
2854 <https://doi.org/10.5194/bg-11-4599-2014>, 2014.
- 2855 Rödenbeck, C., Zaehle, S., Keeling, R., and Heimann, M.: History of El Niño impacts on the global carbon cycle 1957–
2856 2017: a quantification from atmospheric CO₂ data, 373, 20170303, <https://doi.org/10.1098/rstb.2017.0303>, 2018.
- 2857 Rödenbeck, C., DeVries, T., Hauck, J., Le Quéré, C., and Keeling, R. F.: Data-based estimates of interannual sea–air CO₂
2858 flux variations 1957–2020 and their relation to environmental drivers, *Biogeosciences*, 19, 2627–2652,
2859 <https://doi.org/10.5194/bg-19-2627-2022>, 2022.
- 2860 Rosan, T. M., Klein Goldewijk, K., Ganzenmüller, R., O’Sullivan, M., Pongratz, J., Mercado, L. M., Aragao, L. E. O. C.,
2861 Heinrich, V., Randow, C. V., Wiltshire, A., Tubiello, F. N., Bastos, A., Friedlingstein, P., and Sitch, S.: A multi-data
2862 assessment of land use and land cover emissions from Brazil during 2000–2019, *Environ. Res. Lett.*, 16, 074004,
2863 <https://doi.org/10.1088/1748-9326/ac08c3>, 2021.
- 2864 Sakamoto, K., H. Nakano, S. Urakawa, T. Toyoda, Y. Kawakami, H. Tsujino, G. Yamanaka, 2023: Reference manual for the
2865 Meteorological Research Institute Community Ocean Model version 5 (MRI.COMv5), Technical Reports of the
2866 Meteorological Research Institute, No.87, <https://doi.org/10.11483/mritechrepo.87>.
- 2867 Sarma, V. V. S. S., Sridevi, B., Metz, N., Patra, P. K., Lachkar, Z., Chakraborty, K., Goyet, C., Levy, M., Mehari, M., and
2868 Chandra, N.: Air-Sea Fluxes of CO₂ in the Indian Ocean Between 1985 and 2018: A Synthesis Based on Observation-Based
2869 Surface CO₂, Hindcast and Atmospheric Inversion Models, *Glob. Biogeochem. Cycles*, 37, e2023GB007694,
2870 <https://doi.org/10.1029/2023GB007694>, 2023.

- 2871 Schaphoff, S., von Bloh, W., Rammig, A., Thonicke, K., Biemans, H., Forkel, M., Gerten, D., Heinke, J., Jägermeyr, J.,
2872 Knauer, J., Langerwisch, F., Lucht, W., Müller, C., Rolinski, S., and Waha, K.: LPJmL4 – a dynamic global vegetation
2873 model with managed land – Part 1: Model description, *Geosci. Model Dev.*, 11, 1343–1375, [https://doi.org/10.5194/gmd-11-](https://doi.org/10.5194/gmd-11-1343-2018)
2874 1343-2018, 2018.
- 2875 Schimel, D., Alves, D., Enting, I. G., Heimann, M., Joos, F., Raynaud, D., Wigley, T., Prater, M., Derwent, R., Ehhalt, D.,
2876 Fraser, P., Sanhueza, E., Zhou, X., Jonas, P., Charlson, R., Rodhe, H., Sadasivan, S., Shine, K. P., Fouquart, Y.,
2877 Ramaswamy, V., Solomon, S., Srinivasan, J., Albritton, D., Derwent, R., Isaksen, I., Lal, M., and Wuebbles, D.: Radiative
2878 Forcing of Climate Change, in: *Climate Change 1995: The Science of Climate Change, Contribution of Working Group I to*
2879 *the Second Assessment Report of the Intergovernmental Panel on Climate Change* [Houghton, J. T., Meira Rilho, L. G.,
2880 Callander, B. A., Harris, N., Kattenberg, A., and Maskell, K. (eds.)], Cambridge University Press, Cambridge, United
2881 Kingdom and New York, NY, USA, ISBN: 978-0521559621, 1995.
- 2882 Schimel, D., Stephens, B. B., and Fisher, J. B.: Effect of increasing CO₂ on the terrestrial carbon cycle, *Proc Natl Acad Sci*
2883 *USA*, 112, 436–441, <https://doi.org/10.1073/pnas.1407302112>, 2015.
- 2884 Schuh, A. E., Jacobson, A. R., Basu, S., Weir, B., Baker, D., Bowman, K., Chevallier, F., Crowell, S., Davis, K. J., Deng, F.,
2885 Denning, S., Feng, L., Jones, D., Liu, J., and Palmer, P. I.: Quantifying the Impact of Atmospheric Transport Uncertainty on
2886 CO₂ Surface Flux Estimates, *Global Biogeochem. Cycles*, 33, 484–500, <https://doi.org/10.1029/2018GB006086>, 2019.
- 2887 Schwinger, J., Goris, N., Tjiputra, J. F., Kriest, I., Bentsen, M., Bethke, I., Ilicak, M., Assmann, K. M., and Heinze, C.:
2888 Evaluation of NorESM-OC (versions 1 and 1.2), the ocean carbon-cycle stand-alone configuration of the Norwegian Earth
2889 System Model (NorESM1), *Geosci. Model Dev.*, 9, 2589–2622, <https://doi.org/10.5194/gmd-9-2589-2016>, 2016.
- 2890 Schwingshackl, C., Obermeier, W. A., Bultan, S., Grassi, G., Canadell, J. G., Friedlingstein, P., Gasser, T., Houghton, R. A.,
2891 Kurz, W. A., Sitch, S., and Pongratz, J.: Differences in land-based mitigation estimates reconciled by separating natural and
2892 land-use CO₂ fluxes at the country level, *One Earth*, 5, 1367–1376, <https://doi.org/10.1016/j.oneear.2022.11.009>, 2022.
- 2893 Séférian, R., Nabat, P., Michou, M., Saint-Martin, D., Voldoire, A., Colin, J., Decharme, B., Delire, C., Berthet, S.,
2894 Chevallier, M., Sénési, S., Franchisteguy, L., Vial, J., Mallet, M., Joetzjer, E., Geoffroy, O., Guérémy, J.-F., Moine, M.-P.,
2895 Msadek, R., Ribes, A., Rocher, M., Roehrig, R., Salas-y-Méla, D., Sanchez, E., Terray, L., Valcke, S., Waldman, R.,
2896 Aumont, O., Bopp, L., Deshayes, J., Éthé, C., and Madec, G.: Evaluation of CNRM Earth System Model, CNRM-ESM2-1:
2897 Role of Earth System Processes in Present-Day and Future Climate, *Journal of Advances in Modeling Earth Systems*, 11,
2898 4182–4227, <https://doi.org/10.1029/2019MS001791>, 2019.
- 2899 Seiler, C., Melton, J. R., Arora, V. K., Sitch, S., Friedlingstein, P., Anthoni, P., Goll, D., Jain, A. K., Joetzjer, E., Lienert, S.,
2900 Lombardozzi, D., Luysaert, S., Nabel, J. E. M. S., Tian, H., Vuichard, N., Walker, A. P., Yuan, W., and Zachle, S.: Are
2901 Terrestrial Biosphere Models Fit for Simulating the Global Land Carbon Sink?, *J. Adv. Model. Earth Syst.*, 14,
2902 e2021MS002946, <https://doi.org/10.1029/2021MS002946>, 2022.
- 2903 Sellar, A. A., Jones, C. G., Mulcahy, J. P., Tang, Y., Yool, A., Wiltshire, A., O'Connor, F. M., Stringer, M., Hill, R.,
2904 Palmieri, J., Woodward, S., Mora, L., Kuhlbrodt, T., Rumbold, S. T., Kelley, D. I., Ellis, R., Johnson, C. E., Walton, J.,
2905 Abraham, N. L., Andrews, M. B., Andrews, T., Archibald, A. T., Berthou, S., Burke, E., Blockley, E., Carslaw, K., Dalvi,
2906 M., Edwards, J., Folberth, G. A., Gedney, N., Griffiths, P. T., Harper, A. B., Hendry, M. A., Hewitt, A. J., Johnson, B.,
2907 Jones, A., Jones, C. D., Keeble, J., Liddicoat, S., Morgenstern, O., Parker, R. J., Predoi, V., Robertson, E., Siahann, A.,

- 2908 Smith, R. S., Swaminathan, R., Woodhouse, M. T., Zeng, G., and Zerroukat, M.: UKESM1: Description and Evaluation of
2909 the U.K. Earth System Model, *J. Adv. Model. Earth Syst.*, 11, 4513–4558, <https://doi.org/10.1029/2019MS001739>, 2019.
- 2910 Shu, S., Jain, A. K., Koven, C. D., and Mishra, U.: Estimation of Permafrost SOC Stock and Turnover Time Using a Land
2911 Surface Model With Vertical Heterogeneity of Permafrost Soils, *Global Biogeochem. Cy.*, 34, e2020GB006585,
2912 <https://doi.org/10.1029/2020GB006585>, 2020.
- 2913 Shutler, J. D., Land, P. E., Piolle, J.-F., Woolf, D. K., Goddijn-Murphy, L., Paul, F., Girard-Arduin, F., Chapron, B., and
2914 Donlon, C. J.: FluxEngine: A Flexible Processing System for Calculating Atmosphere–Ocean Carbon Dioxide Gas Fluxes
2915 and Climatologies, *J. Atmospheric Ocean. Technol.*, 33, 741–756, <https://doi.org/10.1175/JTECH-D-14-00204.1>, 2016.
- 2916 Sitch, S., Huntingford, C., Gedney, N., Levy, P. E., Lomas, M., Piao, S. L., Betts, R., Ciais, P., Cox, P., Friedlingstein, P.,
2917 Jones, C. D., Prentice, I. C., and Woodward, F. I.: Evaluation of the terrestrial carbon cycle, future plant geography and
2918 climate-carbon cycle feedbacks using five Dynamic Global Vegetation Models (DGVMs): Uncertainty In Land Carbon
2919 Cycle Feedbacks, *Glob. Change Biol.*, 14, 2015–2039, <https://doi.org/10.1111/j.1365-2486.2008.01626.x>, 2008.
- 2920 Smallman, T. L., Milodowski, D. T., Neto, E. S., Koren, G., Ometto, J., and Williams, M.: Parameter uncertainty dominates
2921 C-cycle forecast errors over most of Brazil for the 21st century, *Earth Syst. Dyn.*, 12, 1191–1237,
2922 <https://doi.org/10.5194/esd-12-1191-2021>, 2021.
- 2923 Smith, B., Wårlind, D., Arneth, A., Hickler, T., Leadley, P., Siltberg, J., and Zaehle, S.: Implications of incorporating N
2924 cycling and N limitations on primary production in an individual-based dynamic vegetation model, *Biogeosciences*, 11,
2925 2027–2054, <https://doi.org/10.5194/bg-11-2027-2014>, 2014.
- 2926 Smith, S., Geden, O., Nemet, G., Gidden, M., Lamb, W., Powis, C., Bellamy, R., Callaghan, M., Cowie, A., Cox, E. and
2927 Fuss, S., 2023. The State of Carbon Dioxide Removal–1st Edition, <http://dx.doi.org/10.17605/OSF.IO/W3B4Z>, 2023.
- 2928 Sospedra-Alfonso, R., Merryfield, W. J., Boer, G. J., Kharin, V. V., Lee, W.-S., Seiler, C., and Christian, J. R.: Decadal
2929 climate predictions with the Canadian Earth System Model version 5 (CanESM5), *Geosci. Model Dev.*, 14, 6863–6891,
2930 <https://doi.org/10.5194/gmd-14-6863-2021>, 2021.
- 2931 Stephens, B. B., Gurney, K. R., Tans, P. P., Sweeney, C., Peters, W., Bruhwiler, L., Ciais, P., Ramonet, M., Bousquet, P.,
2932 Nakazawa, T., Aoki, S., Machida, T., Inoue, G., Vinnichenko, N., Lloyd, J., Jordan, A., Heimann, M., Shibistova, O.,
2933 Langenfelds, R. L., Steele, L. P., Francey, R. J., and Denning, A. S.: Weak Northern and Strong Tropical Land Carbon
2934 Uptake from Vertical Profiles of Atmospheric CO₂, *Science*, 316, 1732–1735, <https://doi.org/10.1126/science.1137004>,
2935 2007.
- 2936 Stephens, B. B., Keeling, R. F., Heimann, M., Six, K. D., Murnane, R., and Caldeira, K.: Testing global ocean carbon cycle
2937 models using measurements of atmospheric O₂ and CO₂ concentration, *Glob. Biogeochem. Cycles*, 12, 213–230,
2938 <https://doi.org/10.1029/97GB03500>, 1998.
- 2939 Stocker, T., Qin, D., and Platner, G.-K.: Climate Change 2013: The Physical Science Basis. Contribution of Working Group
2940 I to the Fifth Assessment Report of the Intergovernmental Panel on Climate Change [Intergovernmental Panel on Climate
2941 Change (eds.)], Cambridge University Press, Cambridge, ISBN: 9789291691388, 2013.\

2942 Swart, N. C., Cole, J. N. S., Kharin, V. V., Lazare, M., Scinocca, J. F., Gillett, N. P., Anstey, J., Arora, V., Christian, J. R.,
2943 Hanna, S., Jiao, Y., Lee, W. G., Majaess, F., Saenko, O. A., Seiler, C., Seinen, C., Shao, A., Sigmond, M., Solheim, L., von
2944 Salzen, K., Yang, D., and Winter, B.: The Canadian Earth System Model version 5 (CanESM5.0.3), *Geosci. Model Dev.*, 12,
2945 4823–4873, <https://doi.org/10.5194/gmd-12-4823-2019>, 2019.

2946 SX Coal: Monthly coal consumption estimates, <http://www.sxcoal.com/>, last access: 9 November 2023, 2022.

2947 Takahashi, T., Sutherland, S. C., Wanninkhof, R., Sweeney, C., Feely, R. A., Chipman, D. W., Hales, B., Friederich, G.,
2948 Chavez, F., Sabine, C., Watson, A., Bakker, D. C. E., Schuster, U., Metzl, N., Yoshikawa-Inoue, H., Ishii, M., Midorikawa,
2949 T., Nojiri, Y., Körtzinger, A., Steinhoff, T., Hoppema, M., Olafsson, J., Arnarson, T. S., Tilbrook, B., Johannessen, T.,
2950 Olsen, A., Bellerby, R., Wong, C. S., Delille, B., Bates, N. R., and de Baar, H. J. W.: Climatological mean and decadal
2951 change in surface ocean pCO₂, and net sea–air CO₂ flux over the global oceans, *Deep Sea Research Part II: Topical Studies*
2952 *in Oceanography*, 56, 554–577, <https://doi.org/10.1016/j.dsr2.2008.12.009>, 2009.

2953 Terhaar, J., Frölicher, T. L., and Joos, F.: Southern Ocean anthropogenic carbon sink constrained by sea surface salinity, *Sci.*
2954 *Adv.*, 7, eabd5964, <https://doi.org/10.1126/sciadv.abd5964>, 2021.

2955 Terhaar, J., Frölicher, T. L., and Joos, F.: Observation-constrained estimates of the global ocean carbon sink from Earth
2956 system models, *Biogeosciences*, 19, 4431–4457, <https://doi.org/10.5194/bg-19-4431-2022>, 2022.

2957 Tian, H., Xu, X., Lu, C., Liu, M., Ren, W., Chen, G., Melillo, J., and Liu, J.: Net exchanges of CO₂, CH₄, and N₂O between
2958 China’s terrestrial ecosystems and the atmosphere and their contributions to global climate warming, *J. Geophys. Res.*
2959 *Biogeosciences*, 116, G02011, <https://doi.org/10.1029/2010JG001393>, 2011.

2960 Tian, H., Chen, G., Lu, C., Xu, X., Hayes, D. J., Ren, W., Pan, S., Huntzinger, D. N., and Wofsy, S. C.: North American
2961 terrestrial CO₂ uptake largely offset by CH₄ and N₂O emissions: toward a full accounting of the greenhouse gas budget,
2962 *Climatic Change*, 129, 413–426, <https://doi.org/10.1007/s10584-014-1072-9>, 2015.

2963 Tubiello, F. N., Conchedda, G., Wanner, N., Federici, S., Rossi, S., and Grassi, G.: Carbon emissions and removals from
2964 forests: new estimates, 1990–2020, *Earth Syst. Sci. Data*, 13, 1681–1691, <https://doi.org/10.5194/essd-13-1681-2021>, 2021.

2965 Tuck, C.: 2022 Mineral Commodity Summary: Iron Ore, Tech. rep., U.S. Geological Survey,
2966 <https://pubs.usgs.gov/periodicals/mcs2022/mcs2022-iron-ore.pdf>, 2022.

2967 UNFCCC: Synthesis report for the technical assessment component of the first global stocktake, available at:
2968 <https://unfccc.int/documents/461466>, last access: 9 November 2023, 2022

2969 Urakawa, L. S., Tsujino, H., Nakano, H., Sakamoto, K., Yamanaka, G., and Toyoda, T.: The sensitivity of a depth-
2970 coordinate model to diapycnal mixing induced by practical implementations of the isopycnal tracer diffusion scheme, *Ocean*
2971 *Model.*, 154, 101693, <https://doi.org/10.1016/j.ocemod.2020.101693>, 2020.

2972 Vale, M. M., Berenguer, E., Argollo de Menezes, M., Viveiros de Castro, E. B., Pugliese de Siqueira, L., and Portela, R. de
2973 C. Q.: The COVID-19 pandemic as an opportunity to weaken environmental protection in Brazil, *Biological Conservation*,
2974 255, 108994, <https://doi.org/10.1016/j.biocon.2021.108994>, 2021.

- 2975 van der Laan-Luijkx, I. T., van der Velde, I. R., van der Veen, E., Tsuruta, A., Stanislawski, K., Babenhausser, A.,
 2976 Zhang, H. F., Liu, Y., He, W., Chen, H., Masarie, K. A., Krol, M. C., and Peters, W.: The CarbonTracker Data Assimilation
 2977 Shell (CTDAS) v1.0: implementation and global carbon balance 2001–2015, *Geosci. Model Dev.*, 10, 2785–2800,
 2978 <https://doi.org/10.5194/gmd-10-2785-2017>, 2017.
- 2979 van der Velde, I. R., van der Werf, G. R., Houweling, S., Maasakkers, J. D., Borsdorff, T., Landgraf, J., Tol, P., van
 2980 Kempen, T. A., van Hees, R., Hoogeveen, R., Veeffkind, J. P., and Aben, I.: Vast CO₂ release from Australian fires in 2019–
 2981 2020 constrained by satellite, *Nature*, 597, 366–369, <https://doi.org/10.1038/s41586-021-03712-y>, 2021.
- 2982 van der Werf, G. R., Randerson, J. T., Giglio, L., Collatz, G. J., Mu, M., Kasibhatla, P. S., Morton, D. C., DeFries, R. S., Jin,
 2983 Y., and van Leeuwen, T. T.: Global fire emissions and the contribution of deforestation, savanna, forest, agricultural, and
 2984 peat fires (1997–2009), *Atmospheric Chem. Phys.*, 10, 11707–11735, <https://doi.org/10.5194/acp-10-11707-2010>, 2010.
- 2985 van der Werf, G. R., Randerson, J. T., Giglio, L., van Leeuwen, T. T., Chen, Y., Rogers, B. M., Mu, M., van Marle, M. J. E.,
 2986 Morton, D. C., Collatz, G. J., Yokelson, R. J., and Kasibhatla, P. S.: Global fire emissions estimates during 1997–2016,
 2987 *Earth Syst. Sci. Data*, 9, 697–720, <https://doi.org/10.5194/essd-9-697-2017>, 2017.
- 2988 van Wees, D., van der Werf, G. R., Randerson, J. T., Andela, N., Chen, Y., and Morton, D. C.: The role of fire in global
 2989 forest loss dynamics, *Glob. Change Biol.*, 27, 2377–2391, <https://doi.org/10.1111/gcb.15591>, 2021.
- 2990 von Bloh, W., Schaphoff, S., Müller, C., Rolinski, S., Waha, K., and Zaehle, S.: Implementing the nitrogen cycle into the
 2991 dynamic global vegetation, hydrology, and crop growth model LPJmL (version 5.0), *Geosci. Model Dev.*, 11, 2789–2812,
 2992 <https://doi.org/10.5194/gmd-11-2789-2018>, 2018.
- 2993 Vaittinada Ayar, P., Bopp, L., Christian, J. R., Ilyina, T., Krasting, J. P., Séférian, R., Tsujino, H., Watanabe, M., Yool, A.,
 2994 and Tjiputra, J.: Contrasting projections of the ENSO-driven CO₂ flux variability in the equatorial Pacific under high-
 2995 warming scenario, *Earth Syst. Dynam.*, 13, 1097–1118, <https://doi.org/10.5194/esd-13-1097-2022>, 2022.
- 2996 Vuichard, N., Messina, P., Luysaert, S., Guenet, B., Zaehle, S., Ghattas, J., Bastrikov, V., and Peylin, P.: Accounting for
 2997 carbon and nitrogen interactions in the global terrestrial ecosystem model ORCHIDEE (trunk version, rev 4999): multi-scale
 2998 evaluation of gross primary production, *Geosci. Model Dev.*, 12, 4751–4779, <https://doi.org/10.5194/gmd-12-4751-2019>,
 2999 2019.
- 3000 Walker, A. P., Quaipe, T., Bodegom, P. M., De Kauwe, M. G., Keenan, T. F., Joiner, J., Lomas, M. R., MacBean, N., Xu, C.,
 3001 Yang, X., and Woodward, F. I.: The impact of alternative trait-scaling hypotheses for the maximum photosynthetic
 3002 carboxylation rate (V_{cmax}) on global gross primary production, *New Phytol.*, 215, 1370–1386,
 3003 <https://doi.org/10.1111/nph.14623>, 2017.
- 3004 Walker, A. P., De Kauwe, M. G., Bastos, A., Belmecheri, S., Georgiou, K., Keeling, R. F., McMahon, S. M., Medlyn, B. E.,
 3005 Moore, D. J. P., Norby, R. J., Zaehle, S., Anderson-Teixeira, K. J., Battipaglia, G., Brienen, R. J. W., Cabugao, K. G.,
 3006 Cailleret, M., Campbell, E., Canadell, J. G., Ciais, P., Craig, M. E., Ellsworth, D. S., Farquhar, G. D., Fatichi, S., Fisher, J.
 3007 B., Frank, D. C., Graven, H., Gu, L., Haverd, V., Heilmann, K., Heimann, M., Hungate, B. A., Iversen, C. M., Joos, F., Jiang,
 3008 M., Keenan, T. F., Knauer, J., Körner, C., Leshyk, V. O., Leuzinger, S., Liu, Y., MacBean, N., Malhi, Y., McVicar, T. R.,
 3009 Penuelas, J., Pongratz, J., Powell, A. S., Riutta, T., Sabot, M. E. B., Schleucher, J., Sitch, S., Smith, W. K., Sulman, B.,
 3010 Taylor, B., Terrer, C., Torn, M. S., Treseder, K. K., Trugman, A. T., Trumbore, S. E., van Mantgem, P. J., Voelker, S. L.,

- 3011 Whelan, M. E., and Zuidema, P. A.: Integrating the evidence for a terrestrial carbon sink caused by increasing atmospheric
3012 CO₂, *New Phytol.*, 229, 2413–2445, <https://doi.org/10.1111/nph.16866>, 2021.
- 3013 Watanabe, M., Tatebe, H., Koyama, H., Hajima, T., Watanabe, M., and Kawamiya, M.: Importance of El Niño
3014 reproducibility for reconstructing historical CO₂ flux variations in the equatorial Pacific, *Ocean Sci.*, 16, 1431–1442,
3015 <https://doi.org/10.5194/os-16-1431-2020>, 2020.
- 3016 Watson, A. J., Schuster, U., Shutler, J. D., Holding, T., Ashton, I. G. C., Landschützer, P., Woolf, D. K., and Goddijn-
3017 Murphy, L.: Revised estimates of ocean-atmosphere CO₂ flux are consistent with ocean carbon inventory, *Nat Commun*, 11,
3018 4422, <https://doi.org/10.1038/s41467-020-18203-3>, 2020.
- 3019 Watson, R. T., Rohde, H., Oeschger, H., and Siegenthaler, U.: Greenhouse Gases and Aerosols, in: *Climate Change: The*
3020 *IPCC Scientific Assessment. Intergovernmental Panel on Climate Change (IPCC)*, edited by: Houghton, J. T., Jenkins, G. J.,
3021 and Ephraums, J. J., Cambridge University Press, Cambridge, ISBN: 978-0521403603, 1990.
- 3022 Wenzel, S., Cox, P. M., Eyring, V., and Friedlingstein, P.: Projected land photosynthesis constrained by changes in the
3023 seasonal cycle of atmospheric CO₂, *Nature*, 538, 499–501, <https://doi.org/10.1038/nature19772>, 2016.
- 3024 Wilkenskjeld, S., Kloster, S., Pongratz, J., Raddatz, T., and Reick, C. H.: Comparing the influence of net and gross
3025 anthropogenic land-use and land-cover changes on the carbon cycle in the MPI-ESM, *Biogeosciences*, 11, 4817–4828,
3026 <https://doi.org/10.5194/bg-11-4817-2014>, 2014.
- 3027 Wiltshire, A. J., Burke, E. J., Chadburn, S. E., Jones, C. D., Cox, P. M., Davies-Barnard, T., Friedlingstein, P., Harper, A. B.,
3028 Liddicoat, S., Sitch, S., and Zaehle, S.: JULES-CN: a coupled terrestrial carbon–nitrogen scheme (JULES vn5.1), 14, 2161–
3029 2186, <https://doi.org/10.5194/gmd-14-2161-2021>, 2021.
- 3030 Winkler, K., Yang, H., Ganzenmüller, R., Fuchs, R., Ceccherini, G., Duveiller, G., Grassi, G., Pongratz, J., Bastos, A.,
3031 Shvidenko, A., Araza, A., Herold, M., Wigneron, J.-P., and Ciais, P.: Changes in land use and management led to a decline
3032 in Eastern Europe’s terrestrial carbon sink, *Commun. Earth Environ.*, 4, 1–14, <https://doi.org/10.1038/s43247-023-00893-4>,
3033 2023.
- 3034 Woodward, F. I. and Lomas, M. R.: Vegetation dynamics – simulating responses to climatic change, *Biol. Rev.*, 79, 643–
3035 670, <https://doi.org/10.1017/S1464793103006419>, 2004.
- 3036 Wright, R. M., Le Quéré, C., Buitenhuis, E., Pitois, S., and Gibbons, M. J.: Role of jellyfish in the plankton ecosystem
3037 revealed using a global ocean biogeochemical model, 18, 1291–1320, <https://doi.org/10.5194/bg-18-1291-2021>, 2021.
- 3038 Wunder, S., Kaimowitz, D., Jensen, S., and Feder, S.: Coronavirus, macroeconomy, and forests: What likely impacts?, *For.*
3039 *Policy Econ.*, 131, 102536, <https://doi.org/10.1016/j.forpol.2021.102536>, 2021.
- 3040 Xi, F., Davis, S. J., Ciais, P., Crawford-Brown, D., Guan, D., Pade, C., Shi, T., Syddall, M., Lv, J., Ji, L., Bing, L., Wang, J.,
3041 Wei, W., Yang, K.-H., Lagerblad, B., Galan, I., Andrade, C., Zhang, Y., and Liu, Z.: Substantial global carbon uptake by
3042 cement carbonation, *Nature Geosci*, 9, 880–883, <https://doi.org/10.1038/ngeo2840>, 2016.
- 3043 Xia, J., Chen, Y., Liang, S., Liu, D., and Yuan, W.: Global simulations of carbon allocation coefficients for deciduous
3044 vegetation types, *Tellus B*, 67, 28016, <https://doi.org/10.3402/tellusb.v67.28016>, 2015.

- 3045 Yang, D., Liu, Y., Feng, L., Wang, J., Yao, L., Cai, Z., Zhu, S., Lu, N., and Lyu, D.: The First Global Carbon Dioxide Flux
3046 Map Derived from TanSat Measurements, *Adv. Atmospheric Sci.*, 38, 1433–1443, [https://doi.org/10.1007/s00376-021-](https://doi.org/10.1007/s00376-021-1179-7)
3047 1179-7, 2021.
- 3048 Yang, X., Thornton, P., Ricciuto, D., Wang, Y., and Hoffman, F.: Global evaluation of terrestrial biogeochemistry in the
3049 Energy Exascale Earth System Model (E3SM) and the role of the phosphorus cycle in the historical terrestrial carbon
3050 balance, *Biogeosciences*, 20, 2813–2836, <https://doi.org/10.5194/bg-20-2813-2023>, 2023.
- 3051 Yu, Z., Ciais, P., Piao, S., Houghton, R. A., Lu, C., Tian, H., Agathokleous, E., Kattel, G. R., Sitch, S., Goll, D., Yue, X.,
3052 Walker, A., Friedlingstein, P., Jain, A. K., Liu, S., and Zhou, G.: Forest expansion dominates China’s land carbon sink since
3053 1980, *Nat. Commun.*, 13, 5374, <https://doi.org/10.1038/s41467-022-32961-2>, 2022.
- 3054 Yue, X. and Unger, N.: The Yale Interactive terrestrial Biosphere model version 1.0: description, evaluation and
3055 implementation into NASA GISS ModelE2, *Geosci. Model Dev.*, 8, 2399–2417, <https://doi.org/10.5194/gmd-8-2399-2015>,
3056 2015.
- 3057 Yuan, W., Liu, D., Dong, W., Liu, S., Zhou, G., Yu, G., Zhao, T., Feng, J., Ma, Z., Chen, J., Chen, Y., Chen, S., Han, S.,
3058 Huang, J., Li, L., Liu, H., Liu, S., Ma, M., Wang, Y., Xia, J., Xu, W., Zhang, Q., Zhao, X., and Zhao, L.: Multiyear
3059 precipitation reduction strongly decreases carbon uptake over northern China, *J. Geophys. Res.-Biogeo.*, 119, 881–896,
3060 <https://doi.org/10.1002/2014JG002608>, 2014.
- 3061 Yue, C., Ciais, P., Zhu, D., Wang, T., Peng, S. S., and Piao, S. L.: How have past fire disturbances contributed to the current
3062 carbon balance of boreal ecosystems?, *Biogeosciences*, 13, 675–690, <https://doi.org/10.5194/bg-13-675-2016>, 2016.
- 3063 Zaehle, S. and Friend, A. D.: Carbon and nitrogen cycle dynamics in the O-CN land surface model: 1. Model description,
3064 site-scale evaluation, and sensitivity to parameter estimates: Site-scale evaluation of a C-N model, *Global Biogeochem.*
3065 *Cycles*, 24, GB1005, <https://doi.org/10.1029/2009GB003521>, 2010.
- 3066 Zaehle, S., Ciais, P., Friend, A. D., and Prieur, V.: Carbon benefits of anthropogenic reactive nitrogen offset by nitrous oxide
3067 emissions, *Nature Geosci*, 4, 601–605, <https://doi.org/10.1038/ngeo1207>, 2011.
- 3068 Zaehle, S., Medlyn, B. E., De Kauwe, M. G., Walker, A. P., Dietze, M. C., Hickler, T., Luo, Y., Wang, Y.-P., El-Masri, B.,
3069 Thornton, P., Jain, A., Wang, S., Warlind, D., Weng, E., Parton, W., Iversen, C. M., Gallet-Budynek, A., McCarthy, H.,
3070 Finzi, A., Hanson, P. J., Prentice, I. C., Oren, R., and Norby, R. J.: Evaluation of 11 terrestrial carbon–nitrogen cycle models
3071 against observations from two temperate Free-Air CO₂ Enrichment studies, *New Phytol.*, 202, 803–822,
3072 <https://doi.org/10.1111/nph.12697>, 2014.
- 3073 Zeng, J., Iida, Y., Matsunaga, T., and Shirai, T.: Surface ocean CO₂ concentration and air-sea flux estimate by machine
3074 learning with modelled variable trends, *Front. Mar. Sci.*, 9, <https://doi.org/10.3389/fmars.2022.989233>, 2022.
- 3075 Zheng, B., Ciais, P., Chevallier, F., Chuvieco, E., Chen, Y., and Yang, H.: Increasing forest fire emissions despite the
3076 decline in global burned area, *Sci. Adv.*, 7, eabh2646, <https://doi.org/10.1126/sciadv.abh2646>, 2021.
- 3077 Zou, Y., Wang, Y., Ke, Z., Tian, H., Yang, J., and Liu, Y.: Development of a REgion-Specific Ecosystem Feedback Fire
3078 (RESFire) Model in the Community Earth System Model, *J. Adv. Model. Earth Syst.*, 11, 417–445,
3079 <https://doi.org/10.1029/2018MS001368>, 2019.

3080 Zscheischler, J., Mahecha, M. D., Avitabile, V., Calle, L., Carvalhais, N., Ciais, P., Gans, F., Gruber, N., Hartmann, J.,
3081 Herold, M., Ichii, K., Jung, M., Landschützer, P., Laruelle, G. G., Lauerwald, R., Papale, D., Peylin, P., Poulter, B., Ray, D.,
3082 Regnier, P., Rödenbeck, C., Roman-Cuesta, R. M., Schwalm, C., Tramontana, G., Tyukavina, A., Valentini, R., van der
3083 Werf, G., West, T. O., Wolf, J. E., and Reichstein, M.: Reviews and syntheses: An empirical spatiotemporal description of
3084 the global surface–atmosphere carbon fluxes: opportunities and data limitations, *Biogeosciences*, 14, 3685–3703,
3085 <https://doi.org/10.5194/bg-14-3685-2017>, 2017.

Unit 1	Unit 2	Conversion	Source
GtC (gigatonnes of carbon)	ppm (parts per million) (a)	2.124 (b)	Ballantyne et al. (2012)
GtC (gigatonnes of carbon)	PgC (petagrams of carbon)		1 SI unit conversion
GtCO ₂ (gigatonnes of carbon dioxide)	GtC (gigatonnes of carbon)	3.664	44.01/12.011 in mass equivalent
GtC (gigatonnes of carbon)	MtC (megatonnes of carbon)	1000	SI unit conversion
(a) Measurements of atmospheric CO ₂ concentration have units of dry-air mole fraction. 'ppm' is an abbreviation for micromole/mol, dry air.			
(b) The use of a factor of 2.124 assumes that all the atmosphere is well mixed within one year. In reality, only the troposphere is well mixed and the growth rate of CO ₂ concentration in the less well-mixed stratosphere is not measured by sites from the NOAA network. Using a factor of 2.124 makes the approximation that the growth rate of CO ₂ concentration in the stratosphere equals that of the troposphere on a yearly basis.			

3087 **Table 1.** Factors used to convert carbon in various units (by convention, Unit 1 = Unit 2 × conversion).

3088

3089

3090

Component	Primary reference
Global fossil CO ₂ emissions (EFOS), total and by fuel type	Updated from Andrew and Peters (2022)
National territorial fossil CO ₂ emissions (EFOS)	Gilfillan and Marland (2021), UNFCCC (2022)
National consumption-based fossil CO ₂ emissions (EFOS) by country (consumption)	Peters et al. (2011a) updated as described in this paper
Net land-use change flux (ELUC)	This paper (see Table 4 for individual model references).
Growth rate in atmospheric CO ₂ concentration (GATM)	Lan et al. (2023)
Ocean and land CO ₂ sinks (SOCEAN and SLAND)	This paper (see Table 4 for individual model and data products references).

3091

3092

3093

Table 2. How to cite the individual components of the global carbon budget presented here.

Publication year	Fossil fuel emissions		LUC emissions	Reservoirs			Other changes
	Global	Country (territorial)		Atmosphere	Ocean	Land	
2019	Global emissions calculated as sum of all countries plus bunkers, rather than taken directly from CDIAC.		Average of two bookkeeping models; use of 15 DGVMs	Use of three atmospheric inversions	Based on nine models	Based on 16 models	
Friedlingstein et al. (2019) GCB2019							
2020	Cement carbonation now included in the EFOS estimate, reducing EFOS by about 0.2GtC yr-1 for the last decade	India's emissions from Andrew (2020: India); Corrections to Netherland Antilles and Aruba and Soviet emissions before 1950 as per Andrew (2020: CO2); China's coal emissions in 2019 derived from official statistics, emissions now shown for EU27 instead of EU28. Projection for 2020 based on assessment of four approaches.	Average of three bookkeeping models; use of 17 DGVMs. Estimate of gross land use sources and sinks provided	Use of six atmospheric inversions	Based on nine models. River flux revised and partitioned NH, Tropics, SH	Based on 17 models	
Friedlingstein et al. (2020) GCB2020							
2021	Projections are no longer an assessment of four approaches.	Official data included for a number of additional countries, new estimates for South Korea, added emissions from lime	ELUC estimate compared to the estimates adopted in national GHG inventories (NGHGI)		Average of means of eight models and means of seven data-products. Current year prediction of SOCEAN using a feed-forward	Current year prediction of SLAND using a feed-forward neural network method	
Friedlingstein et al. (2022a) GCB2021							

		production in China.			neural network method		
2022			ELUC provided at country level. Revised components decomposition of ELUC fluxes. Revision of LUC maps for Brazil. New datasets for peat drainage.	Use of nine atmospheric inversions	Average of means of ten models and means of seven data-products	Based on 16 models. Revision of LUC maps for Brazil.	
Friedlingstein et al. (2022) GCB2022							
2023			Refined components decomposition of ELUC. Revision of LUC maps for Indonesia. Use of updated peat drainage estimates.	Use of 14 atmospheric inversions. Additional use of 4 Earth System Models to estimate current year CO2	Additional use of 4 Earth System Models and atmospheric oxygen method to assess SOCEAN. Regional distribution of river flux adjustment revised.	Based on 20 models. Additional use of 4 Earth System Models and atmospheric oxygen method to assess the net atmosphere-land flux.	Inclusion of an estimate of Carbon Dioxide Removal (CDR)
This study							

3095 **Table 3.** Main methodological changes in the global carbon budget since 2019. Methodological changes
3096 introduced in one year are kept for the following years unless noted. Empty cells mean there were no
3097 methodological changes introduced that year. Table S8 lists methodological changes from the first global carbon
3098 budget publication up to 2018.

3099

3100

Model/data name	Reference	Change from Global Carbon Budget 2022 (Friedlingstein et al., 2022b)
<i>Bookkeeping models for land-use change emissions</i>		
BLUE	Hansis et al. (2015)	No change to model, but simulations performed with LUH2-GCB2023 forcing. Update in added peat drainage emissions.
H&C2023	Houghton and Castanho (2023)	H&C2023 replaces the formerly used H&N2017 model. Minor bug fix in fuel harvest estimates. Update in added peat drainage emissions.
OSCAR	Gasser et al. (2020)	No change to model, but land-use forcing changed to LUH2-GCB2023 and FRA2020 (extrapolated to 2022). Constraining based on GCB2022 data for SLAND over 1960-2021. Update in added peat drainage emissions.
<i>Dynamic global vegetation models</i>		
CABLE-POP	Haverd et al. (2018)	Improved representation of nitrogen retranslocation and plant uptake, minor bug fixes, parameter changes
CLASSIC	Melton et al. (2020), Asaadi et al. (2018)	Bug fixes, correct allocation of leaves after summer solstice for latitudes higher than 45°N, improved phenology for several PFTs
CLM5.0	Lawrence et al. (2019)	No change.
DLEM	Tian et al. (2011, 2015)	No change.
<i>EDv3</i>	Moorcroft et al. (2001), Ma et al. (2022)	New this year.
<i>ELM</i>	Yang et al.(2023), Burrows et al.(2020)	New this year.
IBIS	Yuan et al. (2014)	Changes in parameterisation and new module of soil nitrogen dynamics (Ma et al., 2022)
ISAM	Jain et al. (2013), Meiyappan et al. (2015), Shu et al. (2020)	Vertically resolved soil biogeochemistry (carbon and nitrogen) module, following Shu et al. (2020),
ISBA-CTRIP	Delire et al. (2020)	No change.
JSBACH	Mauritsen et al. (2019), Reick et al. (2021)	No change.
JULES-ES	Wiltshire et al. (2021), Sellar et al. (2019), Burton et al. (2019)	Minor bug fixes. (Using JULES v6.3, suite u-co002)
LPJ-GUESS	Smith et al. (2014)	Minor bug fixes.

LPJml	Schaphoff et al., 2018, von Bloh et al., 2018, Lutz et al., 2019 (tillage), Heinke et al., 2023 (livestock grazing)	New this year.
LPJwsl	Poulter et al. (2011) (d)	No change.
LPX-Bern	Lienert and Joos (2018)	No change.
OCN	Zaehle and Friend (2010), Zaehle et al. (2011)	Minor bug fixes
ORCHIDEEv3	Krinner et al. (2005), Zaehle and Friend (2010), Vuichard et al. (2019)	Small update for leaf senescence (ORCHIDEE - V3; revision 8119)
SDGVM	Woodward and Lomas (2004), Walker et al. (2017)	implement gross land-use transitions, tracking of carbon from wood & crop harvest, and tracking of primary & secondary vegetation
VISIT	Ito and Inatomi (2012), Kato et al. (2013)	No change.
YIBs	Yue and Unger (2015)	Inclusion of process-based water cycle from Noah-MP (Niu et al., 2011)
Intermediate complexity land carbon cycle model		
CARDAMOM	Bloom et al. (2016), Smallman et al. (2021)	New this year
Global ocean biogeochemistry models		
NEMO3.6-PISCESv2-gas (CNRM)	Berthet et al. (2019), Séférian et al. (2019)	No change.
FESOM-2.1-REcoM2	Gürses et al. (2023)	No change
NEMO-PISCES (IPSL)	Aumont et al. (2015)	No change.
MOM6-COBALT (Princeton)	Liao et al. (2020)	No change
MRI-ESM2-2	Nakano et al. (2011)	The ocean model has been updated to MRI.COMv5 (Sakamoto et al. 2023). The distribution of background vertical diffusivity is changed to the one proposed by Kawasaki et al. (2021). Model was spun-up with a preindustrial xCO ₂ of 278 ppm.
MICOM-HAMOCC (NorESM-OCv1.2)	Schwinger et al. (2016)	No change.
NEMO-PlankTOM12	Wright et al. (2021)	Minor bug fixes, switch to ERA5 forcing, salinity restoring

CESM-ETHZ	Doney et al. (2009)	Model was spun-up with a preindustrial xCO ₂ of 278 ppm.
MPIOM-HAMOCC6	Lacroix et al. (2021)	No change.
ACCESS (CSIRO)	Law et al. (2017)	Minor bug fixes, extended spinup since last participation 2020.
fCO₂-products		
CMEMS-LSCE-FFNNv2	Chau et al. (2022)	Update to SOCATv2023 measurements and time period 1985-2022. The mapping approach by Chau et al (2022) has been upgraded by increasing spatial resolution from 1° to 0.25°.
JMA-MLR	Iida et al. (2021)	Updated to SOCATv2023
LDEO-HPD	Gloege et al. (2022), Bennington et al. (2022)	Updated with SOCATv2023. Updated with current GCB2023 models and extending back in time using Bennington et al. (2022) method.
MPI-SOMFFN	Landschützer et al. (2016)	update to SOCATv2023. Since GCB2022, fluxes cover open ocean and coastal domains as well as the Arctic Ocean extension.
NIES-ML3	Zeng et al. (2022)	New this year
OS-ETHZ-GRaCER	Gregor et al. (2021)	Updated to SOCATv2023
Jena-MLS	Rödenbeck et al. (2014, 2022)	update to SOCATv2023 measurements, time period extended to 1957-2022
UOEx-Watson	Watson et al. (2020)	Updated to SOCAT v2023. fCO ₂ (sw) corrected to CCI SST v2.1 (Merchant et al. 2019) instead of OI SST v2.1. Updated interpolation datasets to CCI SST v2.1, CMEMS SSS and MLD (Jean-Michel et al. 2021). Monthly cool skin difference calculated using NOAA COARE 3.5 (Edson et al. 2013). CO ₂ flux computed using FluxEngine (Holding et al., 2019; Shutler et al., 2016).
Atmospheric inversions		
Jena CarboScope	Rödenbeck et al. (2003, 2018)	Extension to 2022, re-addition of a 2.5-year relaxation term.
CAMS	Chevallier et al. (2005), Remaud et al. (2018)	Increase of the 3D resolution (4.5 times more 3D cells than the previous submission); extension to year 2022; update of the prior fluxes.
CarbonTracker Europe (CTE)	van der Laan-Luijkx et al. (2017)	Extension to 2022, update of prior fluxes.
NISMON-CO ₂	Niwa et al. (2020, 2022)	Prior terrestrial fluxes include minor fluxes (BVOC and CH ₄) in addition to GPP, RE and LUC.
CT-NOAA	Peters et al. (2005), Jacobson et al. (2023a, 2023b)	New this year.
CMS-Flux	Liu et al. (2021)	Update of OCO-2 observations and prior fluxes.

CAMS-Satellite	Chevallier et al. (2005), Remaud et al. (2018)	Increase of the 3D resolution, extension to year 2022 and the first months of 2023; removal of the pre-OCO-2 period (2010-2014 with GOSAT); update of the prior fluxes.
GONGGA	Jin et al. (2023)	Update of OCO-2 observations and prior fluxes.
THU	Kong et al. (2022)	Updates to the OCO-2 product and the fossil fuel data.
COLA	Liu et al. (2022)	New this year.
GCASv2	Jiang et al. (2021, 2022)	New this year.
UoE in-situ	Feng et al. (2009), Feng et al. (2016), Palmer et al. (2019)	Update of the inversion system by using new version of GEOS-Chem
IAPCAS	Feng et al. (2016), Yang et al. (2021)	New this year.
MIROC4-ACTM	Chandra et al. (2022)	New this year
Earth System Models		
CanESM5	Swart et al. (2019), Sospedra-Alfonso et al. (2021)	New this year.
IPSL-CM6a-CO2-LR	Boucher et al. (2020)	New this year.
MIROC-ES2L	Watanabe et al. (2020)	New this year.
MPI-ESM1-2-LR	Mauritsen et al. (2019), Li et al. (2023)	New this year.

3103

3104 **Table 4.** References for the process models, bookkeeping models, ocean data products, and atmospheric
3105 inversions. All models and products are updated with new data to the end of year 2022, and the atmospheric
3106 forcing for the DGVMs has been updated as described in Section C.2.2 and C.4.1.

3107

		1960s	1970s	1980s	1990s	2000s	2013-2022	2022
Land-use change emissions (ELUC)	Bookkeeping (BK) Net flux (1a)	1.5±0.7	1.3±0.7	1.4±0.7	1.6±0.7	1.4±0.7	1.3±0.7	1.2±0.7
	BK - deforestation (total)	1.7 [1.3,2.1]	1.6 [1.2,1.9]	1.7 [1.3,2.1]	1.9 [1.6,2.2]	2 [1.6,2.4]	1.9 [1.5,2.4]	1.9 [1.4,2.5]
	BK - forest regrowth (total)	-0.8 [-1.1,-0.6]	-0.9 [-1.1,-0.7]	-0.9 [-1.1,-0.7]	-1 [-1.2,-0.7]	-1.1 [-1.3,-0.8]	-1.3 [-1.5,-0.9]	-1.3 [-1.6,-1]
	BK - other transitions	0.4 [0.3,0.4]	0.2 [0.1,0.3]	0.2 [0.2,0.3]	0.1 [0,0.2]	0.1 [0,0.2]	0.1 [0,0.3]	0.1 [0,0.2]
	BK - peat drainage & peat fires	0.2 [0.1,0.2]	0.2 [0.1,0.2]	0.2 [0.2,0.3]	0.3 [0.3,0.3]	0.3 [0.2,0.3]	0.3 [0.3,0.3]	0.2 [0.2,0.3]
	BK - wood harvest & forest management	0.2 [-0.2,0.6]	0.2 [-0.2,0.6]	0.2 [-0.2,0.6]	0.2 [-0.1,0.6]	0.2 [-0.1,0.6]	0.2 [0,0.6]	0.2 [0,0.7]
	DGVMs-net flux (1b)	1.5±0.5	1.3±0.5	1.6±0.6	1.8±0.6	1.8±0.7	1.7±0.6	1.7±0.6
Terrestrial sink (SLAND)	Residual sink from global budget (E _{FOS} +E _{ELUC} (1a)-G _{ATM-S_{OCEAN}}) (2a)	1.7±0.8	1.8±0.8	1.7±0.9	2.7±0.9	2.9±0.9	2.9±0.9	3.7±1
	DGVMs (2b)	1.3±0.5	2±0.7	1.9±0.8	2.5±0.6	2.9±0.7	3.3±0.8	3.8±0.8
Net land fluxes (SLAND-ELUC)	GCB2023 Budget (2b-1a)	-0.2±0.8	0.8±1	0.5±1	0.9±0.9	1.4±1	2.1±1.1	2.6±1.1
	Atmospheric O ₂	---	---	---	1.2±1	1.1±1.1	1.1±1.3	-
	DGVMs-net (2b-1b)	-0.2±0.4	0.7±0.7	0.3±0.6	0.7±0.5	1.1±0.4	1.7±0.6	2.1±0.6
	Inversions*	- [-,-]	- [-,-]	0.5 [0.4,0.6] (2)	0.9 [0.6,1.3] (3)	1.3 [0.7,2] (4)	1.6 [0.5,2.3] (8)	2.7 [1.4-3.8] (13)
	ESMs	---	---	0.6 [0.1,1]	1.7 [1.3,2]	2 [1.4,2.7]	2.4 [1.8,3.3]	3.9 [2.8-5.5]

3108

3109 *Estimates are adjusted for the pre-industrial influence of river fluxes, for the cement carbonation sink, and
3110 adjusted to common E_{FOS} (Sect. 2.7). The ranges given include varying numbers (in parentheses) of inversions
3111 in each decade (Table S4).

3112 **Table 5.** Comparison of results from the bookkeeping method and budget residuals with results from the
3113 DGVMs, as well as additional estimates from atmospheric oxygen, atmospheric inversions and Earth System
3114 Models (ESMs) for different periods, the last decade, and the last year available. All values are in GtCyr⁻¹. See
3115 Figure 7 for explanation of the bookkeeping component fluxes. The DGVM uncertainties represent ±1σ of the
3116 decadal or annual (for 2022) estimates from the individual DGVMs: for the inverse systems the mean and range
3117 of available results is given. All values are rounded to the nearest 0.1 GtC and therefore columns do not
3118 necessarily add to zero.

3119

3120

3121

3122

Product	1960s	1970s	1980s	1990s	2000s	2013-2022	2022
$f\text{CO}_2$ -products	---	---	---	2.3 [2,2.9]	2.4 [2.2,2.7]	3.1 [2.6,3.3]	3.1 [2.5,3.3]
GOBMs	1±0.3	1.2±0.3	1.7±0.3	2±0.3	2.1±0.4	2.6±0.4	2.5±0.4
GCB2023 Budget	1.1±0.4	1.4±0.4	1.9±0.4	2.1±0.4	2.3±0.4	2.8±0.4	2.8±0.4
Atmospheric O ₂	---	---	---	2±0.7	2.6±0.6	3.3±0.6	-
Inversions	- [-,-]	- [-,-]	1.7 [1.6,1.8] (2)	2.2 [1.9,2.5] (3)	2.4 [1.8,3.1] (4)	3 [2.4,4.1] (8)	3 [2.2-4.2] (13)
ESMs	---	---	1.6 [0.7,2.4]	1.8 [1.1,2.5]	2.1 [1.5,2.8]	2.6 [2.2,3.4]	2.7 [2.3-3.5]

3123

3124 **Table 6:** Comparison of results for the ocean sink from the $f\text{CO}_2$ -products, from global ocean biogeochemistry
3125 models (GOBMs), the best estimate for GCB2023 as calculated from $f\text{CO}_2$ -products and GOBMs that is used in
3126 the budget Table 7, as well as additional estimates from atmospheric oxygen, atmospheric inversions and Earth
3127 System Models (ESMs) for different periods, the last decade, and the last year available. All values are in
3128 GtCyr^{-1} . Uncertainties represent $\pm 1\sigma$ of the estimates from the GOBMs ($N > 10$) and range of ensemble members
3129 is given for ensembles with $N < 10$ ($f\text{CO}_2$ -products, inversions, ESMs). The uncertainty of the GCB2023 budget
3130 estimate is based on expert judgement (Section 2 and Supplementary S1 to S4) and for oxygen it is the standard
3131 deviation of a Monte Carlo ensemble (Section 2.8).

3132

		1960s	1970s	1980s	1990s	2000s	2013-2022	2022	2023 (Projection)
Total emissions (EFOS + ELUC)	Fossil CO2 emissions (EFOS) ^a	3±0.2	4.7±0.2	5.5±0.3	6.4±0.3	7.8±0.4	9.6±0.5	9.9±0.5	10.1±0.5
	Land-use change emissions (ELUC)	1.5±0.7	1.3±0.7	1.4±0.7	1.6±0.7	1.4±0.7	1.3±0.7	1.2±0.7	1.1±0.7
	Total emissions	4.6±0.7	6±0.7	6.9±0.8	7.9±0.8	9.2±0.8	10.9±0.8	11.1±0.9	11.2±0.9
Partitioning	Growth rate in atmos CO2 (GATM)	1.7±0.07	2.8±0.07	3.4±0.02	3.1±0.02	4±0.02	5.2±0.02	4.6±0.2	5.1±0.4
	Ocean sink (SOCEAN)	1.1±0.4	1.4±0.4	1.9±0.4	2.1±0.4	2.3±0.4	2.8±0.4	2.8±0.4	2.9±0.6
	Terrestrial sink (SLAND)	1.3±0.5	2±0.7	1.9±0.8	2.5±0.6	2.9±0.7	3.3±0.8	3.8±0.8	2.9±1.2
Budget Imbalance	BIM=EFOS+ELUC-(GATM+SOCEAN+SLAND)	0.4	-0.2	-0.2	0.2	0	-0.4	-0.1	0.3

^aFossil emissions excluding the cement carbonation sink amount to 3±0.2 GtC/yr, 4.7±0.2 GtC/yr, 5.5±0.3 GtC/yr, 6.4±0.3 GtC/yr, 7.9±0.4 GtC/yr, and 9.8±0.5 GtC/yr for the decades 1960s to 2010s respectively and to 10.2±0.5 GtC/yr for 2022, and 10.3±0.5 GtC/yr for 2023.

3133

3134 **Table 7:** Decadal mean in the five components of the anthropogenic CO2 budget for different periods, and last
3135 year available. All values are in GtC yr⁻¹, and uncertainties are reported as ±1σ. Fossil CO2 emissions include
3136 cement carbonation. The table also shows the budget imbalance (B_{IM}), which provides a measure of the
3137 discrepancies among the nearly independent estimates. A positive imbalance means the emissions are
3138 overestimated and/or the sinks are too small. All values are rounded to the nearest 0.1 GtC and therefore
3139 columns do not necessarily add to zero.

3140

		1750-2022	1850-2014	1850-2022	1960-2022	1850-2023
Emissions	Fossil CO ₂ emissions (EFOS)	480±25	400±20	475±25	395±20	485±25
	Land-use change emissions (ELUC)	250±75	210±65	220±65	90±45	220±65
	Total emissions	730±80	610±65	695±70	485±50	705±70
Partitioning	Growth rate in atmos CO ₂ (GATM)	300±5	235±5	280±5	215±5	285±5
	Ocean sink (SOCEAN)	190±40	155±30	180±35	125±25	180±35
	Terrestrial sink (SLAND)	245±60	200±50	225±55	150±35	225±55
Budget imbalance	BIM=EFOS+ELUC-(GATM+SOCEAN+SLAND)	-5	20	15	-5	15

3141

3142 **Table 8.** Cumulative CO₂ for different time periods in gigatonnes of carbon (GtC). Fossil CO₂ emissions
3143 include cement carbonation. The budget imbalance (B_{IM}) provides a measure of the discrepancies among the
3144 nearly independent estimates. All values are rounded to the nearest 5 GtC and therefore columns do not
3145 necessarily add to zero. Uncertainties are reported as follows: E_{FOS} is 5% of cumulative emissions; E_{LUC} prior to
3146 1959 is 1σ spread from the DGVMs, E_{LUC} post-1959 is 0.7*number of years (where 0.7 GtC/yr is the
3147 uncertainty on the annual E_{LUC} flux estimate); G_{ATM} uncertainty is held constant at 5 GtC for all time periods;
3148 S_{OCEAN} uncertainty is 20% of the cumulative sink (20% relates to the annual uncertainty of 0.4 GtC/yr, which is
3149 ~20% of the current ocean sink); and S_{LAND} is the 1σ spread from the DGVMs estimates.

3150

3151

	2003-2012	2013-2022
ELUC from bookkeeping estimates (from Table 5)	1.4	1.3
SLAND on non-intact forest from DGVMs	1.9	2.0
ELUC subtract SLAND on non-intact forests	-0.5	-0.8
National Greenhouse Gas Inventories	-0.4	-0.7

3152 **Table 9:** Translation of global carbon cycle models' land flux definitions to the definition of the LULUCF net
3153 flux used in national Greenhouse Gas Inventories reported to UNFCCC. See Sec. C.2.3 and Table S9 for detail
3154 on methodology and comparison to other datasets. Units are GtC yr⁻¹.

3155

Source of uncertainty	Time scale (years)	Location	Evidence
Fossil CO2 emissions (EFOS; Section 2.1)			
energy statistics	annual to decadal	global, but mainly China & major developing countries	(Korsbakken et al., 2016, Guan et al., 2012)
carbon content of coal	annual to decadal	global, but mainly China & major developing countries	(Liu et al., 2015)
system boundary	annual to decadal	all countries	(Andrew, 2020a)
Net land-use change flux (ELUC; section 2.2)			
land-cover and land-use change statistics	continuous	global; in particular tropics	(Houghton et al., 2012, Gasser et al., 2020, Ganzenmüller et al., 2022, Yu et al. 2022)
sub-grid-scale transitions	annual to decadal	global	(Wilkenskjeld et al., 2014)
vegetation biomass	annual to decadal	global; in particular tropics	(Houghton et al., 2012, Bastos et al., 2021)
forest degradation (fire, selective logging)	annual to decadal	tropics	(Aragão et al., 2018, Qin et al., 2021)
wood and crop harvest	annual to decadal	global; SE Asia	(Arneth et al., 2017, Erb et al., 2018)
peat burning	multi-decadal trend	global	(van der Werf et al., 2010, 2017)
loss of additional sink capacity	multi-decadal trend	global	(Pongratz et al, 2014, Gasser et al, 2020; Obermeier et al., 2021)
Atmospheric growth rate (GATM; section 2.4) no demonstrated uncertainties larger than ± 0.3 GtC yr ⁻¹ . The uncertainties in GATM have been estimated as ± 0.2 GtC yr ⁻¹ , although the conversion of the growth rate into a global annual flux assuming instantaneous mixing throughout the atmosphere introduces additional errors that have not yet been quantified.			
Ocean sink (SOCEAN; section 2.5)			
sparsity in surface fCO2 observations	mean, decadal variability and trend	global, in particular southern hemisphere	(Gloege et al., 2021, Denvil-Sommer et al., 2021, Hauck et al., 2023)

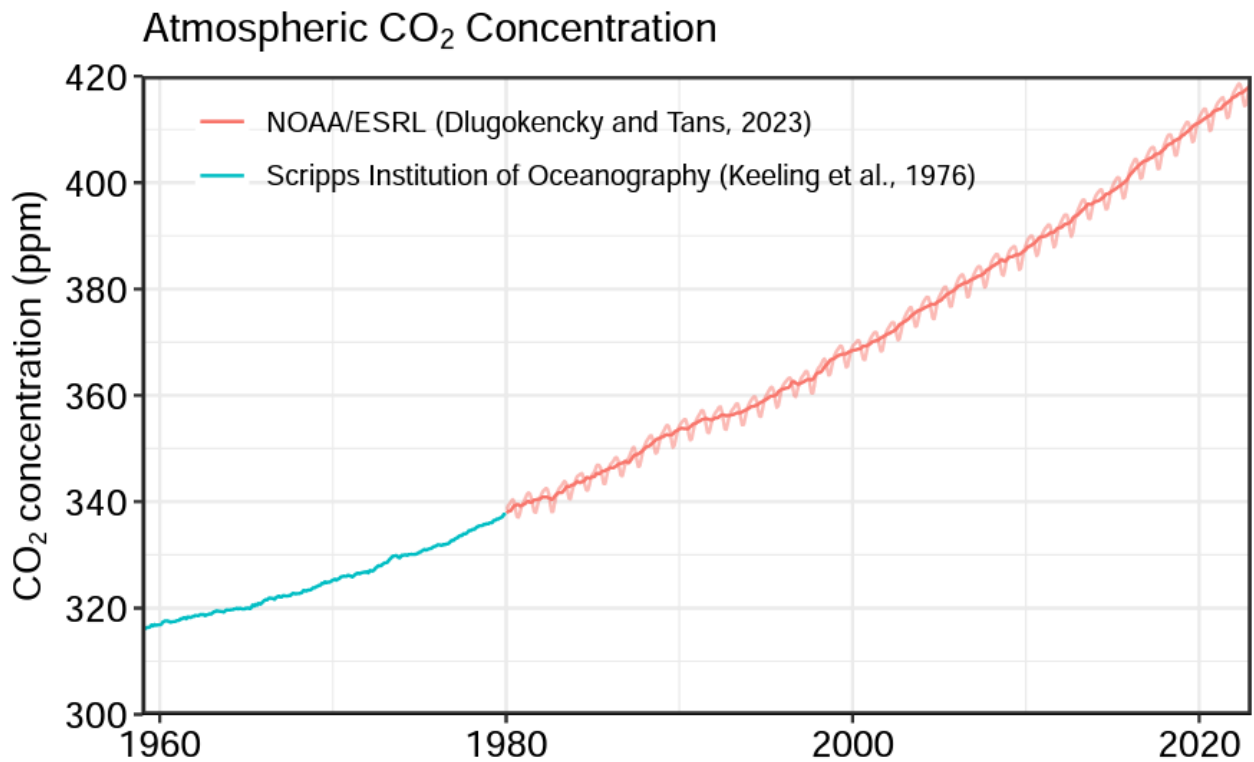
riverine carbon outgassing and its anthropogenic perturbation	annual to decadal	global, in particular partitioning between Tropics and South	(Aumont et al., 2001, Lacroix et al., 2020, Cris et al., 2022)
Models underestimate interior ocean anthropogenic carbon storage	annual to decadal	global	(Friedlingstein et al., 2021, this study, DeVries et al., 2023, see also Terhaar et al., 2022)
near-surface temperature and salinity gradients	mean on all time-scales	global	(Watson et al., 2020, Dong et al., 2022, Bellenger et al., 2023)
Land sink (SLAND; section 2.6)			
strength of CO2 fertilisation	multi-decadal trend	global	(Wenzel et al., 2016; Walker et al., 2021)
response to variability in temperature and rainfall	annual to decadal	global; in particular tropics	(Cox et al., 2013; Jung et al., 2017; Humphrey et al., 2018; 2021)
nutrient limitation and supply	annual to decadal	global	(Zaehle et al., 2014)
carbon allocation and tissue turnover rates	annual to decadal	global	(De Kauwe et al., 2014; O'Sullivan et al., 2022)
tree mortality	annual	global in particular tropics	(Hubau et al., 2021; Brienen et al., 2020)
response to diffuse radiation	annual	global	(Mercado et al., 2009; O'Sullivan et al., 2021)

3157

3158 **Table 10.** Major known sources of uncertainties in each component of the Global Carbon Budget, defined as
3159 input data or processes that have a demonstrated effect of at least $\pm 0.3 \text{ GtC yr}^{-1}$.

3160

3161



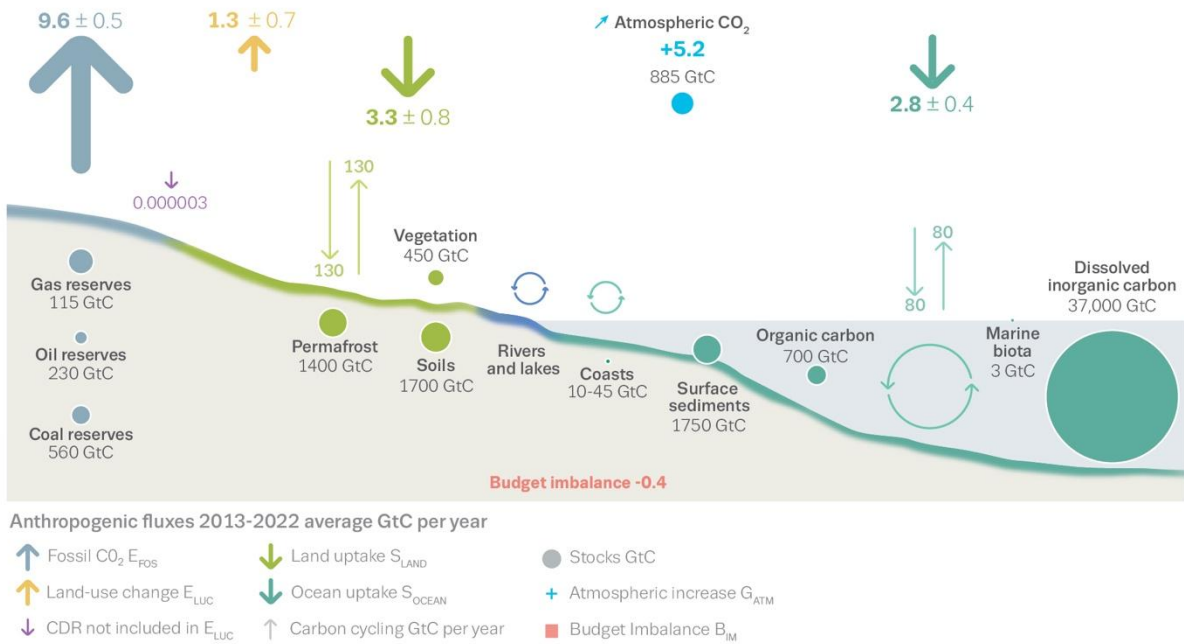
3163

3164 **Figure 1.** Surface average atmospheric CO₂ concentration (ppm). Since 1980, monthly data are from
3165 NOAA/GML (Lan et al., 2023) and are based on an average of direct atmospheric CO₂ measurements from
3166 multiple stations in the marine boundary layer (Masarie and Tans, 1995). The 1958-1979 monthly data are from
3167 the Scripps Institution of Oceanography, based on an average of direct atmospheric CO₂ measurements from the
3168 Mauna Loa and South Pole stations (Keeling et al., 1976). To account for the difference of mean CO₂ and
3169 seasonality between the NOAA/GML and the Scripps station networks used here, the Scripps surface average
3170 (from two stations) was de-seasonalised and adjusted to match the NOAA/GML surface average (from multiple
3171 stations) by adding the mean difference of 0.667 ppm, calculated here from overlapping data during 1980-2012.

3172

3173

The global carbon cycle

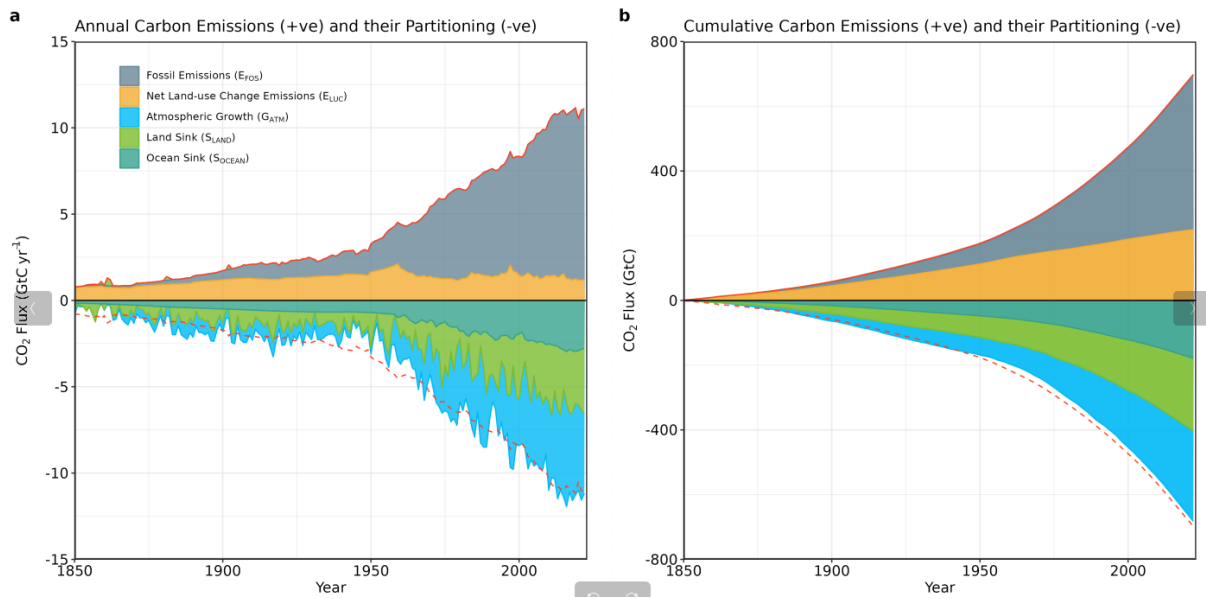


3174

3175

3176 **Figure 2.** Schematic representation of the overall perturbation of the global carbon cycle caused by
 3177 anthropogenic activities, averaged globally for the decade 2013-2022. See legends for the corresponding arrows.
 3178 Fluxes estimates and their 1 standard deviation uncertainty are as reported in Table 7. The uncertainty in the
 3179 atmospheric CO₂ growth rate is very small (± 0.02 GtC yr⁻¹) and is neglected for the figure. The anthropogenic
 3180 perturbation occurs on top of an active carbon cycle, with fluxes and stocks represented in the background and
 3181 taken from Canadell et al. (2021) for all numbers, except for the carbon stocks in coasts which is from a
 3182 literature review of coastal marine sediments (Price and Warren, 2016). Fluxes are in GtC yr⁻¹ and reservoirs in
 3183 GtC.

3184



3185

3186

Figure 3. Combined components of the global carbon budget as a function of time, for fossil CO₂ emissions

3187

(E_{FOS}, including a small sink from cement carbonation; grey) and emissions from land-use change (E_{LUC};

3188

brown), as well as their partitioning among the atmosphere (G_{ATM}; cyan), ocean (S_{OCEAN}; blue), and land (S_{LAND};

3189

green). Panel (a) shows annual estimates of each flux (in GtC yr⁻¹) and panel (b) the cumulative flux (the sum of

3190

all prior annual fluxes, in GtC) since the year 1850. The partitioning is based on nearly independent estimates

3191

from observations (for G_{ATM}) and from process model ensembles constrained by data (for S_{OCEAN} and S_{LAND})

3192

and does not exactly add up to the sum of the emissions, resulting in a budget imbalance (B_{IM}) which is

3193

represented by the difference between the bottom red line (mirroring total emissions) and the sum of carbon

3194

fluxes in the ocean, land, and atmosphere reservoirs. All data are in GtC yr⁻¹ (panel a) and GtC (panel b). The

3195

E_{FOS} estimate is based on a mosaic of different datasets and has an uncertainty of ±5% (±1σ). The E_{LUC} estimate

3196

is from three bookkeeping models (Table 4) with uncertainty of ±0.7 GtC yr⁻¹. The G_{ATM} estimates prior to 1959

3197

are from Joos and Spahni (2008) with uncertainties equivalent to about ±0.1-0.15 GtC yr⁻¹ and from Lan et al.

3198

(2023) since 1959 with uncertainties of about ±0.07 GtC yr⁻¹ during 1959-1979 and ±0.02 GtC yr⁻¹ since 1980.

3199

The S_{OCEAN} estimate is the average from Khatiwala et al. (2013) and DeVries (2014) with uncertainty of about

3200

±30% prior to 1959, and the average of an ensemble of models and an ensemble of fCO₂-products (Table 4)

3201

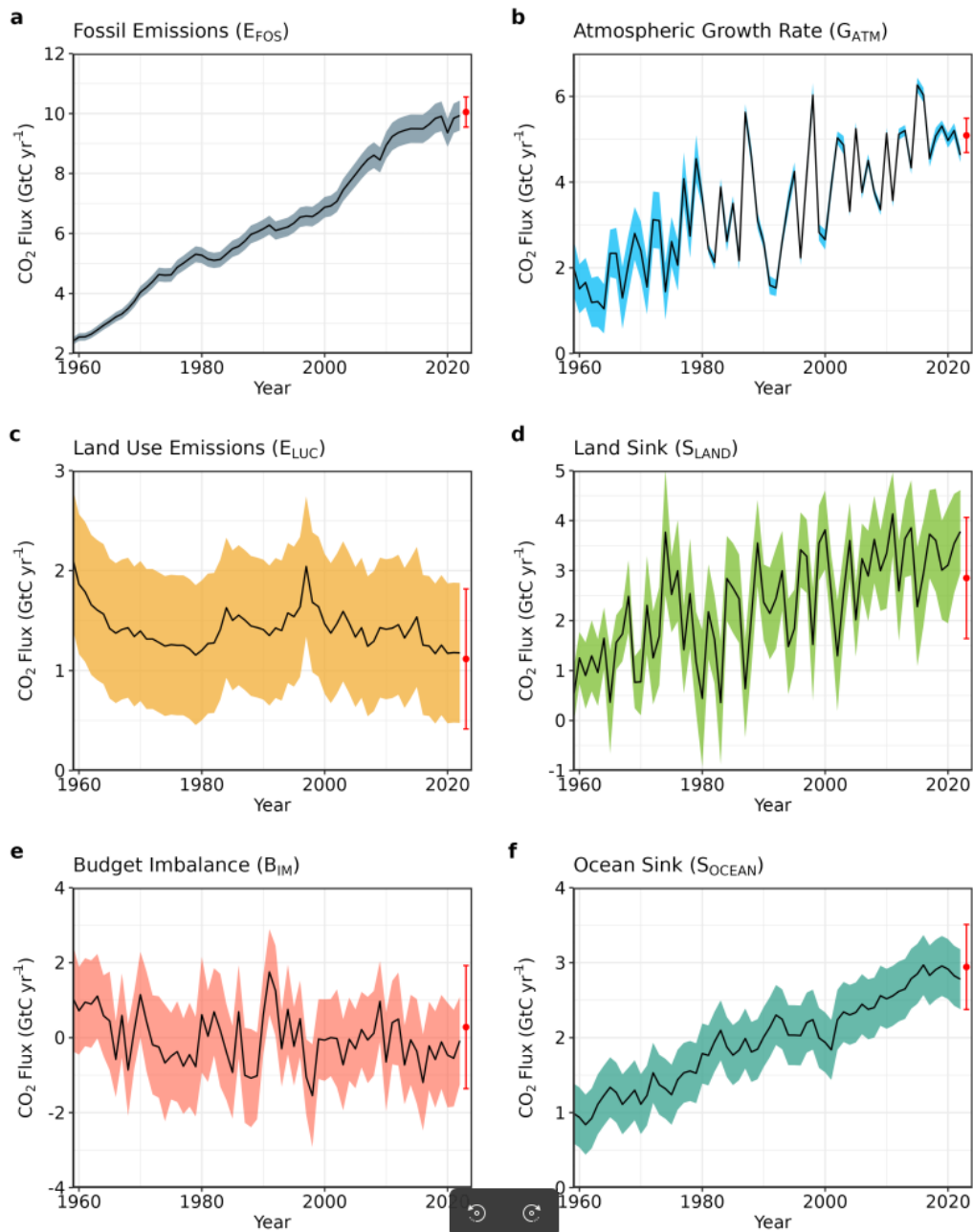
with uncertainties of about ±0.4 GtC yr⁻¹ since 1959. The S_{LAND} estimate is the average of an ensemble of

3202

models (Table 4) with uncertainties of about ±1 GtC yr⁻¹. See the text for more details of each component and

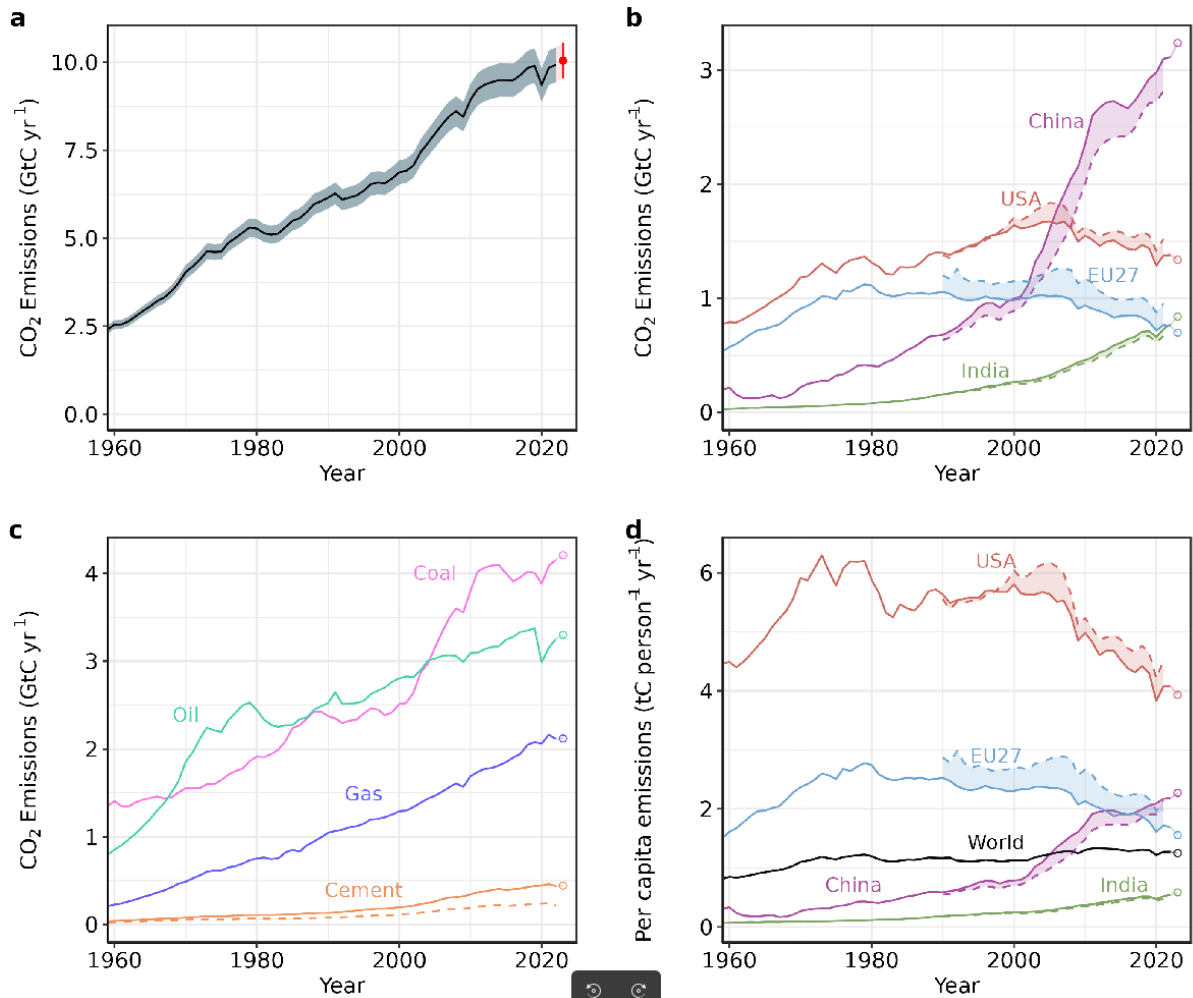
3203

their uncertainties.

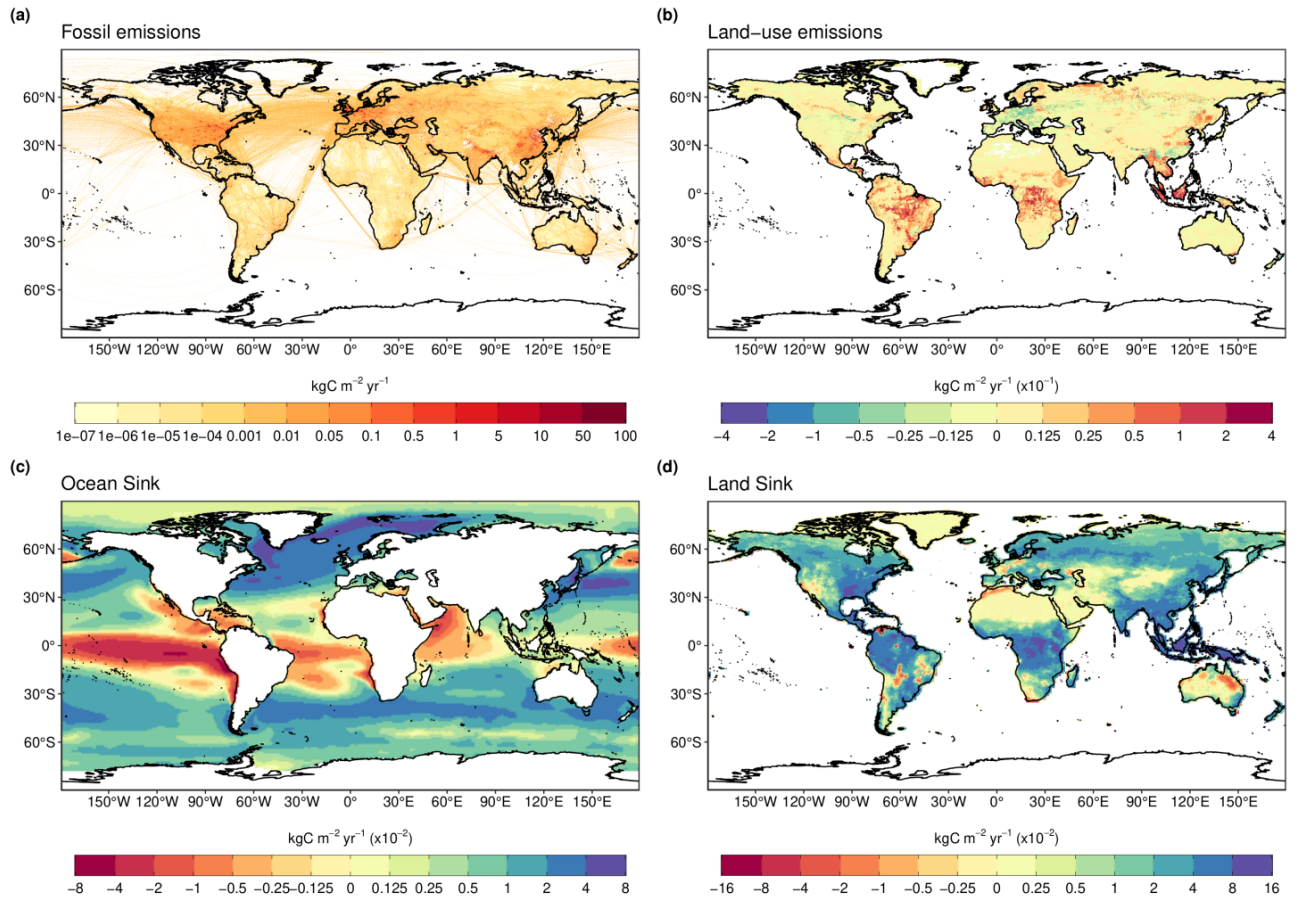


3204

3205 **Figure 4.** Components of the global carbon budget and their uncertainties as a function of time, presented
 3206 individually for (a) fossil CO₂ and cement carbonation emissions (E_{FOS}), (b) growth rate in atmospheric CO₂
 3207 concentration (G_{ATM}), (c) emissions from land-use change (E_{LUC}), (d) the land CO₂ sink (S_{LAND}), (e) the ocean
 3208 CO₂ sink (S_{OCEAN}), (f) the budget imbalance that is not accounted for by the other terms. Positive values of
 3209 S_{LAND} and S_{OCEAN} represent a flux from the atmosphere to land or the ocean. All data are in GtC yr⁻¹ with the
 3210 uncertainty bounds representing ± 1 standard deviation in shaded colour. Data sources are as in Figure 3. The red
 3211 dots indicate our projections for the year 2023 and the red error bars the uncertainty in the projections (see
 3212 methods).

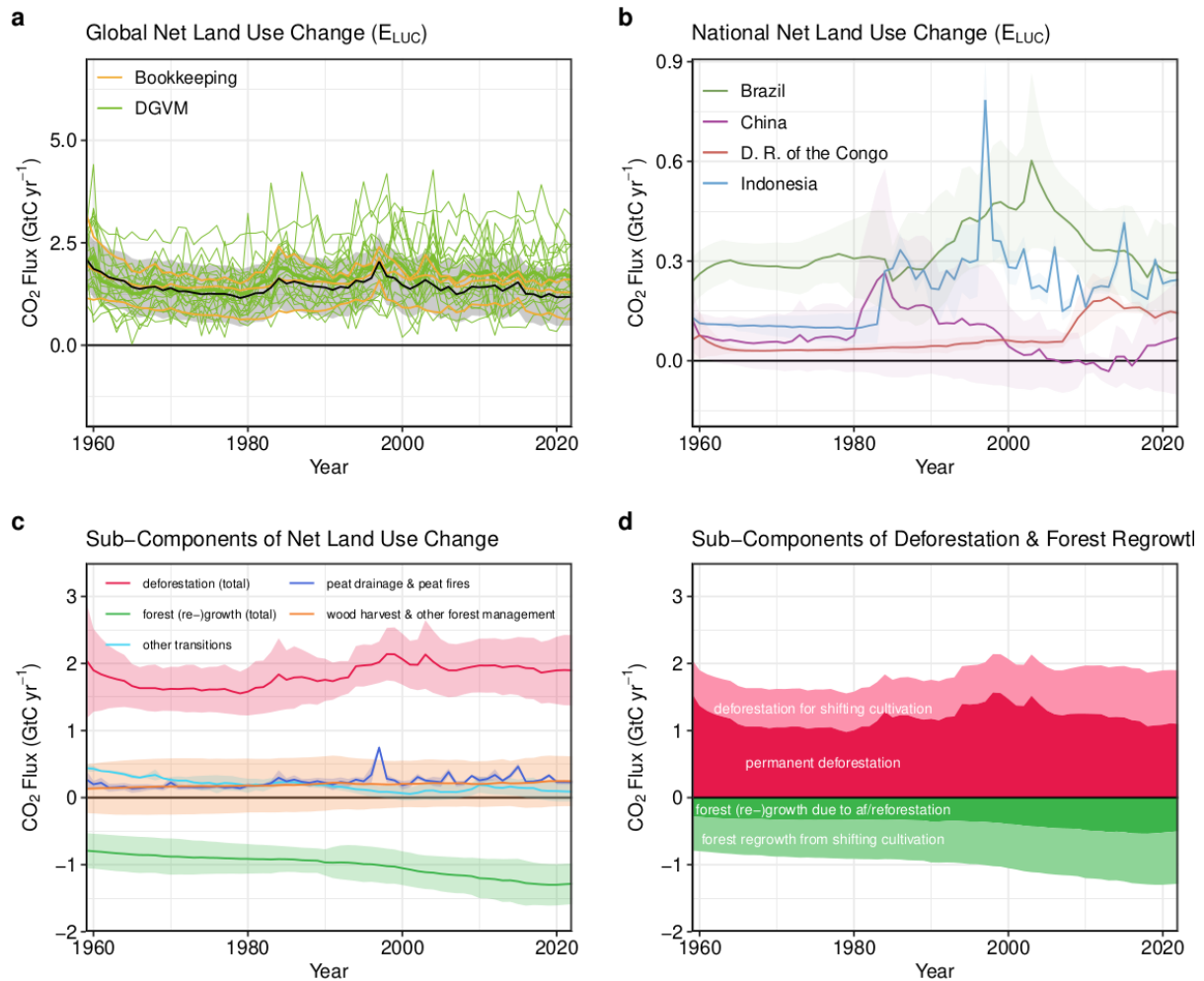


3213
 3214 **Figure 5.** Fossil CO₂ emissions for (a) the globe, including an uncertainty of $\pm 5\%$ (grey shading) and a
 3215 projection through the year 2023 (red dot and uncertainty range), (b) territorial (solid lines) and consumption
 3216 (dashed lines) emissions for the top three country emitters (USA, China, India) and for the European Union
 3217 (EU27), (c) global emissions by fuel type, including coal, oil, gas, and cement, and cement minus cement
 3218 carbonation (dashed), and (d) per-capita emissions the world and for the large emitters as in panel (b). Territorial
 3219 emissions are primarily from a draft update of Gilfillan and Marland (2021) except for national data for Annex I
 3220 countries for 1990-2021, which are reported to the UNFCCC as detailed in the text, as well as some
 3221 improvements in individual countries, and extrapolated forward to 2022 using data from Energy Institute.
 3222 Consumption-based emissions are updated from Peters et al. (2011a). See Section 2.1 and Supplement S.1 for
 3223 details of the calculations and data sources.



3224
 3225
 3226
 3227
 3228
 3229
 3230
 3231
 3232
 3233
 3234
 3235
 3236
 3237
 3238

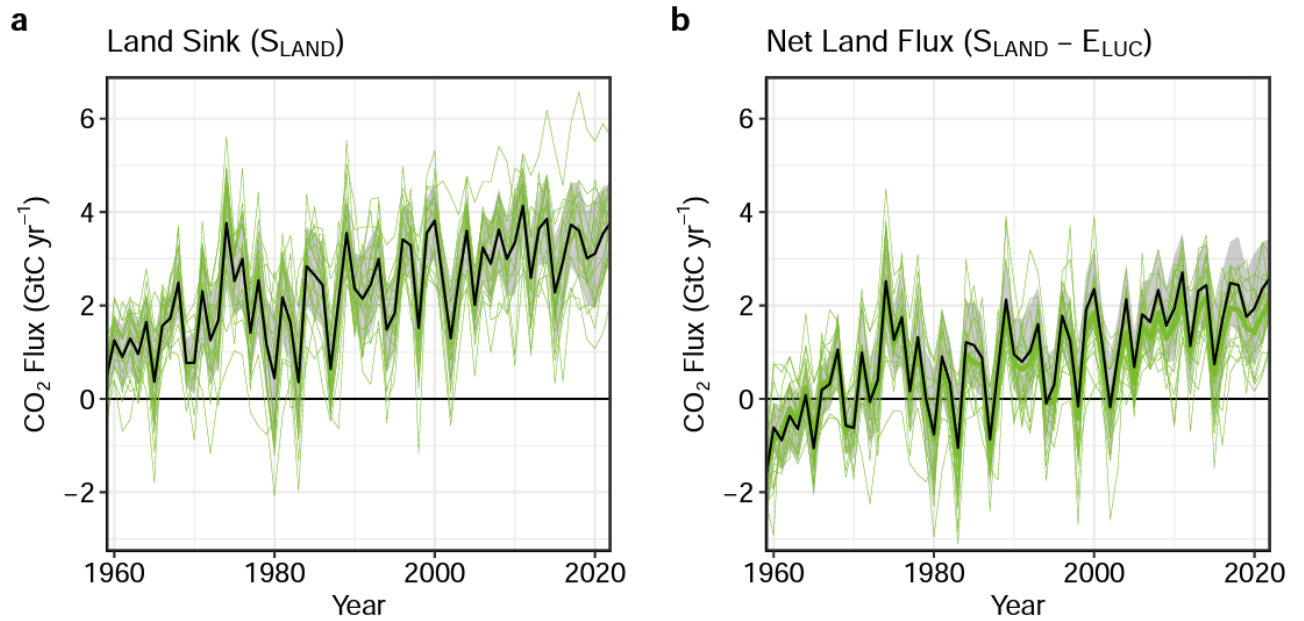
Figure 6. The 2013-2022 decadal mean components of the global carbon budget, presented for (a) fossil CO₂ emissions (E_{FOS}), (b) land-use change emissions (E_{LUC}), (c) the ocean CO₂ sink (S_{OCEAN}), and (d) the land CO₂ sink (S_{LAND}). Positive values for E_{FOS} and E_{LUC} represent a flux to the atmosphere, whereas positive values of S_{OCEAN} and S_{LAND} represent a flux from the atmosphere to the ocean or the land (carbon sink). In all panels, yellow/red colours represent a source (flux from the land/ocean to the atmosphere), green/blue colours represent a sink (flux from the atmosphere into the land/ocean). All units are in $\text{kgC m}^{-2} \text{yr}^{-1}$. Note the different scales in each panel. E_{FOS} data shown is from GCP-GridFEDv2023.1 and does not include cement carbonation. The E_{LUC} map shows the average E_{LUC} from the three bookkeeping models plus emissions from peat drainage and peat fires. Gridded E_{LUC} estimates for H&C2023 and OSCAR are derived by spatially distributing their national data based on the spatial patterns of BLUE gross fluxes in each country (see Schwingshackl et al., 2022, for more details about the methodology). S_{OCEAN} data shown is the average of GOBMs and data-products means, using GOBMs simulation A, no adjustment for bias and drift applied to the gridded fields (see Section 2.5). S_{LAND} data shown is the average of the DGVMs for simulation S2 (see Section 2.6).



3239
3240

Figure 7. Net CO₂ exchanges between the atmosphere and the terrestrial biosphere related to land use change.

3241 (a) Net CO₂ emissions from land-use change (E_{LUC}) with estimates from the three bookkeeping models (yellow
3242 lines) and the budget estimate (black with $\pm 1\sigma$ uncertainty), which is the average of the three bookkeeping
3243 models. Estimates from individual DGVMs (narrow green lines) and the DGVM ensemble mean (thick green
3244 line) are also shown. (b) Net CO₂ emissions from land-use change from the four countries with largest
3245 cumulative emissions since 1959. Values shown are the average of the three bookkeeping models, with shaded
3246 regions as $\pm 1\sigma$ uncertainty. (c) Sub-components of E_{LUC} : (i) emissions from deforestation (including permanent
3247 deforestation and deforestation in shifting cultivation cycles), (ii) emissions from peat drainage & peat fires, (iii)
3248 removals from forest (re-)growth (including forest (re-)growth due to afforestation and reforestation and forest
3249 regrowth in shifting cultivation cycles), (iv) fluxes from wood harvest and other forest management (comprising
3250 slash and product decay following wood harvest, regrowth after wood harvest, and fire suppression), and (v)
3251 emissions and removals related to other land-use transitions. The sum of the five components is E_{LUC} shown in
3252 panel (a). (d) Sub-components of ‘deforestation (total)’ and of ‘forest (re-)growth (total)’: (i) deforestation in
3253 shifting cultivation cycles, (ii) permanent deforestation, (iii) forest (re-)growth due to afforestation and/or
3254 reforestation, and (iv) forest regrowth in shifting cultivation cycles.

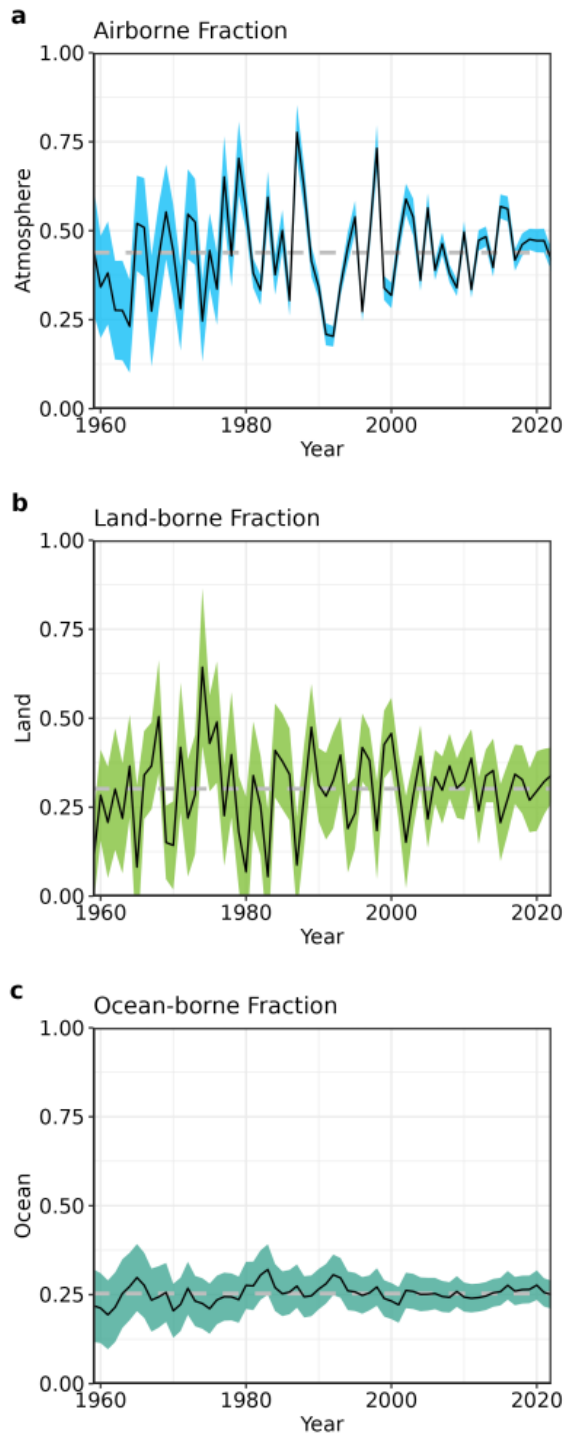


3255

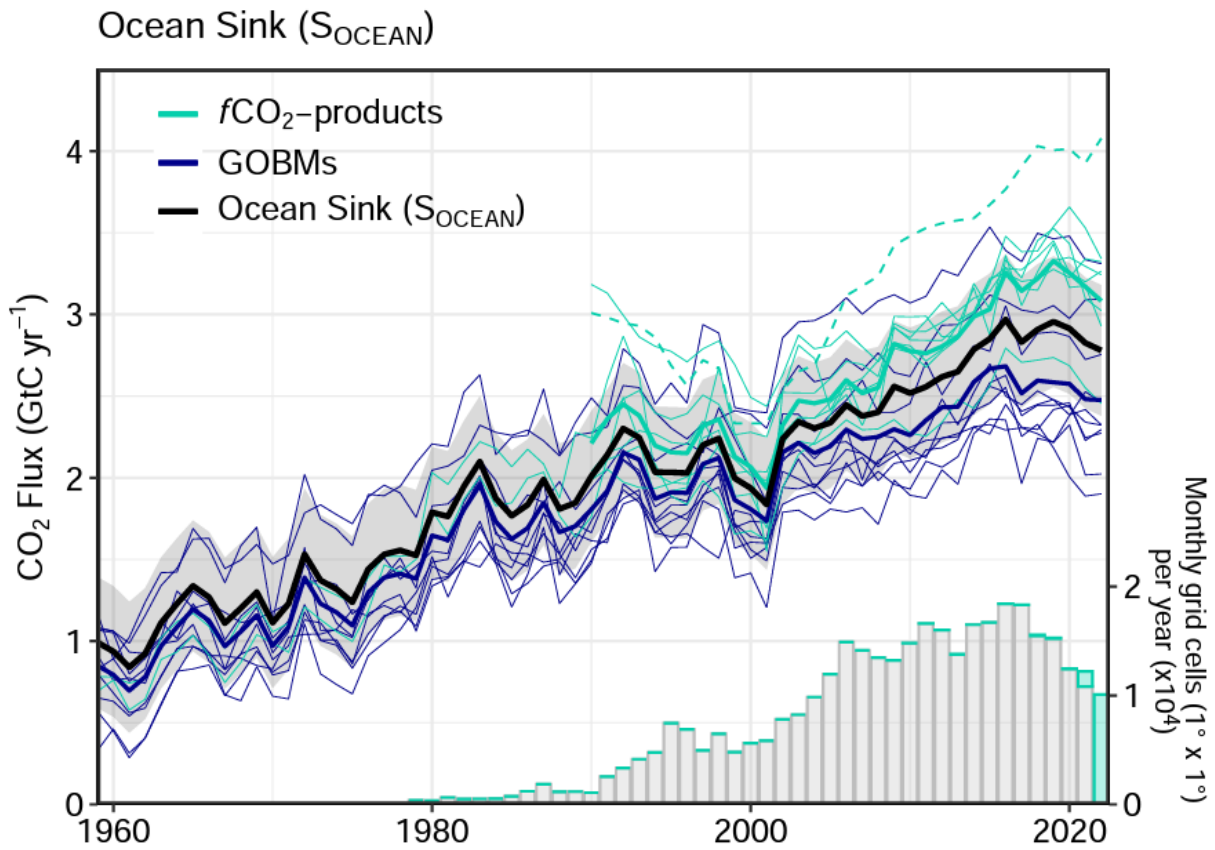
3256 **Figure 8.** (a) The land CO₂ sink (S_{LAND}) estimated by individual DGVMs (green), as well as the budget estimate
 3257 (black with $\pm 1\sigma$ uncertainty), which is the average of all DGVMs. (b) Net atmosphere-land CO₂ fluxes ($S_{\text{LAND}} -$
 3258 E_{LUC}). The budget estimate of the net land flux (black with $\pm 1\sigma$ uncertainty) combines the DGVM estimate of
 3259 S_{LAND} from panel (a) with the bookkeeping estimate of E_{LUC} from Figure 7a. Uncertainties are similarly
 3260 propagated in quadrature. DGVMs also provide estimates of E_{LUC} (see Figure 7a), which can be combined with
 3261 their own estimates of the land sink. Hence panel (b) also includes an estimate for the net land flux for
 3262 individual DGVMs (thin green lines) and their multi-model mean (thick green line).

3263

3264



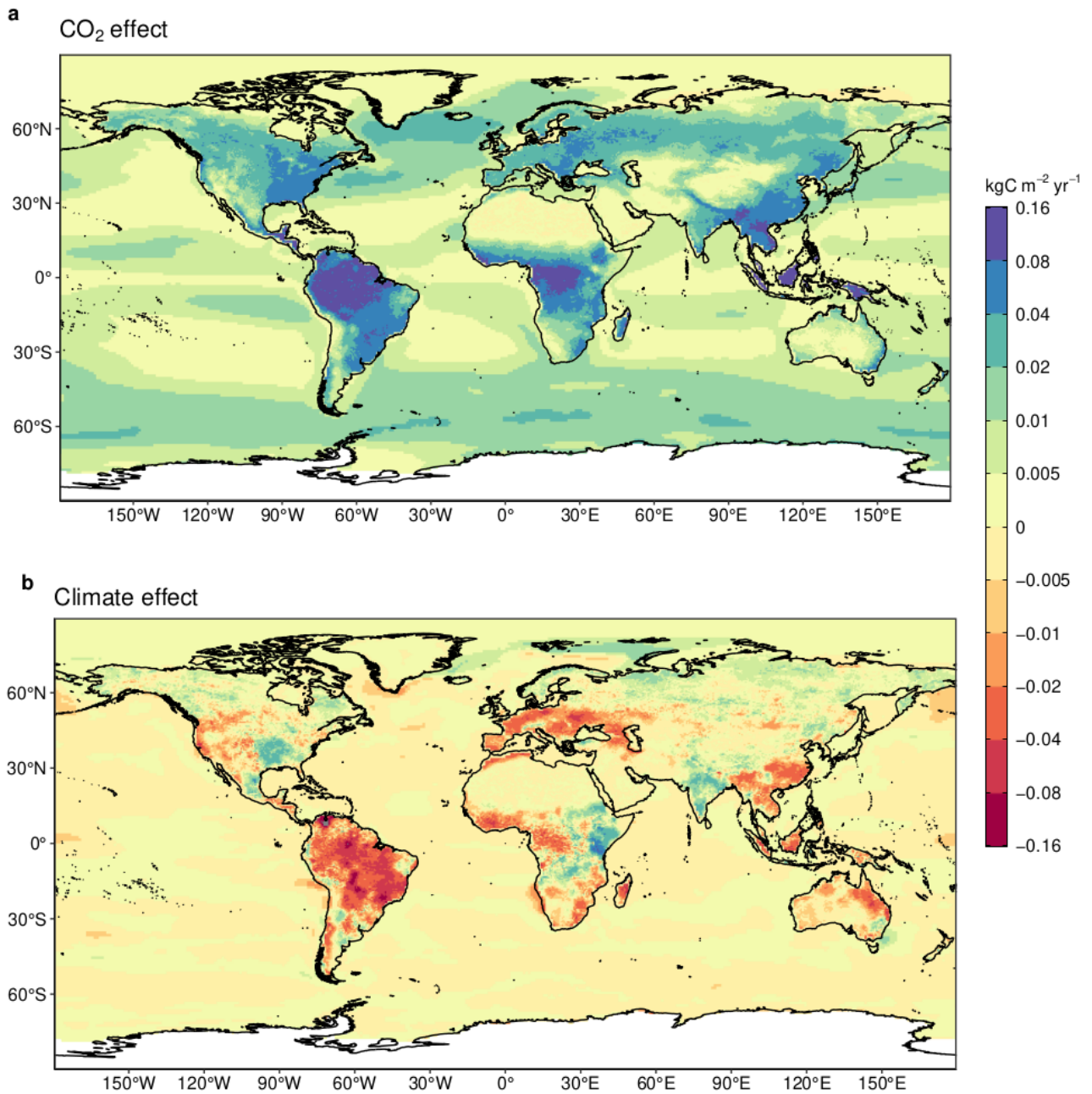
3310 **Figure 9.** The partitioning of total anthropogenic CO₂ emissions ($E_{\text{FOS}} + E_{\text{LUC}}$) across (a) the atmosphere
 3311 (airborne fraction), (b) land (land-borne fraction), and (c) ocean (ocean-borne fraction). Black lines represent the
 3312 central estimate, and the coloured shading represents the uncertainty. The grey dashed lines represent the long-
 3313 term average of the airborne (44%), land-borne (30%) and ocean-borne (25%) fractions during 1960-2022 (with
 3314 a B_{IM} of 1%).
 3315



3316

3317 **Figure 10.** Comparison of the anthropogenic atmosphere-ocean CO₂ flux showing the budget values of S_{OCEAN}
 3318 (black; with the uncertainty in grey shading), individual ocean models (royal blue), and the ocean $f\text{CO}_2$ -products
 3319 (cyan; with Watson et al. (2020) in dashed line as not used for ensemble mean). Only one $f\text{CO}_2$ -product (Jena-
 3320 MLS) extends back to 1959 (Rödenbeck et al., 2022). The $f\text{CO}_2$ -products were adjusted for the pre-industrial
 3321 ocean source of CO₂ from river input to the ocean, by subtracting a source of 0.65 GtC yr⁻¹ to make them
 3322 comparable to S_{OCEAN} (see Section 2.5). Bar-plot in the lower right illustrates the number of $f\text{CO}_2$ observations
 3323 in the SOCAT v2023 database (Bakker et al., 2023). Grey bars indicate the number of data points in SOCAT
 3324 v2022, and coloured bars the newly added observations in v2023.

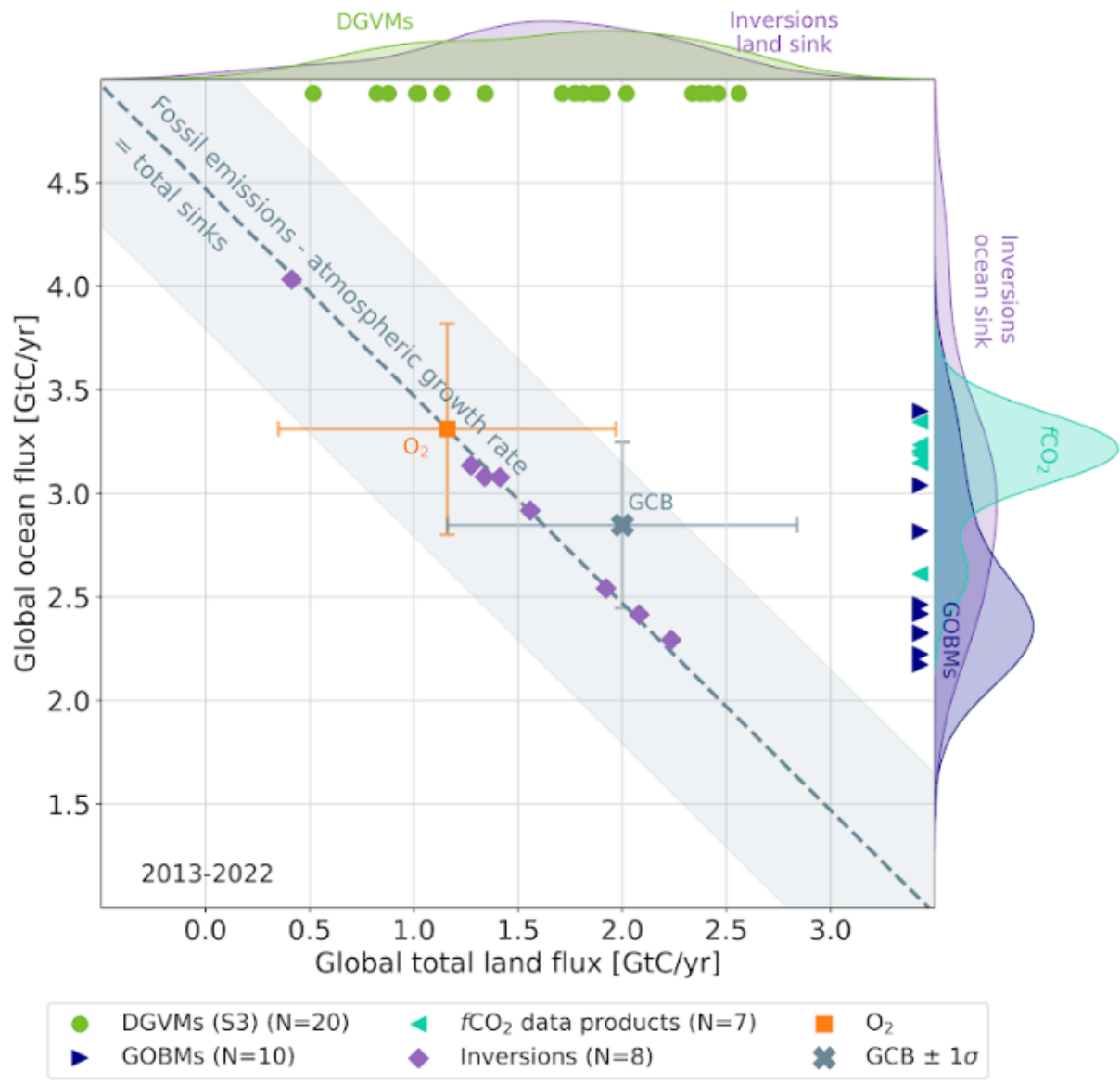
3325



3326

3327 **Figure 11.** Attribution of the atmosphere-ocean (S_{OCEAN}) and atmosphere-land (S_{LAND}) CO₂ fluxes to (a)
 3328 increasing atmospheric CO₂ concentrations and (b) changes in climate, averaged over the previous decade 2013-
 3329 2022. All data shown is from the processed-based GOBMs and DGVMs. Note that the sum of ocean CO₂ and
 3330 climate effects shown here will not equal the ocean sink shown in Figure 6 which includes the f_{CO_2} -products.
 3331 See Supplement S.3.2 and S.4.1 for attribution methodology. Units are in kgC m⁻² yr⁻¹ (note the non-linear
 3332 colour scale).

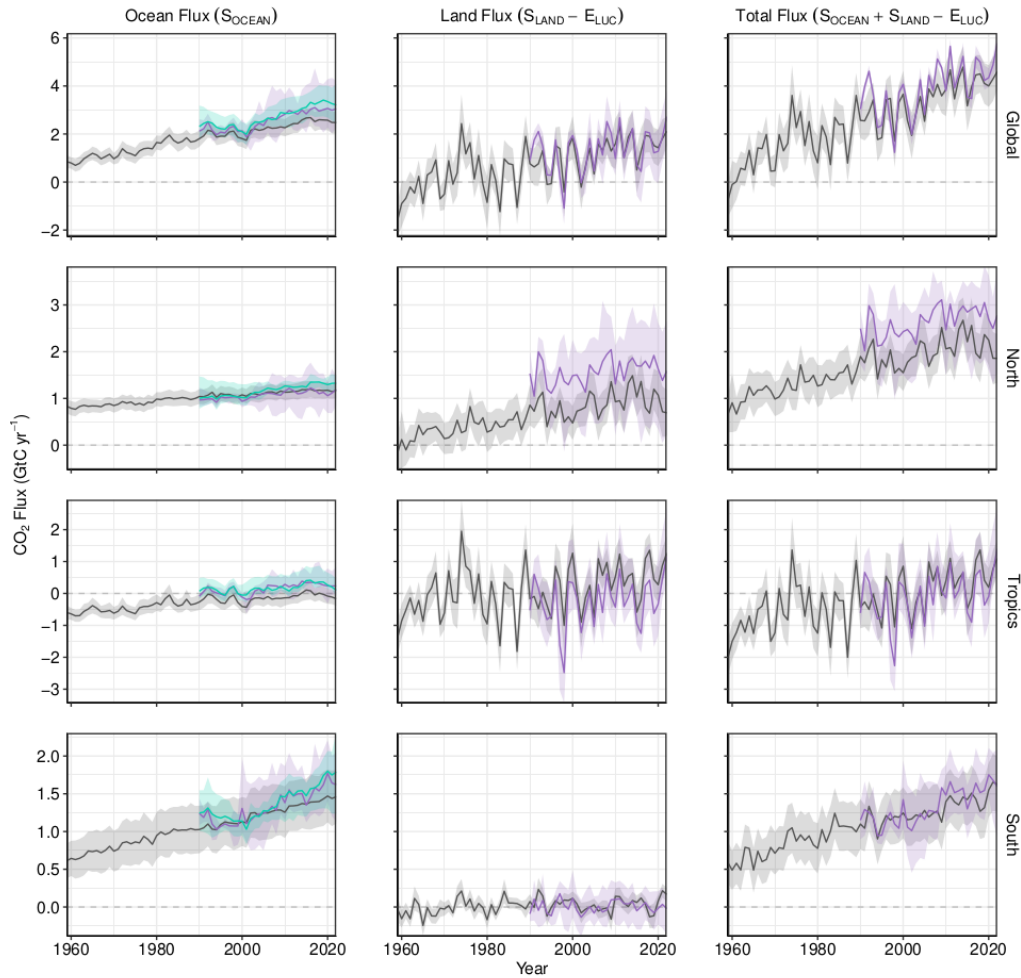
3333



3334

3335 **Figure 12.** The 2013-2022 decadal mean global net atmosphere-ocean and atmosphere-land fluxes derived from
 3336 the ocean models and $f\text{CO}_2$ products (y-axis, right and left pointing blue triangles respectively), and from the
 3337 DGVMs (x-axis, green symbols), and the same fluxes estimated from the atmospheric inversions (purple
 3338 symbols). The shaded distributions show the densities of the ensembles of individual estimates. The grey central
 3339 cross is the mean ($\pm 1\sigma$) of S_{OCEAN} and $(S_{\text{LAND}} - E_{\text{LUC}})$ as assessed in this budget. The grey diagonal line
 3340 represents the constraint on the global land + ocean net flux, i.e. global fossil fuel emissions minus the
 3341 atmospheric growth rate from this budget ($E_{\text{FOS}} - G_{\text{ATM}}$). The orange cross represents the same global net
 3342 atmosphere-ocean and atmosphere-land fluxes as estimated from the atmospheric O_2 constraint ($\pm 1\sigma$ for each of
 3343 the fluxes although caution is needed to interpret these error bars, since solutions outside the grey band are
 3344 unlikely, as outside of the 1σ uncertainty). Positive values are CO_2 sinks. Note that the inverse estimates have
 3345 been scaled for a minor difference between E_{FOS} and GridFEDv2023.1 (Jones et al., 2023).

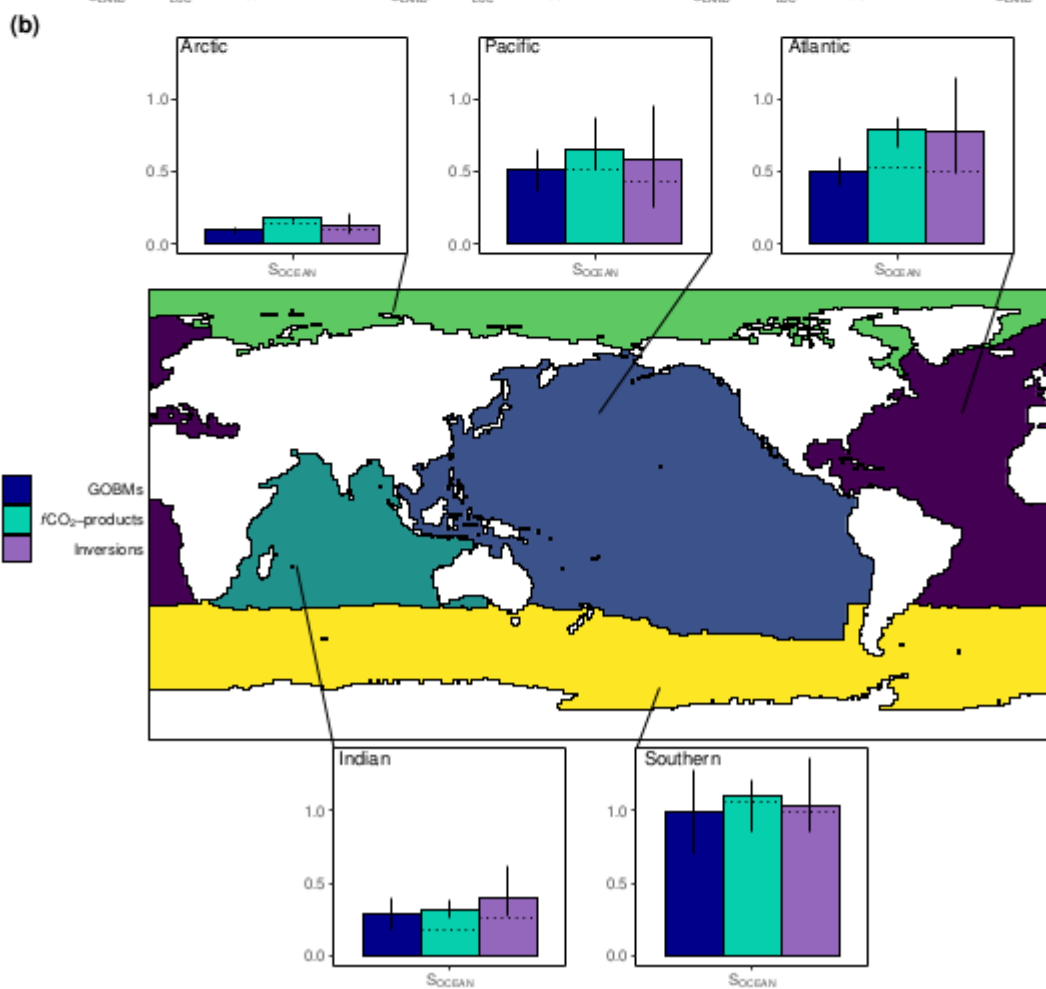
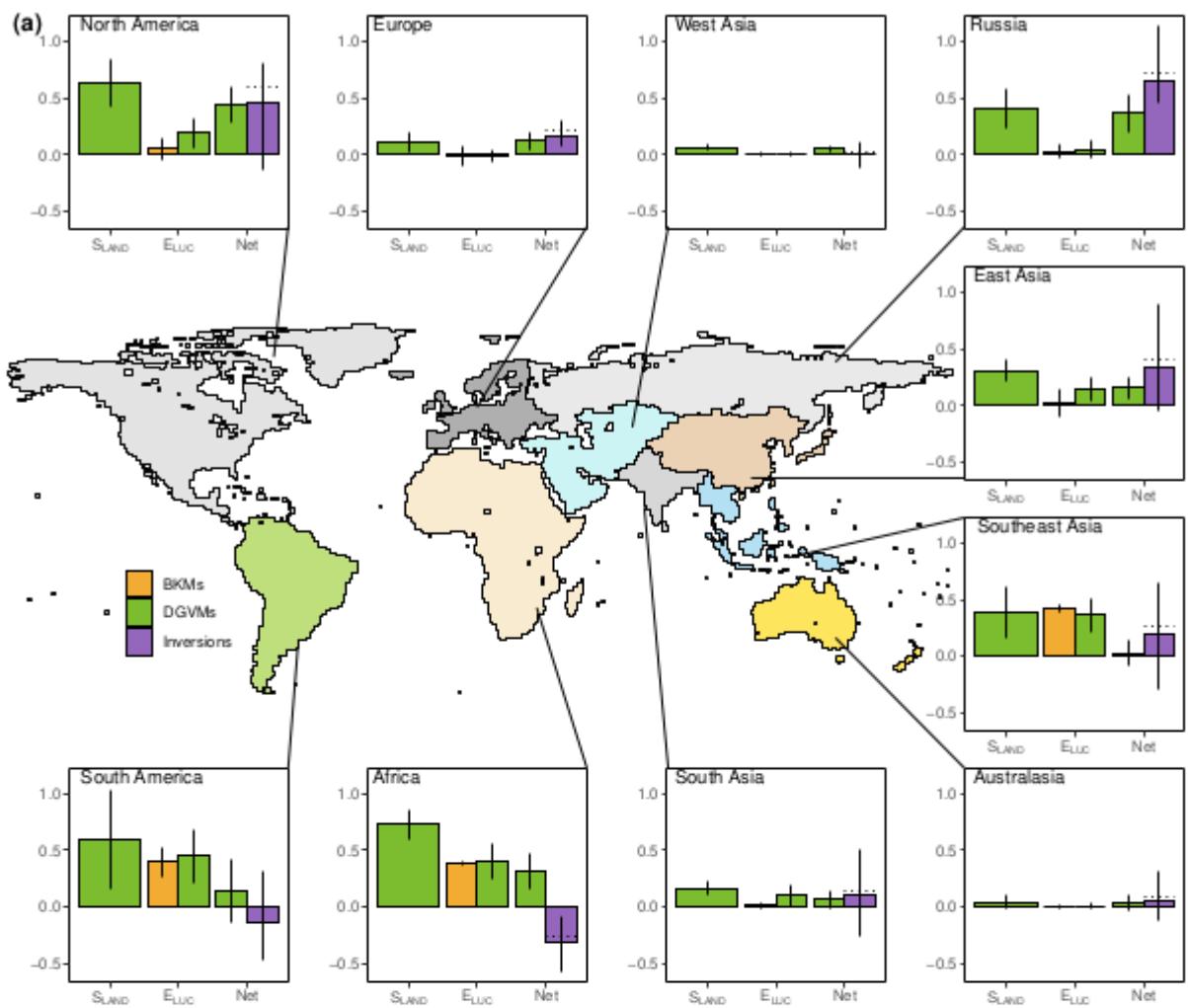
Annual Carbon Fluxes to (-ve) or from (+ve) the Atmosphere



— Process-based models (DGVMs and GOBMs) — Inversions — fCO_2 -products

3346

3347 **Figure 13.** CO₂ fluxes between the atmosphere and the Earth's surface separated between land and oceans,
3348 globally and in three latitude bands. The ocean flux is S_{OCEAN} and the land flux is the net atmosphere-land fluxes
3349 from the DGVMs. The latitude bands are (top row) global, (2nd row) north (>30°N), (3rd row) tropics (30°S-
3350 30°N), and (bottom row) south (<30°S), and over ocean (left column), land (middle column), and total (right
3351 column). Estimates are shown for: process-based models (DGVMs for land, GOBMs for oceans); inversion
3352 systems (land and ocean); and $f\text{CO}_2$ -products (ocean only). Positive values are CO₂ sinks. Mean estimates from
3353 the combination of the process models for the land and oceans are shown (black line) with $\pm 1 \sigma$ of the model
3354 ensemble (grey shading). For the total uncertainty in the process-based estimate of the total sink, uncertainties
3355 are summed in quadrature. Mean estimates from the atmospheric inversions are shown (purple lines) with their
3356 full spread (purple shading). Mean estimates from the $f\text{CO}_2$ -products are shown for the ocean domain (light blue
3357 lines) with full model spread (light blue shading). The global S_{OCEAN} (upper left) and the sum of S_{OCEAN} in all
3358 three regions represents the anthropogenic atmosphere-to-ocean flux based on the assumption that the
3359 preindustrial ocean sink was 0 GtC yr⁻¹ when riverine fluxes are not considered. This assumption does not hold
3360 at the regional level, where preindustrial fluxes can be significantly different from zero. Hence, the regional
3361 panels for S_{OCEAN} represent a combination of natural and anthropogenic fluxes. Bias-correction and area-
3362 weighting were only applied to global S_{OCEAN} ; hence the sum of the regions is slightly different from the global
3363 estimate (<0.05 GtC yr⁻¹).

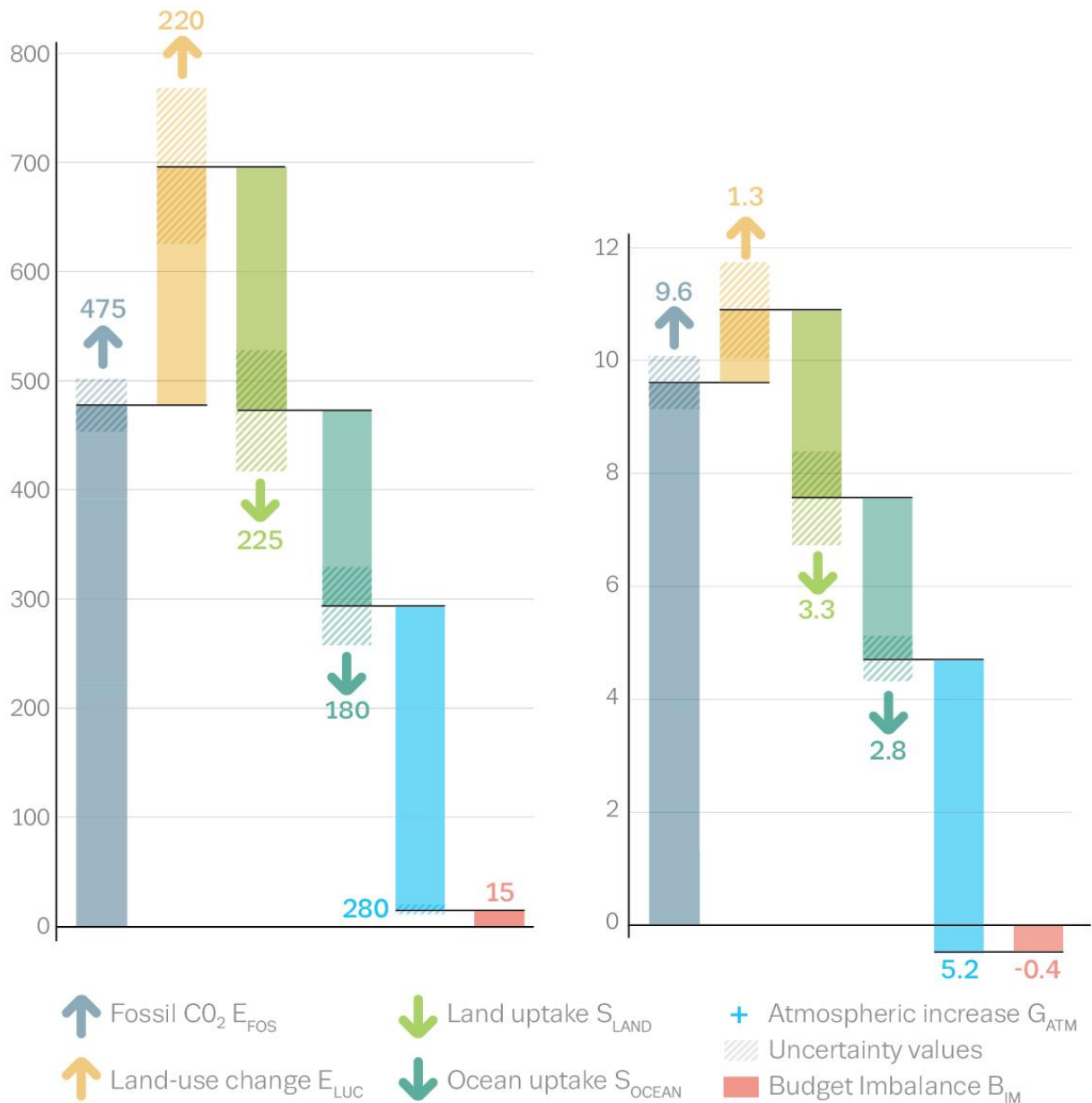


3365 **Figure 14.** Decadal mean (a) land and (b) ocean fluxes for RECCAP-2 regions over 2013-2022. For land fluxes,
3366 S_{LAND} is estimated by the DGVMs (green bars), with the error bar as $\pm 1\sigma$ spread among models. A positive
3367 S_{LAND} is a net transfer of carbon from the atmosphere to the land. E_{LUC} fluxes are shown for both DGVMs
3368 (green) and bookkeeping models (orange), again with the uncertainty calculated as the $\pm 1\sigma$ spread. Note, a
3369 positive E_{LUC} flux indicates a loss of carbon from the land. The net land flux is shown for both DGVMs (green)
3370 and atmospheric inversions (purple), including the full model spread for inversions. The net ocean sink (S_{OCEAN})
3371 is estimated by GOBMs (royal blue), $f\text{CO}_2$ -products (cyan), and atmospheric inversions (purple). Uncertainty is
3372 estimated as the $\pm 1\sigma$ spread for GOBMs, and the full model spread for the other two products. The dotted lines
3373 show the $f\text{CO}_2$ -products and inversion results without river flux adjustment. Positive values are CO_2 sinks.

Anthropogenic carbon flows

Cumulative changes 1850-2022 GtC

Mean fluxes 2013-2022 GtC per year



3374

3375 **Figure 15.** Cumulative changes over the 1850-2022 period (left) and average fluxes over the 2013-2022 period
 3376 (right) for the anthropogenic perturbation of the global carbon cycle. See the caption of Figure 3 for key
 3377 information and the methods in text for full details.



3378

3379 **Figure 16.** Kaya decomposition of the main drivers of fossil CO₂ emissions, considering population, GDP per
 3380 person, Energy per GDP, and CO₂ emissions per energy, for China (top left), USA (top right), EU27 (middle
 3381 left), India (middle right), Rest of the World (bottom left), and World (bottom right). Black dots are the annual
 3382 fossil CO₂ emissions growth rate, coloured bars are the contributions from the different drivers to this growth
 3383 rate. A general trend is that population and GDP growth put upward pressure on emissions (positive values),
 3384 while energy per GDP and, more recently, CO₂ emissions per energy put downward pressure on emissions
 3385 (negative values). Both the COVID-19 induced drop during 2020 and the recovery in 2021 led to a stark contrast
 3386 to previous years, with different drivers in each region. The EU27 had strong Energy/GDP improvements in
 3387 2022.